Theses and Dissertations

August 2013

Zinc Chemical Biology: The Pursuit of the Intracellular Targets of Zinquin

Andrew Nowakowski
University of Wisconsin-Milwaukee

Follow this and additional works at: https://dc.uwm.edu/etd

Part of the Biochemistry Commons, and the Chemistry Commons

ZINC CHEMICAL BIOLOGY: THE PURSUIT OF THE INTRACELLULAR TARGETS OF ZINQUIN

by

Andrew B. Nowakowski

A Dissertation Submitted in

Partial Fulfillment of the

Requirements for the Degree of

Doctor of Philosophy

in Chemistry

at

The University of Wisconsin-Milwaukee

August 2013

ABSTRACT

ZINC CHEMICAL BIOLOGY: THE PURSUIT OF THE INTRACELLULAR TARGETS OF ZINQUIN

by

Andrew B. Nowakowski

The University of Wisconsin-Milwaukee, 2013
Under the Supervision of Distinguished Professor David H. Petering, Ph.D.

Abstract

Fluorescent sensors have been a main microscopic tools used to understand Zn^{2+} physiology on a cellular level. The use of the fluorescent Zn^{2+} sensor Zinquin (ZQ) and its analogues have revealed that transient Zn^{2+} is a chief component in a variety of biochemical pathways. Yet, little work has been performed to validate the exact targets of Zinquin in a cellular environment. The goals of this investigation are to determine the types of Zinquin reactions that take place in the cell as well as the identities of its cellular targets.

It has been hypothesized that Zinquin reacts with free Zn^{2+} within cells at nanomolar concentrations. Instead, by using robust analytical methods such as fluorescence spectrophotometry, column chromatography, and ICP-MS, this report shows a consistent pattern across seven cell and tissue types that Zinquin reacts in micromolar concentrations with Zn^{2+} bound to proteins. The main source of evidence for this reaction is a unique emission spectrum for a ZQ-Zn-protein adduct compared to $Zn(ZQ)_2$. $Zn(ZQ)_2$ can be generated by Zinquin sequestering Zn^{2+} from members of the Zn-

proteome and can undergo additional ligand substitution reactions with apo-Zn-binding sites within the proteome to form new ZQ-Zn-protein adducts.

With these new insights in mind, previously published investigations were revisited to reevaluate the conclusions drawn using Zinquin as a Zn-reporter molecule. A parallel investigation was also performed using a Zinquin analogue, TSQ, which revealed that the reactions and fluorescence observed were dependent on the chemical properties of the sensor used, not on the physiology being evaluated.

Lastly, the development of a novel affinity chromatography method led to a partial isolation of the intracellular targets of Zinquin. In addition, a high resolution native polyacrylamide gel electrophoresis method was developed to sufficiently separate protein mixtures while still retaining their metal cofactors. These gels can then be analyzed using laser ablation-inductively coupled plasma-mass spectrometry to assess the metal content of the protein bands. The development of these two techniques enhances the ability to isolate and identify members of the Zn-proteome, and thus are great tools for advancing the field of metallomics.

To my family,
whose love and guidance have made my success possible

To my friends,
whose support will never go unrecognized or unappreciated

To all the people who've stoked my passion for science,
your intellectual stimulations have lead me to a fulfilling career

TABLE OF CONTENTS

LIST OF FIGURES

LIST OF TABLES

LIST OF ABREVIATIONS

AAS	Flame Atomic Absorption Spectroscopy
AU	Arbitrary Units
ADH	Alcohol Dehydrogenase
AP	Alkaline Phosphatase
β-Gal	β-Galactosidase
BN-PAGE	Blue Native- Polyacrylamide Gel Electrophoresis
CA	Carbonic Anhydrase
DPBS	Dulbecco's Phosphate Buffered Saline
EDC	1-ethyl-3-(3-dimethylaminopropyl)carboiimide
EDTA	Ethylenediaminetetraacetic acid
FCS	Fetal Calf Serum
GSH	Glutathione
LDS	Lithium Dodecyl Sulfate
LMW	Low Molecular Weight
LA-ICP-MS	Laser Ablation-Inductively Coupled Plasma-Mass Spectrometry
HMW	High Molecular Weight
MES	2-(N-morpholino)ethanesulfonic acid
MOPS	3-(N-morpholino)propanesulfonic acid
MTT	3(4,5-dimethyl-2-thiazoyl)-2,5-diphenyl-2H-tetrazolium bromide
NBT	Nitro Blue Tetrazolium
NSDS-PAGE	Native Sodium Dodecyl Sulfate-Polyacrylamide Gel Electrophoresis
PMS	Phenazine Methosulfate
$SC_{10}S$	Sodium Decyl Sulfate
SDS	Sodium Dodecyl Sulfate
SDS-PAGE	Sodium Dodecyl Sulfate-Polyacrylamide Gel Electrophoresis
SOD	Superoxide Dismutase
SOS	Sodium Octyl Sulfate
STS	Sodium Tetradecyl Sulfate
TPEN	*N,N,N',N'*-Tetrakis(2-pyridylmethyl)ethylenediamine
ZQ_{ACID}	(2-methyl-8-*p*-toluenesulfonamido-6-quinolyloxy)acetate
ZQ_{EE}	ethyl(2-methyl-8-*p*-toluenesulfonamido-6-quinolyloxy)acetate

1. <u>Introduction</u>

The use of Zinc (Zn^{2+}) in biological systems is both ubiquitous and varied. Traditional Zn^{2+} biochemists view this metal ion in two lights: that of a structural element stabilizing the three dimensional protein scaffolding and that of an essential cofactor in the active site of many enzymes.[1,2] Such examples of Zn-proteins include Zn-finger transcription factors, carbonic anhydrase, and carboxypeptidase.[1,3] By mass, zinc is the second most prevalent transition metal ion used in a biological systems.[4] Recently, a bioinformatics study was undertaken to determine the depth of the Zn-proteome.[2,5] Based on binding motifs of known catalytic and structural Zn^{2+} sites, a survey of the human genome suggested that approximately 2,800 proteins have a theoretical capability to bind Zn^{2+}, corresponding to approximately 10% off the coding genome.[5] If correct, this proposed Zn-proteome dwarfs other metallomes including the Cu-proteome (near 100 proteins) and the non-heme Fe-proteome (near 250 proteins).[5]

Besides static associations with proteins as a co-factor, more recent research has focused on transient Zn^{2+} and the role it plays in various physiological pathways. One of the most well-studied pathways involves the stimulation of metallothionein synthesis.[6-9] Here, increased intracellular Zn^{2+} binds to apo-Zn-fingers on the MTF-1 transcription factor. Now active, MTF-1 binds to a gene promoter region and stimulates the transcription of metallothionein mRNA. The synthesized metallothionein protein then

binds the excess Zn^{2+} as a stable Zn-metallothionein structure. Hence, through this pathway, the intracellular Zn^{2+} concentration can be maintained.

Zn^{2+} has also emerged as a major player in brain physiology. High concentrations of Zn^{2+} are located in synaptic vesicles throughout the brain.[10] Upon activation, Zn^{2+} is released into the extracellular space to interact with different extracellular targets.[11] Therefore, it is believed that Zn^{2+} acts as a neurotransmitter in the brain.[11,12] Furthermore, localization of Zn^{2+} in the hippocampal region has suggested that Zn^{2+} may play a significant role in cognitive function and memory formation.[10,13] In addition, the accumulation of Zn^{2+} within the extracellular space of neural tissues has been a hallmark of cerebral trauma and several neurodegenerative disorders such as Alzheimer's disease.[14-16]

Due to its extensive cellular interactions, maintenance of Zn^{2+} homeostasis is of paramount importance to the cell. Pathways involving Zn^{2+} import/export, compartmentalization, and protein association must all be tightly regulated.[17,18] Thus, understanding the dynamic nature of intracellular Zn^{2+} metabolism has been at the forefront of metallo-biochemistry over the past few decades.

In general, the metabolically active Zn^{2+} within the cell can be described as reactions 1.1.

$$Zn^{2+}+L_1 \rightleftarrows Zn\text{-}L_1 \,; Zn\text{-}L_1 +L_2 \rightleftarrows Zn\text{-}L_2 + L_1 ... Zn\text{-}L_n + L_{n-1} \qquad (1.1)$$
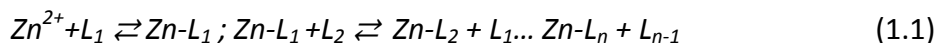
The Zn^{2+} that participates in these general reactions is considered to be metabolic, that is, able to move among ligands. It is typically described within the field as

"exchangeable," "chelatable," "labile," or "free" Zn^{2+}.[11,19-21] The ligands in these reactions represent the sum of all biomolecules present within the cell that have an appreciable affinity for Zn^{2+} that might contribute to the dynamics of Zn^{2+} within the cell. Thus, this general reaction is chiefly dependent on the thermodynamic and kinetic properties of the individual ligands as well as their intracellular concentrations.[22] The cytosolic "free" Zn^{2+} concentration is estimated to be in the low nM to high pM range.[4,23]

The idea of transient Zn^{2+} hinges on the ability of the equilibria in reaction 1.1 to be modified. More specifically, the introduction of a cellular stimulus results in either the release of Zn^{2+} from a specific ligand (reaction 1.2), or the modification of a ligand forming an active Zn-ligand complex (reaction 1.3).

$$Zn\text{-}Ligand + stimulus \rightleftarrows Zn^{2+} + Ligand \qquad (1.2)$$

$$Zn\text{-}Ligand + stimulus \rightleftarrows Zn\text{-}Ligand_{REACTIVE} \qquad (1.3)$$

The products of either reaction—free Zn^{2+} or an activated Zn-Ligand—then react with a new ligand that is a critical participant in a pathway that ultimately gives rise to a change in physiology (reaction 1.4 or 1.5).

$$Zn^{2+} + Ligand^* \rightleftarrows Zn\text{-}Ligand^* \qquad (1.4)$$

$$Zn\text{-}Ligand_{REACTIVE} + Ligand^* \rightleftarrows Zn\text{-}Ligand^* + Ligand_{REACTIVE} \qquad (1.5)$$

Therefore, to truly understand Zn-mediated physiological events, the chemistry of these reactions need to be investigated.

Investigating Zn^{2+} requires a different strategy than that used in studying other transition metals. Unlike many other transition metal cofactors, Zn^{2+} is not redox active under physiological conditions. Moreover, the d^{10} electronic configuration of Zn^{2+} makes it invisible to most spectroscopic methods. Hence inorganic techniques such as electron paramagnetic resonance spectroscopy and absorption spectroscopy used for studying copper and iron cannot be employed to investigate Zn^{2+}. These limitations have led to the development of Zn^{2+} sensors as a means for studying Zn^{2+} biochemistry.

Fluorescent Zn^{2+} sensors have been the main tool for studying transient Zn^{2+} within the cellular environment.[24-26] It has been assumed that these sensors exhibit fluorescence changes when interacting with free Zn^{2+} within the cell (reaction 1.6).

$$Zn^{2+} + sensor \rightleftarrows Zn\text{-}sensor \qquad\qquad (1.6)$$

Therefore, changes in intracellular free Zn^{2+} can be evaluated by monitoring fluorescence changes after a given stimulus. In order for the sensor to function properly, the equilibrium constant of reaction 1.6 must lie within the range of the transient Zn^{2+} concentration. If the sensor binds Zn^{2+} too weakly, minute changes in the free Zn^{2+} concentration will not be detected. Conversely, if the sensor binds Zn^{2+} too strongly, the sensor may become saturated and a discernible Zn^{2+} flux cannot be evaluated. More importantly, a sensor with an exceptionally high affinity for Zn^{2+} may in sequester Zn^{2+} from members of the non-transient zinc population (i.e. Zn-proteins). Therefore, a more accurate representation of the chemistry involved in Zn-sensor investigations is described in reaction 1.7, the combination of reactions 1.1 and 1.6.

$$\Sigma \text{ Zn-Ligand} + \text{sensor} \rightleftarrows \text{Zn-sensor} + \Sigma \text{ Ligand} \qquad (1.7)$$
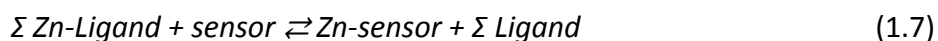
The extent to which the sensor interacts with the non-transient Zn^{2+} pool is again dependent on the thermodynamic and kinetic properties associated with those Zn-proteins and the sensor. These interactions must be minimal in order to draw proper conclusions about the changes in transient Zn^{2+}.

With this is mind, a variety of fluorescent Zn^{2+} sensors have been employed over the years to study Zn^{2+} biochemistry within cells.[26] One of the most common classes of fluorescent probes used is the quinolinesulfonamides.[24] 6-methoxy-(8-*p*-toluenesulfonamido)quinoline, or TSQ, was one of the first sensors developed and was used as a histochemical stain for Zn^{2+} in brain tissue (**Figure 1.1**).[27] TSQ reacts with Zn^{2+} to form 2:1 complexes resulting in a substantial increase in fluorescence.[28] Importantly, fluorescence enhancement does not occur with any other biologically relevant metal ion, making it a sole reporter for Zn^{2+}.[28] Using fluorescence microscopy, cells stained with TSQ typically display a punctate staining pattern attributed to the localization of high concentrations of Zn^{2+}.[28]

Second generation quinoline fluorophores such as (2-methyl-8-p-toluenesulfonamido-6-quinolyloxy)acetate, or Zinquin (ZQ), have overtaken TSQ in its use as a Zn^{2+} sensor (**Figure 1.1**).[26,29] Zinquin was synthesized to overcome the perceived shortcomings of its predecessor. Since both TSQ and $Zn(TSQ)_2$ are neutrally charged, cellular efflux of the
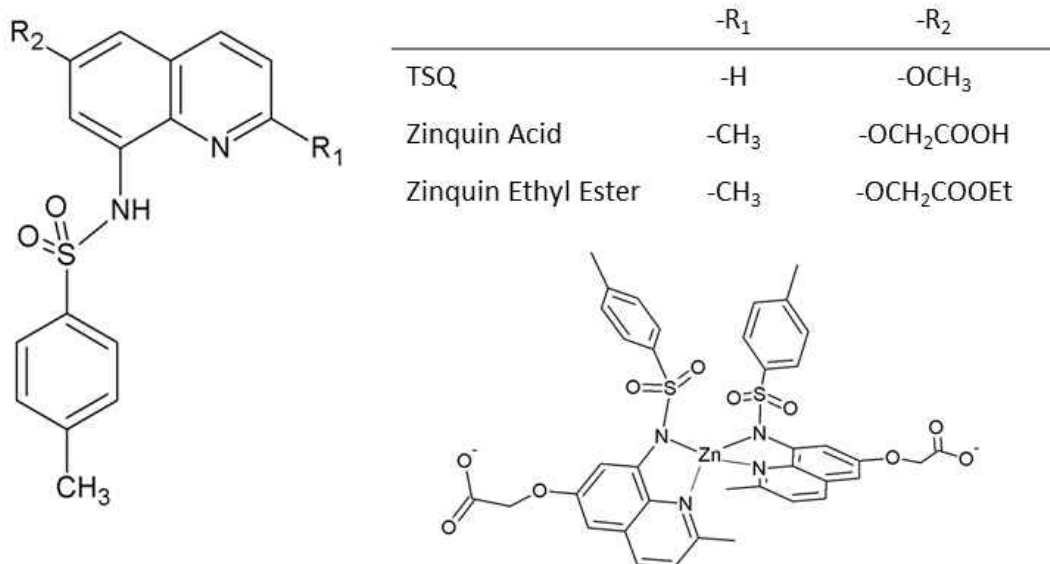
Figure 1.1. Chemical structures of quinoline based Zn^{2+} sensors. The structure of Zn(ZQ)$_2$ was inferred from the crystal structure of Zn(2-Me-TSQ)$_2$.[30]

probe or metal-probe complex is conceivable. To circumvent this, an ethyl ester moiety was added to the methoxy group at the 6 position of the quinoline ring. This neutral molecule passively enters cells and, once inside, is hydrolyzed by intracellular esterases to a negatively charged carboxylic acid, presumably trapping it within the cell. Another modification included the addition of a methyl group at the 2 position on the quinoline ring. This methyl group hinders the formation of square planar and octahedral complexes via steric clash in 2:1 binding, thus stabilizing the more favorable distorted tetrahedral coordination.[30] This modification contributes to the higher Zn^{2+} binding affinity of Zinquin than TSQ.[28,30,31]

The literature is rife with examples of utilizing Zinquin in conjunction with fluorescence microscopy to image Zn^{2+} within cells.[15,20,29,30,32-50] In most cases, cultured cells are loaded with Zinquin ethyl ester (ZQ_{EE}) for a given time to determine basal Zn^{2+} fluorescence and distribution. Then, a chemical stimulus is applied and fluorescence changes are monitored. Depending on the Zn^{2+} pathway being studied, these stimuli can range from exposure to heavy metals, to sulfhydral modifying agents, to compounds inducing oxidative stress via nitric oxide (NO) release.[35,40,45,51] Based on changes in fluorescence, conclusions are drawn as to how the stimulus affects the Zn^{2+} status within the cell.

The main pitfall of using fluorescent Zn^{2+} sensors is the tendency to infer detailed chemical reactions from fluorescent micrographs. For example, one study examined the effects of metallothionein in mouse lung fibroblasts in relation to exposure to NO as

measured by Zinquin.[45] In wild type cells, exposure to *S*-nitrosocysteine, a nitric oxide donor, resulted in an instantaneous increase in Zinquin fluorescence. Conversely, the treatment of metallothionein knockout cells with NO did not result in an immediate fluorescence response. Thus, the authors concluded that metallothionein plays a significant role in Zn^{2+} homeostasis by quickly responding to oxidative stress induced by nitric oxide. Yet, *in vitro* studies have shown that the metallothionein does not readily react with nitric oxide.[52] Therefore, the chemical mechanisms causing the fluorescence enhancement are probably more complex than the sole interaction of NO with metallothionein.[52]

Another potential complication when using fluorescent sensors such as Zinquin is the formation of 1:1 Zn-Sensor complexes. It has been posited that, in a biological setting, bidentate quinoline probes like Zinquin may react with openly coordinated Zn-proteins, forming ZQ-Zn-protein complexes (reaction 1.8).[22,53,54]

$$Zn\text{-}Ligand + ZQ \rightleftarrows ZQ\text{-}Zn\text{-}Ligand \qquad (1.8)$$

This hypothesis was supported by work showing that Zinquin acid can form ternary adducts with small organic ligands that still exhibit fluorescence.[53] Therefore, if such adducts are formed *in vivo*, they would most likely be indistinguishable from a $Zn(ZQ)_2$ species as viewed through a fluorescence microscope.

Furthermore, this problem is expanded when considering $Zn(ZQ)_2$ in a cellular environment.   The cytosol of a human colon cancer cell was estimated to have approximately 28 µM of unoccupied Zn^{2+}-binding sites with an average dissociation

constant of 83 pM.[55] Assuming that that these values are applicable to other cell types, it may be possible that intracellular ligands compete with one of the Zinquin molecules in the $Zn(ZQ)_2$ complex (reaction 1.9). This reaction would further obscure the identity of the fluorescent species being imaged using fluorescence microscopy.

$$Zn(ZQ)_2 + L_{INTRACELLULAR} \rightleftarrows ZQ\text{-}Zn\text{-}L_{INTRACELLULAR} + ZQ \qquad (1.9)$$

Therefore, there is a pressing need for more comprehensive studies involving techniques besides fluorescence microscopy to determine the intracellular chemistry of these fluorescent sensors. This need is even more apparent when considering the vast number of investigations that employ Zinquin and its analogues as a means to monitor changes in free Zn^{2+} concentration.

An initial investigation to elucidate the source of TSQ-based fluorescence in cells was performed by Dr. Jeff Meeusen from the Petering Lab.[56] By using multiple analytical techniques, it was determined that TSQ reacts almost exclusively with Zn^{2+} bound to proteins and not free Zn^{2+} within the cell.[56] This conclusion was drawn not only from the gel filtration experiments, but also by using fluorescence data obtained from entire emission spectra. Specifically, a TSQ-Zn-protein adduct was characterized as having an emission spectrum that is blue-shifted from the spectrum of $Zn(TSQ)_2$, which can be distinguished spectrophotometrically. These findings shed new light on how TSQ functions in cells and provided the initial evidence for the formation of fluorescent adducts with cellular proteins.[56]

In this context, the purpose of this dissertation research is to expand upon the initial premise of adduct formation to include the intracellular reactions of Zinquin. Although TSQ and Zinquin are closely related, there are known chemical differences. First, the formation of $Zn(ZQ)_2$ may be favored over an adduct species since Zinquin binds Zn^{2+} several orders of magnitude more strongly than TSQ.[31,56] Also, Zinquin acid is negatively charged at physiological pH. Hence, it is more soluble than TSQ in an aqueous environment which may affect the intracellular distribution of the probe.[43,57] Furthermore, the charged carboxylate may hinder adduct formation with some proteins due to electrostatic interactions. Along the same line, the 2' methyl group may also sterically clash with potential Zn-protein targets. Therefore, Zinquin may react differently than TSQ in a cellular context.

In summation, fluorescent probes such as Zinquin have been used as tools to visualize Zn^{2+} flux within cells. Yet, there have been limited accompanying data to support what chemistries these fluorescent sensors may be participating in. With these ideas in mind, the following goals were set to understand the chemical biology of Zinquin:

Project Goals

1. Identify the source(s) of Zinquin-based fluorescence as it relates to intracellular Zn^{2+}

2. Characterize the possible intracellular reactions of Zinquin

3. Use the information from goals **1** and **2** to reevaluate published Zinquin studies

4. Develop novel biochemical techniques to aid in the identification of the intracellular targets for Zinquin

cells were detached via treatment with 1 mL of trypsin/EDTA solution and divided into either flasks or 100 cm^2 cell culture plates.

Epithelial kidney cells from *Sus scofa* (pig) (LLC-PK$_1$, ATCC #CL-101) were grown in M199/HEPES modified media (Sigma) supplemented with 4% fetal calf serum (FCS). Human medulloblastoma cells (TE-671, ATCC #CCL-136) were cultured in Dulbecco's modified essential media-low glucose (Sigma) supplemented with 5% FCS. Human astrocytoma/glioblastoma cells (U-87 mg, ATCC #HTB-14) were grown in Eagles' minimal essential media supplemented with 5% FCS. Human epithelial lung carcinoma cells (A549, ATCC #CCL-185) were maintained in Ham's F-12 Nutrient Mixture-Kaighn's Modification media (Sigma) supplemented with 10% FCS. Rat brain glioma (C6, ATCC #CCL-107) were grown in Ham's F-12 Nutrient Mixture-Kaighn's Modification media supplemented with 2.5% FCS and 10% horse serum. Human lymphocytic leukemia cells (CCRF-CEM, ATCC# CCL-199) were donated by Dr. Christopher Chitambar at the Medical College of Wisconsin and cultured in RPMI-1640 media (Sigma) supplemented with 10% FCS. All media were additionally supplemented with 50 mg/L streptomycin and 75-100KU/L penicillin G. LLC-PK$_1$, C6, and A549 cell lines were grown in the presence of 5% CO$_2$; TE-671, U-87 mg, and CCRF-CEM cell lines were grown in the presence of 6% CO$_2$.

CCRF-CEM cells were maintained in suspension until a concentration of 1 x 10^6 cells/mL was reached. Cells were then collected via centrifugation at 680 x g for 4 minutes and resuspended in complete media to an approximate concentration of 1-2 x 10^5 cells/mL.

Mixed neuron-astrocyte (9:1) cell suspensions from fetal mice were provided by Dr. Douglas Lobner at Marquette University.

2.2.1. Culturing ^{70}Zn LLC-PK$_1$ cells

^{70}Zn (as ZnO, ≥96% pure) was obtained from Cambridge Isotope Laboratories and prepared by dissolving the oxide powder in 1 mL of 6M HCl. 3.25 g of Chelex-100 resin (Bio-Rad) was added directly to a 500 mL bottle of FCS. A stir bar was added and the suspension was stirred overnight at 4 °C to chelate out all of the Zn^{2+} from the FCS. The suspension was then spun at 1,000 g for 4 minutes to pellet the Zn-Chelex-100 resin. The Zn-depleted FCS was filter-sterilized 3 times using a 0.22 μm bottle top filter. Before the last sterilization, 40 μM of ^{70}Zn was added back to the FCS. LLC-PK$_1$ cells were cultured as described above using 4% ^{70}Zn-FCS in M199 media additionally supplemented with 4 μM ^{70}Zn. Cells became isotopically stable after one pass.

2.2.2. Viability Assay

The toxicity of various reagents was determined in a dose and time dependent fashion. A 1 mL suspension of approximately 1×10^6 cells/mL in complete media was grown in 24 well plates for 1-2 days before experiments were performed. Cells were exposed to a given reagent at varying concentrations and lengths of exposure. After incubation, the viability of the cells was examined via the MTT Assay.[58] This assay evaluates the ability to convert a tetrazolium salt (3-(4,5-dimethyl-2-thiazolyl)-2,5-diphenyl-2H-tetrazolium bromide, or MTT) to formazan. This reduction reaction occurs within active

mitochondria, which therefore can be correlated to the overall health of the cell. An MTT solution (5 mM) was prepared by dissolving the dry powder in Dulbecco's Phosphate Buffered Saline (DPBS) and syringe filter-sterilized. The media was decanted and 1 mL of fresh complete media was added to each well along with 100 µL of the MTT solution and incubated 2-4 hours at 37 °C. One mL of isopropanol containing 0.04M HCl was added to each well and suspensions were mixed with a transfer pipette to dissolve the formazan crystals. Absorbance was measured at 570 and 630 nm and the difference between A_{570} and A_{630} was used to calculate viability based on normalization from cells with no exposure to the tested reagent.

2.2.3. Fluorescent Spectroscopy of Whole Cells

Cells were grown on 100 cm^2 culture plates until confluency was reached. Media was decanted and the plates were washed 3 times in cold choline phosphate buffered saline (4.7 g NaH_2PO_4, 1.0 g Na_2HPO_4, 32.2 g NaCl, and 25.0 g Choline Chloride in 3.8 L ddH_2O). One mL of Dulbecco's phosphate buffered saline (DPBS, Sigma) was added to the plate and cells were gently lifted into suspension using a rubber cell scraper. Clumps of cells were brought into suspension by pipetting the solution up and down multiple times. For suspension CCRF-CEM cells, cultures were pooled into 50 mL centrifuge tubes and spun at 680 x g for 4 min. The cell pellet was resuspended in 10 mL of DPBS and the process was repeated three times using fresh DPBS to wash the cells. The amount of cells in each suspension was determined by loading a 10 µL aliquot onto a

hemacytometer for cell counting. The cell suspensions were diluted to 5 x 10^6 cells/mL with DPBS in a fluorescence cuvette.

Spectrofluorimetry settings are described in section 2.4.1. Suspended cells were placed in the fluorometer and a background emission spectrum was taken to account for light scatter between cells and auto fluorescence.   Cells were then exposed to 25 µM Zinquin or 30 µM TSQ in the dark for at least 30 minutes. Cells were mixed periodically using a plastic pipet to ensure a homogenous mixture of the suspension. Additional fluorescence spectra were taken and the initial background spectrum was mathematically subtracted from these spectra.

2.2.4. Preparation of cell lysate

Cells from 10-50 100 cm^2 plates were harvested into DPBS as described in section 2.2.3. Cells were collected via centrifugation at 680 x g for 4 minutes at room temperature. The cell pellet was resuspended in one mL of cold ddH_2O per 10 plates of cells. A sonicator equipped with a flat tip was placed in an ice water bath for 5 minutes to chill the tip. Approximately one mL of the concentrated suspension was transferred to a plastic cut-off tube. The suspension was sonicated at power 5 for 60 pulses for a total time of 24 seconds. The sonicate was transferred to a 15 mL Corex® tubes and the process was repeated until the entire suspension was lysed. For experiments resulting in the isolation of the cellular proteome, 1000 units of Benzonase® nuclease (Sigma) and 500 µM phenylmethanesulfonyl fluoride protease inhibitor were added. The sonicate was then spun at 47,000 x g for 30 minutes at 4 °C using a Sorvall ultracentrifuge. The

resulting supernatant—termed the cell lysate—was further separated using chromatographic techniques described in section 2.3.

2.3. Chromatography

2.3.1. *Sephadex G-75, G-50, and G-25 Gel Filtration*

Various types of size exclusion chromatography were employed to separate complex mixtures. For fractionation of Zinquin-exposed cell lysates, Sephadex G-75 beads were used. Sephadex G-50 gel filtration was performed on isolated proteomes and purified proteins. For the isolation of the cellular proteome from a cell lysate, Sephadex G-25 beads were used. For the construction of the size exclusion columns, Sephadex G-75, G-50, and G-25 gel filtration beads (GE Healthcare) were hydrated using 20 mM Tris-Cl buffer pH 7.4 for 24, 3 and 3 hours, respectively. After rehydration, the bead suspensions were degassed in a sidearm flask for one hour via aspiration. Sephadex G-75 beads were poured—approximately 5 mL at a time—into a 0.75 cm x 80 cm borosilicate glass column supported by a small amount of glass wool. In a similar manner, Sephadex G-50 beads were poured into a 0.75 cm x 40 cm borosilicate glass supported with glass wool. Sephadex G-25 beads were transferred into a 1.5 cm x 28 cm low-pressure chromatography column (Bio-Rad). One liter round bottom buffer reservoirs were connected to the top of the columns using Tygon tubing and columns were eluted by gravity. Unless otherwise noted, columns were eluted using degassed 20 mM Tris-Cl pH 7.4. When the columns lost their seal and dried out or when the

flow rate exceeded 1 drop every 20 seconds, the Sephadex beads were resuspended in new buffer, degassed, and repacked.

Typical fractionation involved collecting 25-50 drop fractions, corresponding to 1.0-2.0 mL. For Sephadex G-75 separation, 50 one- mL fractions were collected with a total fractionation time of 1.5-3.5 hours. The first 8 mL corresponded to the void volume of the column. Fractions 10-20 represented the high molecular weight (HMW), proteome pool with molecular sizes >10 kDa, fractions 20-30 contained molecules with molecular weights around 10 kDa, and fractions greater than 30 contained the low molecular weight (LMW) species with weights lower than 10 kDa. In Sephadex G-50 gel filtration experiments, thirty 1.0-mL fractions were collected taking 0.3-1.0 hour to complete. The first 5 mL were the void volume; fractions 5-15 corresponded to the HMW while fractions 15-30 were the LMW pool. For separation using Sephadex G-25 size exclusion beads, 25 two-mL fractions were collected with the HMW eluting from fraction 7 to fraction 13 and LMW from fraction 14 to fraction 25. This separation took approximately 30 minutes to complete.

2.3.2. Sephacryl S-300 Gel Filtration

For higher resolution size exclusion separations, Sephacryl S-300 beads (Sigma) were used. The beads were supplied in a suspension of 20% ethanol. This suspension was transferred to a 500 mL side-arm Erlenmeyer flask and allowed to settle. The ethanol solution above the beads was removed and replaced with 50 mM Tris-Cl pH 7.4 buffer containing 150 mM NaCl. The bead/buffer solution was then put back into a slurry and

allowed to settle once again. The supernatant was again removed and replaced with buffer. This process was repeated 3 times to replace the storage ethanol solution with buffer. The suspension was then degassed for 1 hour and poured into a 1.5 cm x 60 cm column. The column was eluted 50 mM Tris-Cl pH 7.4 buffer containing 150 mM NaCl. A buffer reservoir was connected to a peristaltic pump via Tygon tubing which connected to the top of the column. Elutions were performed at a constant flow rate of 1 mL/min. To determine the approximate molecular weights of analytes in the eluted fractions, gel filtration standards (Bio-Rad) containing thyroglobulin (670,000 Da), gamma-globulin (158,000 Da), albumin (44,000 Da), myoglobin (17,000 Da), and vitamin B12 (1350 Da) were run under these conditions and peaks were determined via absorbance at 280 nm.

2.3.3. *DEAE Ion Exchange Chromatography*

5-mL Macro-Prep DEAE ion exchange cartridges were purchased from Bio-Rad. The ion exchange matrix was generated by elution with 5 column volumes of 5 mM Tris-Cl pH 8.0 containing 1 M NaCl followed by an additional 5 column volumes with 5 mM Tris-Cl pH 8.0 containing no salt. Protein samples were loaded onto the column using a peristaltic pump—set at 1 mL/min—in a loop, meaning the flow through from the column was directed back into the protein sample feeding the column. This cycle was performed for 30 minutes to ensure maximal sample load onto the DEAE matrix. Elution of the column was done using a stepwise gradient. In brief, a 10 mL upside down syringe—without the plunger—was connected to the peristaltic pump using Tygon tubing which then fed the column. Using a constant flow rate of 1 mL/min, 7 mL of

buffer—5 mM Tris-Cl pH 8.0—was loaded into the syringe and allowed to flow until empty. The syringe was then replenished with 7 mL of new buffer containing a higher salt concentration. A typical stepwise gradient was conducted using 50 mM NaCl increments from 0-500 mM NaCl. 1 mL fractions were collected from the column and the conductivity was determined using a Radiometer CDM 3 conductivity meter. For smaller protein samples, a 1 mL Pall DEAE Ceramic HyperD F column was used, eluting with 1 mL of buffer for each gradient step.

2.3.4. Zinquin- Affinity Chromatography

Synthesis of a Zinquin-Affinity column was performed using a CarboyxLink^{TM} Immobilization Kit purchased from Thermo Scientific. In brief, 500 µL of 13 mM Zinquin Acid (2.5 mg) was diluted with 1,500 µL of Coupling Buffer (0.1 M MES, 0.9% NaCl, pH 4.7). Approximately 2.0 mL of the CarboxyLink^{TM} coupling resin—diaminodipropylamine immobilized to 4% beaded agarose—was washed with 10 mL of the coupling buffer and allowed to drain. The 2 mL Zinquin sample was then loaded onto the resin and put into a slurry suspension. 500 µL of coupling buffer was added to 60 mg of EDC [1-ethyl-3-(3-dimethylaminopropyl)carbodiimide] and immediately added to the suspension. The slurry was placed on an end-over-end shaker and allowed to react for 3 hours. In this reaction, the carbodiimide reacts with the carboxylic acid group on Zinquin, forming an activated ester. The primary amine on the coupling resin then performs a nucleophilic attack on the activated ester to form a stable amide linkage between the resin and Zinquin (**Figure 2.1**).
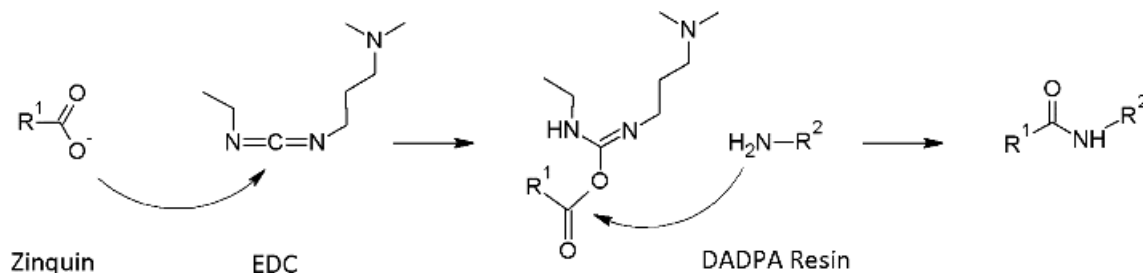
Figure 2.1. Synthesis of Zinquin Affinity Column.

After reaction, the column was washed with 10 mL of 1 M NaCl to remove any unbound

Zinquin and reaction byproducts. The column was stored in 20 mM Tris-Cl pH 7.4 buffer

at 4 °C. An acetate affinity column was synthesized in a similar manner by replacing 2.5

mg of Zinquin with 2.5 mg of sodium acetate.

For affinity purifications, protein samples were first loaded into the acetate affinity

column, the protein-resin mixture was put into a slurry, and mixed end-over-end for 45

minutes.   The slurry mixture was then allowed to settle, and unbound protein was

washed off the column with 20 mM Tris-Cl pH 7.4, collecting 8 to 12 one-mL fractions.

To elute the bound proteins, the column was washed with either 20 mM Tris-Cl pH 7.4

containing 1 M NaCl (native conditions) or 0.2 M glycine-Cl pH 2.8 (denaturing

conditions), collecting 8 to 12 on-mL fractions. Unbound protein was loaded onto the

Zinquin affinity column and affinity purification was done using the same conditions as

above. The protein concentration of each fraction was determined using the DC Assay

(section 2.4.3) and the $[Zn^{2+}]$ was determined using AAS (section 2.4.2)

2.4. Analytical Measurements and Determinations

2.4.1. Fluorescence Spectrophotometry

All fluorescence measurements were performed using an Hitachi F-4500 Fluorescence Spectrophotometer. For measuring fluorescence emission spectra using TSQ or Zinquin, an excitation wavelength of 370 nm was used while recording emissions from 400-600 nm. For Zinquin, the excitation and emission slit widths were fixed at 10 and 5 nm, respectively, and the photomultiplier voltage was set at 950 volts. Emission wavelength scans were performed at either 240 or 1200 nm per second. Emission maxima were determined by the x-intercept of the first derivative plot of the fluorescence spectra. Since the spectra were unique for a given Zinquin or TSQ complex, the fluorescence of fractions from chromatography experiments was reported as the sum of arbitrary units from 400-600 nm.

For kinetics experiments, the excitation wavelength was set at 370 nm while the emission wavelength was recorded at the spectral maximum of the fluorescent species, usually 470 nm or 492 nm. After recording a baseline, a competitive ligand was added and the fluorescence trace was monitored. Observed pseudo-first order rate constants were determined by recording the loss of fluorescence and fit to the first order rate expression:

$$\ln[\text{ZQ-Zn-Species}]_t = \ln[\text{ZQ-Zn-Species}]_o - k_{obs} \times t$$

where k_{obs} is the observed rate constant

$$k_{obs} = k \times [\text{Ligand}]$$

This equation was used to determine the dependence of k_{obs} on the concentration of the competitive ligand.

2.4.2. Zn^{2+} determination by Flame Atomic Absorption Spectroscopy (AAS)

For most experiments, zinc concentrations were determined using a GBC 904 flame atomic absorption spectrometer. Solutions were nebulized into an 80:20 air-acetylene flame and the absorbance was recorded using a zinc cathode lamp and a deuterium background lamp. Data were acquired in running mean mode with a sampling time of 1 second. Prior to the analysis of the samples, a calibration curve was constructed using standards containing 0.5, 1.0, and 2.0 ppm Zn^{2+} corresponding to 7.6, 15.2, and 30.4 µM Zn^{2+}. Any solution with a concentration above 30 µM was diluted and remeasured.

2.4.3. Protein determination via DC Protein Assay

The amount of protein in a given sample was determined using the DC Protein Assay kit from Bio-Rad. This colorimetric assay is based on the reaction of the protein sample with alkaline copper tartrate followed by a Folin reagent, similar to the Lowry assay. Solutions containing 1.36, 0.68, 0.34, 0.17, and 0.085 mg/mL BSA were used as protein standards. 25 µL of protein sample was reacted first with 125 µL of Reagent A (copper

solution), followed by 1 mL of Reagent B (Folin solution).   Solutions were vortexed, and after 15 minutes, the absorbance at 750 nm was recorded. The protein concentrations of unknown samples were determined using a linear regression analysis of the BSA standards.

2.4.4. *Sulfhydral determination using DTNB*

Thiol concentration was determined using Ellman's reagent (5,5-dithiobis-2-nitrobenzoic acid, DTNB).[59]   A 10 mM solution was made by adding 100 mg of DTNB in 25 mL of ddH$_2$O. DTNB was not soluble at low pH, so Tris was slowly added to the system under vigorous stirring until reaching pH 6.5 and most of the DTNB was dissolved.   Any undissolved DTNB was then removed by filtering the solution through Whatman #2 filter paper. Solutions were stored in the dark and used within one month. For analysis, 100 μL of 10 mM DTNB was added to the samples and vortexed. After one hour, the absorbance was recorded at 412 nm and the sulfhydral concentration was determined using an extinction coefficient of 13,400 cm^{-1} M^{-1}.

2.5.   Poly Acrylamide Gel Electrophoresis (PAGE)

All gel electrophoretic methods were performed using Novex® NuPAGE® precast gels in conjunction with the XCell SureLock^{TM} Mini-Cell electrophoresis chamber available from Invitrogen.

2.5.1. Denaturing Sodium Dodecyl Sulfate (SDS) PAGE

Protein samples—diluted with ddH$_2$O to 7.5 µL—were mixed with 2.5 µL of 4X NuPAGE®

LDS Sample Buffer (106 mM Tris HCl, 141 mM Tris Base, 2% Lithium Dodecyl Sulfate,

10% glycerol, 0.51 mM EDTA, 0.22 mM SERVA Blue G250, 0.175 mM Phenol Red, pH

8.5). Samples were placed in a heat block set at 70 °C for 10 minutes before being

loaded into 10 well (25 µL) NuPAGE® 12% Bis-Tris precast gels. One lane was reserved

for 2.5-5.0 µL of prestained SDS-PAGE protein markers (Bio-Rad) for approximate

molecular weight determination. Both cathode and anode chambers were filled with 1X

MOPS SDS running buffer (50 mM MOPS, 50 mM Tris, 1 mM EDTA, 0.1% SDS, pH 7.7)

and gels were run at constant voltage (200V) for 40-50 minutes until the dye front

migrated 60 mm. Protein bands on gels were stained using 100 mL of SimplyBlue^{TM} Safe

Stain (section 2.6.3.), or by following the Coomassie R-250 protocol (section 2.6.4.) or

silver staining protocol (section 2.6.5.).

2.5.2. Blue-Native PAGE (BN-PAGE)

In BN-PAGE, Coomassie G-250 is used as a negative charge-shift molecule that binds to

proteins without perturbing the native structure. Protein samples were prepared in 4X

NativePAGE^{TM} sample buffer (50 mM Bis-Tris, 6 N HCl, 50 mM NaCl, 10% glycerol,

0.001% Ponceau S, pH 7.2) and immediately added into 10 well (25 µL) NativePAGE^{TM} 4-

16% Bis-Tris precast gels. 5 µL of NativeMark^{TM} Unstained Protein Standards were used

for estimation of molecular weights. After samples were loaded and the gel was locked

in place, the cathode (inner) chamber was filled with 200 mL of cathode buffer (50 mM

Bis-Tris, 50 mM Tricine, 0.002% Coomassie G-250, pH 6.8) while the anode (outer) chamber was filled with approximately 600 mL of anode buffer (50 mM Bis-Tris, 50 mM Tricine, pH 6.8). Electrophoresis was performed at 150V for 95-105 minutes until the dye front had migrated 60 mm. Protein was visualized by using the Coomassie R-250 staining protocol (section 2.6.4.).

2.5.3. Native Sodium Dodecyl Sulfate (NSDS) PAGE

Before protein preparation, NSDS run buffers (50 mM Tris, 50 mM MOPS, 0.0375% SDS, pH 7.6) were chilled on ice for 30 minutes to 4 °C. In addition, NuPAGE® 12% Bis-Tris precast gels were assembled in the electrophoresis chamber and run at 200V for at least 30 minutes using ddH$_2$O as the run buffer. Protein samples were mixed with 4X sample buffer (100 mM Tris HCl, 150 mM Tris Base, 10% glycerol, 0.0185% Coomassie G-250, 0.00625% Phenol Red, pH 8.5) and loaded into pre-run gels. The ddH$_2$O was replaced with the chilled run buffer and the electrophoresis was performed at 150V for 75-85 minutes until the dye front migrated 60 mm. Gels were stained for protein using SimplyBlue^{TM} Safe Stain (section 2.6.3.), Coomassie R-250 stain (Section 2.6.4.), or silver stain (section 2.6.5.).

2.6. Gel Staining Techniques

Except for TSQ-staining, all gel images were recorded using a digital scanner. Densitometry line plots were constructed using ImageJ image processing freeware available from the National Institutes of Health.

2.6.1. In-gel Activity Assays

The detections of active proteins within gels were performed based on published methods by Manchenko with modifications (original sources are listed with the individual assays).[60] After the given electrophoretic technique was complete, gels were washed 3 times in ddH$_2$O for 5 minutes before assays were performed.

(1) Alcohol dehydrogenase activity[61] (E.C. 1.1.1.1)

Gels were placed in 50 ml of 50 mM Tris-Cl pH 8.5 buffer containing 10 mg of nicotinamide adenine dinucleotide (NAD), 10 mg of 3-(4,5-Dimethylthiazol-2-yl)-2,5-diphenyltetrazolium bromide (MTT), 0.2 mg of phenazine methosulfate (PMS) and 2 mL of 100% ethanol. Gels were incubated on a shaker until blue bands appeared (10-20 minutes) and fixed in 25% ethanol.

(2) β-galactosidase activity[62] (E.C. 3.2.1.23)

Gels were incubated in 50 mL of 100 mM Na$_2$HPO$_4$ buffer pH 7.4 containing 10 mg of 5-bromo-4-chloro-indolyl-β-D-galactopyranoside (X-Gal) and 5 mg of Nitro Blue Tetrazolium (NBT) and placed on a shaker until blue bands appeared (approximately 15 minutes). The reaction ceased upon fixing the gel in 25% ethanol.

(3) Superoxide dismutase activity[63] (E.C. 1.15.1.1)

Gels were placed in 50 mL of 50 mM Tris-Cl pH 8.5 containing 10 mg MTT, 6 mg PMS, and 10 mg MgCl$_2$. The gels were placed on a shaker under a 100W lamp for at least one hour. SOD activity was seen as clear bands on a dark blue background.

(4) Alkaline phosphatase activity[64] (E.C. 3.1.3.1)

Gels were soaked in 50 mL of 100 mM Tris-HCl pH 9.0 containing 10 mg of anhydrous MgCl$_2$, 20 mg of 5-Bromo-4-Chloro-3-Indyl Phosphate, and 10 mg of NBT. After incubation on a shaker for 15 minutes, gels were fixed in 3% acetic acid. Dark blue bands indicated enzymatic activity.

(5) Urease activity[65] (E.C. 3.5.1.5)

Gels were put in 50 mL of 23.7 mM citrate buffer pH 6.0 containing 79 mM Urea, 10 mg NBT and 5 mg dithiotheritol. The gel container was wrapped in Syran wrap and gently shook for at least 1 hour. The activity solution was replaced with 20 mM hydrochloric acid and activity was visualized by the appearance of light purple bands.

(6) Peroxidase activity[66] (E.C. 1.11.1.7)

Gels were submersed in 50 mL of 50 mM Na$_2$HPO$_4$ pH 7.0 buffer containing 5.5 mg of reduced NAD, 4 mg of phenol, 3 mg of NBT, and 0.02% hydrogen peroxide. The gel container was sealed and incubated on a shaker in the dark for 30 minutes. The reaction was again halted using a 25% ethanol solution after the appearance of light brown bands.

(7) Carbonic anhydrase activity[67] (E.C. 4.2.1.1.)

Gels were placed in 50 mL of 100 mM Tris-Cl pH 9.0 containing 0.1% bromothymol blue for 15 minutes on a shaker. The solution was decanted and the gel was gently blotted in the gel container. Approximately 150 mL of water were added to a 500 mL side arm

flask connected with a rubber hose. A few chips of dry ice were added, the flask was corked, and the evolution of carbon dioxide from the end of the rubber hose was streamed over the gel surface. Active carbonic anhydrase appeared as yellow bands on a blue background.

(8) L-amino oxidase activity[68] (E.C. 1.4.3.2)

Covered gels were incubated in 75 mL of 65 mM NaH_2PO_4 buffer pH 6.8 containing 10 mM L-Lysine, 5 mg NBT and 2.5 mg PMS on a rotary shaker for 30 minutes. Gel was rinsed in ddH_2O and fixed in 25% ethanol, revealing blue bands for oxidase activity.

(9) Glucose-6-phosphate dehydrogenase activity[69] (E.C. 1.1.1.49)

30 mg of D-glucose, 10.6 mg of adenosine triphosphate, 10 mg $MgCl_2$ and 20 U of hexokinase were dissolved to 50 mL of 100 mM Tris-Cl pH 8.4 and the solution was allowed to react for 2 hours. During this time, glucose was converted to glucose-6-phosphate by the hexokinase enzyme. Next, 10 mg of NAD, 10 mg of MTT, and 1 mg PMS were added and the solution was poured into the gel container. After incubating the gels on a shaker for 30 minutes, the reaction was stopped using 25% ethanol. Dark blue bands on the gel signified glucose-6-phosphate dehydrogenase activity.

2.6.2. TSQ/ZQ staining of gels

All TSQ/ZQ gel staining experiments were carried out at the Great Lakes Water Institute. Electrophoresis of protein samples was done using the NSDS-PAGE technique (Section 2.5.3.). After the plastic casting was removed, gels were washed twice in 100 mL of

ddH_2O. Initial background of the gel was taken to rule out auto-fluorescent protein bands. The gel was transferred into a UVP EpiChemi II Darkroom UV transilluminator gel box set at the long UV wavelength (approximately 365 nm). Images of the gel were taken using a digital camera with a 470 nm emission filter and processed using LabWorks software version 4.5. Typical exposure times for fluorescent images were between 3-7 seconds. After the initial picture was taken, gels were soaked in 50 mL of ddH_2O containing 25 μM TSQ or ZQ_{EE} on a rotary shaker for 40 minutes and washed twice in fresh ddH_2O for 5 minutes each. Pictures of the stained gel were captured using the same exposure times and software settings. In some cases, the gels were additionally incubated in 50 mL of ddH_2O containing 100 μM TPEN for 30 minutes and additional images were captured.

2.6.3. SimplyBlue^{TM} Safe Stain

Gels were washed three times in 100 mL of ddH_2O for 5 minutes. After the final rinse, the water was decanted and approximately 50 mL of SimplyBlue^{TM} Safe Stain (Invitrogen) were added to the gel container. Gels were placed on a shaker for 1 hour. The staining solution was decanted, replaced with 100 mL of ddH_2O, and incubated on a shaker for 1 hour. If need be, gels were additionally destained in fresh ddH_2O overnight.

2.6.4. Coomassie R-250 protein band staining

After being removed from their casings, gels were placed in 100 mL of fixing solution containing 40% methanol and 10% acetic acid, microwaved for 45 seconds, and put on a

shaker for 30-45 minutes. For BN-PAGE gels, this process was repeated twice with new fixing solution to remove the Coomassie dye in the gel from the electrophoresis process. The fixing solution was decanted and 50 mL of staining solution (30% methanol, 10% acetic acid, 0.002% Coomassie R-250) was added. Gels were microwaved for 45 seconds and placed on a shaker for 30 minutes. The gels were destained by incubating in 100 mL of microwaved 8% acetic acid and agitating for 45 minutes. The destaining solution was replaced and the gel was allowed to destain overnight on a shaker.

2.6.5. Silver Staining

For protein bands that were undetectable using the Coomassie R-250 protocol, a silver staining method was employed. Gels were first fixed in 100 mL of 50% methanol solution containing 12% acetic acid and 0.05% formalin (35% formaldehyde) overnight. The fixing solution was decanted and gels were washed three times using 35% ethanol for 20 minutes each rinse. Gels were then placed in 100 mL of sensitizing solution consisting of 0.02% sodium thiosulfate for 2 minutes and washed three times in ddH$_2$O for 5 minutes. After decanting the rinse, a staining solution (0.2% silver nitrate and 0.076% formalin) was added and gel was agitated for 20 minutes. After three 1 minute rinses in ddH$_2$O, the gel was placed in 100 mL of the developer solution (6% sodium carbonate, 0.05% formalin, 0.0004% sodium thiosulfate). The container was moved to a light box where the developing process was monitored until the gel had reached the proper exposure time. The silver staining process was halted by incubation in 100 mL of 50% methanol and 12% acetic acid.

2.7. Laser Ablation-Inductively Coupled Plasma-Mass Spectrometry (LA-ICP-MS)

2.7.1. Passive Drying of PAGE gels

PAGE gels were dried in partial accordance with the Invitrogen DryEase® Mini-Gel Drying System. First, gels were soaked in a drying solution (30% methanol, 5% glycerol) for 10 minutes. One side of the gel drying frame was placed on the drying base followed by a piece of cellophane wetted in the drying solution. The gel was placed on top of the piece of cellophane, followed by a piece of cut saran wrap and a second piece of wetted cellophane. Care was taken to remove any air bubbles trapped between the layers of gel, saran wrap, and cellophane. The other half of the drying frame was placed on the base and the frame was secured with binder clamps. The frame, now holding the cellophane-gel sandwich, was placed in a closed fume hood with an atmospheric humidity of 55%. This high humidity prevented the gel from drying too quickly and cracking. After 24 hours, the dried sandwich was removed from the frame and placed under weight—to prevent warping—until the gel was ready for analysis via LA-ICP-MS.

2.7.2. Laser Ablation

Laser Ablation was performed using a Cetac LSX-213 Laser Ablation unit. The laser unit power supply was run for at least one hour before ablation. In addition, the laser was activated and allowed to warm up until the operating temperature reached 34.8 °C, the optimal temperature for the laser to perform ablation. Dried gels were cut in half lengthwise and the cellophane sandwich was opened, exposing the gel on one side

while leaving the cellophane on the other side. The gel was attached to the large format ablation cell using double-sided tape. For semi-quantification purposes, 0.5 µL of standards containing 1250, 625, 313, 156, 78.1, 39.1 and 19.5 ppb Zn^{2+} were spotted on the edge of the gel and allowed to dry for at least one hour before ablation. Since the laser cannot move the entire width of the sample cell, the stage was moved toward one side and the top half of the gel was ablated first before repositioning the stage to ablate the bottom half.

Ablation parameters and laser energy were controlled by DigiLaz III software (Cetac Industries, Ohama, NB). Using the video controls, the microscope was zoomed in 100% and brought into focus to assure ablation occurred at the surface of the gel. The microscope was then zoomed out, and ablation lines were drawn in each lane consisting of 2-3 lines per lane with a spacing of 300 µm between lines. For most experiments, the laser was set at 20 Hz with 100% energy and a scan rate of 40 µm per second.   There was also a trigger and shutter delay of 10 seconds to allow enough time for the laser to reposition itself in between scan lines. After both the plasma and laser power supply had been running for at least an hour, ablation was begun with the final Helium carrier gas flow rate set at 1000 mL/min (see section 2.7.3).

2.7.3. Inductively Coupled Plasma-Mass Spectrometry (ICP-MS)

Elemental analysis was performed using a MicroMass Platform ICP-MS powered by MassLynx software (Waters Corporation, Milford, MA). The argon gas settings used to ignite and maintain the inductively coupled plasma included a cool gas flow rate of 13.5

L/min and an intermediate gas flow rate of 0.8 L/min. Once the plasma torch was ignited, helium from the LA unit was introduced at the minimal flow rate of 100 mL/min. Slowly, the helium flow rate was increased in 200 mL/min increments until the operational flow rate of 1000 mL/min was reached. Occasionally, the introduction of helium to the plasma caused to the plasma to extinguish. To prevent this, the argon cool gas was increased to 16 L/min and the plasma ignition process was repeated. Once the plasma was stable, the cool gas flow rate was lowered back down to 13.5 L/min. The plasma was run for at least one hour before the ablation was performed. Data were collected in the MassLynx software and transfer to Microsoft Excel for further analysis.

3.   Results

3.1.   Fluorescence Spectroscopy of Zn(ZQ)$_2$ and Zinquin Treated Cells

3.1.1.   Zn binding of Zinquin

The use of more analytical methods than microscopy or single wavelength fluoremetry is paramount in understanding the chemical species responsible for Zinquin-based fluorescence.   Observing entire fluorescence spectra may allow for better chemical understanding of what types of zinc sources are being sensed by Zinquin.   To begin this study, Zinquin was incubated with increasing concentrations of ZnCl$_2$ (**Figure 3.1**).
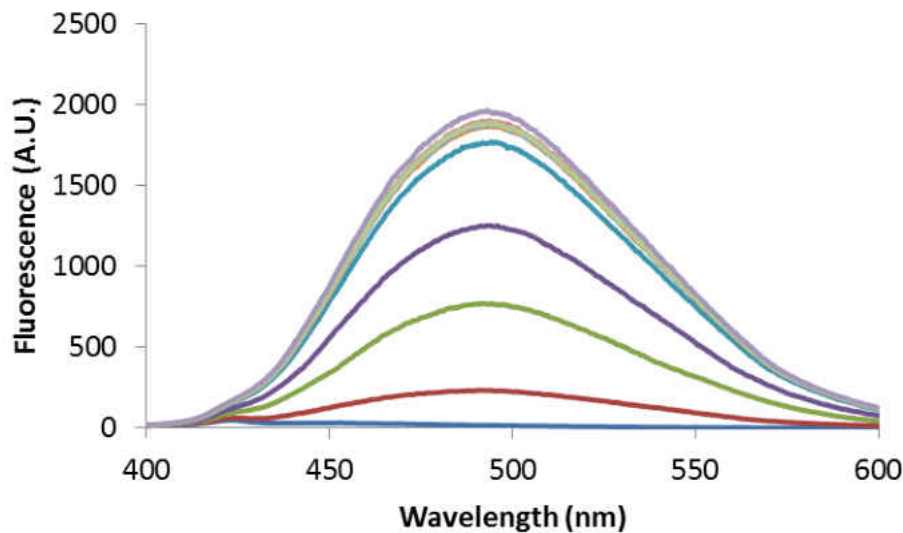
Figure 3.1. Fluorescence Spectra of ZQ$_{ACID}$ with ZnCl$_2$. 10 µM Zinquin Acid in 1 mL of 20 mM Tris-Cl pH 7.4 was titrated with 0-50 µM of ZnCl$_2$. Using an excitation wavelength of 370nm, the fluorescence emission was recorded from 400-600nm using an Hitachi F4500 Fluorescence Spectrophotometer.

In agreement with published studies of Zinquin, there was an increase in fluorescence in tandem with an increased [Zn^{2+}] with a fluorescence maximum centered at 492 nm.[28-30] Similar emission spectra have been seen with the related quinoline based fluorophore TSQ.[28,56] This emission profile serves as a model as to what would be expected for a fluorescent $Zn(ZQ_{ACID})_2$ species.   Corresponding UV-Vis absorbance spectroscopy showed a unique absorbance spectrum with peak absorbance at 259 and 360 nm, troughs at 242 and 283 nm, and isosbestic points at 250 and 277 nm (**Figure 3.2**). Plotting the absorbance at 259 nm versus the $ZnCl_2$ concentration yielded a saturation curve to similar to that seen in the fluorescence data.   In addition, the increase in absorbance at 370 nm was small enough not to warrant concern of an inner filter effect of absorption at the excitation wavelength at the given concentrations.[70]
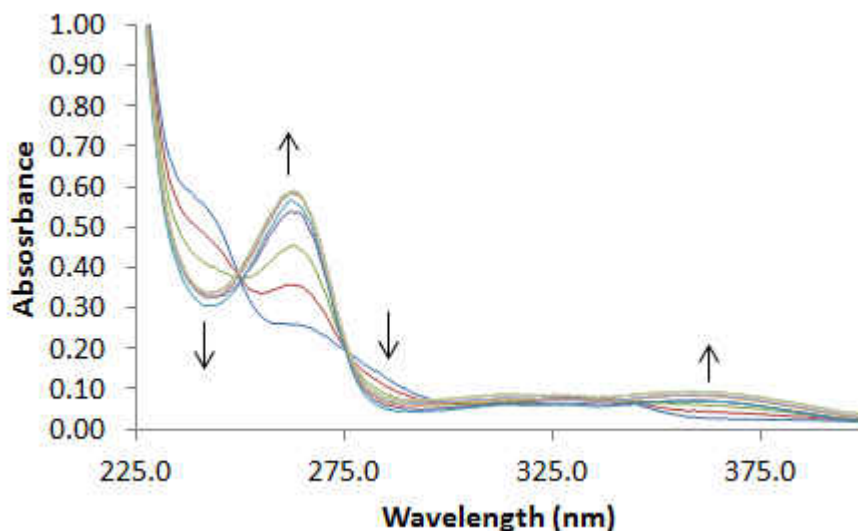
Figure 3.2. UV-Vis Spectroscopy of Zn(ZQ$_{ACID}$)$_2$. 10 μM ZQ$_{ACID}$ was reacted with 0-50 μM ZnCl$_2$ in 20 mM Tris-Cl pH 7.4. Absorbance was recorded from 225-400 nm using a Beckman DU-640 Spectrometer

3.1.2. Exposing cells to Zinquin in vivo

In order to detect Zn^{2+} in living systems, cells were grown in culture, gently scraped into a suspension using phosphate buffered saline and exposed to Zinquin in a fluorescence cuvette. In order to obtain a more complete picture of how Zinquin reacts within cells, a variety of different cell types were used as shown in **Table 3.1.**

cell line, species	tissue	growth properties	Zinquin fluorescence[a]	λ_{max} (nm)
LLC-PK1, *Sus scofa* (pig)	kidney epithelial	adherent	39.8 ± 4.1	471
TE-671, *Homo sapien* (human)	medulloblastoma	adherent	165.1 ± 8.7	471
U87 mg, *Homo sapien* (human)	glioblastoma	adherent	153.2 ± 9.5	475
C6, *Rattus norvegicus* (rat)	brain glioma	adherent	78.9 ± 8.2	473
CCRF-CEM, *Homo sapien* (human)	T-cell lymphoblast	suspension	68.0 ± 1.9	471
A549, *Homo sapien* (human)	lung carcinoma	adherent	83.7 ± 10.8	473
mouse, *Mus muculus* (Swiss-Webster)	whole brain, > 9:1 neuron: astrocyte	suspension of primary dissection	46.7	474

[a] Five $\times 10^6$ cells/mL, sum of fluorescence from 400 to 600 nm in thousand units, $n = 3$, except for mouse whole brain cells where $n = 1$.

Table 3.1. Cell models used for fluorescence spectroscopy of Zinquin. Taken from *Nowakowski, et. al.* (2011)[71]

This group represents a diverse sample set from not only multiple species, but also diverse tissues, morphologies and growth properties. Due to interest in the Zn^{2+} trafficking within neural tissues, a glioblastoma (U87 mg), a medulloblastoma (TE-671), and a brain glioma (C6) cell lines were used.[10-12,35] In addition, microscopic studies of both the C6 glioma and A549 lung carcinoma cell types have been previously investigated in conjunction with Zinquin, so these cell types were reinvestigated.[20,34,35] The reactivity of the Zn-proteome from $LLC-PK_1$ cells has been extensively studied, so this cell line was included as well.[56,72,73] The suspension lymphocytic CCRF-CEM cell line was used as a comparison to adherent cells. Finally, a brain suspension obtained from

the dissection of a fetal mouse was used to determine possible differences between primary tissues and cultured cells.

After exposure to 25 µM ZQ_{EE} for 30 minutes—the typical conditions used in microscopic experiments—all cell types displayed an enhancement of fluorescence (**Figure 3.3**).[35,36,41]
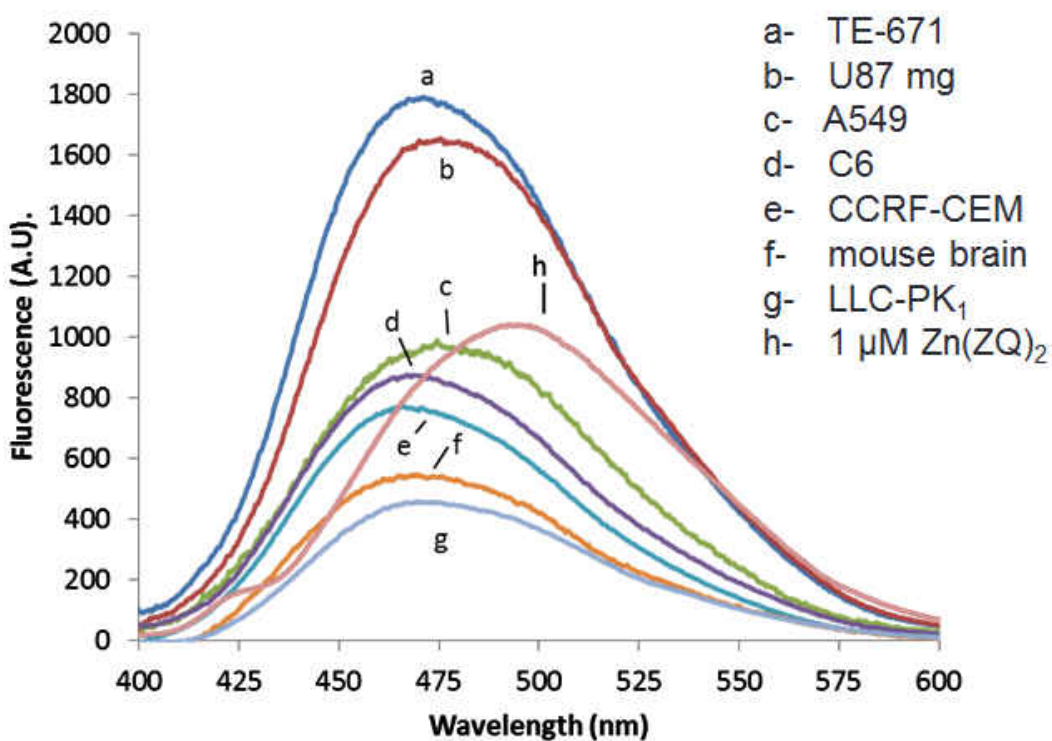
Figure 3.3. Fluorescence spectra of ZQ-exposed cells. Five x 10^6 cells (a-g) were suspended in DPBS and reacted with 25 µM ZQ_{EE} for 30 minutes and the fluorescence spectra was recorded, subtracting any initial fluorescence from unexposed cells. Spectral maxima in all cell lines were blue shifted to 470 nm from the normal emission of 492 nm for 1 µM $Zn(ZQ_{ACID})_2$ (h). Spectra represent the average of three replicates, except for the mouse brain (f) where n=1. Adapted from *Nowakowski et.al.* (2011)[71]

Using a hemocytometer to determine the number of cells in suspension, fluorescence intensity was normalized to five x 10^6 cells for each cell line. Interestingly, each cell type displayed a different amount of fluorescence, suggesting that there were varying amounts of Zn^{2+} measured in each cell type. More importantly, the fluorescence spectra for all cell types were blue shifted in comparison with the spectrum of $Zn(ZQ_{ACID})_2$, showing a spectral maximum near 470 nm. These spectra were different from the expected emission profile for Zinquin bound to "free" Zn^{2+} which has a λ_{MAX} centered at 492nm (**Figure 3.3h**). This variance in emission spectra provided initial evidence that ZQ_{ACID} may not be reacting with Zn^{2+} ions within the cell. Rather, it is hypothesized that ZQ_{ACID} might be reacting with open coordination sites of Zn-proteins to form ternary adducts that display this blue-shifted emission spectrum (reaction 3.1)

$$ZQ_{ACID} + Zn\text{-}Protein \rightleftarrows ZQ_{ACID}\text{-}Zn\text{-}Protein \qquad (3.1)$$

3.1.3. Fluorescence and Zn^{2+} distribution of Zinquin-exposed cells

To further investigate where the fluorescence is located within cells exposed to Zinquin, treated cells from **Table 3.1** were lysed, cellular debris was removed via centrifugation, and lysates were eluted using Sephadex G-75 gel filtration. This type of size exclusion chromatography separates the cytosol into three possible Zn^{2+} pools: the Zn-proteomic or high molecular weight (HMW) region containing molecules >10 kDa, the Zn-metallothionein (MT) region (MW≈ 10 kDa), and the low molecular weight (LMW) region

containing molecules less than 10 kDa.[33,56,74] Analysis of the resultant fractions from the LLC-PK$_1$ cytosol showed that both fluorescence and Zn—measured by AAS—were confined solely to the Zn-proteomic fractions of the chromatogram (**Figure 3.4A**). Furthermore, spectral analysis of these proteomic fractions revealed fluorescence profiles with blue-shifted emission maxima near 463 nm, similar to what was seen in intact cells. Taken together, these data of this cell line further support the hypothesis that Zinquin-based fluorescence is due to adduct formation with Zn-proteins.

Analysis of Zinquin treated TE-671 cells after gel filtration also showed a significant amount of fluorescence in the proteomic region that has the blue-shifted emission spectrum (**Figure 3.4B**). In addition, there existed a LMW pool of fluorescence and Zn^{2+}, which has the identical spectrum of that of Zn(ZQ)$_2$ which has a λ_{MAX} at 492nm. In a control experiment in which untreated cells were fractionated and analyzed for Zn^{2+} content, this LMW pool did not exist. This demonstrates that not only is adduct formation possible between Zinquin and a Zn-protein, but that Zinquin can compete for proteomic Zn^{2+}, sequestering Zn^{2+} from the HMW proteome that elutes as a Zn(ZQ)$_2$ species in the LMW portion of the chromatogram as proposed in reaction 3.2**.**

$$2\ ZQ_{ACID} + Zn\text{-}protein \rightleftarrows Zn(ZQ_{ACID})_2\ + apo\text{-}protein \qquad\qquad (3.2)$$
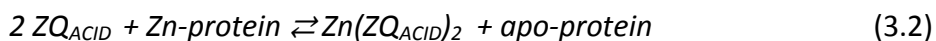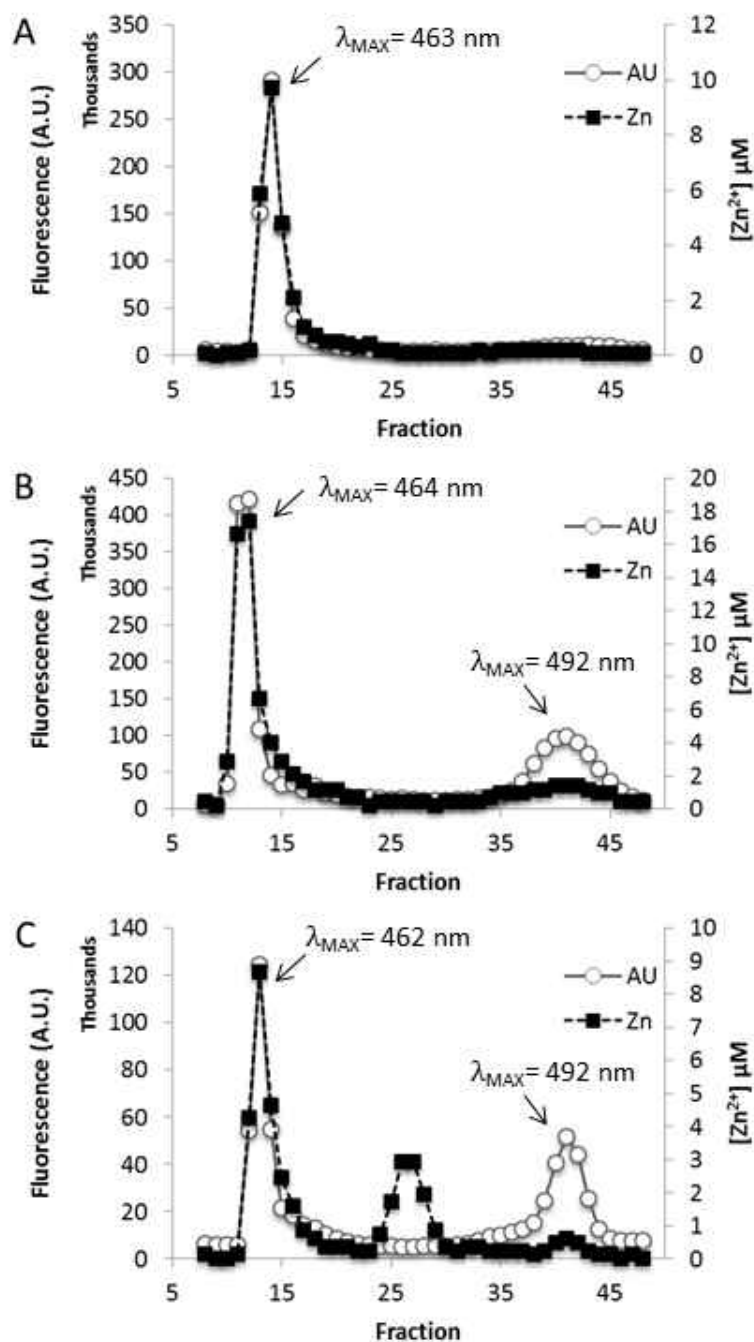
Figure 3.4. Fluorescence and Zn^{2+} distribution of Zinquin-exposed cells. 10^8 LLC-PK$_1$ (A), TE-671 (B), and U87-mg (C) cells were exposed to 25 µM ZQ$_{EE}$ for 30 minutes, lysed and eluted over a Sephadex G-75 column using 20 mM Tris-Cl pH 7.4. Fluorescence spectra from 400-600 nm were recorded and [Zn^{2+}] was determined via AAS. Spectral maxima for each pool of fluorescence was reported. Adapted from *Nowakowski et. al.* (2011)[71]

The only cell type tested that had a detectable amount of basal metallothionein was the U87 mg cell line (fractions 20-30 of **Figure 3.4.C**) Metallothionein is a cysteine-rich protein capable of tightly binding up to 7 Zn^{2+} with stability constants near 10^{11} M^{-1}.[75] However, unlike the HMW Zn-proteome pool, the MT fractions in this experiment exhibited no fluorescence. Comparing the amount of Zn^{2+} in this pool to a control experiment in which unexposed cells were fractionated showed that the Zn^{2+} was not perturbed upon exposure. In addition, when the MT fractions were assayed with 10 μM ZQ_{ACID} *in vitro*, no fluorescence enhancement was observed over a 30 minute period. Therefore, this pool of Zn^{2+} is unaffected by the presence of Zinquin.

Table 3.2 describes the extent of reaction of the proteomic region for the seven cell types tested. The data include three replicates (except mouse brain) for each cell type using different cell preparations normalized to 10^8 cells per experiment.

| cell line | Zn-proteome pool[a] | | Zn-fluorescence (nmoles)[c] | % Zn reacted | λ_{max} (nm) |
	Zn-AAS (nmoles)	fluorescence (AU)[b]			
LLC-PK1[d]	23.6 ± 2.1	48.3 ± 12.6	4.2	18	462
C6[d]	12.5 ± 2.4	28.0 ± 3.0	2.5	20	463
TE671[d]	50.1 ± 4.9	112.2 ± 12.1	9.9	20	464
U87 mg[d]	18.6 ± 1.6	32.7 ± 4.7	2.8	15	462
CCRF-CEM[d]	17.4 ± 1.3	50.0 ± 9.1	4.4	25	463
A549[d]	17.1 ± 2.1	59.4 ± 15.5	5.1	30	465
mouse brain	18.8	67.1	5.9	31	463

[a] Per 10^8 cells. [b] Sum of fluorescence from 400 to 600 nm in ten thousand units. [c] Amount of Zn^{2+} sensed by fluorescence based on a standard curve of titration of ZQ_{ACID} with Zn^{2+}. [d] Average ± standard deviation of at least 3 replicates using different cell preparations.

Table 3.2. Survey of proteomic Zn^{2+} in multiple cell types exposed to 25 μM ZQ_{EE}. Taken from *Nowakowski et. al.* (2011)[71]

In concert with what is seen in LLC-PK$_1$ and TE-671 cells, all the proteomes tested had blue shifted emission spectra centered near 463 nm, not near 492nm, the emission profile of Zn(ZQ)$_2$. This is consistent with the hypothesis that Zinquin is reacting with Zn^{2+} bound to the proteome to form adducts.

Using a standard curve of ZQ$_{ACID}$ titrated with known amounts of Zn$^{2+,}$ the fluorescence observed was converted to [Zn^{2+}] (Zn-fluorescence in **Table 3.2**). This calculation was supported by the fact that a 1:1 ZnZQ complex has similar quantum yield to a 1:2 Zn(ZQ)$_2$ complex.[43] By dividing the converted fluorescence intensity by the total amount of Zn^{2+} measured using AAS, the extent of the reactivity of Zn^{2+} within the proteome was estimated. Approximately 30% of the Zn^{2+} within the proteome of both the A549 lung carcinoma cells and the mouse brain formed adducts with Zinquin, representing the most reactive proteomes tested. The U87 mg proteome, on the other hand, was least reactive, with only 15% of the Zn^{2+} within the proteome coordinated with Zinquin. Nevertheless, these values indicate that a substantial fraction of the Zn-proteome is accessed by Zinquin, thus enforcing the idea that the Zn-proteome is a main target for Zinquin.

As stated early, some cell types also exhibited LMW pools of fluorescence and Zn^{2+} ions as outlined in **Table 3.3**. The amounts of fluorescence and Zn^{2+} within these pools varied amongst the cell types with the largest being from the TE-671 cell line where nearly 20% of the total Zn^{2+} eluted in this pool. Conversely, the amount of Zn^{2+} and fluorescence of LLC-PK$_1$ cell line was near the limit of detection for both AAS and fluorescence and thus

negligible.   It is important to reemphasize that in control experiments where unexposed cells were fractionated, there were no LMW pools of Zn^{2+} for any cell type.   This underscores the plausibility that Zn^{2+} can be chelated out from members of the Zn-proteome by Zinquin (Reaction 3.2), thus negating the notion that Zinquin is only a passive observer of transient, loosely bound Zn^{2+} within a given cell.

| cell line | LMW Zn pool[a] | | % of | λ_{max} |
	Zn-AAS (nmoles)	fluorescence (AU)[b]	total Zn	(nm)
LLC-PK1[c]	0.6	5.9	2	
C6[d]	1.5 ± 0.3	10.0 ± 2.2	11	491
TE671[d]	11.1 ± 1.3	57.5 ± 6.2	18	492
U87 mg[d]	2.9 ± 0.6	19.8 ± 8.7	9	493
CCRF-CEM[d]	1.3 ± 0.4	17.8 ± 2.7	6	491
A549[d]	2.2 ± 0.6	19.0 ± 5.4	11	492
mouse brain	1.5	21.0	7	492

[a] Per 10^8 cells. [b] Sum of fluorescence from 400 to 600 nm in ten thousand units. [c] At limit of detection using flame atomic absorption spectroscopy. [d] Average $\pm$ standard deviation of at least 3 replicates using different cell preparations

Table 3.3. Survey of LMW Zn^{2+} in multiple cell types exposed to 25 µM ZQ$_{EE}$. Taken from *Nowakowski et. al.* (2011)[71]

3.1.4. Solvent effects of Zn(ZQ)$_2$

Another possible explanation of the fluorescence spectra and distribution in the cell may be that a Zn(ZQ)$_2$ complex is formed, but it migrates with the proteome and experiences a blue-shifted emission due to solvent effects that occur during its binding to proteins. To test this, 5 µM Zn(ZQ$_{ACID}$)$_2$ was added to an array of different solvents and the fluorescence spectra were recorded (**Figure 3.5**). Comparing Zn(ZQ)$_2$ in an aqueous environment—both pure water and 20 mM Tris-Cl pH 7.4—to a non-polar environment such as acetone or DMSO shows that although there is a change in fluorescence intensity, there is no blue shift in the emission maximum (**Figure 3.5** inset). This also holds true for solvents with both polar and non-polar character, namely ethanol, 1-octanol, and sodium dodecyl sulfate (SDS). 1-octanol did show a slightly blue-shifted spectrum with a λ_{MAX} of 486 nm.

The SDS solution used is at a concentration feasible for micelle formation.[76] It, therefore, can act as a surrogate for a possible microsomal environment occurring *in vivo*. Multiple microscopic studies have inferred the existence of such microsomes— referred to as zincosomes—containing high concentrations of "free" Zn^{2+}.[34,35,77] However, Zn(ZQ)$_2$ in this SDS environment did not exhibit the blue-shifted spectrum seen in the fluorescence spectroscopy of whole cells, but rather a slightly red-shifted spectra centered near 498 nm. Therefore, if zincosomes containing free Zn^{2+} survived both sonication and centrifugation and eluted with the proteome after gel filtration, it is

unlikely this is the source of the Zinquin-based fluorescence. Further characterization of

the reactivity of Zn(ZQ)$_2$ is described in section 3.4.
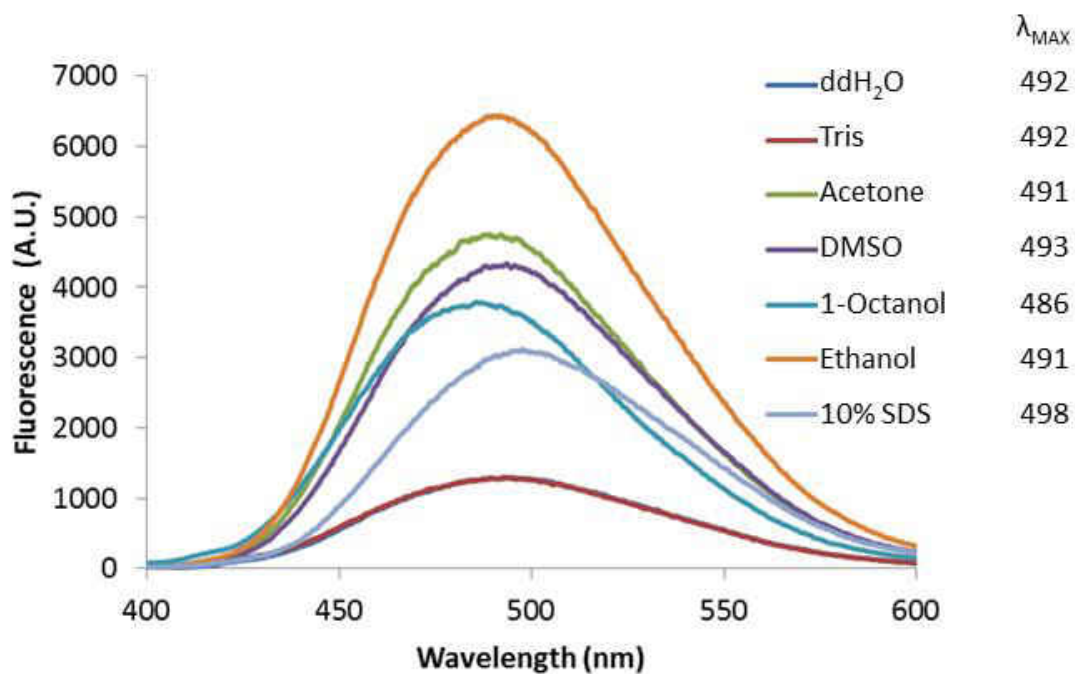
Figure 3.5. Solvent effects of Zn(ZQ)$_2$. 1 mM Zn(ZQ$_{ACID}$)$_2$ in DMSO was diluted to 5 µM (5 µL in 1 mL) in a variety of solvents and the fluorescence was recorded. The emission maxima are listed to the right of the solvent. (Note: the spectra for Zn(ZQ$_{ACID}$)$_2$ in ddH$_2$O and Tris buffer are overlapped)

3.2. Reactions of Zinquin with the proteome and model proteins

3.2.1. Reactions of Zinquin with the isolated TE-671 proteome

Since the Zn-proteome was a major source of the fluorescence in cells exposed to Zinquin, further characterization of the reaction of Zinquin with the proteome fractions was performed. First, TE-671 cells were lysed, centrifuged, and fractionated over a Sephadex G-25 size exclusion column, collecting fractions with absorbance at 280 nm and determining the $[Zn^{2+}]$ using AAS. Based on Zn^{2+}, 10 µM of proteome was then titrated separately with ZQ_{ACID} or ZQ_{EE} (**Figure 3.6A and B**, respectively). The fluorescence enhancement observed in both cases displayed blue-shifted emission spectra with a λ_{MAX} of 470 nm for ZQ_{ACID} and 468 nm for ZQ_{EE}. When these reaction mixtures were chromatographed using Sephadex G-50 size exclusion resin, the majority of the fluorescence was retained in the HMW region for each proteome reacted with ZQ_{ACID} or ZQ_{EE} (**Figure 3.6C and D**, respectively). In addition, these fluorescent proteomic fractions have emission spectra that are centered at 468 nm and 466 nm for the acid and ethyl ester, respectively, which again are blue shifted from the $Zn(ZQ)_2$ species. However, both reaction mixtures also contained a small amount ($\approx$10%) of LMW fluorescence and Zn^{2+}. This LMW pool represents the Zn^{2+} capable of being chelated from Zn-proteins using Zinquin. Taken together, these data underscore the notion that Zinquin reacts extensively with Zn^{2+} in the proteome, forming predominantly fluorescent adducts as well as sequestering ions from native Zn-proteins.
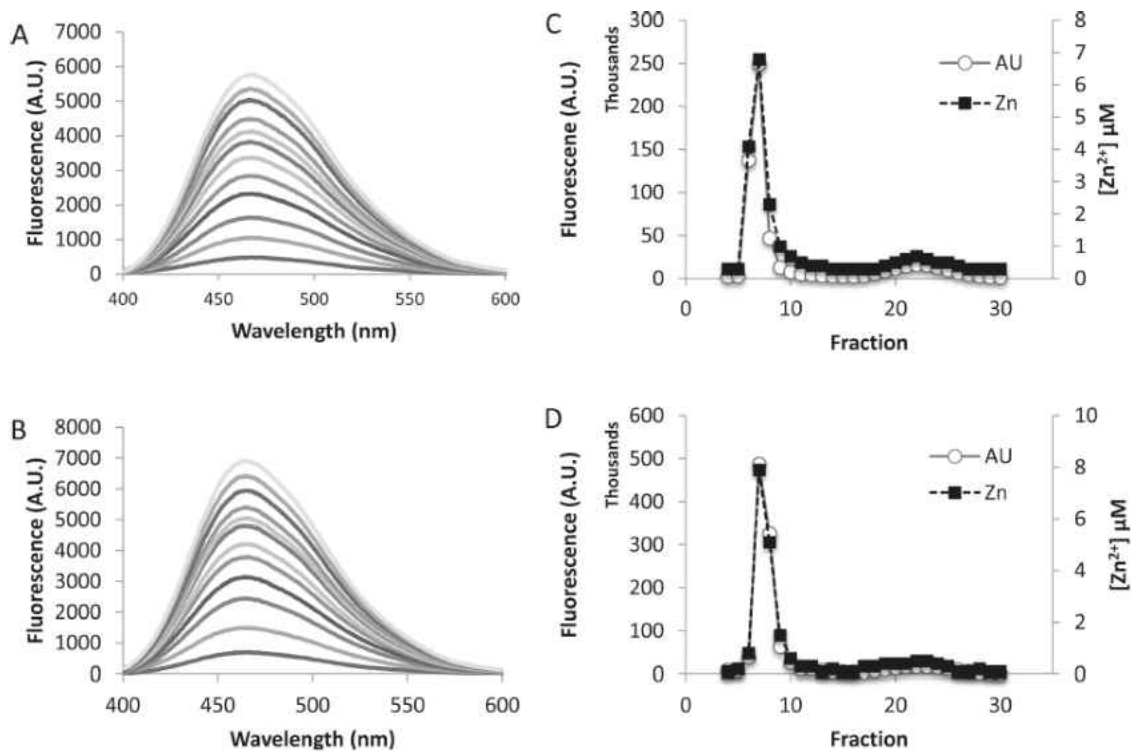
Figure 3.6. Titrations of the Zn-proteome with ZQ$_{ACID}$ and ZQ$_{EE}$. 10 µM Zn-proteome (based on Zn^{2+}) was titrated with Zinquin acid (A) and Zinquin ethyl ester (B) in 20 mM Tris-Cl pH 7.4. Reaction mixtures of both the ZQ$_{ACID}$- (C) and ZQ$_{EE}$-treated proteomes (D) were chromatographed over Sephadex G-50 gel filtration columns eluted with 20 mM Tris-Cl pH 7.4 recording fluorescence and [Zn^{2+}]. Taken from *Nowakowski et. al.* (2011)[71]

Higher resolution size exclusion chromatography was also employed. TE-671 cells were sonicated and centrifuged at 100,000 x g to remove not only cell debris but any intact organelles. This cytosol was then eluted using a Sephacryl S-300 column, which can separate complex protein mixtures with molecular weights ranging from 1×10^4 to 1×10^6 daltons (**Figure 3.7**). After elution, the fractions were assayed with 5 µM ZQ_{ACID} and fluorescence was recorded. Also, by the use of gel filtration standards, the approximate molecular weights of the macromolecules within the eluted fractions were determined. The resulting chromatogram showed that the majority of the fluorescence resided in the 100,000 to 10,000 Da region, indicative of Zinquin associating with Zn-proteins within that region. The spectra of these fractions were centered near 470 nm, further supporting the hypothesis that the blue-shifted spectrum seen in Zinquin-exposed cells is due to Zinquin binding to members of the Zn-proteome.
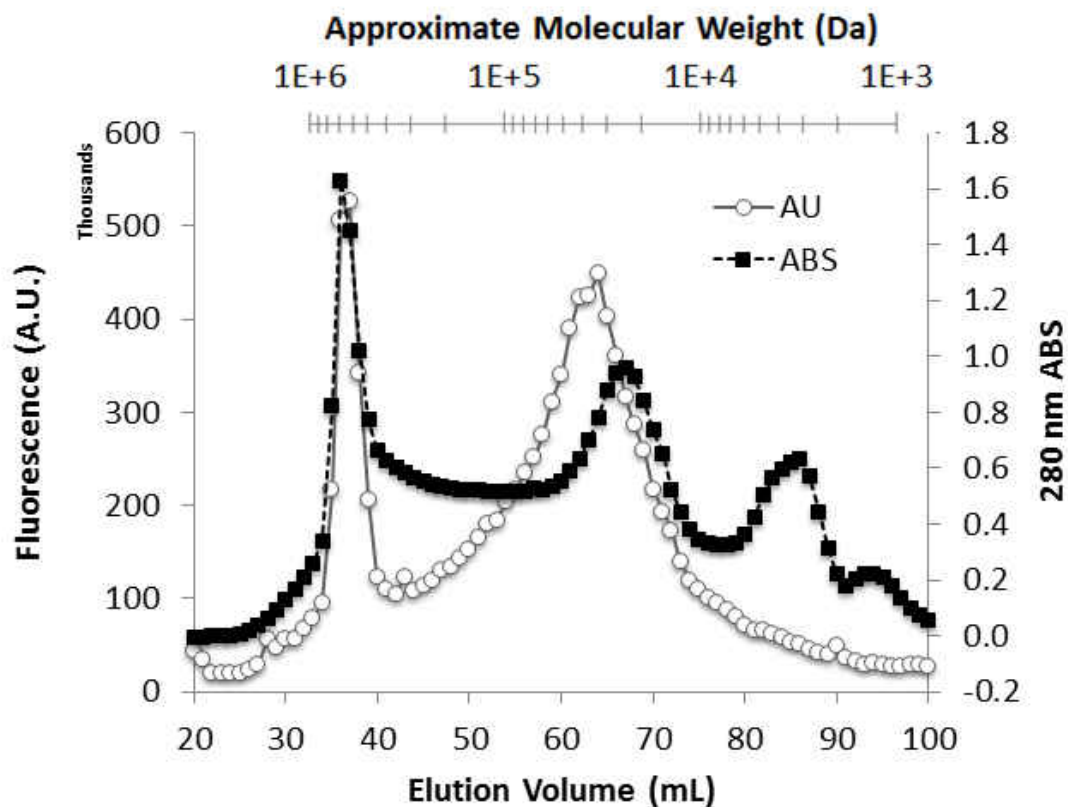
Figure 3.7. Sephacryl S-300 separation of TE-671 cytosol. Cytosol from 3×10^8 TE-671 cells was chromatographed over a Sephacryl S-300 gel filtration column eluted with 50 mM Tris-Cl, 150 mM NaCl, pH 7.4. Fractions were assayed with 5 µM ZQ_{ACID} and fluorescence and absorbance at 280 nm were recorded. Approximate molecular weights of macromolecules in eluted fractions were determined using gel filtration standards.

3.2.2. Reactions of Zinquin with Model Protein Zn-Alcohol Dehydrogenase

To further investigate the how Zinquin reacts with Zn-proteins, yeast alcohol dehydrogenase (Zn_2-ADH) was used as a model system. Zn_2-ADH is a tetramer containing two heterodimers ($Zn_2\alpha\beta)_2$, each dimer containing both a structural Zn^{2+} and a catalytic Zn^{2+}.[78] First, 5 μM Zn_2-ADH was titrated with ZQ_{EE}, resulting in an increase in fluorescence with a spectral maximum centered at 471 nm, suggestive of a formation of a ZQ_{EE}-Zn_2-ADH ternary adduct (**Figure 3.8**). When the fluorescent solution was fractionated via Sephadex G-50 size exclusion chromatography, all the fluorescence and Zn^{2+} was retained in the HMW proteomic region with the fluorescence being blue-shifted as well. This provides additional evidence that Zinquin can react with Zn^{2+} ligated to a protein which results in fluorescent enhancement that is characteristically blue-shifted from the spectra seen from $Zn(ZQ)_2$. (reaction 3.3)

$$ZQ_{EE} + Zn_2\text{-}ADH \rightleftarrows ZQ_{EE}\text{-}Zn_2\text{-}ADH \qquad\qquad (3.3)$$
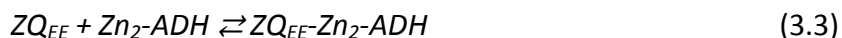
The titration was repeated, this time using the free acid form of Zinquin. When 5 μM Zn_2-ADH was titrated with Zinquin acid, the fluorescence increased showing a broad spectrum with a λ_{MAX} centered at 480 nm, halfway in between the 490nm λ_{MAX} for a $Zn(ZQ)_2$ complex and 470 λ_{MAX} for a hypothetical ternary adduct (**Figure 3.9**). The solution was then chromatographed, yielding two fluorescence and Zn^{2+} pools. The LMW pool—containing half of the total Zn^{2+}—displayed the fluorescence pattern
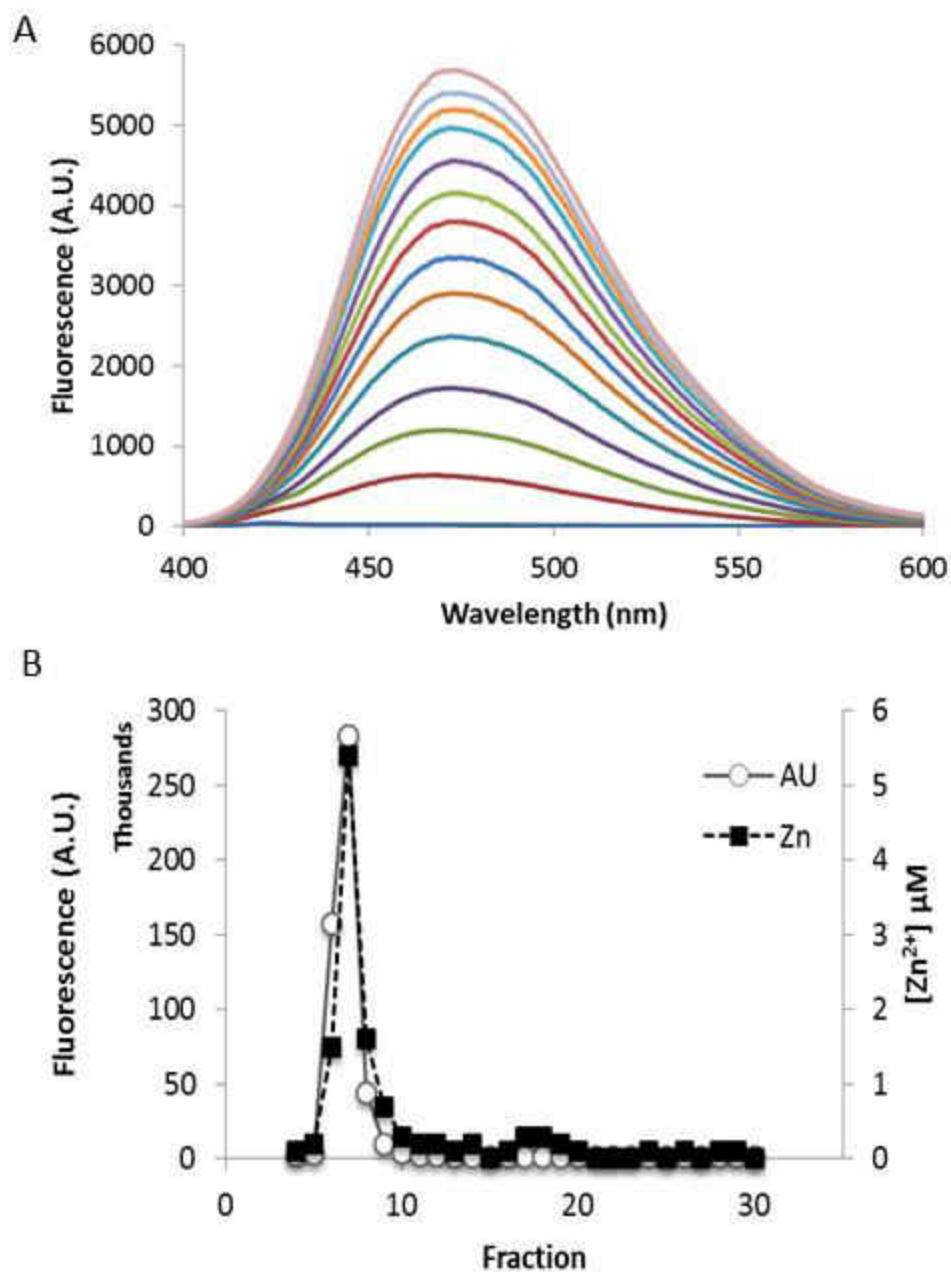
Figure 3.8. Titration of Zn$_2$-ADH with ZQ$_{EE}$. (A) 5 µM Zn$_2$-ADH (10 µM total Zn^{2+}) was titrated with ZQ$_{EE}$ in 20 mM Tris-Cl pH 7.4. (B) Reaction mixture was eluted over a Sephadex G-50 gel filtration column using 20 mM Tris-Cl pH 7.4. Fluorescence and [Zn^{2+}] was recorded for each fraction. Taken from *Nowakowski et. al.* (2011)[71]
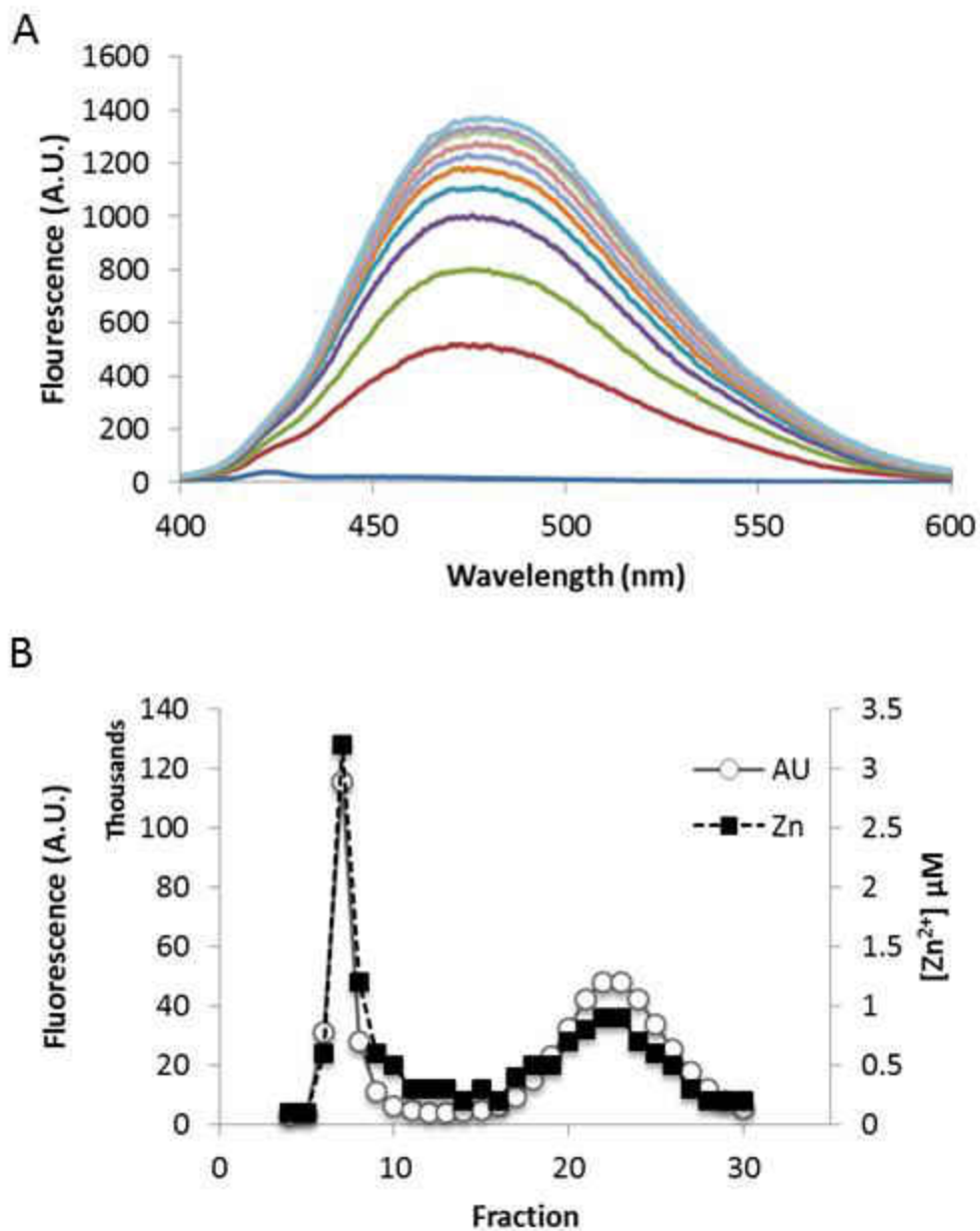
Figure 3.9. Titration of Zn₂-ADH with ZQ_ACID. 5 µM Zn₂-ADH (10 µM total Zn^{2+}) was titrated with ZQ_{ACID} in 20 mM Tris-Cl pH 7.4. (B) Reaction mixture was eluted over a Sephadex G-50 gel filtration column using 20 mM Tris-Cl pH 7.4. Fluorescence and $[Zn^{2+}]$ was recorded for each fraction. Taken from *Nowakowski et. al.* (2011)[71]

expected for a Zn(ZQ)$_2$ complex with an emission maximum at 492 nm. The other half

of the total Zn eluted in the proteomic pool. It too was fluorescent, displaying an

emission pattern that was blue shifted to 472 nm, similar to that observed with the

ethyl ester form of the enzyme. These data imply that ZQ$_{ACID}$ not only can engage in

adduct formation with Zn-proteins, but also can extract Zn^{2+} from Zn-proteins (reaction

3.4).

$$2\ ZQ_{ACID} + Zn_2\text{-}ADH \rightleftarrows Zn(ZQ_{ACID})_2 + Zn\text{-}ADH \tag{3.4}$$
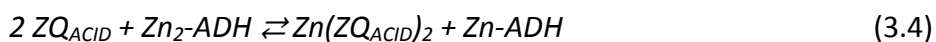
3.2.3.   Reactions of Zinquin with Model Proteins Zn-Alkaline Phosphatase

Another Zn-protein was tested for its reactivity with Zinquin, Zn-Alkaline Phosphatase

(Zn$_2$-AP). This dimer contains two Zn^{2+} ions within both of its active sites as well as a

Mg^{2+} ion.[79] Upon titration of 5 μM Zn$_2$-AP with ZQ$_{EE}$, the fluorescence increased showing

a λ$_{MAX}$ at 475 nm, indicative of the formation of a sensor-protein ternary adduct (**Figure

3.10**). Furthermore, when the mixture was separated using size exclusion, fluorescence

and Zn^{2+} eluted together in the HMW region. In addition, the fluorescence maintained

its blue-shifted emission spectrum seen before separation.   This reinforces the

hypothesis that Zinquin forms ternary adducts with Zn-proteins (reaction 3.5).

$$ZQ_{EE} + Zn_2\text{-}AP \rightleftarrows ZQ_{EE}\text{-}Zn_2\text{-}AP \tag{3.5}$$

Upon the reaction of Zn$_2$-AP and ZQ$_{ACID}$, there was a fluorescence increase; however, it

displayed the emission profile of that of Zn(ZQ)$_2$ and was not blue-shifted.   Once the

reaction mixture was chromatographed, most of the fluorescence eluted in the LMW

region of the chromatogram which did have the expected 492nm emission maximum of a $Zn(ZQ)_2$ complex. The small fluorescence that remained in proteomic fractions was spectrally the same as that of the initial spectrum of 5 µM Zn_2-AP in solution. Hence this fluorescence was due to the background fluorescence of Zn_2-AP or possible contaminants retained during purification (see PAGE gel in section 3.7.4.). As seen with Zn_2-ADH, half of the Zn^{2+} eluted as LMW while the other half remained with the protein. These data infer that ZQ_{ACID} chelated one of the two Zn^{2+} from Zn_2-AP, but was not reactive with the other protein-bound Zn^{2+} (reaction 3.6).

$$2\ ZQ_{ACID} + Zn_2\text{-}AP \rightleftarrows Zn(ZQ_{ACID})_2 + Zn\text{-}AP \qquad (3.6)$$
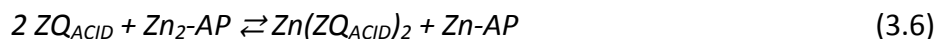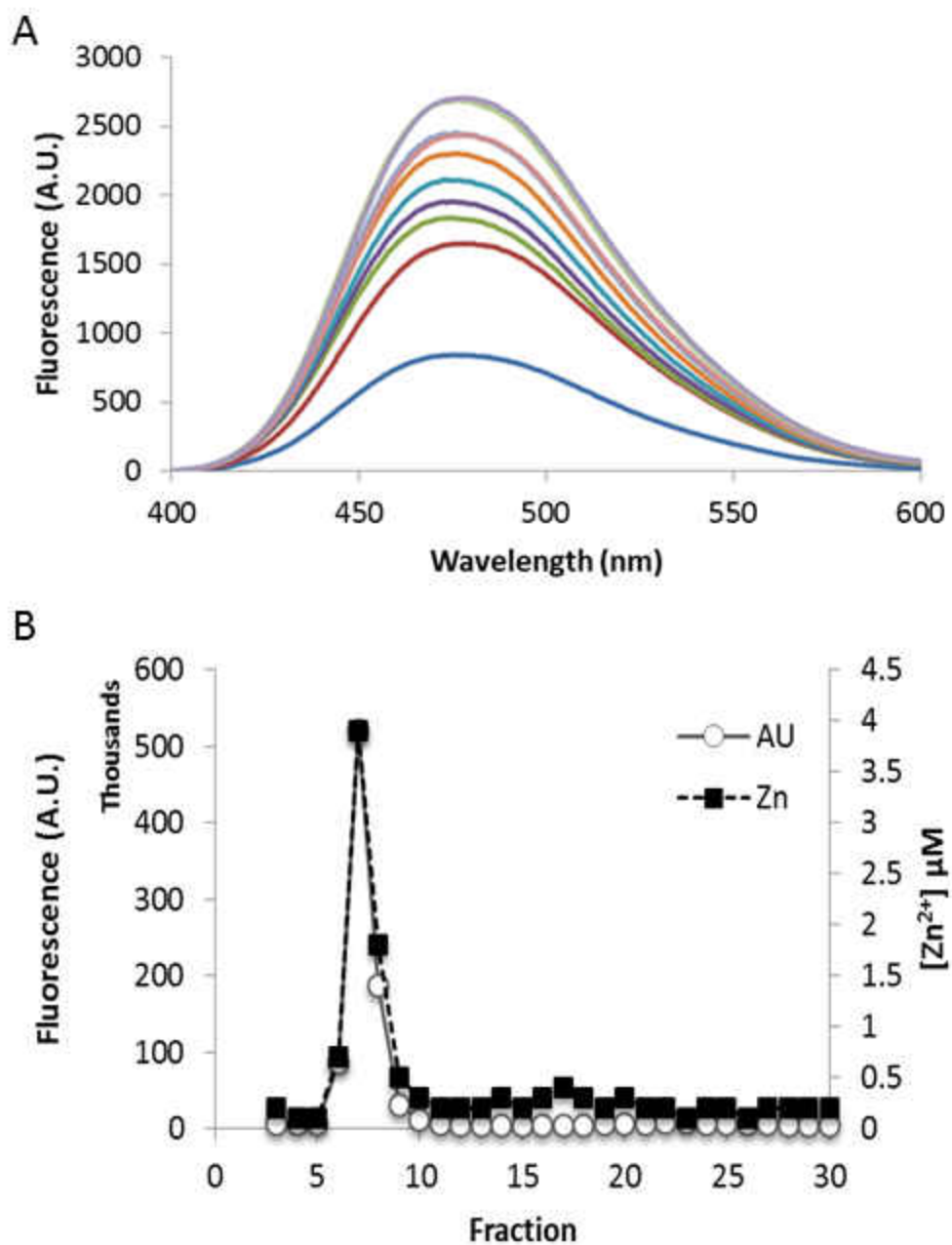
Figure 3.10. Titration of Zn$_2$-AP with ZQ$_{EE}$. 5 µM Zn$_2$-AP (10 µM total Zn^{2+}) was titrated with ZQ$_{EE}$ in 20 mM Tris-Cl pH 7.4. (B) Reaction mixture was eluted over a Sephadex G-50 gel filtration column using 20 mM Tris-Cl pH 7.4. Fluorescence and [Zn^{2+}] was recorded for each fraction. Taken from *Nowakowski et. al.* (2011)[71]

3.2.4. Reactions of Zinquin with Zn-Carbonic Anhydrase and Bovine Serum Albumin

Carbonic Anhydrase, Zn-CA, was also used to test for reactivity. Dr. Jeff Meeusen from the Petering Lab demonstrated that the related sensor, TSQ, was able to bind to Zn-CA, demonstrated by a fluorescence enhancement with a shifted emission spectrum.[56] However, when Zn-CA was titrated with either ZQ_{EE} or ZQ_{ACID}, no fluorescence enhancement was observed, indicating that no binding had occurred.   The most likely explanation for this difference is that both forms of ZQ have a methyl group at the 2 position on the quinoline ring whereas TSQ does not. Since this group is adjacent to the coordination site of Zn^{2+}, there may be some form of steric hindrance involved with the binding of Zinquin to the active site Zn^{2+}.

The titration of Zn-CA with ZQ provides an additional insight in terms of the source of fluorescence within a cell. This negative result downplays the possible hypothesis that ZQ is associating non-specifically—meaning not coordinated to metal—with a protein, which in turn is the source of the blue-shifted emission spectra. To further negate this hypothesis, a non-metal protein, bovine serum albumin (BSA) was also titrated with Zinquin. This too resulted in no significant fluorescence increase, further supporting that Zinquin needs to be coordinated in order for it to exhibit fluorescence enhancement.

3.3. Cellular Chemistry of TPEN

3.3.1. Cellular Quenching of Fluorescence using TPEN

N,N,N',N'-Tetrakis(2-pyridylmethyl)ethylenediamine, known as TPEN, has been a standard reagent used within the Zn^{2+} sensor arena. Due to its high binding affinity for Zn^{2+} ($K_A \approx 10^{15.6}$) and cell permeability, exposure to TPEN has been thought to perturb the intracellular "free" or "transient" Zn^{2+} concentration within a cell (reaction 3.7).

$$Zn^{2+}_{TRANSIENT} + TPEN \rightleftarrows Zn\text{-}TPEN \qquad (3.7)$$

It has been used as a model for inducing intracellular Zn^{2+} deficiency.[80-82] In addition, it is employed in conjunction with Zn-sensor experiments as a proof of principle that fluorescent changes caused by the Zn-sensor are due to binding Zn^{2+} which can be quenched via treatment with TPEN (reaction 3.8).[29,46]

$$Zn\text{-}sensor + TPEN \rightleftarrows Zn\text{-}TPEN + sensor \qquad (3.8)$$
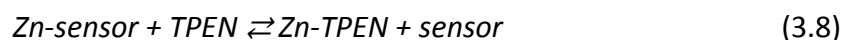
In these experiments, the source of Zn-based fluorescence to be quenched by TPEN was thought to be from preformed Zn-sensor complexes. However, it has now been demonstrated that Zinquin fluorescence enhancement is due primarily to ternary adduct formation, not $Zn(ZQ)_2$ complexes. In light of these new data, more chemical analyses of the interactions of TPEN with intracellular Zn^{2+} sources must be conducted.

To begin, 5 x 10^6 LLC-PK_1 cells—corresponding to 5 μM total Zn^{2+}—were put in suspension and reacted with 10 μM ZQ_{EE} reaching peak fluorescence intensity after 10

minutes. Then, under pseudo first order conditions, the suspension was reacted with 100 μM TPEN and the fluorescence was monitored at 470 nm (◊ in **Figure 3.11**).

Plotting the log of fluorescence vs. time showed that, within 5 minutes, about 80% of the fluorescence was quenched in a first-order reaction. After 10 minutes, the fluorescence was diminished to 10% of the initial signal and remained constant for another 20 minutes. This result was then compared to an isolated proteome in which 5 μM proteome—based on Zn—was reacted with 10 μM ZQ_{ACID} (blue of **Figure 3.11**) or ZQ_{EE} (red in **Figure 3.11**) for 30 minutes before being quenched with 100 μM TPEN. The quenching of the ZQ_{ACID}-exposed proteome was multi-phasic and occurred within a time frame qualitatively similar to that seen in intact cells; however, the major initial phase happened at a slightly faster rate than seen in cells. The opposite was true for the proteome initially reacted with the ethyl ester form of Zinquin, in which fluorescence quenching occurred more slowly. Nonetheless, both proteomes reacted at similar overall rates when compared to cells. Chemically, the loss of fluorescence can be ascribed to either a ligand substitution reaction between TPEN and a ZQ-Zn-protein or a chelation of Zn from those proteins, described in reactions 3.9 and 3.10.

$$ZQ\text{-}Zn\text{-}protein + TPEN \rightleftarrows TPEN\text{-}Zn\text{-}protein \tag{3.9}$$
$$ZQ\text{-}Zn\text{-}protein + TPEN \rightleftarrows apo\text{-}protein + ZQ + Zn\text{-}TPEN \tag{3.10}$$
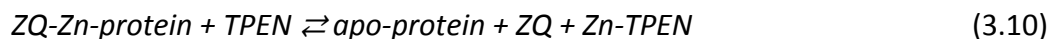
The extent to which these two reactions occur will be investigated in section 3.3.5.
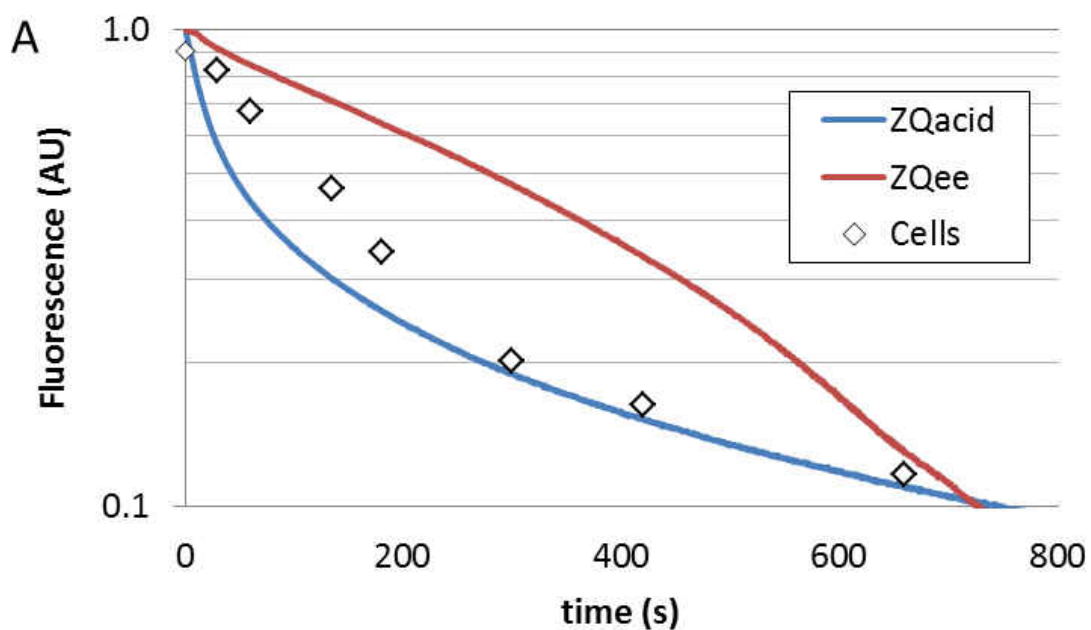
Figure 3.11. Kinetics of ZQ-exposed LLC-PK$_1$ and ZQ-proteomes with TPEN. LLC-PK$_1$ cells (5 x 10^6 in DPBS, approximately 5 µM Zn^{2+}) were reacted with 10 µM ZQ$_{EE}$ (◊) for 15 minutes before fluorescence was quenched using 100 µM TPEN. Similarly, 5 µM Zn-proteome reacted with Zinquin for 15 minutes in 20 mM Tris-Cl pH 7.4 at 25 °C. Fluorescence of ZQ$_{ACID}$-Zn-proteome (blue) and ZQ$_{EE}$-Zn-proteome (red) was quenched with 100 µM TPEN. (λ$_{EX}$=370 nm, λ$_{EM}$=470 nm) Adapted from *Meeusen et. al.* (2012)[73]

A possible reason for the difference in rates between cells and the two isolated ZQ-proteomes may be attributed to the fact that upon entering the cell, ZQ_{EE} can either be hydrolyzed to the acid form or react immediately with a member of the Zn-proteome as outlined in the scheme in **Figure 3.12.**

$$ZQ_{EE(o)}$$

$$ZQ_{EE}\text{-Zn-protein} \rightleftharpoons ZQ_{EE(i)} \longrightarrow ZQ_{ACID} \rightleftharpoons ZQ_{ACID}\text{-Zn-protein}$$
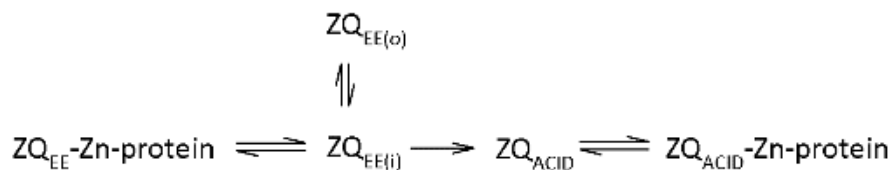
Figure 3.12. Reaction scheme of the cellular fate of Zinquin

Therefore, it is likely that cellular fluorescence is due to a mixture of both forms of Zinquin ligating to the Zn-proteome. Since TPEN reacts with the acid and ethyl ester treated proteomes at different rates, the overall rate of quenching within cells is a combination of the rates of the reactions of TPEN with the specific form of Zinquin bound to a protein. This results in a rate that lies in between the rates of TPEN reacting with either form of the Zinquin treated proteome. Moreover, this rate is not only dependent on which form of Zinquin is reacting with a Zn-protein, but also dependent on the identity of the Zn-protein. Some ZQ-Zn-proteins may react faster or slower with TPEN depending on the coordination environment around the Zn^{2+} attached to the protein and mechanism of reaction. Therefore, this observed rate is the result of rates for potentially thousands of different reactions each with its own kinetic parameters. This helps explains why even though this experiment was performed under pseudo-first

order conditions, the rates observed for both cells and isolated proteomes did not yield exact first order plots.

3.3.2. Reactions of TPEN with Zn(ZQ$_{EE}$)$_2$ and Zn(ZQ$_{ACID}$)$_2$

As models for quenching of intracellular ZQ-based fluorescence, the reactivity of TPEN with Zn(ZQ$_{ACID}$)$_2$ and Zn(ZQ$_{EE}$)$_2$ was investigated. When 5 µM Zn(ZQ$_{ACID}$)$_2$ was reacted 100 µM TPEN, the fluorescence quickly diminished to near baseline levels within the first minute. (**Figure 3.13**) Interestingly, this reaction was zero-order with respect to TPEN as higher concentrations of TPEN had no effect on the overall rate. The reactions were repeated 3 times for each concentration of TPEN and yielded an overall first order rate constant of 4.8 x 10^{-2} sec^{-1}.
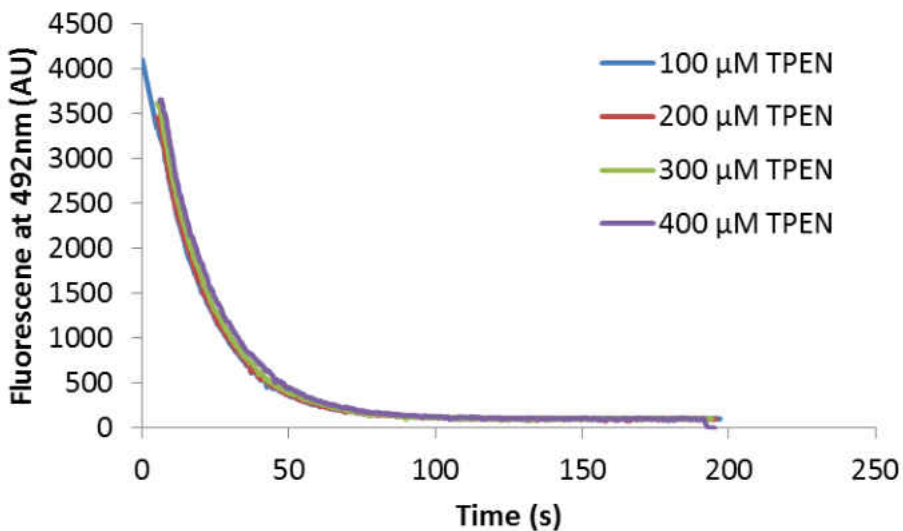
Figure 3.13. Kinetics of Zn(ZQ$_{ACID}$)$_2$ with TPEN. 5 µM Zn(ZQ$_{ACID}$)$_2$ was reacted with 100-400 µM TPEN in 20 mM Tris-Cl pH 7.4 at 25 °C. (λ_{EX}=370 nm, λ_{EM}=492 nm)

The experiment was then repeated using $Zn(ZQ_{EE})_2$ instead of $Zn(ZQ_{ACID})_2$. **Figure 3.14** shows the fluorescence quenching traces of 5 µM $Zn(ZQ_{EE})_2$ with various concentrations of TPEN.   Unexpectedly, this reaction occurred at a much slower rate than the $Zn(ZQ_{ACID})_2$ reaction with a significant amount of fluorescence still remaining after 30 minutes.   In addition, this reaction obeyed second-order kinetics, first order to both $Zn(ZQ_{EE})_2$ and TPEN. After three replicates at multiple concentrations, the observed rate of reaction (k_{obs}) was plotted versus the concentration of TPEN, giving a rate constant for this reaction of 1.82 M^{-1} s^{-1} with a nonzero *y*-intercept of 3.0 x 10^{-4} s^{-1} compared to 4.8 x 10^{-2} s^{-1} observed in the previous reaction (**Figure 3.15** inset).   For purposes of showing k_{obs} vs. [TPEN] for both ZQ_{ACID} and ZQ_{EE} on the same graph, there is a scale break in the y-axis.

These pseudo-first order rates of reactions of TPEN with the two $Zn(ZQ)_2$ species occurred either much faster or much slower than that of exposed cells (**Figure 3.15**).   In addition, the multi-phasic nature of the cellular fluorescence quenching reaction fits more closely with the reaction of ZQ_{ACID}-Zn-protein with TPEN than either of the two $Zn(ZQ)_2$ species, providing more evidence that the ZQ_{ACID}-Zn-protein species is the dominant source of fluorescence within the cellular environment.
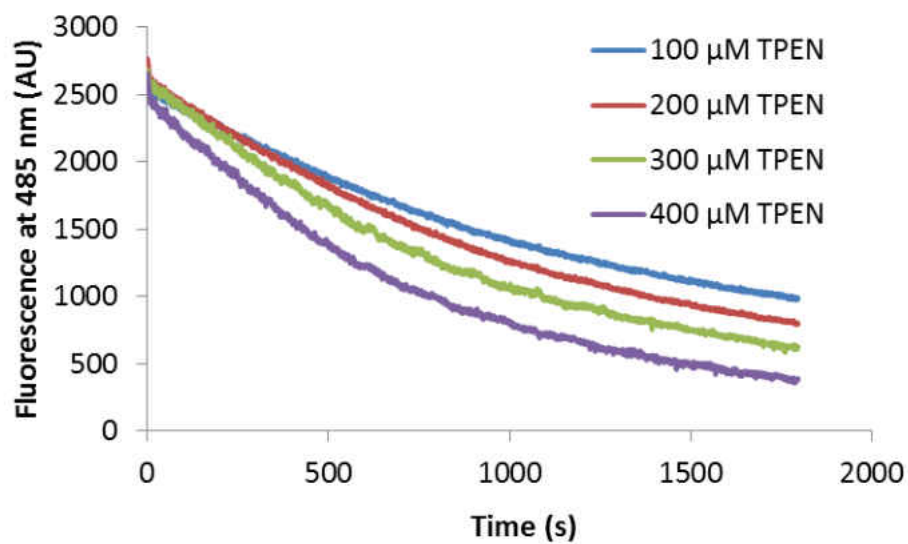
Figure 3.14. Kinetics of Zn(ZQ$_{EE}$)$_2$ with TPEN. 5 µM Zn(ZQ$_{EE}$)$_2$ was reacted with 100-400 µM TPEN in 20 mM Tris-Cl pH 7.4 at 25 °C. (λ_{EX}=370 nm, λ_{EM}=492 nm)
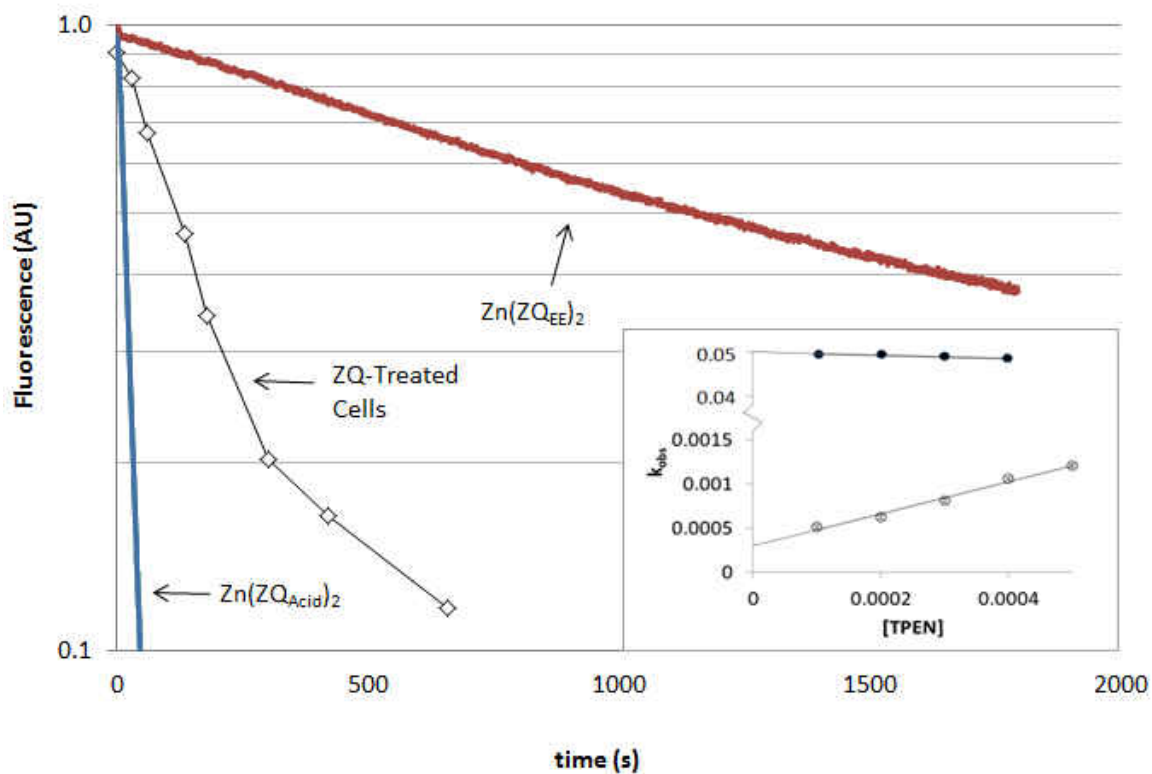
Figure 3.15. Quenching kinetics of Zn(ZQ)$_2$ verse ZQ-treated cells with TPEN. Natural logarithm plot of fluorescence decay of 5 µM Zn(ZQ$_{ACID}$)$_2$ (blue) and Zn(ZQ$_{EE}$)$_2$ (red) reacted with 100 µM TPEN in 20 mM Tris-Cl pH 7.4 at 25 °C. Results are compared to ZQ-exposed LLC-PK$_1$ cells (◊) in DPBS reacted with 100 µM TPEN.   Inset: linear regression of k$_{obs}$ versus [TPEN] for the reactions of 5 µM Zn(ZQ$_{ACID}$)$_2$ (●) and 5 µM Zn(ZQ$_{EE}$)$_2$ (○) with TPEN. (R^2 = 0.99). Adapted from *Meeusen et. al.* (2012)[73]

3.3.3. Proposed Mechanism of Zn(ZQ)$_2$ + TPEN

The kinetic data obtained from the reactions of Zn(ZQ$_{ACID}$)$_2$ and Zn(ZQ$_{EE}$)$_2$ with TPEN can provide insight into a possible pathway for these reactions.   The hypothetical mechanism for the reaction of Zn(ZQ$_{ACID}$)$_2$ with TPEN is outlined in **Figure 3.16**.
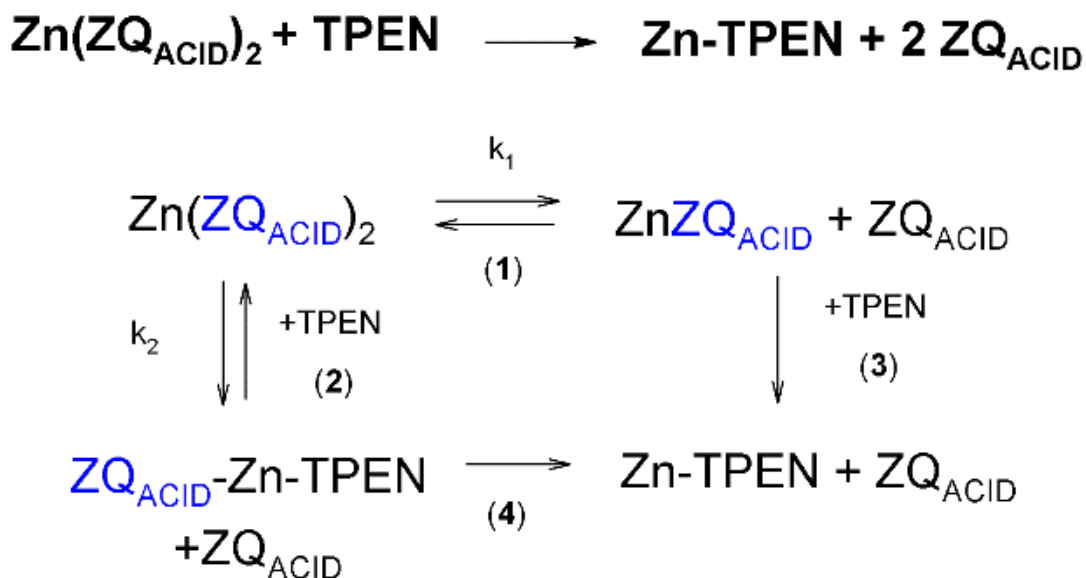
Figure 3.16. Proposed mechanism of the reaction Zn(ZQ$_{ACID}$)$_2$ + TPEN.

The two possible routes for fluorescence quenching are as follows: (1) There is a rate limiting dissociation of one of the two ZQ$_{ACID}$ molecules from Zn(ZQ$_{ACID}$)$_2$ (reaction 1) followed by a rapid attack from TPEN chelating Zn^{2+} from the other ZQ$_{ACID}$ molecule (reaction 4) or (2) a rate limiting bimolecular attack by TPEN first displacing one of the two ZQ$_{ACID}$ molecules and forming a TPEN-Zn-ZQ$_{ACID}$ adduct (reaction 2). This is followed

by a displacement of the second ZQ molecule. In this model the observed rate of reaction would be described as

$$k_{obs} = k_1 + k_2[TPEN] \quad\quad\quad (3.11)$$

Experimental data show that this reaction is zero-order with respect to TPEN (**Figure 3.15** inset). This implies that the rate constant of reaction 1 is much greater than that of reaction 2, i.e.

$$k_1 >> k_2[TPEN] \quad\quad\quad (3.12)$$

Therefore, the predominant pathway by which this reaction procedes is the first pathway described, a ZQ dissociation followed by direct chelation of Zn^{2+}. Moreover, the TPEN-independent nature of this reaction dictates that reaction 3 is much faster than reaction 1, and that the dissociation of the first ZQ_{ACID} molecule is the rate-limiting step in this process. Therefore, the observed rate constant of is equal to the rate constant of reaction 1, $4.8 \times 10^{-2} s^{-1}$.

The hypothetical pathways for the reaction of $Zn(ZQ_{EE})_2$ with TPEN are the same as for $Zn(ZQ_{ACID})_2$ shown here in **Figure 3.17**.

$$\text{Zn(ZQ}_{EE})_2 + \text{TPEN} \longrightarrow \text{Zn-TPEN} + 2\ \text{ZQ}_{EE}$$
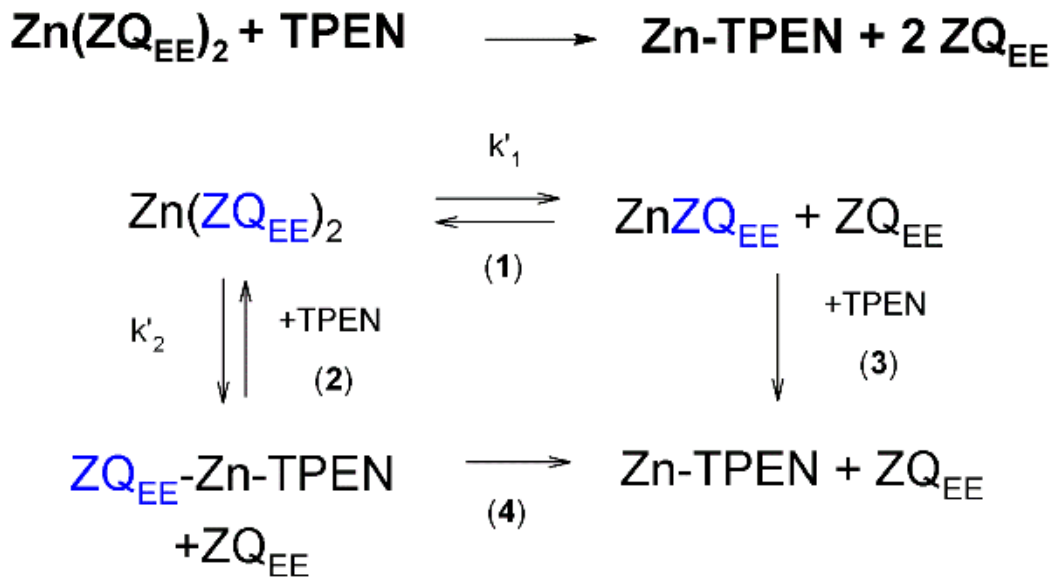
Figure 3.17. Proposed mechanism of the reaction Zn(ZQ$_{EE}$)$_2$ + TPEN.

In this system, however, the observed reaction rate is dependent on the concentration of TPEN (**Figure 3.12** inset). This implies that the reaction proceeds in part through a bimolecular reaction between Zn(ZQ$_{EE}$)$_2$ and TPEN (pathway 2). However, according to **Figure 3.12**, the observed rate can also be described as a reaction also including a component that is independent of the TPEN concentration. Thus,

$$k'_{obs} = k'_1 + k'_2[TPEN] \qquad\qquad (3.13)$$

In this case, both rate constants are of the same order of magnitude and both make significant contributions to the overall rate expression for the observed rate constant. Thus, k'$_1$ is equal to 3.0 x 10^{-4} s^{-1}. This dissociation step of the first ZQ from Zn(ZQ)$_2$ is much slower with the ethyl ester than the acid (3.0 x 10^{-4} s^{-1} vs. 4.8 x 10^{-2} s^{-1}). This is

presumably because the electrostatic repulsion of the two negatively charged ZQ_{ACID} ligands increases the rate of the dissociation process. In addition, the slope of first-order plot represents the rate constant for reaction 2, k'_2, with a value of 1.82 $M^{-1}s^{-1}$.

3.3.4. Reactions of the Zn-Proteome with TPEN and other metal chelators

The high binding affinity of TPEN for Zn^{2+} ions has the potential for not only scavenging free Zn^{2+} ions in cells as intended, but more importantly, removing Zn^{2+} from the basal distribution of Zn-proteins. To test this, the isolated Zn-proteome from LLC-PK$_1$ cells was reacted with a 10-fold excess (100 µM) of TPEN for 30 minutes before being subjected to Sephadex G-75 gel filtration to determine the extent of sequestration. In addition, each fraction was assayed with 10 µM ZQ_{ACID} to determine the residual activity of the treated proteome (**Figure 3.18**). This was compared to a proteome that was not treated with TPEN, fractionated, and assayed for fluorescence.

Exposure to TPEN removed nearly 35% of the total Zn^{2+} from the proteome so that it eluted in the LMW fractions, presumably as Zn-TPEN. Furthermore, the reactivity of the proteome to Zinquin was reduced by approximately 75%. These data indicate that the introduction of TPEN significantly affects the natural distribution of Zn^{2+} in the affected proteome. Additionally, the removal of Zn^{2+} resulted in significant loss of fluorescence, suggesting that the Zn-proteins affected by TPEN are also members of the Zn-proteome that form adducts with Zinquin.
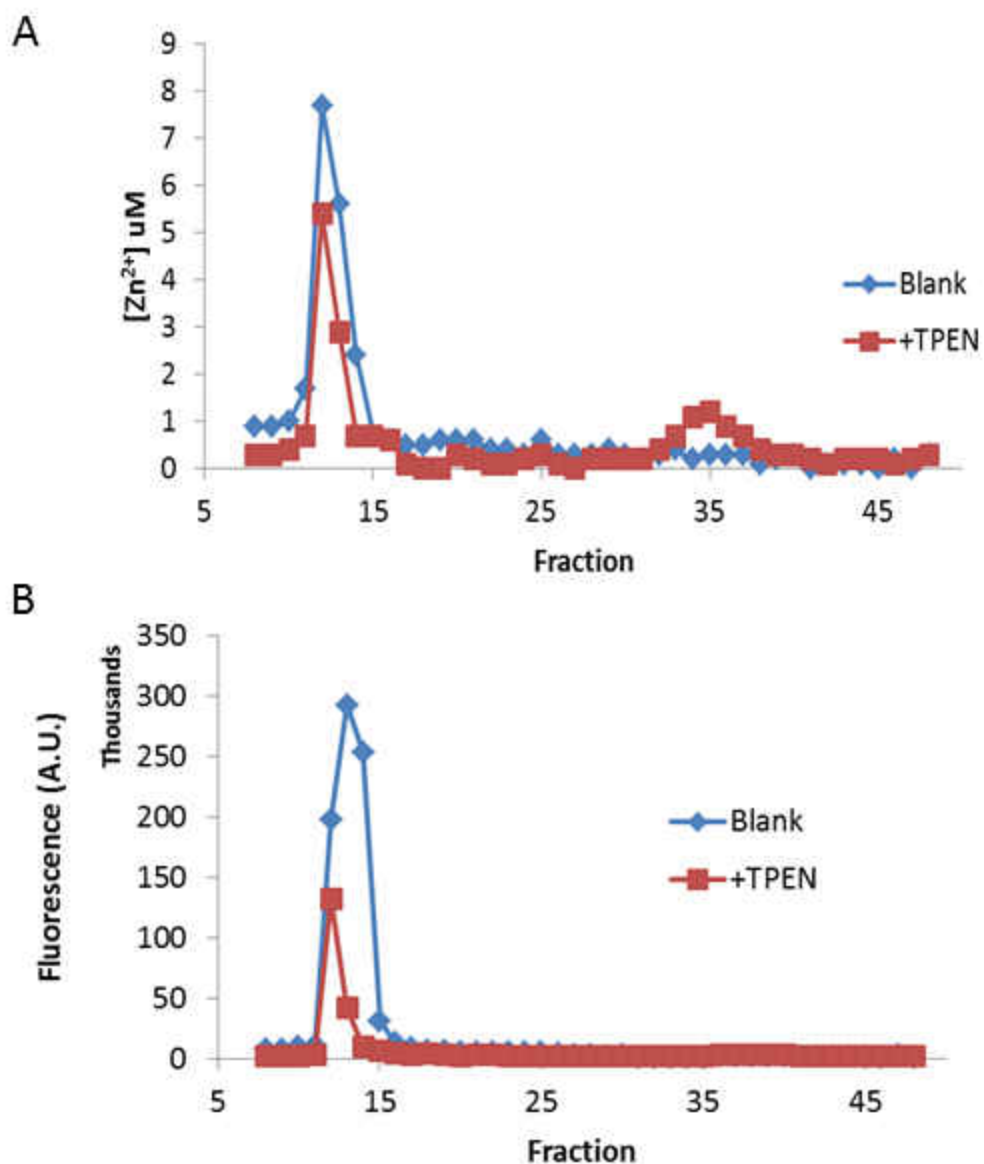
Figure 3.18. Effects of the Zn-proteome reacted with 100 μM TPEN. 10 μM of LLC-PK$_1$ Zn-proteome was reacted with 100 μM TPEN (red) for 30 minutes and eluted over a Sephadex G-75 gel filtration column with 20 mM Tris-Cl pH 7.4. Fractions were assayed with 10 μM ZQ$_{ACID}$ and the [Zn^{2+}] and fluorescence was recorded. Results were compared to 10 μM of unreacted Zn-proteome (blue).

This study was further expanded by repeating the experiment in triplicate with not just

TPEN, but other Zn^{2+} chelators including tris(2-aminoethyl)amine (TREN), ethylenediaminetetraacetic acid (EDTA), ethylene glycol triacetic acid (EGTA), and nitrilotriacetate (NTA). The stability constants, as well as the percent chelation of Zn^{2+} from the proteome and subsequent loss of Zinquin-based fluorescence are summarized in **Table 3.4.**

competitive ligand	log K^b	% Zn^{2+} chelation[c]	% decrease in ZQ fluorescence[c]
NTA	10.5^{32}	25 ± 3	30 ± 14
EGTA	8.8^{33}	25 ± 3	51 ± 23
TREN	14.4^{32}	26 ± 2	43 ± 7
EDTA	13.6^{34}	30 ± 5	75 ± 9
TPEN	15.4^{16}	35 ± 2	77 ± 3

[a]Reaction conditions: Zn−proteome (10 μM Zn^{2+}), treated for 30 min with 100 μM chelator in 20 mM Tris-Cl, pH 7.4, buffer at 25 °C. [b]Conditional stability constant, pH 7. [c]Average ± standard deviation, n = 3.

Table 3.4. Reactions of the LLC-PK$_1$ Zn-proteome with chelating agents. Taken from *Meeusen et. al.* (2012)[73]

Although the Zn^{2+} binding affinities of these chelators range over seven orders of magnitude, all removed approximately 30% of the total Zn^{2+} from the proteome. This was in agreement with what was done in a previous study in which an array of metal chelators removed 30-35% of the Zn^{2+} from the proteome as well.[72] Interestingly, from a qualitative standpoint, the reactivity with Zinquin of each chelated proteome was

inversely proportional to the stability constant of the chelating agent used. For example, the TPEN-treated proteome displayed a 75% loss of fluorescence whereas the proteome incubated with the weaker chelator NTA showed only a 30% loss in fluorescence. Since relatively the same amount of Zn^{2+} was removed regardless of the chelator used, it is likely that the sequestered Zn^{2+} in each experiment came from similar cellular sources. But, the fact that there is more Zinquin fluorescence in the proteome treated with a weaker chelator than a stonger chelator suggests that these chelators are also forming adducts with Zn-proteins that Zinquin can, in some cases, out compete. In general, these results imply that these metal ligands interact differently with the Zn-proteome as determined by their ability to be sensed by Zinquin.

Interestingly, when Zinquin was added to the LMW fractions—containing the Zn-chelator complexes—there was fluorescence for the NTA, EGTA, and TREN treated samples. Moreover, the emission spectra of the fractions in all three samples had fluorescence peaks near 474nm (**Figure 3.19**).

Since these spectra are not characteristic of a spectrum associated with a $Zn(ZQ_{ACID})_2$ species, the result indicates that Zinquin is able to form ternary adducts with these chelators. Likewise, it underscores the fact that Zinquin-Zn-ligand ternary adducts are distinguishable by blue-shifted emissions. Stepping further back, since cells exposed to Zinquin have this spectra, it reinforces the hypothesis that Zinquin is forming ternary adducts *in vivo*.
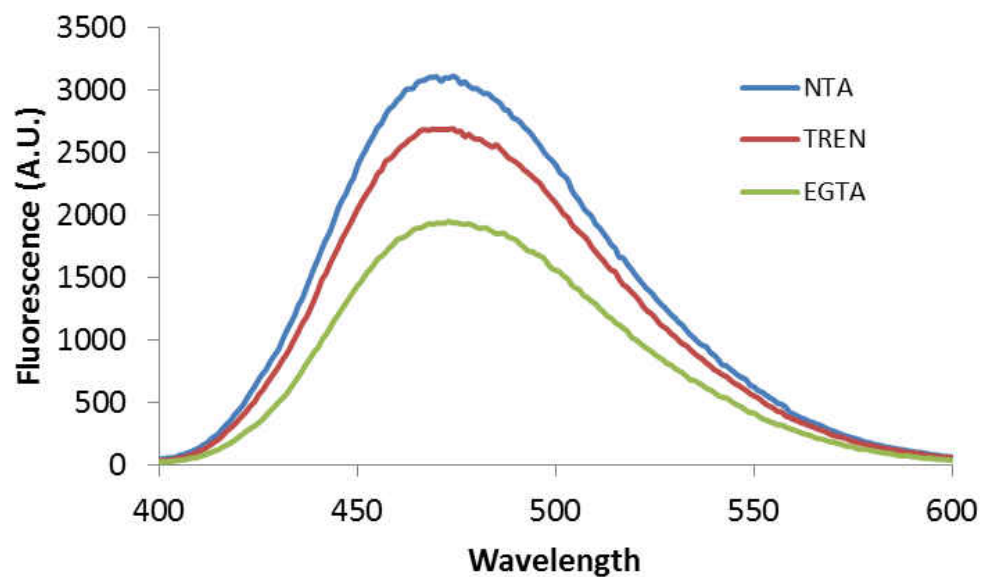
Figure 3.19. Fluorescence of Zn-NTA, -EGTA and -TREN with ZQ$_{ACID}$. Peak fluorescence spectra of LMW fractions from Sephadex G-75 gel filtration of 10 µM LLC-PK$_1$ Zn-proteome reacted with 100 µM NTA (blue), TREN (red), and EGTA (green) as assayed with 10 µM ZQ$_{ACID}$ in 20 mM Tris-Cl pH 7.4. Emission λ_{MAX} = 474 nm (NTA), 474 nm (TREN), 473 nm (EGTA)

3.3.5. Reactions of TPEN with model Zn-proteins exposed to Zinquin

The model proteins Zn_2-ADH and Zn_2-AP were revisited to investigate possible interactions with TPEN. First, 5 µM Zn_2-ADH was reacted with 20 µM ZQ_{ACID} for 30 minutes. After the addition of 100 µM TPEN, the fluorescence was monitored at 480 nm for 30 minutes (**Figure 3.20**).

The fluorescence decay over time suggested a two-step process, including distinguishable fast and slow steps. Recalling that the reaction of ZQ_{ACID} with Zn_2-ADH resulted in the removal of one Zn^{2+} from the protein, it is likely the first phase of the reaction is between TPEN and the extracted Zn^{2+} ligated to Zinquin (reaction 3.14)

$$Zn(ZQ_{ACID})_2 + TPEN \rightleftarrows Zn\text{-}TPEN + 2\ ZQ_{ACID} \qquad \text{(fast)} \qquad\qquad (3.14)$$

This is supported by the fact that the rate of this phase is consistent with the rate of the above reaction as described in section 3.3.2. To investigate the nature of the second phase of the reaction, the reaction product was separated using Sephadex G-50 size exclusion (**Figure 3.21**).

After fractionation, half of the total Zn^{2+} remained with the protein while the other half eluted in the LMW fractions. In addition, the fluorescence within the proteomic fractions was extinguished. Taken together, this suggests that the slow step of the reaction is a ligand substitution reaction between TPEN and the ZQ_{ACID} coordinated to Zn-ADH as stated in reaction 3.15.

Figure 3.20. Fluorescence quenching of ZQ treated Zn$_2$-ADH with TPEN. 5 μM Zn$_2$-ADH was reacted with 20 μM ZQ$_{ACID}$ (red) and 20 μM ZQ$_{EE}$ (blue) for 30 minutes before quenching the fluorescence with with 100 μM TPEN in 20 mM Tris-Cl pH 7.4 at 25 °C.

Figure 3.21. Sephadex G-50 of Zn$_2$-ADH + ZQ$_{ACID}$ + TPEN. 5 µM Zn$_2$-ADH was reacted with 20 µM ZQ$_{ACID}$ followed by 100 µM TPEN was chromatographed over a Sephadex G-50 gel filtration column eluted with 20 mM Tris-Cl pH 7.4. [Zn^{2+}] was determined via AAS. Taken from *Meeusen et. al.* (2012)[73]

$$TPEN + ZQ_{ACID}\text{-}Zn\text{-}ADH \rightleftarrows TPEN\text{-}Zn\text{-}ADH + ZQ_{ACID} \quad\quad\quad (3.15)$$

To provide some evidence as to which Zn^{2+} ion was being chelated and which was forming an adduct, the Zn-ADH from the proteome fractions of the gel filtration column were tested for enzymatic activity and compared to the activity of the holo-enzyme (**Figure 3.22**). This assay was performed by monitoring the conversion of NAD to NADH, signified by an increase in absorbance at 340 nm. Treatment with ZQ and, subsequently, TPEN reduced the activity of the enzyme by 27%. Because the enzyme still maintained 73% of its catalytic activity, the results lend support to the conclusion that the catalytic Zn^{2+} remained with the protein while the structural Zn^{2+} was removed. This was in agreement with other investigations that showed that the removal of the structural Zn^{2+} only had modest effects on the enzymatic activity.[78]

In a parallel reaction, 5 μM Zn_2-ADH was reacted directly with 100 μM TPEN. After 30 minutes, when the reaction product was separated using gel filtration, half of the total Zn^{2+} was removed from the protein. Altogether, the interaction of TPEN with Zn_2-ADH as model for cellular exposure to TPEN shows that this strong chelating agent can disturb Zn^{2+} distribution by removing Zn^{2+} from an accessible Zn-protein as well as form adducts with Zn^{2+} sites within a protein.

The quenching kinetics of the reaction of Zinquin-treated Zn_2-AP with TPEN was investigated. First, 5 μM Zn_2-AP was reacted with 20 μM ZQ_{ACID} for 30 minutes before quenching the fluorescence with 100 μM TPEN. Monitoring the fluorescence at

Figure 3.22. Activity Assay of Zn₂-ADH. Zn-ADH (red) from gel filtration in **Figure 3.21** was assessed for activity. Assay was performed in 20 mM Tris-Cl pH 7.4 at 25 °C containing 1.5 mM NAD, 0-100 mM ethanol and 3.7 µg enzyme. Initial rate was monitored at 340 nm for 30 seconds. Results were compared to enzyme not reacted with ZQ$_{ACID}$ or TPEN (blue).

492 nm shows that the fluorescence is quickly diminished within the first minute of the reaction (**Figure 3.23**).

Recalling that the result of the reaction between Zn_2-AP and ZQ_{ACID} is the chelation of one of the two Zn^{2+} ions as $Zn(ZQ_{ACID})_2$, what is being observed upon addition of TPEN is the direct reaction with $Zn(ZQ_{ACID})_2$ (reaction 3.6 followed by reaction 3.14). This is supported by the finding that the rate of decay for the Zn_2-AP reaction is similar to that of the rate of decay of the $Zn(ZQ_{ACID})_2$ reaction. Furthermore, when the reaction mixture was eluted over a Sephadex G-50 column, half of the Zn^{2+} eluted as a LMW species (**Figure 3.24**). This result was expected since the reaction of Zn_2-AP with ZQ_{ACID} alone removes one of the two Zn^{2+} ions.

Yet, when 5 µM Zn_2-AP was reacted only with 100 µM TPEN, it too resulted in the removal of one of the two Zn^{2+} ions from Zn_2-AP. This implies that not only Zinquin acid, but also TPEN, can chelate Zn^{2+} from Zn-proteins.

To give insight as to how the protein was affected by the treatment with ZQ_{ACID} and TPEN, an activity assay was performed on the remaining protein isolated after size exclusion chromatography (**Figure 3.25**). This assay is performed by monitoring the conversion of 4-nitrophenyl phosphate to 4-nitrophenol, which absorbs at 405 nm. Comparing the activity of the treated enzyme versus the untreated enzyme shows only a 20% decrease in activity. This is consistent with previous work which showed that partial depletion of Zn^{2+} from alkaline phosphatase has a modest effect on the enzymatic activity.[83]
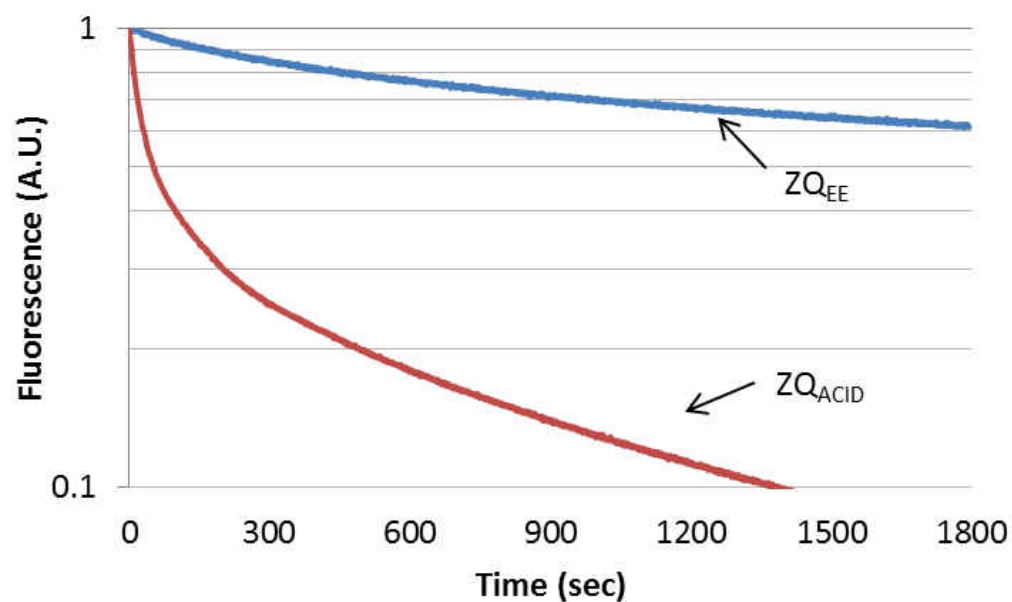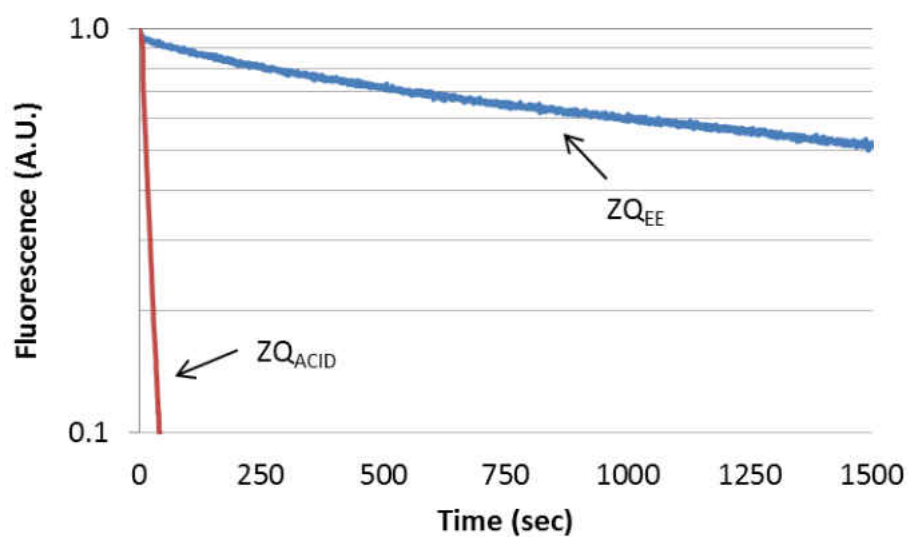
Figure 3.23. Fluorescence quenching of ZQ treated Zn$_2$-AP with TPEN. 5 µM Zn$_2$-AP was reacted with 20 µM ZQ$_{ACID}$ (red) and 20 µM ZQ$_{EE}$ (blue) for 30 minutes before quenching the fluorescence with with 100 µM TPEN in 20 mM Tris-Cl pH 7.4 at 25 °C
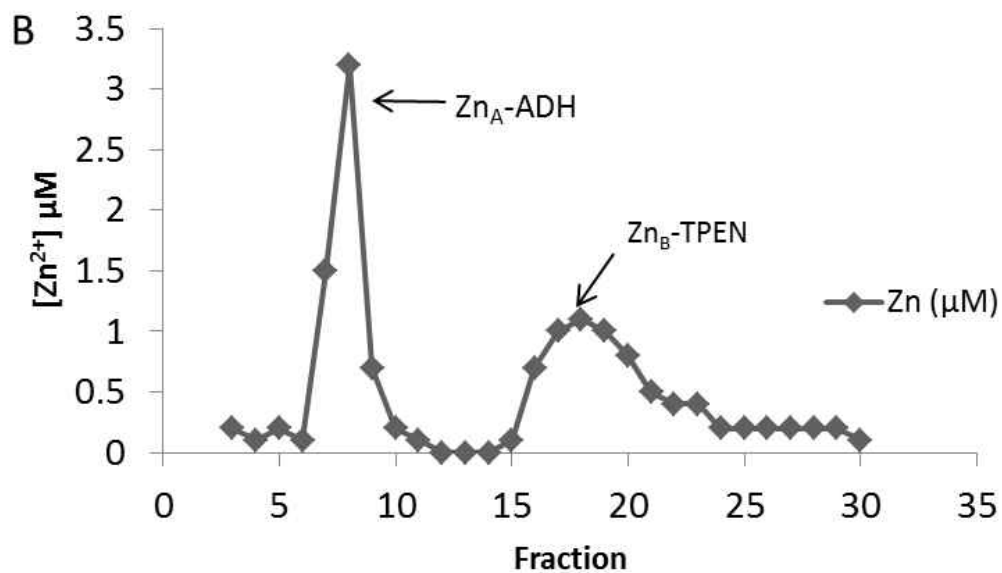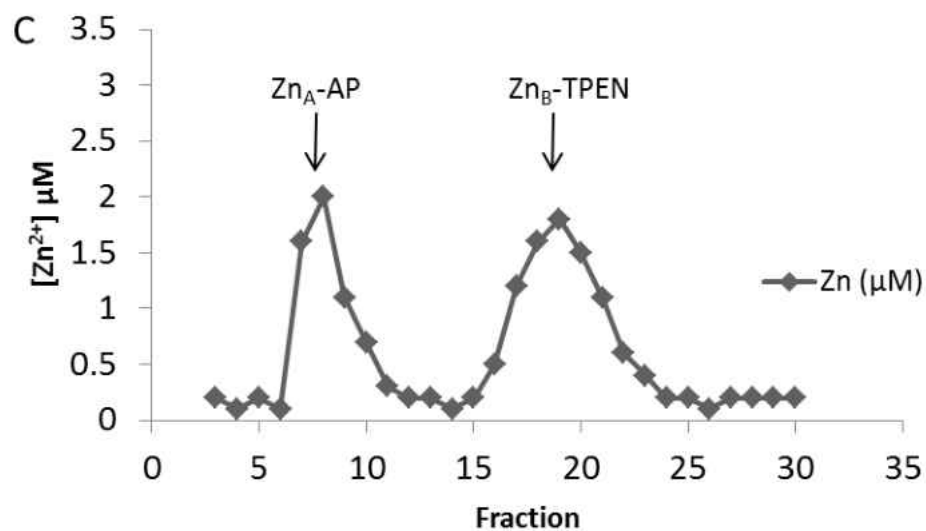
Figure 3.24. Sephadex G-50 of Zn$_2$-AP + ZQ$_{ACID}$ + TPEN. 5 µM Zn$_2$-AP was reacted with 20 µM ZQ$_{ACID}$ followed by 100 µM TPEN was chromatographed over a Sephadex G-50 gel filtration column eluted with 20 mM Tris-Cl pH 7.4. [Zn^{2+}] was determined via AAS. Taken from *Meeusen et. al.* (2012)[73]

In toto, the data from these experiments layout potential pitfalls of the use of TPEN within a cellular system. It has the ability to affect members of the Zn-proteome by either sequestering the Zn^{2+} cofactor from Zn-proteins or by forming adducts with Zn-proteins. Therefore, caution must be taken when using this powerful chelator in proof of principle Zn-sensor experiments or to mimic Zn-deficiency.
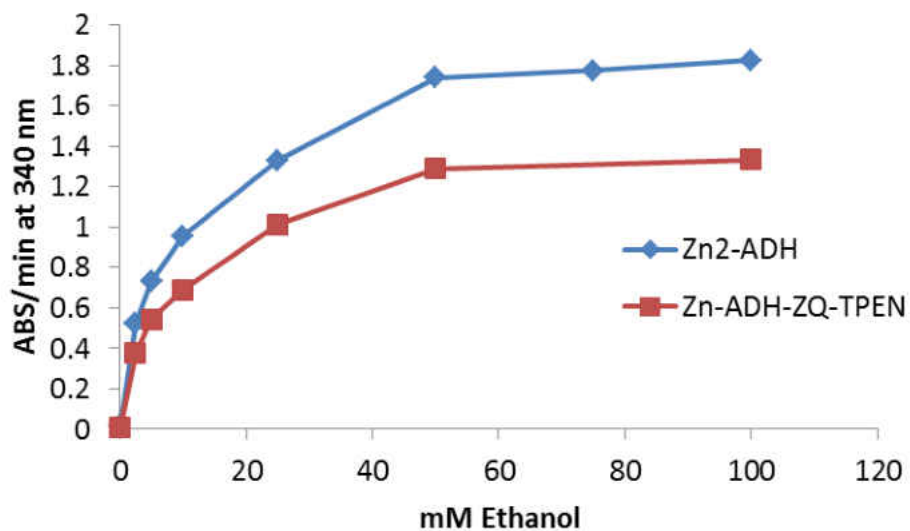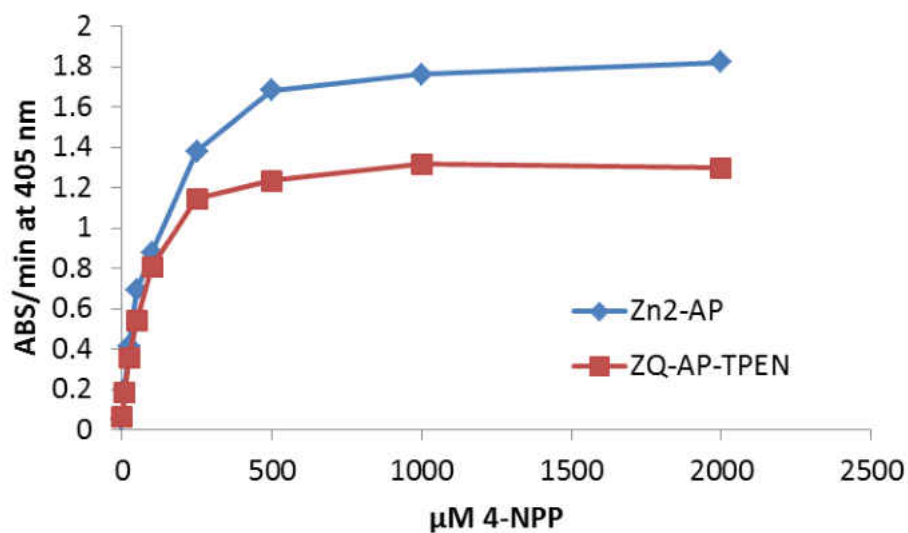
Figure 3.25. Activity Assay of Zn$_2$-AP. Zn-AP (red) from gel filtration in **Figure 3.24** was assessed for activity. Assay was performed in 50 mM Tris-Cl pH 9.0 at 25 °C containing 0-2000 μM 4-nitrophenol phosphatel and 5 μg enzyme. Initial rate was monitored at 405 nm for 30 seconds. Results were compared to enzyme not reacted with ZQ$_{ACID}$ or TPEN (blue).

3.4. Chemical stability of Zn(ZQ)$_2$ within a proteomic environment

The evidence that the main targets of Zinquin in cells are members of the Zn^{2+} proteome lends itself to the question of what roles a Zn(ZQ)$_2$ species may play in the overall scheme of adduct formation, possibly as an intermediate. To begin, LLC-PK$_1$ cells in suspension were incubated with 2 μM Zn(ZQ$_{EE}$)$_2$ and the fluorescence was tracked over time (**Figure 3.26**). During the course of 30 minutes, the fluorescence intensity decreased, but more importantly, there was a blue shift in the emission spectrum, emphasized by comparing the fluorescence at 482 nm, the spectral maximum of Zn(ZQ$_{EE}$)$_2$, to the fluorescence at 470 nm, the spectral maximum of Zinquin adducts.

The blue shifting of the emission spectrum lends to the hypothesis that upon entering the cell, Zn(ZQ$_{EE}$)$_2$ reacts with a Zn-binding site within the proteome and forms a ZQ-Zn-protein adduct, releasing a Zinquin molecule to then react with a native Zn-protein (reactions 3.16 and 3.17)

$$Zn(ZQ)_2 + apo\text{-}proteome \rightleftarrows ZQ\text{-}Zn\text{-}proteome + ZQ \qquad (3.16)$$
$$ZQ + Zn\text{-}proteome \rightleftarrows ZQ\text{-}Zn\text{-}proteome \qquad (3.17)$$
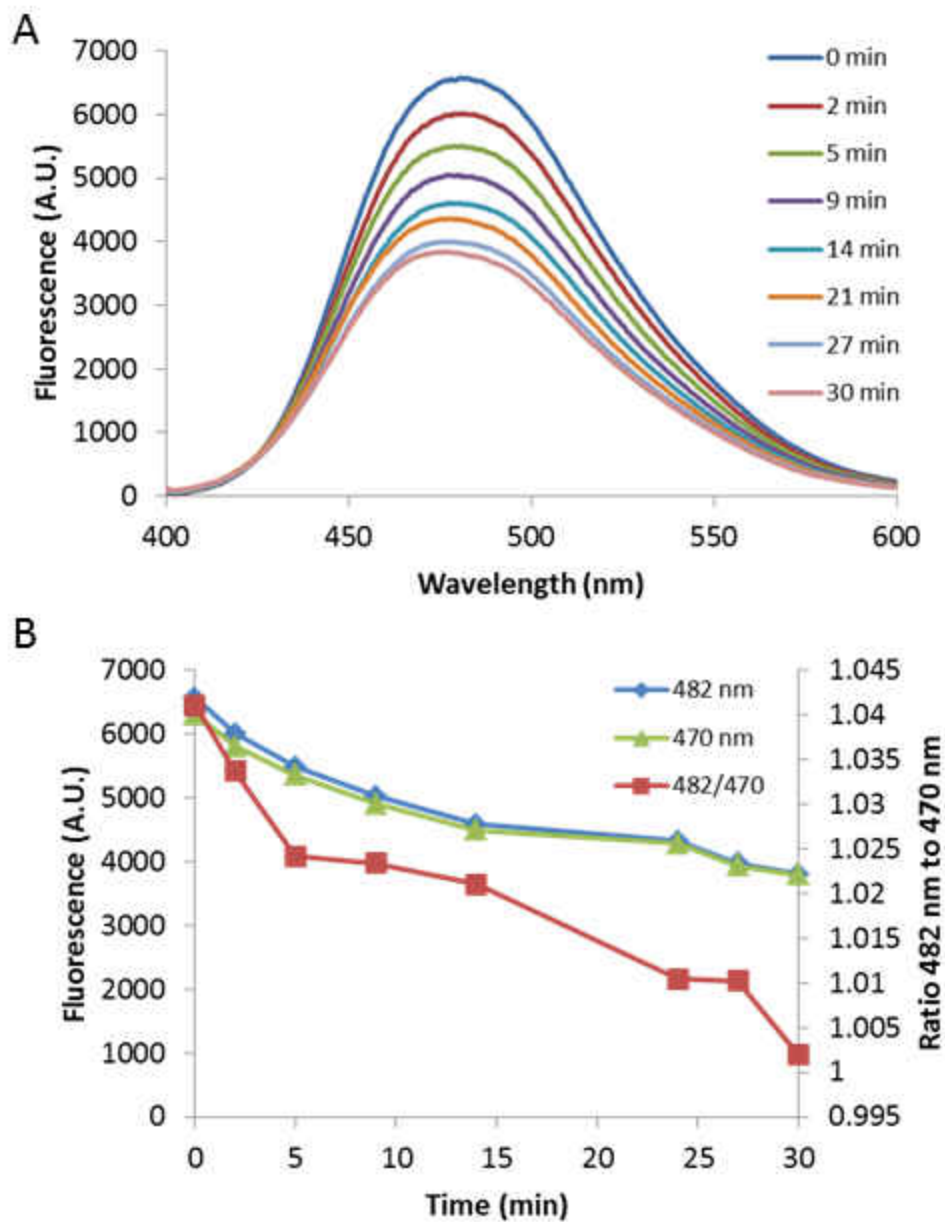
Figure 3.26. Fluorescence of LLC-PK$_1$ cells exposed to Zn(ZQ$_{EE}$)$_2$. 5 x 10^6 LLC-PK$_1$ cells were suspended in 1 mL of DPBS and treated with 10 µL of 200 µM Zn(ZQ$_{EE}$)$_2$ (final [Zn(ZQ$_{EE}$)$_2$] = 2 µM) monitoring the fluorescence (A) and changes in spectra maximum (B).

3.4.1. Reaction of Zn(ZQ)$_2$ with Bovine Serum Albumin

To test the plausibility of reaction 3.16, Zn(ZQ)$_2$ was titrated with increasing amounts of

BSA. BSA is a serum transport protein that modestly binds Zn^{2+} with an affinity constant

of $10^{7.3}$ M^{-1}.[84] Solutions were set up in 20 mM Tris-Cl pH 7.4 containing 0, 1, 2.5, 5, 10,

25, 50, 100, and 200 μM BSA and 10 μM Zn(ZQ$_{ACID}$)$_2$ was added to each solution and

allowed to react for 30 minutes before the emission spectra were recorded (**Figure**

3.27).
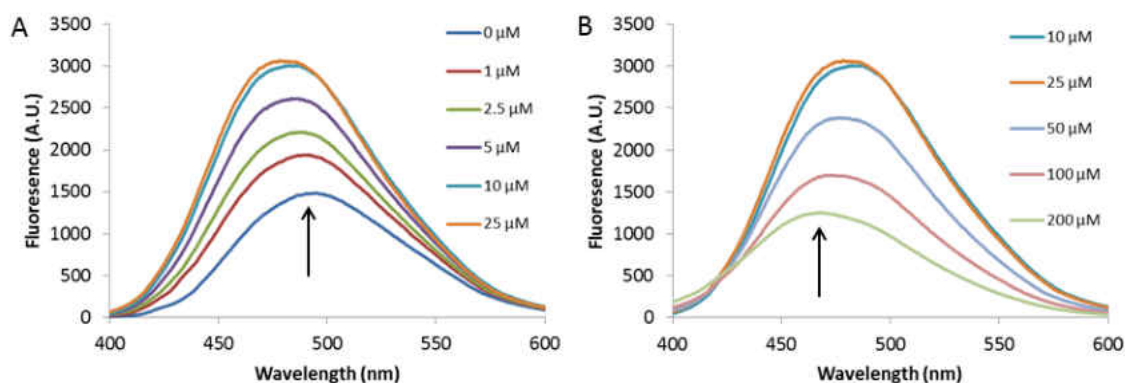
Figure 3.27. Fluorescence titration of Zn(ZQ$_{ACID}$)$_2$ with BSA. 10 μM Zn(ZQ$_{ACID}$)$_2$ was reacted with 0-200 μM BSA (0-25 μM in A, 10-200 μM in B) in 20 mM Tris-Cl pH 7.4 for 30 minutes before fluorescence was recorded. Arrows signify spectra at the start and end of the reaction.

As the concentration of BSA was increased, the fluorescence spectra became more and

more blue-shifted. At a final concentration of 200 μM BSA, the emission maximum had

shifted all the way to 467 nm from an original maximum at 492 nm (0 μM BSA). This

supports the hypothesis of Zn(ZQ$_{ACID}$)$_2$ reacting with the apo-Zn-site on BSA and forming

a ZQ-Zn-BSA ternary adduct (reaction 3.18).

$$Zn(ZQ_{ACID})_2 + BSA \rightleftarrows ZQ_{ACID}\text{-}Zn\text{-}BSA + ZQ_{ACID} \hspace{2cm} (3.18)$$
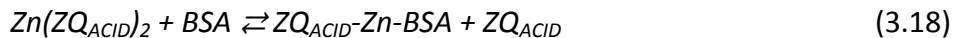
Importantly, the fluorescence intensities of the $Zn(ZQ_{ACID})_2$ species and the proposed ZQ_{ACID}-Zn-BSA adduct species were relatively equal to one another (arrowed spectra in **Figure 3.27**). This provides credence for the use of a $Zn(ZQ_{ACID})_2$ standard curve as a surrogate for measuring the approximate amount of Zn^{2+} being imaged within the Zn-proteome as outlined in section 3.1.3.

The solutions of 0, 25, and 200 μM BSA with $Zn(ZQ_{ACID})_2$ were chromatographed over Sephadex G-50 size exclusion columns, tracking both the fluorescence and Zn^{2+} (**Figure 3.27**). Based on the results in **Figure 3.26**, these concentrations represent the initial, midway, and final points in the titration, respectively. As expected, the chromatography of the solution containing only 10 μM $Zn(ZQ_{ACID})_2$ resulted in localization of both Zn^{2+} and fluorescence in the LMW pool. Additionally, the emission profiles of the fractions in this pool were centered at 492 nm, indicative of unperturbed $Zn(ZQ_{ACID})_2$. When the solution containing 25 μM BSA was separated using gel filtration, half of the Zn^{2+} was removed from the LMW pool in comparison with the 0 μM BSA solution. However, this Zn^{2+} was recovered in the proteomic region. The λ_{MAX} of these proteomic fractions was 468 nm, supporting the hypothesis of the formation of a ZQ-Zn-BSA adduct. Finally, the chromatographed 200 μM BSA solution showed that all the fluorescence and Zn^{2+} had migrated to the proteomic region of the chromatogram. Additionally, the fluorescence spectra of these fractions had a maximum emission at 465 nm. In these conditions, $Zn(ZQ_{ACID})_2$ had completely dissociated and rearranged itself as a ZQ_{ACID}-Zn-BSA adduct
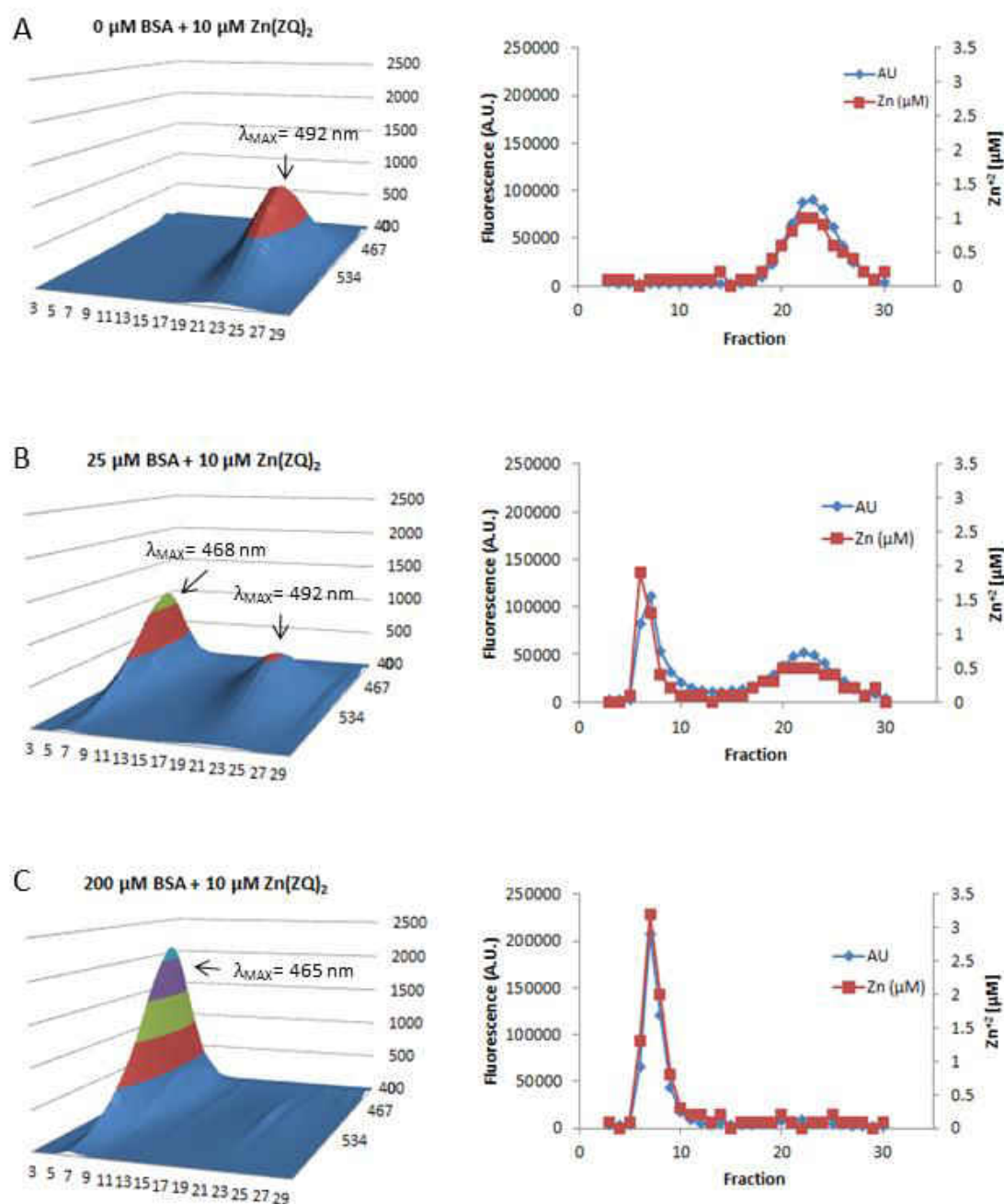
Figure 3.28. Sephadex G-50 gel filtration of Zn(ZQ_{ACID})_2 + BSA. Reaction mixtures of 10 μM Zn(ZQ_{ACID})_2 with 0 μM (A), 25 μM (B), and 200 μM (C) BSA were chromatographed using Sephadex G-50 gel filtration columns eluted with 20 mM Tris-Cl pH 7.4. Fluorescence and [Zn^{2+}] were recorded for each fraction.

species, thus suggesting that $Zn(ZQ)_2$ formed *in situ* is not immune to reacting with modest Zn^{2+} binding sites within the cellular proteome to form fluorescent adducts.

3.4.2. Reaction of $Zn(ZQ)_2$ with trypsin

To provide additional evidence for adduct formation and not simply a non-specific interaction between $Zn(ZQ_{ACID})_2$ and a protein causing a fluorescence shift, the experiment was repeated using trypsin, a protein not known to bind Zn^{2+}. Again, 0-200 μM Trypsin was treated with 10 μM $Zn(ZQ_{ACID})_2$ for 30 minutes before observing the fluorescence (**Figure 3.29**).

At all concentrations of Trypsin, there was no change in spectral intensity or position. Thus, the likelihood of a protein causing blue-shifted Zinquin emission spectra via non-specific interactions is minimized. Furthermore, when the 0, 25 and 200 μM Trypsin solutions were eluted over Sephadex G-50 size exclusion columns, the fluorescence and Zn^{2+} eluted within the LMW pool in all three cases. The emission spectra for these fractions were again centered at 492 nm, indicative of an intact $Zn(ZQ_{ACID})_2$ complex. Tracking the migration of Trypsin through the elution, the absorbance was recorded at 280 nm (Δ in **Figure 3.30C**). It was confirmed that Trypsin eluted in the HMW region while $Zn(ZQ_{ACID})_2$ migrated separately in the LMW fractions.
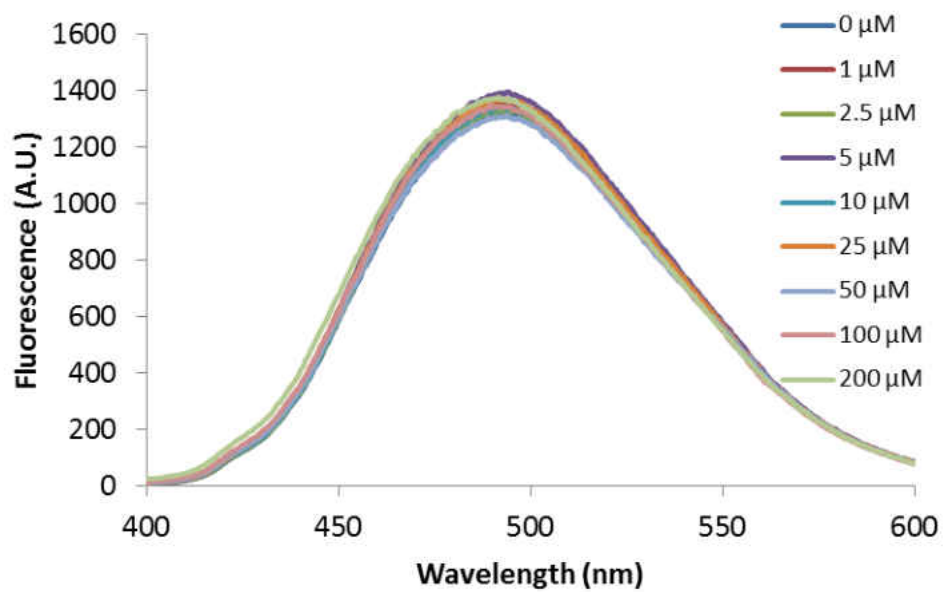
Figure 3.29. Fluorescence titration of Zn(ZQ$_{ACID}$)$_2$ with Trypsin 10 µM Zn(ZQ$_{ACID}$)$_2$ was reacted with 0-200 µM Trypsin in 20 mM Tris-Cl pH 7.4 for 30 minutes before fluorescence was recorded.
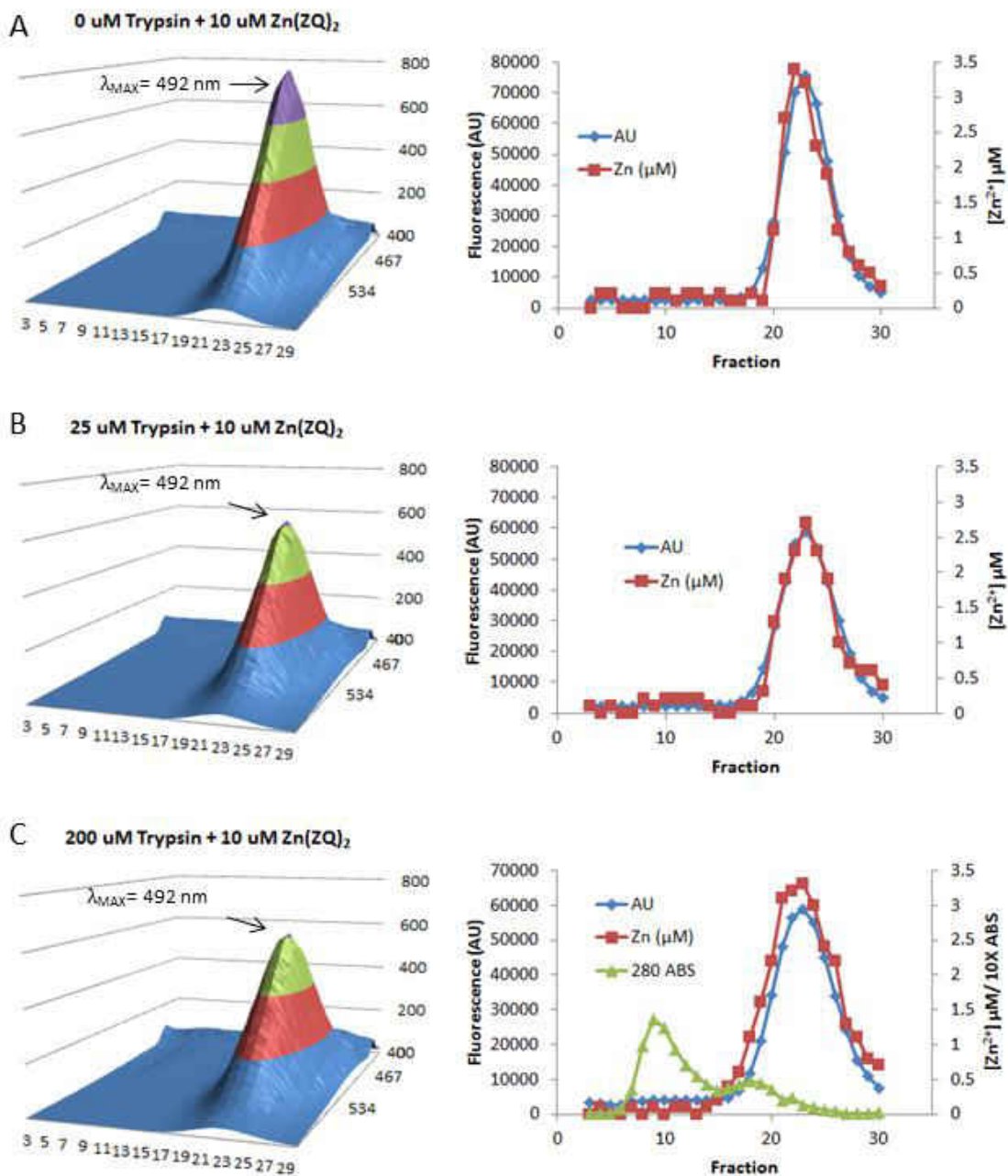
Figure 3.30. Sephadex G-50 gel filtration of Zn(ZQ$_{ACID}$)$_2$ + Trypsin Reaction mixtures of 10 μM Zn(ZQ$_{ACID}$)$_2$ with 0 μM (A), 25 μM (B), and 200 μM (C) Trypsin were chromatographed using Sephadex G-50 gel filtration columns eluted with 20 mM Tris-Cl pH 7.4. Fluorescence and [Zn^{2+}] were recorded for each fraction.

3.4.3. Reactions of $Zn(ZQ)_2$ with the LLC-PK$_1$ Zn-proteome

The reaction of $Zn(ZQ)_2$ with BSA provides support for the hypothesis that, in cells, the formation of ZQ-Zn-protein adducts from $Zn(ZQ)_2$ is possible given the existence of Zn-binding sites in the cellular environment (reaction 3.18). To strengthen this view, 10 µM LLC-PK$_1$ Zn-proteome was reacted with 10 µM $Zn(ZQ_{ACID})_2$ monitoring changes in the fluorescence emission (**Figure 3.31**). Within the time of mixing, the fluorescence maximum had immediately shifted to 482 nm (red line in **Figure 3.31A**) from 492 nm, the spectral maximum of $Zn(ZQ_{ACID})_2$. Over time, the fluorescence both increased and blue-shifted, underscored by comparing the ratio of fluorescence at 492nm to 470nm (**Figure 3.31B**). This fluorescence enhancement points to the formation of new Zn-ZQ species. The reaction neared completion after 30 minutes, resulting in a spectrum with λ_{MAX} =470 nm. Running the reaction mixture over a G-50 size exclusion column showed that the 10 nmoles of $Zn(ZQ_{ACID})_2$ added to the proteome had been absorbed into the HMW fractions, with a trace amount eluting in the LMW fractions (**Figure 3.31C,D**).

Furthermore, the HMW proteome fractions had emission profiles centered at 465 nm, indicative of ternary adducts, not $Zn(ZQ_{ACID})_2$. These fractions contained nearly all of the Zn^{2+} as well. Taken together, these data suggest that upon introduction to a proteomic environment, $Zn(ZQ)_2$ breaks down into ZnZQ, which binds to an apo-Zn-binding site (reaction 3.16), and ZQ, which reacts with a member of the Zn-proteome (reaction 3.17).
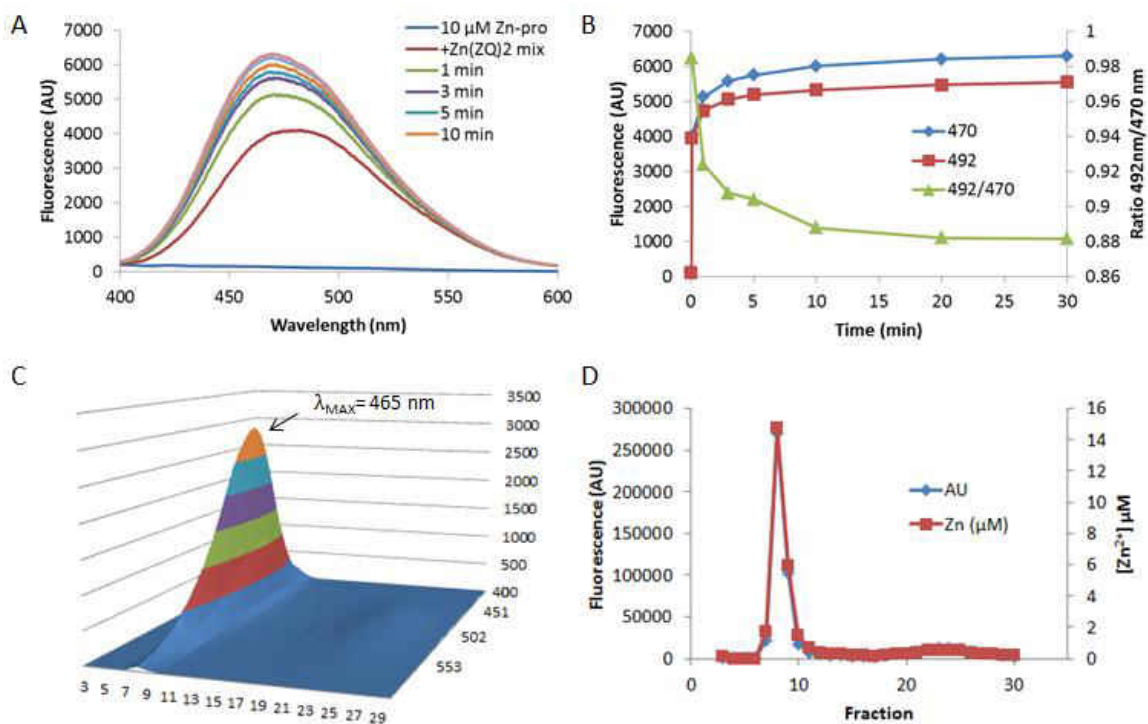
Figure 3.31. Fluorescence spectra of Zn-proteome + Zn(ZQ$_{ACID}$)$_2$. 10 μM isolated LLC-PK$_1$ Zn-proteome was reacted with 10 μM Zn(ZQ$_{ACID}$)$_2$ in 20 mM Tris-Cl pH 7.4 monitoring the fluorescence spectra (A) and the change in spectral maximum (B). Reaction mixture was chromatographed over a Sephadex G-50 gel filtration column eluted with 20 mM Tris-Cl pH 7.4. Fluorescence and [Zn^{2+}] were recorded in the eluted fractions (C, D).

Interestingly, the fluorescence enhancement seen here was different than that seen when $Zn(ZQ_{EE})_2$ was reacted with whole cells in which the fluorescence decreased (**Figure 3.26**). A possible explanation for this is that, in cells, the ethyl ester was being converted to the acid form, which is does not fluoresce as much when bound to Zn^{2+} when compared to the ethyl ester. Also, since $Zn(ZQ_{EE})_2$ is shuttled inside the cell, the photon generated from fluorescence must travel through a membrane in order to be detected, which may result in some scattering that gives the appearance of a decrease in fluorescence. Nevertheless, the shift in the emission maximum provides strong evidence for a chemical rearrangement of $Zn(ZQ)_2$ in both of these situations.

To provide further evidence for this reaction scheme, the Zn-proteome was reacted first with ZQ_{ACID}. Fully saturating the Zn-proteome with ZQ_{ACID} beforehand will effectively halt the second reaction (reaction 3.17) from occurring. As a result, without the Zn-proteome to react with, the concentration of free ZQ_{ACID} will increase, thus forcing the equilibrium of reaction 3.16 to left. This would result in a higher concentration of $Zn(ZQ_{ACID})_2$ at equilibrium versus an unsaturated Zn-proteome. Hence, 10 µM Zn-proteome was titrated with ZQ_{ACID} to a final concentration of 10 µM. The fluorescence increased with a λ_{MAX} of 470 nm, consistent with the formation of ZQ-Zn-protein ternary adducts (blue line in **Figure 3.32A**).

Upon addition of 10 µM $Zn(ZQ_{ACID})_2$, the total fluorescence was enhanced and red-shifted as expected for the addition of another fluorescent species with an emission maximum at a longer wavelength. However, the blue-shift back towards 470 nm was

less pronounced than the previous experiment. This is highlighted in **Figure 3.31B** and **Figure 3.32B** when comparing the 492/470 nm ratio for both the untreated and Zinquin treated proteomes (0.88 vs 0.95, respectively). In addition, the Zinquin-treated proteome reached completion much faster than the untreated proteome (5 min vs. 30 min). These two pieces of data indicate that the extent of reaction 3.16 had been altered. Fractionating the sample over a Sephadex G-50 size exclusion column showed that, unlike the untreated proteome, there was a significant amount of Zn^{2+} in the LMW pool (**Figure 3.32C,D**). Presumably, this was unreacted $Zn(ZQ_{ACID})_2$ as evidenced by the 492 nm fluorescence maximum. Taken together, this experiment provides credence for the hypothesis that $Zn(ZQ_{ACID})_2$ is not inert to reactions with the proteome, so long as there are available ZQ-Zn binding sites as well as ZQ binding sites within the proteome.

Additionally, the fact that the reaction of $Zn(ZQ_{ACID})_2$ with the proteome can be blocked by the addition of ZQ_{ACID} suggests that both sources of Zinquin—either from free ZQ_{ACID} or $Zn(ZQ_{ACID})_2$—interact with the same Zn-proteins. This hypothesis will be revisited in section 3.8.2.
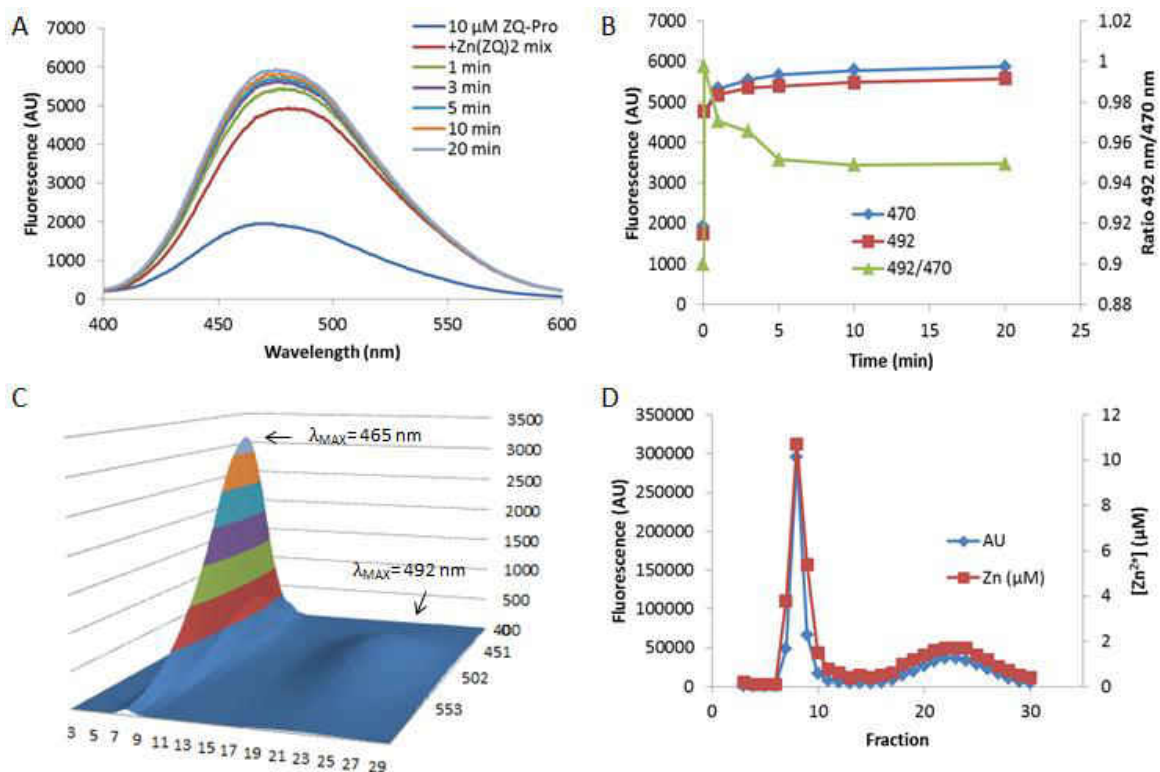
Figure 3.32. Fluorescence spectra of ZQ$_{ACID}$-Zn-proteome + Zn(ZQ$_{ACID}$)$_2$. 10 µM isolated LLC-PK$_1$ Zn-proteome was reacted with 10 µM ZQ$_{ACID}$ in 20 mM Tris-Cl pH 7.4 for 30 minutes (blue line in A). The solution was then reacted with 10 µM Zn(ZQ$_{ACID}$)$_2$ monitoring the fluorescence spectra (A) and the change in spectral maximum (B). Reaction mixture was chromatographed over a Sephadex G-50 gel filtration column eluted with 20 mM Tris-Cl pH 7.4. Fluorescence and [Zn^{2+}] were recorded in the eluted fractions (C, D).

3.5. Reexamination of Zinquin studies: *N*-ethylmaleimide with C6 rat glioma cells

Given the new perspective on how Zinquin functions, it calls into question previous chemical conclusions drawn from using such fluorophores in cellular experiments. One set of studies involved the use of Zinquin in conjunction with *N*-ethylmaleimide (NEM) as a way to understand zinc distribution and transport in C6 rat glioma cells.[34,35,85] NEM is a commonly used reagent that readily reacts with sulfhydryl groups.[86-88] Chemically, it acts as an excellent electrophile for nucleophilic attack from a thiol group resulting in the formation of a stable covalent bond (**Figure 3.33**).

N-ethylmaleimide
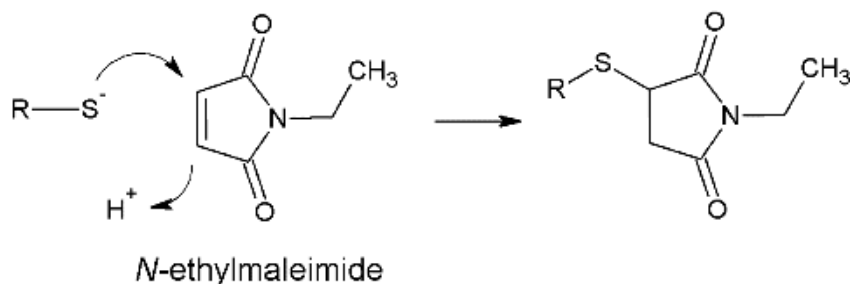
Figure 3.33. Reaction scheme of NEM with sulfhydryls

In a cellular environment, NEM attacks thiols on cysteine residues which may be coordinated to Zn^{2+}. With this in mind, NEM has been used as a trigger for stimulating Zn^{2+} release to which cellular responses are measured via the use of fluorescent probes such as Zinquin.[35,85,89] The studies involving cellular exposure of C6 rat glioma cells to NEM were revisited to understand the nature of the chemical species of the Zn^{2+} with which Zinquin is interacting.

3.5.1. Cytotoxicity of N-ethylmaleimide

Since the overall thiol concentration, and thus the reductive environment, can be vastly affected by this agent, the MTT viability assay was performed to monitor the toxicity of acute exposures to NEM in C6 glioma cells (**Figure 3.34**). The cytotoxic effects were a function not only of concentration, but more importantly length of incubation. An exposure for greater than 30 minutes led to significant decreases in cell viability. For this reason, experiments involving the use of live cells were kept to a maximum NEM exposure of half an hour.
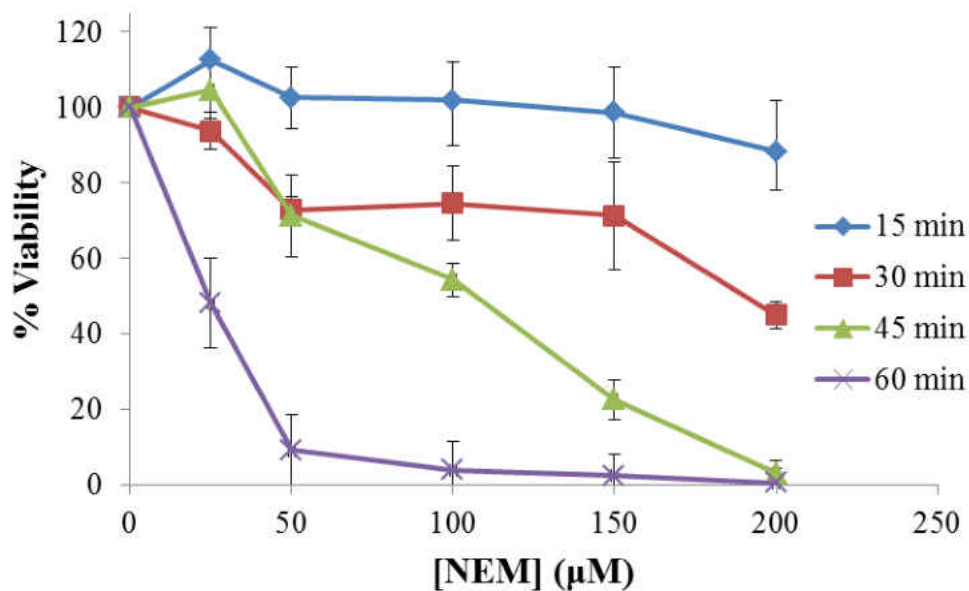
Figure 3.34. Toxicity of *N*-ethylmaleimide to C6 cells. C6 cells were treated with *N*-ethylmaleimide at varying concentrations and lengths of exposure. Viability was measured using the MTT cytotoxicity assay (average ± standard deviation, n=3). Taken from *Nowakowski et. al.* (2012)[90]

3.5.2. Effects of intracellular Zn^{2+} in response to N-ethylmaleimide as detected by

Zinquin

Moving forward, approximately five x 10^6 C6 cells were put into suspension with 1 mL of

DPBS. Exposing cells to 25 µM ZQ$_{EE}$ for 30 minutes resulted in a fluorescence

enhancement centered at 468 nm, consistent with the primary formation of ZQ-Zn-

protein adducts within the cell (blue line in **Figure 3.35A**). The cells were then treated

with 100 µM NEM and the fluorescence was monitored over time. In agreement with

previous studies, the fluorescence enhanced immediately after exposure. During a 20-

minute incubation period, the fluorescence increased 37±10% (average ± standard

deviation from three independent cell preparations). However, unlike previous studies

examining only one wavelength, fluorescence data from the entire spectrum showed an

increase in the ratio of fluorescence emissions at 492 nm (λ$_{MAX}$ of Zn(ZQ$_{ACID}$)$_2$) to 467 nm

(λ$_{MAX}$ of ZQ$_{ACID}$-Zn-Protein). This is indicative of a release of thiolate-bound Zn^{2+} which is

then sensed by Zinquin (reactions 3.19 and 3.20).

$$Zn\text{-}S\text{-}protein + NEM \rightarrow NEM\text{-}S\text{-}protein + Zn^{2+} \tag{3.19}$$
$$Zn^{2+} + 2\ ZQ_{ACID} \rightleftarrows Zn(ZQ_{ACID})_2 \tag{3.20}$$

In addition, this newly formed Zn(ZQ$_{ACID}$)$_2$ did not undergo further reaction with the

proteome (see section 3.4.3.) This is most likely due to the fact that the cells were

already treated with Zinquin. Hence, the reactive Zn-proteins were saturated with

Zinquin which lessened the reactivity of Zn(ZQ$_{ACID}$)$_2$ with the proteome (see section

3.4.3).

Figure 3.35. Fluorescence of Zinquin-treated C6 cells exposed to NEM. 5×10^6 C6 cells were suspended in 1 mL DPBS and reacted with 25 μM ZQ_{EE} for 30 minutes (blue line in A). Cells were treated with 100 μM NEM and the fluorescence (A) and changes in spectral maximum (B) were monitored for 20 minutes. Adapted from *Nowakowski et. al.* (2012)[90]

To further support this hypothesis, 2×10^8 C6 cells exposed to Zinquin and subsequently NEM were collected, lysed and fractionated over a Sephadex G-75 gel filtration column (**Figure 3.36**). The effects of exposure to 100 µM NEM were compared to cells exposed only to ZQ_{EE} under the same time and concentration conditions. Fractionating the NEM-treated cells showed that most of the fluorescence still remained in the proteomic region still having blue-shifted emission spectra, indicative of ZQ-Zn-protein adducts. However, the total fluorescence in this region was 16 ± 8% (n=3) higher compared to cells solely exposed to Zinquin. Looking further down the chromatograph showed that the LMW fluorescence had also increased 30 ± 11% in comparison to control cells. Fractions were then analyzed using AAS to determine the effect of NEM on Zn^{2+} distribution (**Figure 3.36B**). Importantly, cells exposed to neither Zinquin nor NEM retained all of the Zn^{2+} in the proteomic fractions. Exposure to ZQ_{EE} resulted in a decrease of Zn^{2+} within the pool that was recovered in the LMW region. The subsequent treatment with NEM resulted in a modest reduction of the Zn^{2+} in the proteome (9 ± 4%, n=3) versus the Zinquin-exposed cells. This reduction (2.2 ± 0.9 nmoles) was again recovered in the LMW pool. Thus, the addition of NEM mobilized some zinc from the Zn-proteome as detected by Zinquin.

Ellman's reagent was used to determine the amount sulfhydrals remaining after NEM treatment (**Figure 3.36C**). The formation of covalent linkages between NEM and reactive thiols makes these products undetectable by this assay. The introduction of

Figure 3.36. Sephadex G-75 gel filtration of ZQ-C6 cells exposed to NEM. Lysates of 2 x 10^8 C6 cells exposed to 25 µM ZQ_{EE} (o) followed by treatment with 100 µM NEM (■) were chromatographed over Sephadex G-75 gel filtration columns eluted with 20 mM Tris-Cl pH 7.4. Fluorescence (A), $[Zn^{2+}]$ (B), and thiol concentration of the eluted fractions were determined. (B) contains Zn^{2+} distribution of untreated cells control cells (◊). Taken from *Nowakowski et. al.* (2012)[90]

NEM to this system led to a 29 ± 5% reduction of reactive thiols in the proteome fraction. Furthermore, the LMW thiol pool—presumably glutathione—was completely extinguished. These chromatography experiments report that NEM reacts widely with cysteine residues from both the proteome as well as glutathione pools. This results in the release of Zn^{2+} from the proteome as detected by an increase in the amount of $Zn(ZQ_{ACID})_2$ in the LMW region (reactions 3.19 and 3.20). Additionally, NEM introduces new Zinquin binding sites within the proteome as evidenced by an increase in fluorescence compared to control despite the depletion of some Zn^{2+} from this pool (reactions 3.21 and 3.22).

$$NEM + Zn\text{-}protein \rightarrow Zn^*\text{-}protein\text{-}NEM \qquad (3.21)$$
$$ZQ_{ACID} + Zn^*\text{-}protein\text{-}NEM \rightleftarrows ZQ_{ACID}\text{-}Zn^*\text{-}protein\text{-}NEM \qquad (3.22)$$
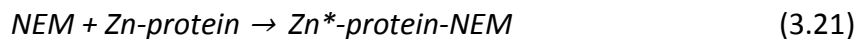
Whether this was mediated by the modification of an existing Zn-protein or the release of Zn^{2+} captured by Zinquin that reacted with a Zn-binding site on the proteome is yet to be determined.

3.5.3. Effects of intracellular Zn^{2+} in response to N-ethylmaleimide as detected by TSQ

The generality of these results were investigated by using a related quinosulfonamide probe, TSQ.   C6 cells were reacted with 25 µM TSQ and again the emission spectrum was monitored overtime. After a 30-minute incubation, the fluorescence had enhanced with a spectrum centered at 471 nm, indicative of the formation of TSQ-Zn-protein ternary adducts (blue line of **Figure 3.37A**).[56] Once the cells were reacted with 100 µM NEM, the fluorescence intensity increased similar to the Zinquin-treated cells with an
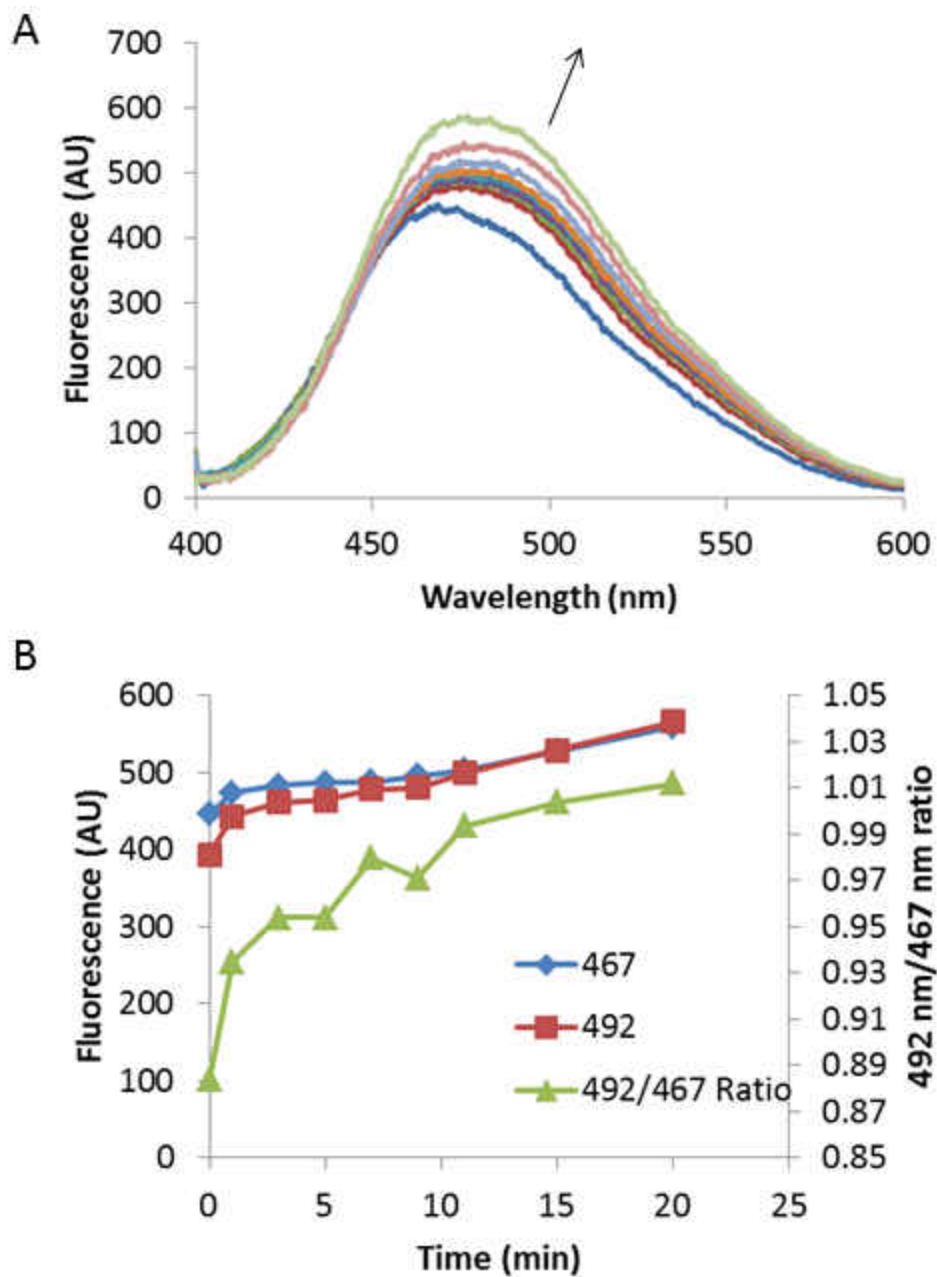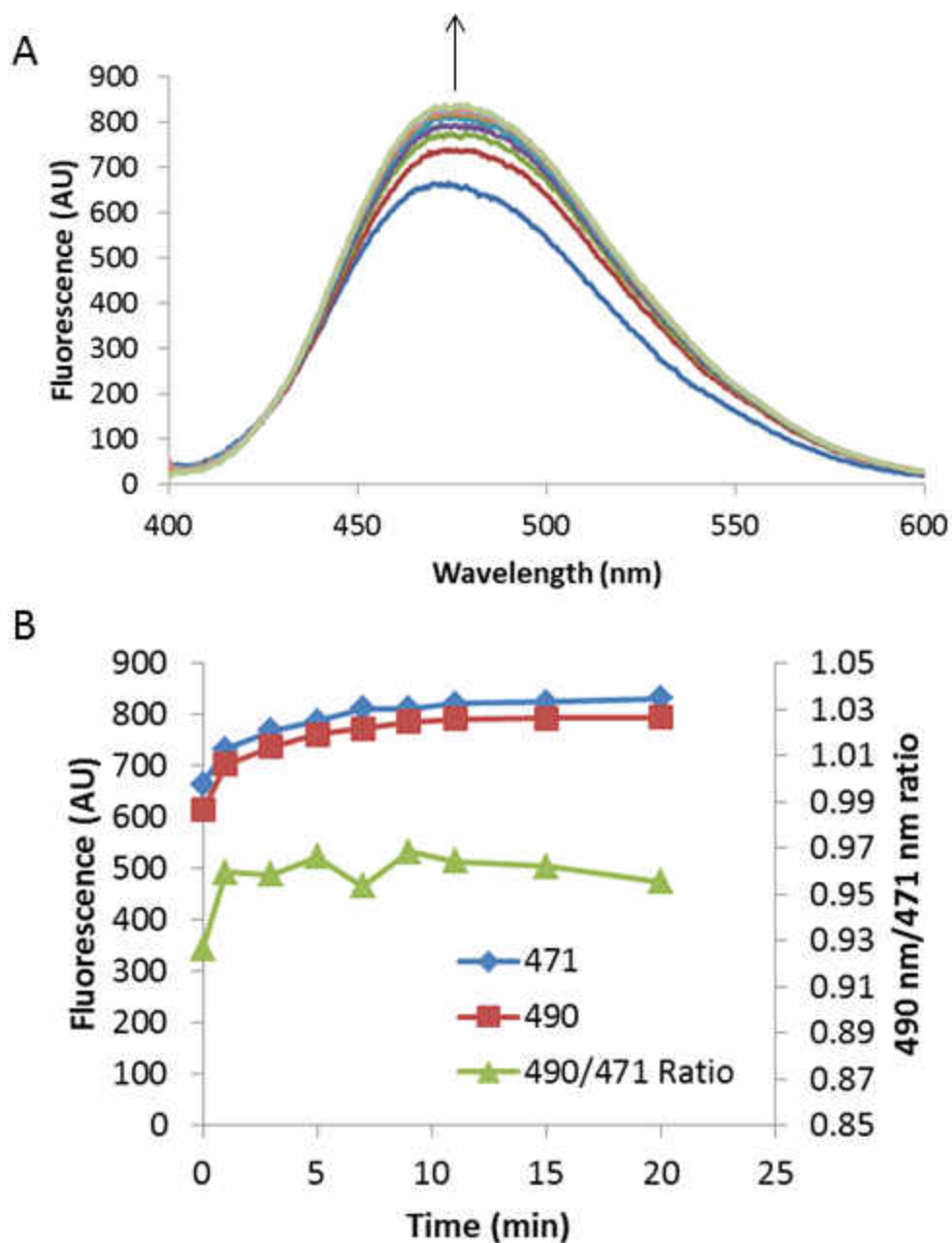
Figure 3.37. Fluorescence of TSQ-treated C6 cells exposed to NEM. 5 x 10^6 C6 cells were suspended in 1 mL DPBS and reacted with 25 µM TSQ for 30 minutes (blue line in A). Cells were treated with 100 µM NEM and the fluorescence (A) and changes in spectral maximum (B) were monitored for 20 minutes. Adapted from *Nowakowski et. al.* (2012)[90]

average enhancement of 28 ± 6% for three replicates. However, unlike the Zinquin-treated cells, after a small initial jump, the ratio of fluorescence between 490 nm (free Zn(TSQ)$_2$) and 471 nm (TSQ-Zn-protein ternary adducts) did not vary during the duration of the experiment (**Figure 3.37B**). This result implies that NEM did not release Zn^{2+} ions into the system, but rather coordination sites were opened for TSQ to form new adduct species (reactions 3.23 and 3.24).

$$NEM + Zn\text{-}protein \rightarrow Zn^*\text{-}protein\text{-}NEM \qquad (3.23)$$
$$TSQ + Zn^*\text{-}protein\text{-}NEM \rightleftarrows TSQ\text{-}Zn^*\text{-}protein\text{-}NEM \qquad (3.24)$$
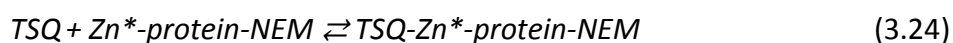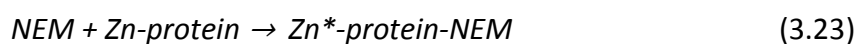
To provide further evidence for reactions 3.21 and 3.23, the cellular contents of 2 x 10^8 C6 cells exposed to TSQ and NEM were eluted over a Sephadex G-75 size exclusion column (**Figure 3.38**). The elution profile was again compared to cells exposed only to the fluorophore, in this case TSQ. Reacting C6 cells with TSQ resulted in fluorescence only in the HMW with no evidence of the formation of Zn(TSQ)$_2$. Notably, the λ_{MAX} of the fluorescence in the proteomic region was 468 nm, indicative of TSQ-Zn-protein species. Exposing these TSQ-treated cells to 100 µM NEM resulted in an increase of fluorescence in this region with an average enhancement of 30 ± 18% for three cell preparations. Interestingly, treatment with NEM did not mobilize any Zn^{2+} to the LMW (**Figure 3.38B**). This is in contrast to the result of NEM reacted cells monitored with Zinquin. Analyzing the fractions with DTNB showed that there was a 30 ± 6% reduction of sulfhydrals in the proteome and a complete depletion in the glutathione pool (**Figure 3.38C**). These changes in thiol concentration were identical to that seen in the cells reacted with Zinquin versus TSQ. Taken together, these data provide evidence for
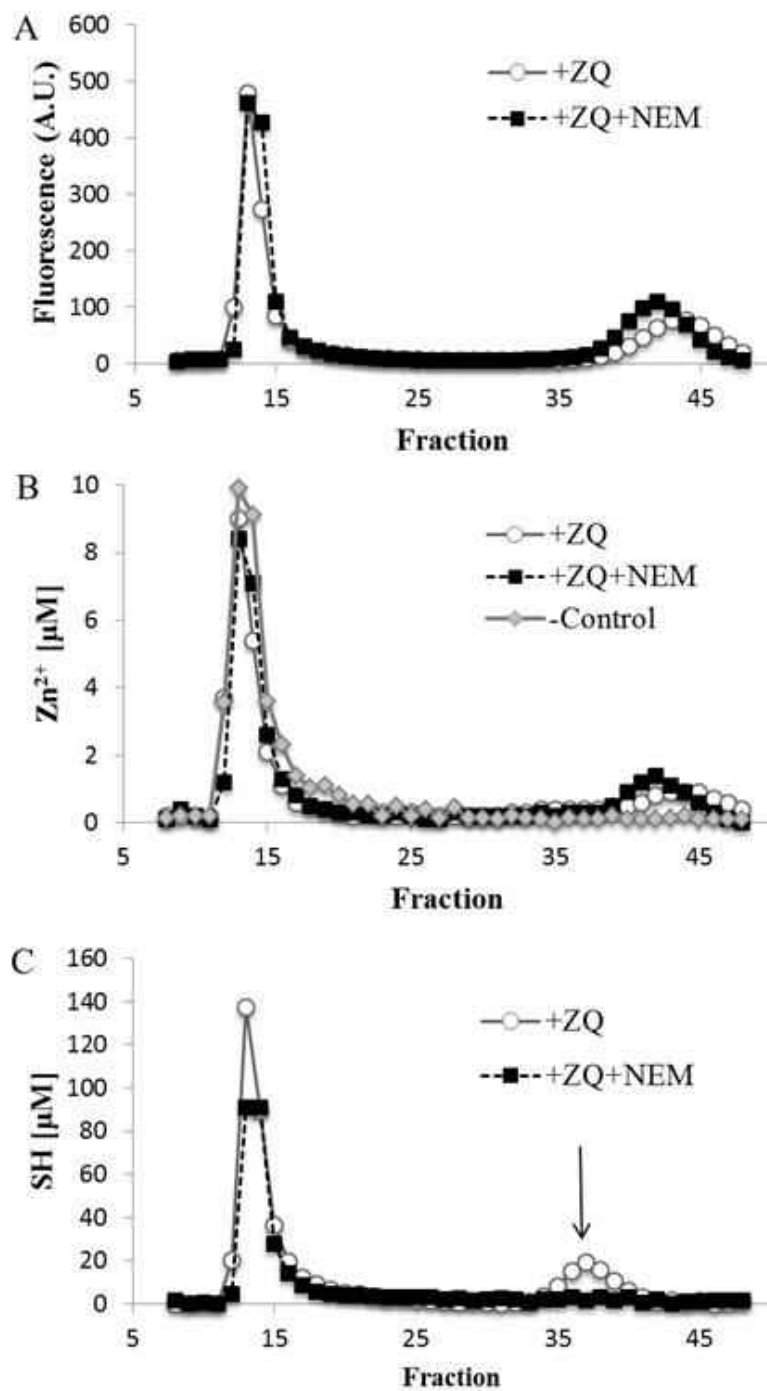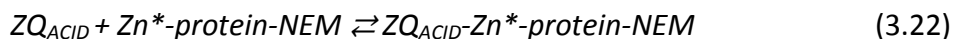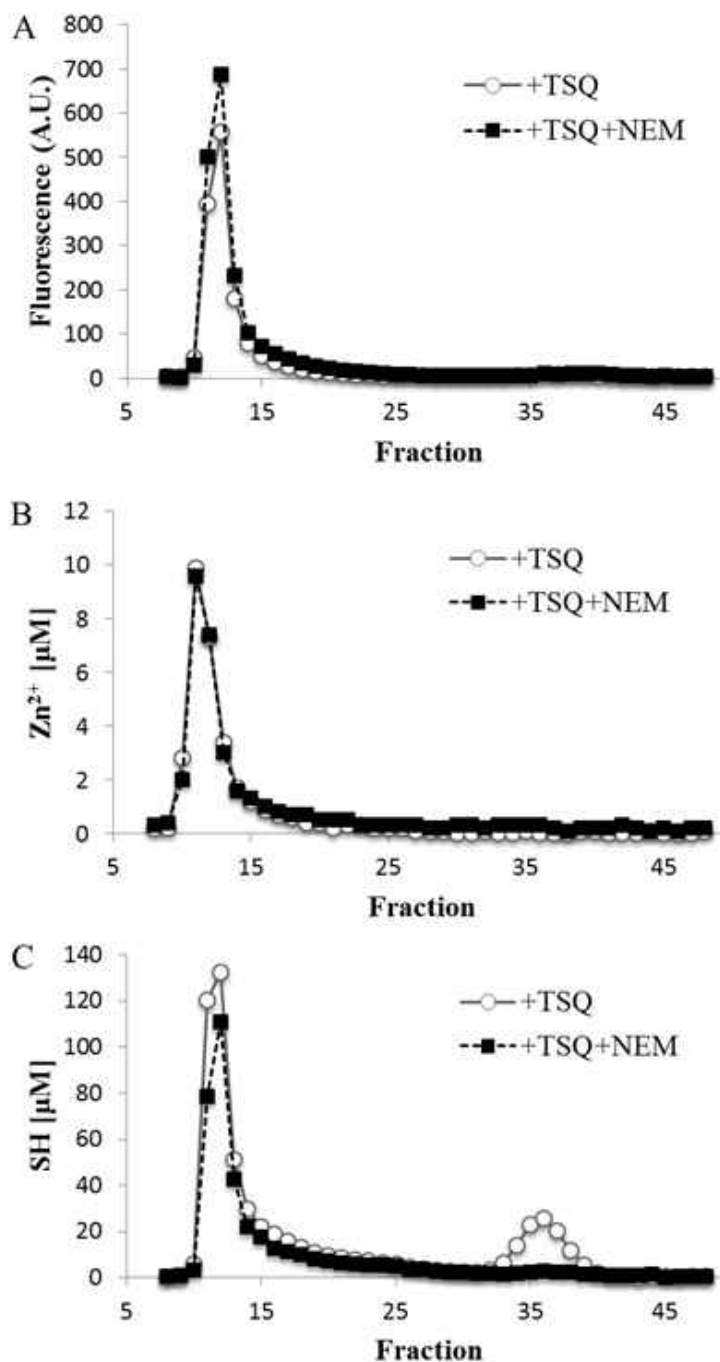
Figure 3.38. Sephadex G-75 gel filtration of TSQ-C6 cells exposed to NEM. Lysates of 2 x 10^8 C6 cells exposed to 25 µM TSQ (○) followed by treatment with 100 µM NEM (■) were chromatographed over Sephadex G-75 gel filtration columns eluted with 20 mM Tris-Cl pH 7.4. Fluorescence (A), [Zn^{2+}] (B), and thiol concentration of the eluted fractions were determined. (B) contains Zn^{2+} distribution of untreated cells control cells (◊).Taken from *Nowakowski et. al.* (2012)[90]

reactions 3.23 and 3.24 in which treatment with NEM results in formation of additional TSQ-Zn-protein adducts, which is in contrast to cells assayed with Zinquin. In all likelihood, the nature of reaction 3.21 and 3.23 in which NEM reacts with the proteome is similar in both systems. However, since the binding affinity for Zn^{2+} is higher for Zinquin than TSQ, Zinquin chelates some Zn^{2+} from these affected proteins while TSQ only forms additional adducts.

3.5.4. Reactions of the Zn-proteome with N-ethylmaleimide measured by Zinquin/TSQ

Further experiments were performed to determine the nature of interaction of NEM with the Zn-proteome in terms of its reactivity with these fluorescent probes. To begin, 10 µM of isolated proteome was reacted with 20 µM ZQ_{ACID} for 30 minutes followed by 100 µM NEM for an additional 30 minutes. A control was also performed by reacting the proteome with just ZQ_{ACID} under the same time conditions. Both reaction mixtures were then fractionated over Sephadex G-50 gel filtration columns (**Figure 3.39**).

After the elution of the control, the proteomic fractions retained a large majority of the fluorescence as well as the Zn^{2+} (**Figure 3.39A**). In addition, a small but noticeable amount of Zn^{2+} eluted as $Zn(ZQ_{ACID})_2$ in the LMW region. Reacting the Zn-proteome with NEM resulted in a significant change in the distribution of both Zn^{2+} and fluorescence (**Figure 3.39B**). Although the HMW still exhibited fluorescence (λ_{MAX} = 470 nm), it was significantly diminished to about 10% of the control. The majority of the fluorescence eluted in the LMW fractions having an emission maximum at 492 nm, indicative of $Zn(ZQ_{ACID})_2$. Furthermore, the amount of Zn^{2+} in the LMW fractions nearly doubled
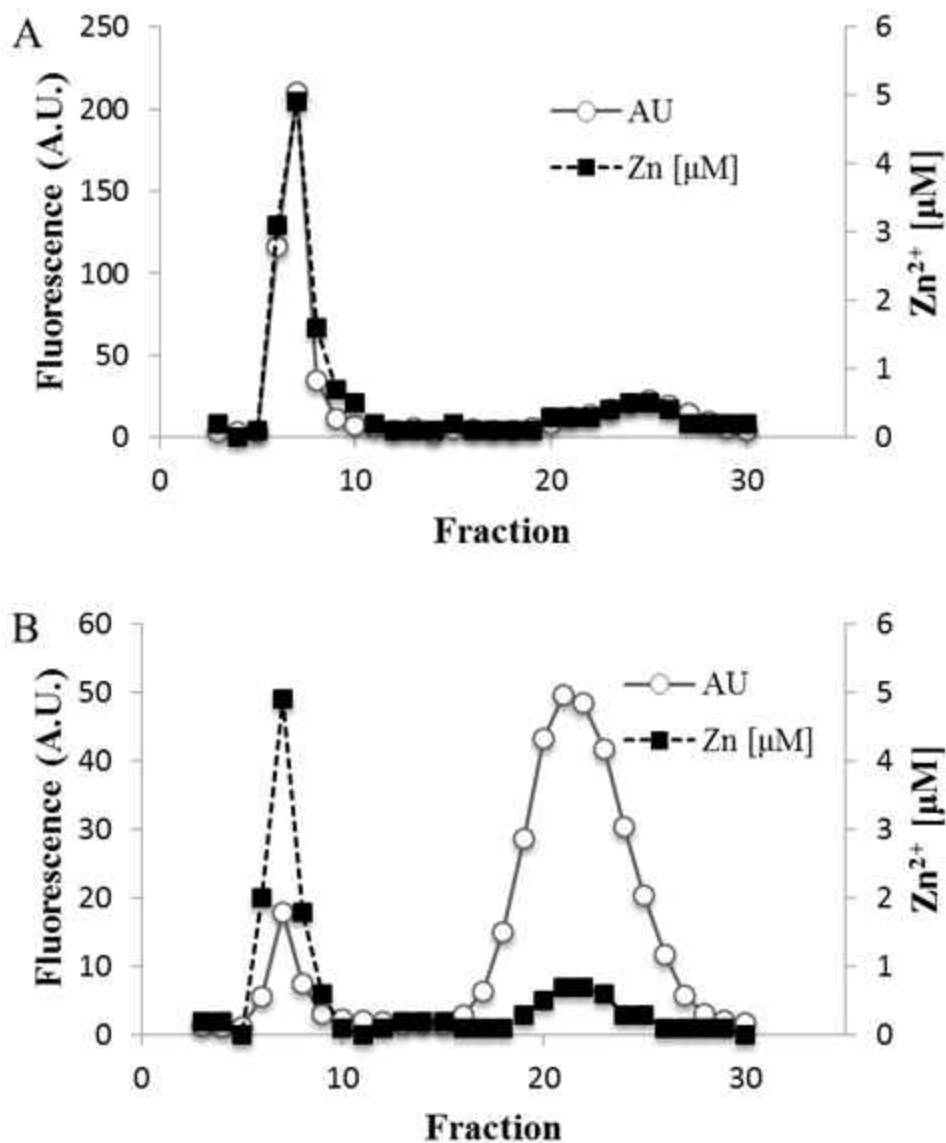
Figure 3.39. Sephadex G-50 of C6 Zn-proteome + ZQ$_{ACID}$ + NEM. 10 µM of isolated C6 Zn-proteome was reacted with 20 µM ZQ$_{ACID}$ in 20 mM Tris-Cl pH 7.4 for 30 minutes (A) followed by treatment with 100 µM NEM for 30 minutes (B). Reaction mixtures were chromatographed over Sephadex G-50 gel filtration columns eluted with 20 mM Tris-Cl pH 7.4. Fluorescence and [Zn^{2+}] were measured in each fraction. Taken from *Nowakowski et. al.* (2012)[90]

compared to the control (3.4 vs. 1.8 nmoles). Analysis of the sulfhydral content showed that the reaction of NEM was stoichiometric and went to completion. More specifically, 166 nmoles of thiols in the proteome reacted with 100 nmoles of NEM, resulting in 54 nmoles of reactive thiols remaining. Overall, these data indicate that NEM reacted with sulfhydryls in the proteome causing a Zinquin mediated release of Zn^{2+} as $Zn(ZQ_{ACID})_2$. Furthermore, the major reduction of the proteomic fluorescence after NEM exposure suggests that the Zn^{2+} ions in the Zinquin ternary complexes formed *in vivo* are most likely coordinated by thiols.[91]

Repeating this experiment using TSQ in place of Zinquin led to a markedly different result. Here, when TSQ was reacted with the proteome and eluted over the column, there was only fluorescence associated with the HMW fractions (**Figure 3.40A**). The emission maxima of these fractions were centered at 470 nm, indicative of TSQ-Zn-protein adducts. However, unlike the Zinquin-treated sample, no Zn^{2+} eluted in the LMW fraction as $Zn(TSQ)_2$. Even more striking was the difference in the reaction with NEM. Instead of a release of Zn^{2+} from the Zn-proteome recovered in the LMW, all the Zn^{2+} eluted in the HMW fractions (**Figure 3.40B**). However, the fluorescence intensity of these fractions was 90% higher versus the control, but stayed centered at 470 nm. These data imply that NEM opened up more Zn^{2+} sites for TSQ to form new fluorescent adducts without chelating any of the Zn^{2+}.

Generally speaking, these results state that even closely-related Zn-sensors, such as ZQ and TSQ, can yield surprisingly different fluorescent products. Hence, the overall effect
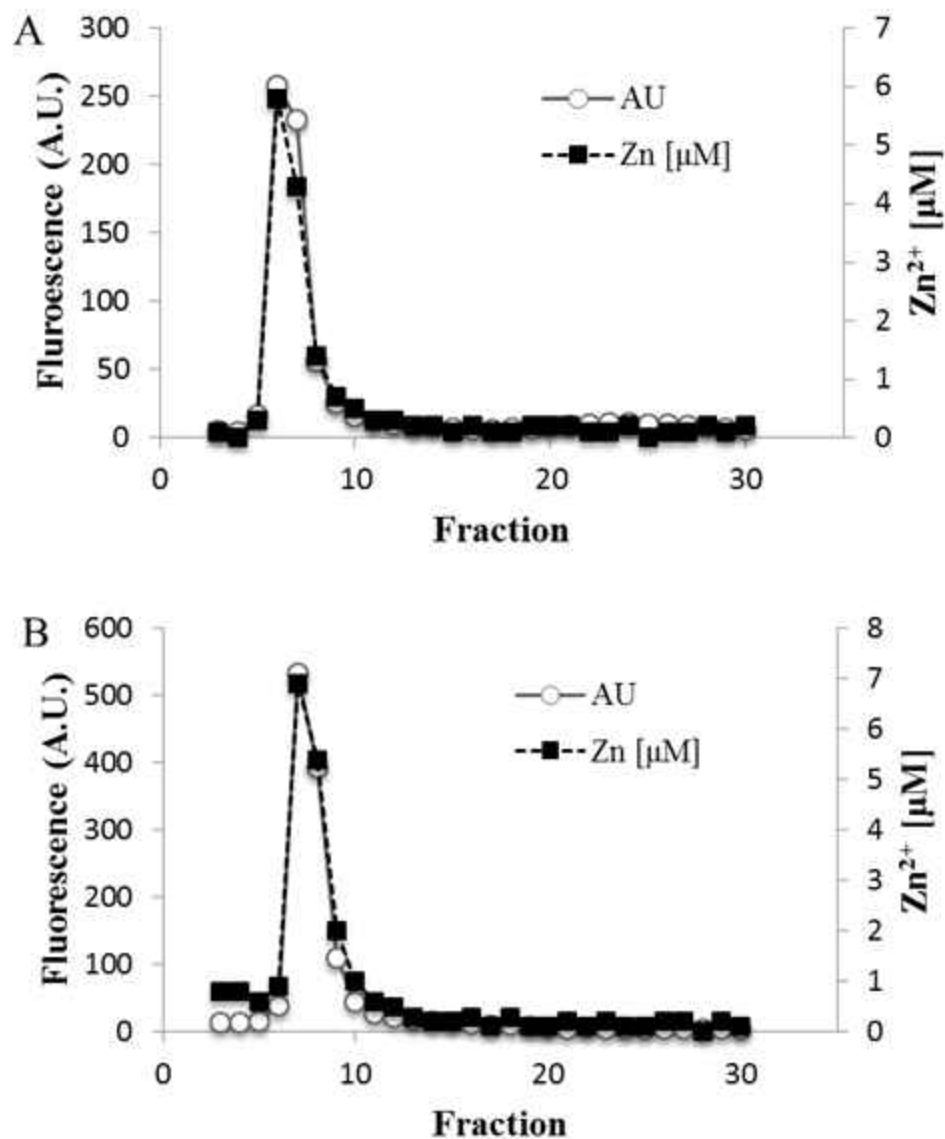
Figure 3.40. Sephadex G-50 of C6 Zn-proteome + TSQ + NEM. 10 µM of isolated C6 Zn-proteome was reacted with 20 µM TSQ in 20 mM Tris-Cl pH 7.4 for 30 minutes (A) followed by treatment with 100 µM NEM for 30 minutes (B). Reaction mixtures were chromatographed over Sephadex G-50 gel filtration columns eluted with 20 mM Tris-Cl pH 7.4. Fluorescence and $[Zn^{2+}]$ were measured in each fraction. Taken from *Nowakowski et. al.* (2012)[90]

of NEM on Zn^{2+} distribution is more so a function of the properties of the probe used rather than the direct reaction of NEM with intracellular thiols. Therefore, the authors' conclusion that NEM induced Zn^{2+} redistribution to intracellular compartments may simply be a result of using Zinquin as the reporter molecule and not necessarily Zn^{2+} release.

3.5.5. Effects of Glutathione on NEM exposure

In both Zinquin and TSQ treated cells, the glutathione pool was completely exhausted after exposure to N-ethylmaleimide. In addition, the extent of Zn^{2+} chelation with Zinquin was quantitatively less in whole cells compared to reactions with just the proteome. Given that cells contain millimolar concentrations of GSH, it stands to reason that glutathione provides some protection for thiols within the proteome.[92] To test this, the reactions of the proteome with NEM in the presence of Zinquin were repeated, supplementing back in different concentrations of GSH. Adding 50 nmoles of GSH to the reaction mixture resulted in a significant change in fluorescence and Zn^{2+} distribution compared to the reaction of the Zn-proteome with NEM without any glutathione (**Figure 3.41A** vs. **Figure 3.39B**). Fractionating the reaction mixture showed that the amount of liberated Zn^{2+} in the form of $Zn(ZQ_{ACID})_2$ was significantly diminished in the sample with glutathione. Also, no glutathione thiols were detected in the LMW fraction while the HMW thiols decreased by approximately 50 nmoles (115 nmoles of SH vs. 167 nmoles of SH in the control proteome). Supplementing the Zinquin treated proteome with 100 nmoles of GSH before the reaction with 100 nmoles of NEM gave an elution profile that
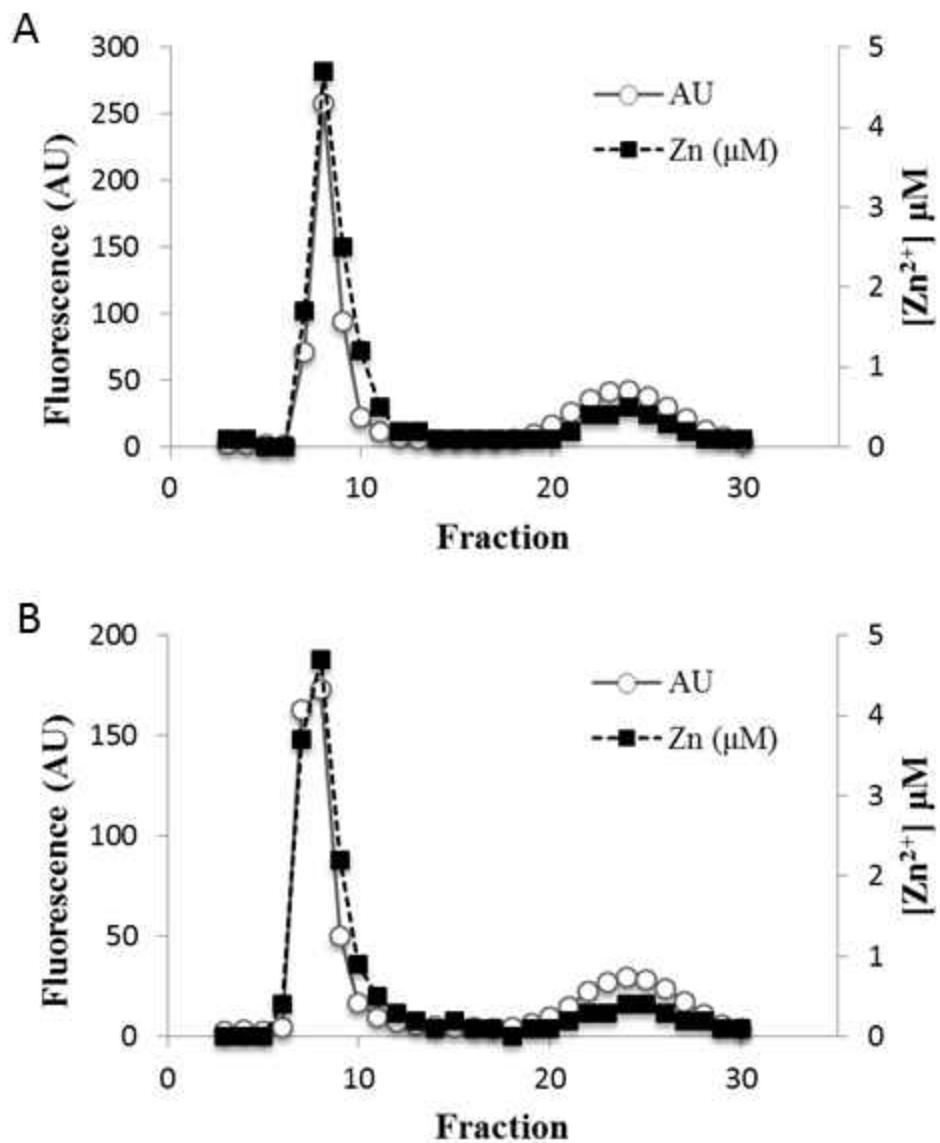
Figure 3.41. Sephadex G-50 of C6 Zn-proteome + ZQ$_{ACID}$ + NEM + GSH. 10 µM of isolated C6 Zn-proteome supplemented with 50 (A) and 100 (B) nmoles of glutathione was reacted with 20 µM ZQ$_{ACID}$ in 20 mM Tris-Cl pH 7.4 for 30 minutes followed by treatment with 100 µM NEM for 30 minutes. Reaction mixtures were chromatographed over Sephadex G-50 gel filtration columns eluted with 20 mM Tris-Cl pH 7.4. Fluorescence and [Zn^{2+}] were measured in each fraction.

was nearly identical to a proteome only reacted with Zinquin (**Figure 3.41B** vs. **Figure 3.40A**). In this case, the amount of reactive thiols in the proteome was not altered significantly (160 nmoles of SH vs. 167 nmoles of SH) and no reactive glutathione was recovered in the LMW region. Therefore, NEM reacts preferentially with glutathione over sulfhydryls located in the proteome, providing evidence for the protective nature of glutathione against thiol-modifying agents such as NEM.

To test this conclusion on a cellular level, C6 cells were treated with buthionine sulphoximine (BSO). BSO is a potent inhibitor of γ-glutamylcysteine synthetase, the first enzyme in the glutathione biosynthesis pathway, leading to a depletion in the glutathione concentration inside cells after exposure.[92]   C6 cells were grown in the presence of 700 μM BSO for 72 hours before being placed in suspension and reacted with 25 μM Zinquin ethyl ester and subsequently 100 μM NEM. (**Figure 3.42**)

After exposure to NEM, the fluorescence quickly increased with a 60% enhancement after a 20 minute period. This result was 20% higher than cells not grown in the glutathione biosynthesis inhibitor (**Figure 3.35**). Furthermore, the large increase in the ratio of fluorescence at 492 nm to 467 nm suggested a significant release of Zn^{2+} in the form of $Zn(ZQ_{ACID})_2$. In addition, the sulfhydryls in the BSO-treated proteome decreased 50% from the treatment with NEM, a 20% larger reduction than in cells with normal amounts of glutathione. This supports the hypothesis that the presence of GSH ameliorates some of the effects of *N*-ethylmaleimide exposure in cells.
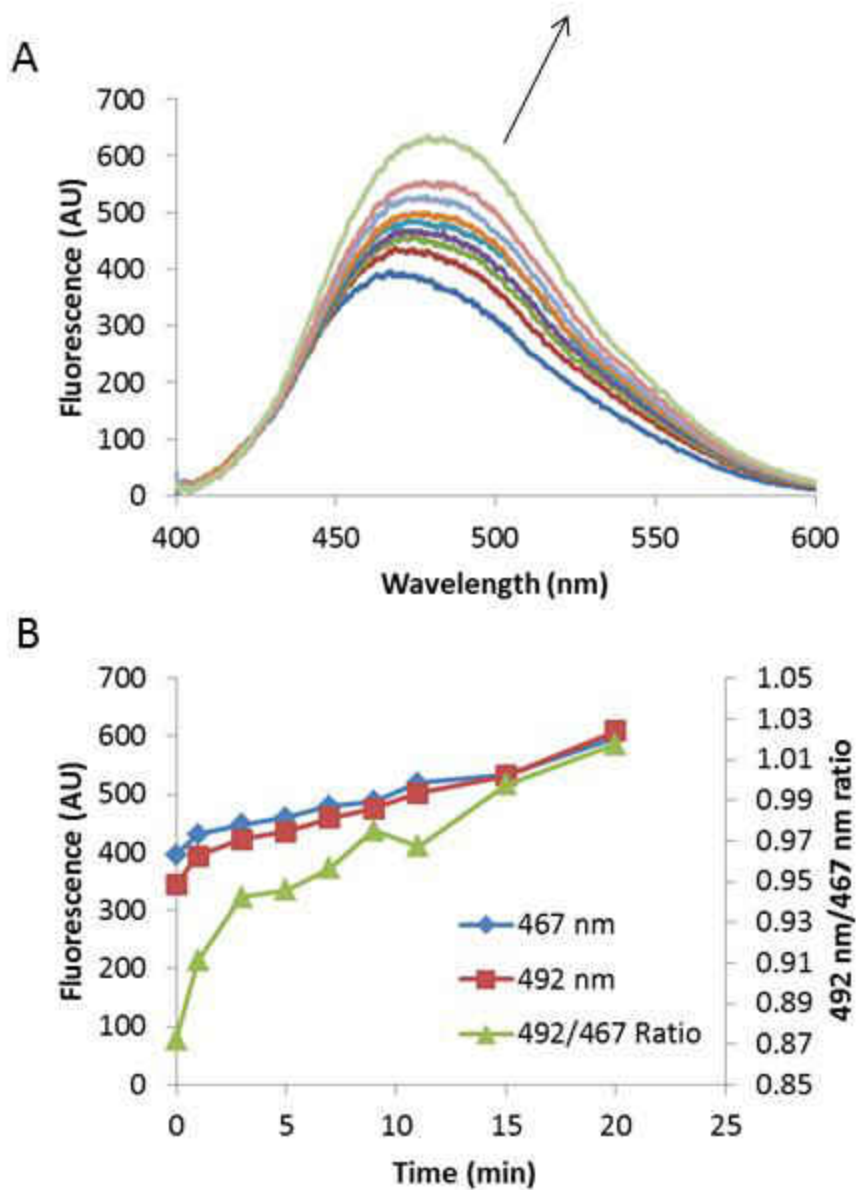
Figure 3.42. Fluorescence of BSO-treated C6 cells exposed ZQ$_{EE}$ followed NEM. 5×10^6 glutathione depleted C6 cells were suspended in 1 mL DPBS and reacted with 25 μM ZQ$_{EE}$ for 30 minutes (blue line in A). Cells were treated with 100 μM NEM and the fluorescence (A) and changes in spectral maximum (B) were monitored for 20 minutes.

3.5.6. Subcellular distribution of Zinquin fluorescence

Several reports using fluorophores such as Zinquin have claimed that Zn^{2+} ions are confined to intracellular vesicles sometimes referred to as "zincosomes."[34,35,77] One study claimed that exposure to NEM resulted in the accumulation of Zn^{2+} within these vesicles.[35] To determine whether Zinquin fluorescence was associated with a particular organelle, sequential centrifugal fractionation was performed on homogenized C6 cells exposed to Zinquin (**Figure 3.43**).
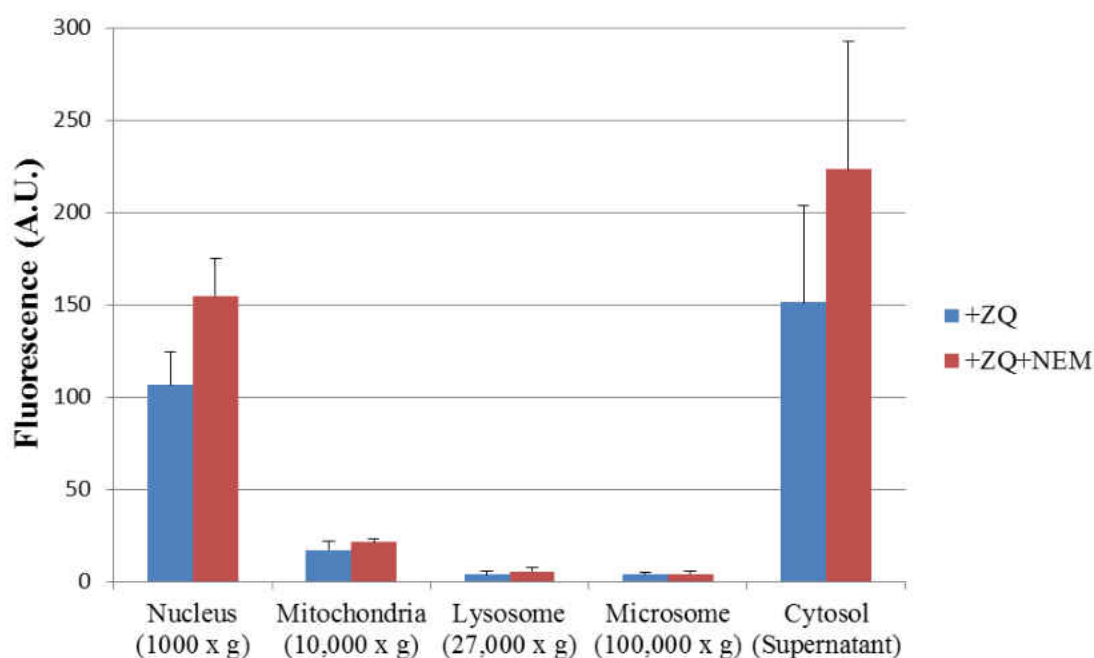
Figure 3.43. Subcellular Fractionation of ZQ-C6 cells treated with NEM. 2×10^8 C6 cells were exposed to 25 µM ZQ_{EE} for 30 min (blue) followed by 100 µM NEM for 30 min (red). Cells were homogenized and differentially centrifuged to isolate nuclear, mitrochondrial, lysosomal, microsomal, and cytosolic fractions. Fluorescence was recorded in each fraction adjusted for volume (bars indicate average intensity ± standard deviation, n=4). Taken from *Nowakowski et. al.* (2012)[90]

This was run in parallel with cells treated with NEM in addition to Zinquin. After subcellular fractionation, 37 ± 3% (n=4) of the total fluorescence was found in the first pool, considered the nuclear and cell membrane/debris fraction. The majority of the fluorescence was confined in the cytosol (supernatant), accounting for 57 ± 9% of the fluorescence. On the other hand, almost no fluorescence appeared in the microsomal fraction, suggesting that microsomes play a minimal role as intracellular targets for Zinquin. Comparing these results with cells additionally reacted with NEM showed that fluorescence enhancement occurred in both the nuclear and cytosolic fractions. Also, the emission spectrum for the NEM-treated cytosol fraction was red-shifted to 483 nm whereas the emission spectrum for the NEM-treated nuclear fraction remained at 467 nm. This suggests that the increase in "free" Zn^{2+} observed in the chromatography experiments of Zinquin-treated cells was likely due to the reaction of NEM with cytosolic Zn-proteins which resulted in the chelation of Zn^{2+} by Zinquin.

With these results in mind, the observations made by the authors were revisited.[35] The authors noted that an initial exposure of Zinquin-treated C6 cells to 100 μM NEM resulted in fluorescence enhancement throughout the entire cell, claiming a broad release of intracellular Zn^{2+}. Here, spectral and chromatographic data support a release of Zn^{2+} that was observed using Zinquin, but also an enhancement of fluorescence due to the formation of new ZQ-Zn-protein adducts. Therefore, what is being observed in fluorescence microscopy is likely a combination of these two fluorescent products.

Next, the authors state that over a 5 minute period, the fluorescence pattern became more punctate, causing the authors to surmise that the Zn^{2+} had been transported to an intracellular compartment. Yet, no such organelle was isolated during the subcellular fractionation. A possible rational would be that NEM allows Zinquin to chelate Zn^{2+} from proteins as described in reaction 3.2. Some of the newly formed $Zn(ZQ_{ACID})_2$ then reacts with proteins that are in fixed positions within the cell resulting in punctate fluorescent bodies. However, the increase in $Zn(ZQ)_2$ obtained after gel filtration as a result of exposure to NEM suggests that this reaction is limited. Moreover, since the authors reported micrographs of different cells during the incubation with NEM, it is unclear where inside the cell the punctate staining developed in reference to the basal Zinquin fluorescence. Therefore, it is difficult to assess these reactions with their data. Nevertheless, the reactions and results of exposing cells to NEM are more complex than the authors first claim.

3.6. Zinquin-Affinity Chromatography

3.6.1. Development of Zinquin-Affinity Chromatography

This thesis research provides compelling evidence that Zinquin binds to members of the Zn-proteome and not solely to Zn^{2+} ions. Therefore, to capture these intracellular targets, the Zinquin molecule was ligated to an agarose bead matrix to form a Zinquin affinity column (**Figure 3.44**).
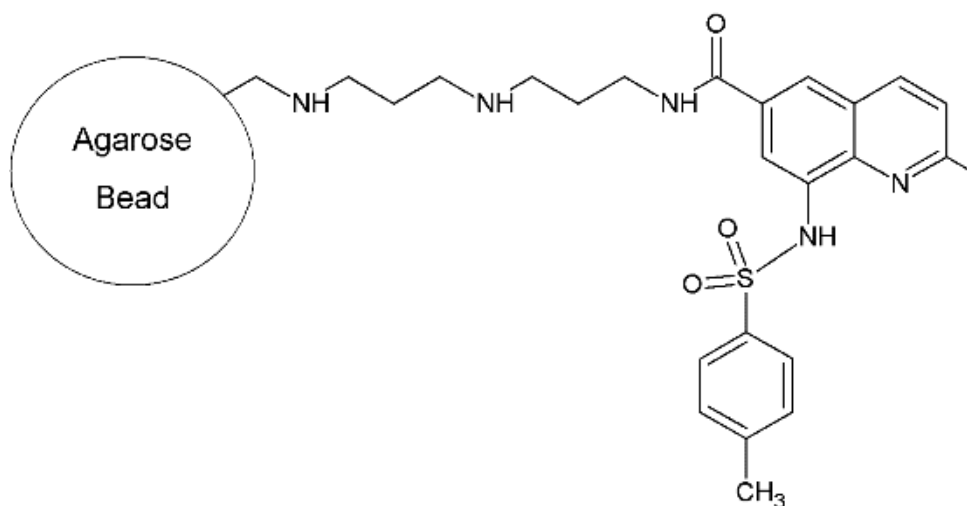
Figure 3.44. Schematic of Zinquin-affinity bead.

In theory, when the cell lysate is eluted over this column, the cellular proteins to which Zinquin binds can be purified. The LLC-PK$_1$ cell line was primarily used in these experiments because there is a minimal amount of Zn^{2+} chelation due to cellular exposure to Zinquin (see section 3.1.3). Therefore, the Zn-proteins eluted over the

column will more likely form ZQ-Zn-protein adducts and not surrender their metal cofactor to the column.

To begin, the proteome was isolated first by Sephadex gel filtration of the cellular lysate and then reacted in suspension with the Zinquin-beads. After one hour, the beads in suspension were transferred into a cuvette and the fluorescence was recorded. This result was compared to the fluorescence from beads reacted with 50 µM ZnCl$_2$ (**Figure 3.45**).
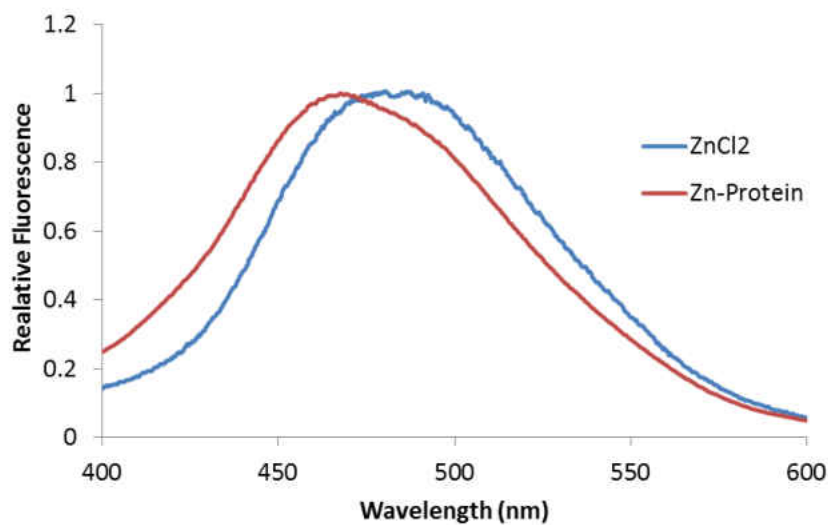
Figure 3.45. Fluorescence of ZQ-Aff beads with Zn-proteome and ZnCl$_2$.12.5 mg of Isolated LLC-PK$_1$ Zn-proteome were put in suspension with the Zinquin Beads in 20 mM Tris-Cl pH 7.4 for 1 hour and the fluorescence was recorded (red, λ_{MAX} = 465 nm). Fluorescence was compared to Zinquin beads treated with 50 µM ZnCl$_2$ in 20 mM Tris-Cl pH 7.4 (blue, λ_{MAX} = 481 nm)

As expected, the emission spectrum of the Zinquin beads treated with the proteome was blue-shifted, indicative of the formation of Zinquin bead-Zn-protein adducts. This was in contrast to the fluorescence of beads in the presence of Zn^{2+} ions alone which

had a maximum emission at 481 nm. Presumably, the reason for the emission maximum at 480 nm and not 492 nm (λ_{MAX} for Zn(ZQ$_{ACID}$)$_2$) is due to the conversion of the carboxylic acid on Zinquin to an amide linkage during the synthesis process. Since the amide bond is chemically more similar to an ester than a carboxylate, the fluorescence properties of these beads are more similar to Zn(ZQ$_{EE}$)$_2$, which has a λ_{MAX} of 481 nm.

After transferring the beads back to the column, the affinity column was washed with 20 mM Tris-Cl pH 7.4 and the bound protein was eluted using 0.2M Glycine-Cl pH 2.8 (**Figure 3.46**).
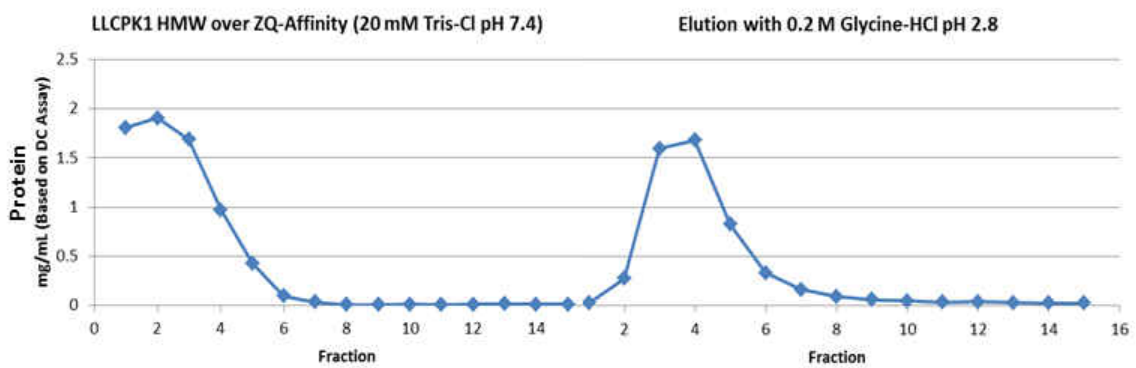
Figure 3.46. Elution of ZQ-aff column. Zinquin beads from **Figure 3.47** were washed in 20 mM Tris-Cl pH 7.4 and eluted with 0.2 M Glycine-Cl pH 2.8. The amount of protein in collected fractions was determined using the DC protein assay.

Assaying the fractions for protein showed that nearly 40% of the protein loaded became bound onto the column. This result was unexpectedly high since Zn-proteins comprise of approximately 10% of the total cellular proteome and Zinquin only reacts with about 15% of this Zn-proteome (see section 3.1.3).[5] This led to the hypothesis that there was

significant non-specific protein binding to the column matrix. In an attempt to reduce these non-specific interactions, the buffering system was modified. Unfortunately, running the column in higher conductivity (25 mM Tris-Cl pH 7.2 containing 0.10 M NaCl) or in a different buffer (50 mM HEPES pH 7.5) showed no significant variance in the percentage of bound protein. This lead to the synthesis of another affinity column, this time made with sodium acetate instead of Zinquin (**Figure 3.47**).
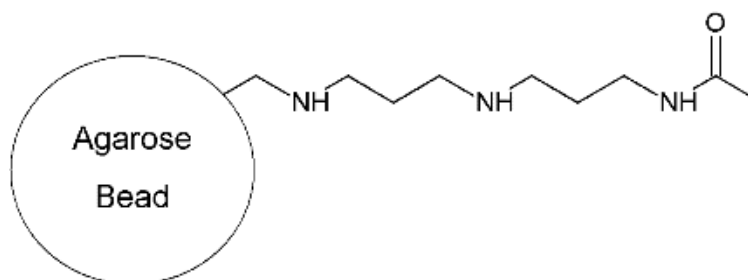
Figure 3.47. Schematic of acetate column.

The proteome was run over this column first in order to in the remove proteins that have an affinity for the bead matrix (**Figure 3.48A**). Interestingly, just over 50% of the protein loaded was captured by the acetate column, signifying significant amounts of non-specific protein interactions with the agarose beads. The protein that did not bind to the acetate column was then loaded onto the Zinquin affinity column (**Figure 3.48B**). Here, a significantly smaller amount of protein associated with the Zinquin beads, accounting for approximately 5% (by mass) of the total protein used in this prep. It was hypothesized that the proteins within this pool represent the subset of proteome to which Zinquin binds in cells.
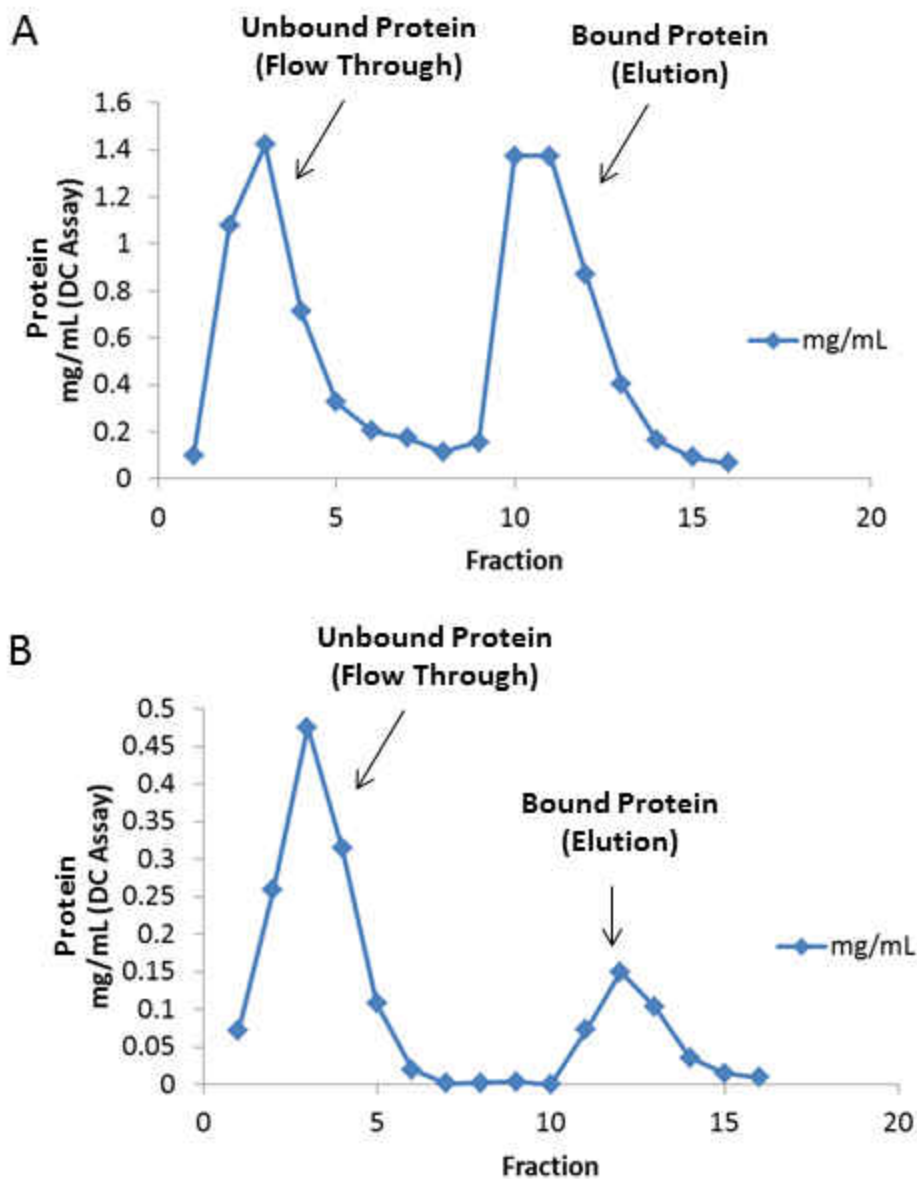
Figure 3.48. Elution of acetate and ZQ-aff columns. 10 mg of isolated LLC-PK$_1$ Zn-proteome were put in suspension with acetate beads in 20 mM Tris-Cl pH 7.4 for 45 minutes. Column beads were washed in 20 mM Tris-Cl pH 7.4 and eluted with 0.2 M glycine-Cl pH 2.8 (A). Unbound protein was put in suspension with Zinquin affinity beads for 1 hour. Beads were washed in 20 mM Tris-Cl pH 7.4 and eluted with 0.2 M glycine-Cl pH 2.8 (B). Protein concentration was determined via DC protein assay.

3.6.2. Reexamination of the reaction of the Zn-proteome with N-ethylmaleimide using Zinquin-affinity chromatography

In order to validate this method as well as provide additional evidence for the conclusions drawn in section 3.5.4, the reaction between the Zn-proteome and *N*-ethylmaleimide was revisited. After isolation of the proteome from C6 cells, 1.4 mL of 14 μM Zn-proteome (20 nmoles of Zn^{2+}) was chromatographed through the acetate column. The protein that did not bind to the beads was then run over the Zinquin affinity column. After the bound proteins were eluted using 0.2 M glycine-Cl pH 2.8, the protein and Zn^{2+} concentrations of the sample fractions were measured (**Figure 3.49**). Since Zn^{2+} analysis via AAS results in sample loss, the amount of Zn^{2+} in the acetate flow through pool was inferred from the sum of the Zn^{2+} recovered off the Zinquin column. 17% of the total protein was captured by the Zinquin column and 14% of the total Zn^{2+} (2.9 nmoles). This Zn^{2+} result was slightly lower than the value reported in section 3.1.3 in which it was suggested that 20% of the proteomic Zn^{2+} was being sensed by Zinquin in cells. This lower result can be explained by Zn-proteins that bind to Zinquin but also have an affinity for the agarose beads and thus being removed in the acetate step. In addition, the ligated Zinquin molecule on the agarose bead may induce steric hinderance in a ZQ-Zn-protein adduct.
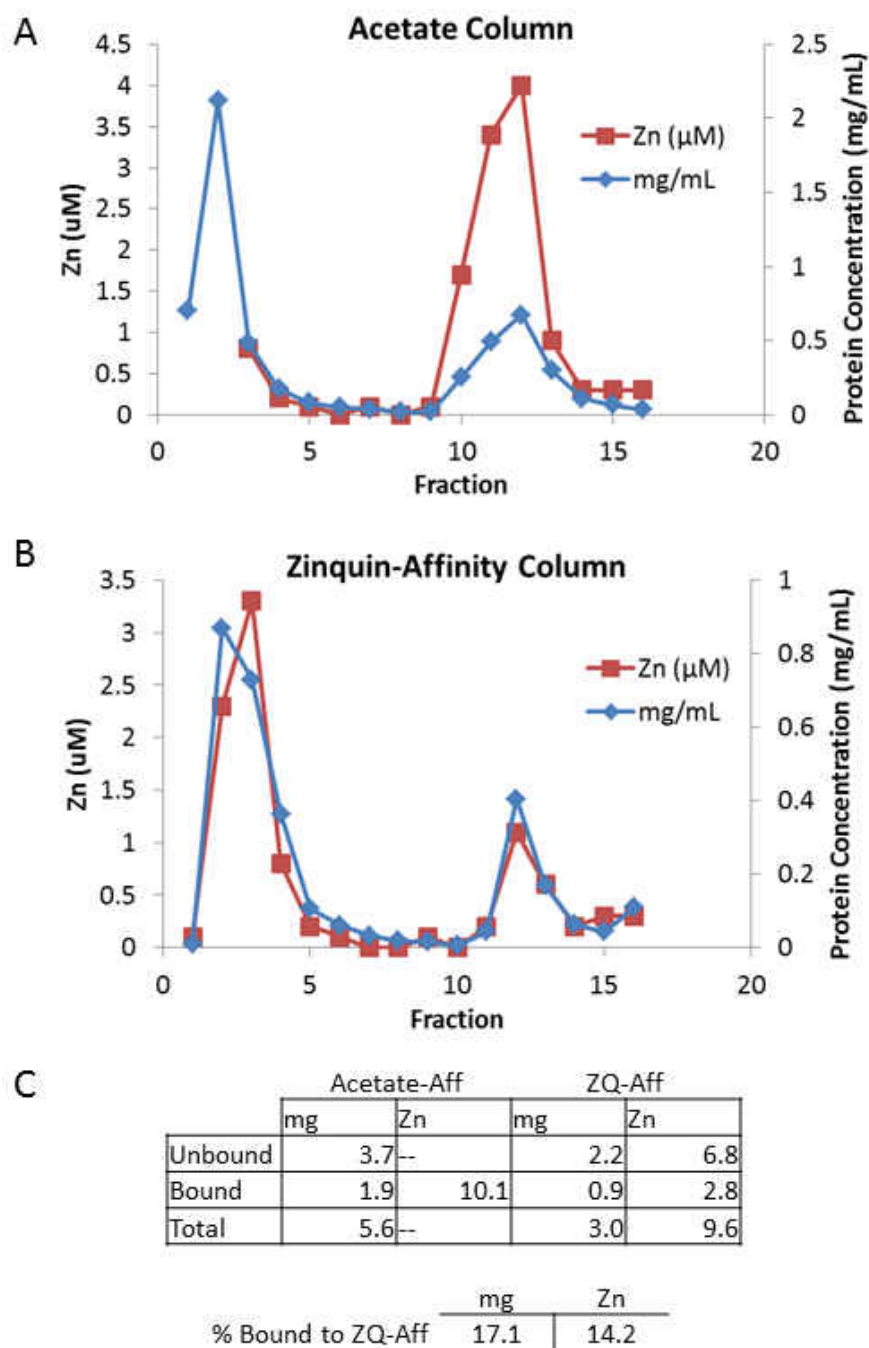
Figure 3.49. C6 proteome over acetate and ZQ-aff columns. 20 nmoles (based on Zn^{2+}) of isolated C6 Zn-proteome were suspended in acetate beads for 40 min. Beads were washed using 20 mM Tris-Cl pH 7.4 and eluted using 0.2 M glycine-Cl pH 2.8 (A). Unbound protein was suspended in Zinquin-affinity beads for 40 min. washed with 20 mM Tris-Cl pH 7.4, and eluted with 0.2 M glycine-Cl pH 2.8 (B). The amounts of protein and Zn^{2+} in each pool are listed in (C).
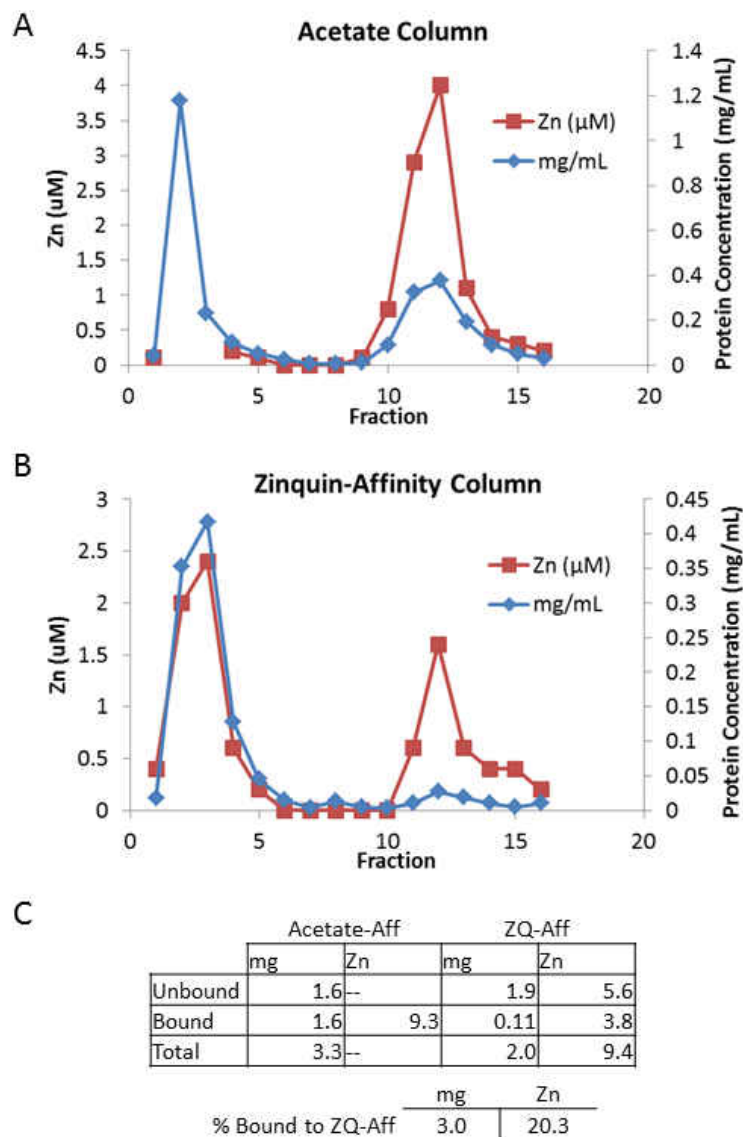
Figure 3.50. NEM treated C6 proteome over acetate and ZQ-Aff columns. 20 nmoles (based on Zn^{2+}) of isolated C6 Zn-proteome were reacted with 100 µM NEM for 30 min in 20 mM Tris-Cl pH 7.4. Reaction mixture was suspended in acetate beads for 40 min. Beads were washed using 20 mM Tris-Cl pH 7.4 and eluted using 0.2 M glycine-Cl pH 2.8 (A). Unbound protein was suspended in Zinquin-affinity beads for 40 min. washed with 20 mM Tris-Cl pH 7.4, and eluted with 0.2 M glycine-Cl pH 2.8 (B). The amounts of protein and Zn^{2+} in each pool are listed in (C).

The experiment was then repeated with 20 nmoles of a proteome exposed to 100 µM NEM for 30 minutes (**Figure 3.50**). The analysis of Zn^{2+} in the column fractions showed that 20% of the total Zn^{2+} (3.8 nmoles) was bound to the Zinquin column. This was a 30% increase in the amount of Zn^{2+} bound to the column versus control (3.9 vs. 2.9 nmoles Zn^{2+}). In contrast, the amount of protein that was captured by the Zinquin column was diminished down to 3%. This result was consistent with the conclusions drawn from the size exclusion data in section 3.5.4. Specifically, the exposure of the isolated proteome to NEM results in the ability for Zinquin to bind more Zn^{2+} ions. In the size exclusion experiments, this was achieved in solution as free $Zn(ZQ_{ACID})_2$, while here it was done with Zinquin immobilized to a matrix (**Figure 3.39B**). In addition, treatment with NEM causes the proteome to lose its ability to form adducts with Zinquin, demonstrated here by the decline in protein bound to the Zinquin column. Taken together, these data provide validity for this new method of isolating proteins that react with Zinquin in cells.

3.6.3. *Optimization of elution conditions*

Another consideration taken into account during the development of this purification method was the manner of eluting the bound proteins from the affinity columns. Under the manufacturer's suggestion, the initial experiments were performed using a low pH buffer, specifically 0.2 M glycine-Cl pH 2.8. However, putting a Zn-protein in such an environment can lead to not only protein denaturation, but also the release of their metal cofactors. This procedure leads to the inability to perform subsequent analytical techniques to test the protein for bound Zn^{2+}, as seen in their reactivity with Zinquin.

To overcome this obstacle, new elution buffers were tested. The most logical alteration would be a buffer containing an excess of the ligand attached to the affinity column, in this case Zinquin. This is how antibodies are eluted off of affinity columns ligated with a peptide of interest (CarboxyLink^{TM} technical guide). It was determined by running a standard Zn^{2+} solution over the column that approximately 180 nmoles of Zinquin were ligated to this column, corresponding to a rough concentration of 95 μM Zinquin in the bead matrix. Per the manufacturer's recommendation, a proteome bound to the Zinquin column was eluted in a buffer with 10X the free ligand concentration, in this case a Tris buffer containing 950 μM of Zinquin acid. However, putting the column in suspension with this buffer over a two hour period resulted in a minimal elution of the proteins that were bound (<5%, near the limit of detection using the DC protein assay). Therefore, in order to successfully compete with the Zinquin ligated to the agarose beads, a higher concentration of free Zinquin in solution would be needed.

There exist two major experimental challenges with a concentrated Zinquin buffer. First, a concentration of 950 μM Zinquin acid approaches the solubility limit in an aqueous environment. Thus, organic solvents need to be added to the buffer as well, which could potentially denature the eluted proteins within this system. Second, creating a usable amount of highly concentrated Zinquin buffer would require hundreds of milligrams of this expensive reagent, making it cost prohibitive. Therefore, other elution buffers were explored.

The next elution system tested was that of a high ionic strength. Hence, the 33 nmoles of isolated proteome from C6 cells was chromatographed over the acetate and Zinquin-affinity columns, this time eluting the bound proteins with a 20 mM Tris-Cl pH 7.4 buffer containing 1 M potassium chloride (**Figure 3.51**).

Interestingly, when the DC protein assay was performed on the eluted fractions, the solution mixtures turned slightly cloudy. Visually inspecting the fractions showed that the copper product was only found in a few fractions containing protein. Yet the turbidity of the samples was enough to affect the absorbance values in all the elution fractions. Thus, an accurate measurement of protein concentration using this assay could not be determined in the fractions containing this salt. Furthermore, when AAS was performed on the fractions, there was an extremely high Zn^{2+} background response (>3.0 µM) in the eluted fractions. This was most likely due to absorbance interference on the AAS from the high potassium concentration, but also could be due to actual zinc contamination in the potassium chloride powder used to make the buffer. Either way, elution with a high concentration of KCl was not an ideal buffer condition.

Next, an elution was repeated swapping out potassium chloride buffer for 20 mM Tris-Cl pH 7.4 containing 1 M sodium chloride. Unlike the KCl solution, this buffering system did not interfere with the DC protein assay. Unfortunately, there still was some interference from the sodium ions when measuring Zn^{2+} using AAS, but it was less than the KCl solution (Zn^{2+} equivalents ≈ 1.0 µM). This system allowed for an elution of
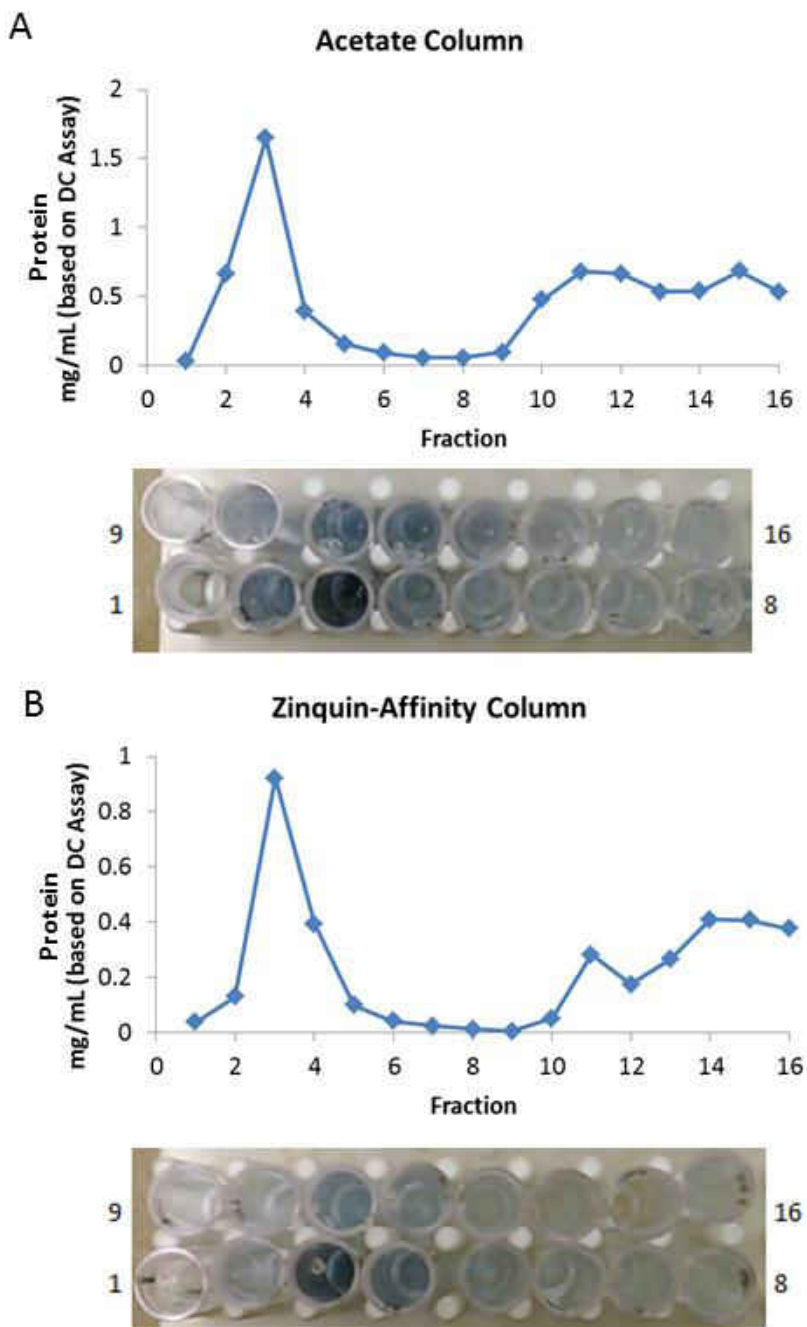
native proteins and thus was used in subsequent experiments. A more detailed account

of this experiment is described in section 3.6.4.

3.6.4.   Isolation of the Zinquin proteome from LLC-PK$_1$ cells

By utilizing this new method of Zinquin affinity chromatography to isolate proteins that

interact with Zinquin, it is possible to start the identification of specific Zinquin targets

within the entire proteome. The general strategy for isolation is outlined in **Figure 3.52**.
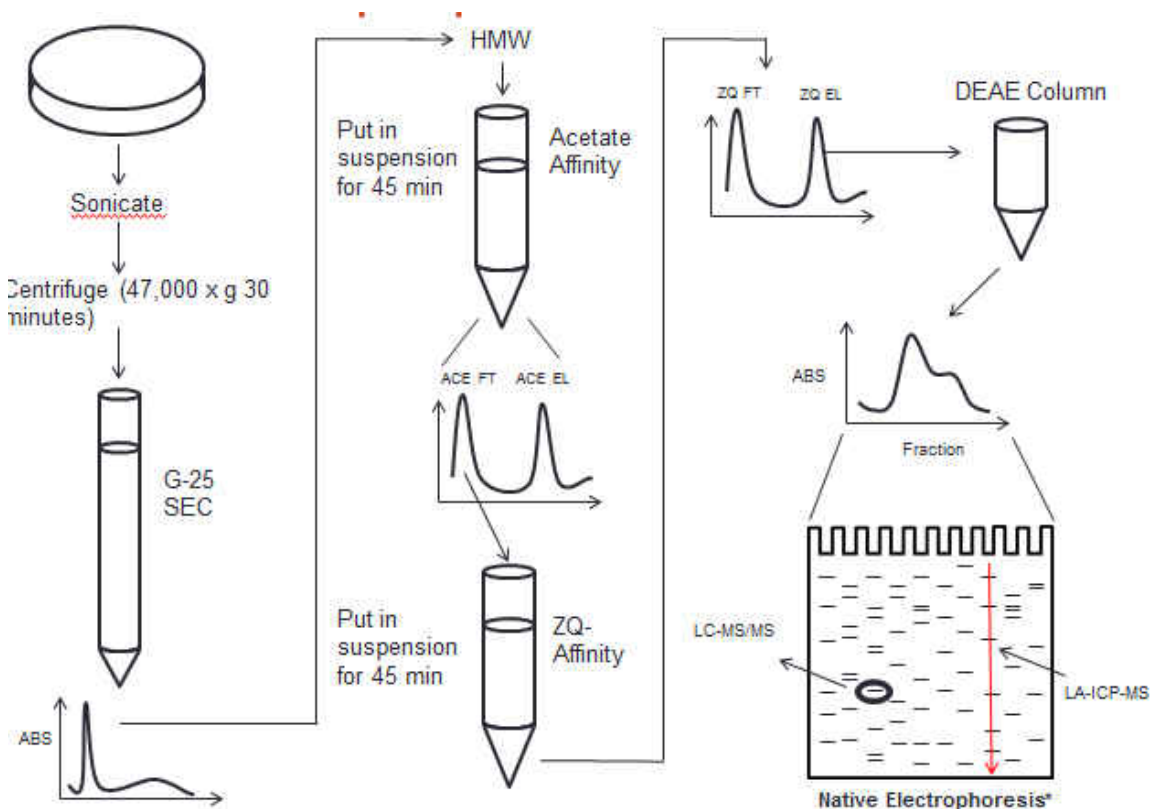
Figure 3.52. General protocol for Isolation of Zinquin-proteins
*Developed in section 3.7

Cells grown in culture are collected, lysed via sonication, and centrifuged. The cellular contents are run over a size exclusion column to obtain the proteome which is then eluted through the acetate column. The unbound proteins are chromatographed over the Zinquin-affinity column and bound proteins are eluted. This pool of Zinquin proteins is separated using ion exchange chromatography and the eluted fractions are then electrophoresed through polyacrylamide gels. Bands within these gels can then be excised for identification using LC-MS/MS techniques, or ablated using LA-ICP-MS to determine the metal content (see section 3.8.1.)

To begin, the HMW proteome from LLC-PK$_1$ cells was isolated and 25 nmoles (based on Zn^{2+}) was run over both the acetate and Zinquin-affinity columns (**Figure 3.49**). Approximately 3% of the total proteome was recovered off the Zinquin-affinity column. This result was slightly less than that seen in a previous prep, but still an acceptable result (see **Figure 3.48**). In order to show that this method is not only a native process but also a purification, the three protein pools (acetate elution, ZQ-Aff flow through, and ZQ-Aff elution) were assayed with Zinquin. First, to remove any effects of the sodium ion concentration on Zinquin binding, the elution fractions from both the acetate and Zinquin columns were desalted using a 3 kDa MWCO centrifugal filter. This was done three times, replacing the salt buffer with 20 mM Tris-Cl pH 7.4 each time. The product samples were then reacted with 10 μM ZQ$_{ACID}$ for 30 minutes and the observed fluorescence was correlated to the amount of protein in each sample (**Figure 3.50**).
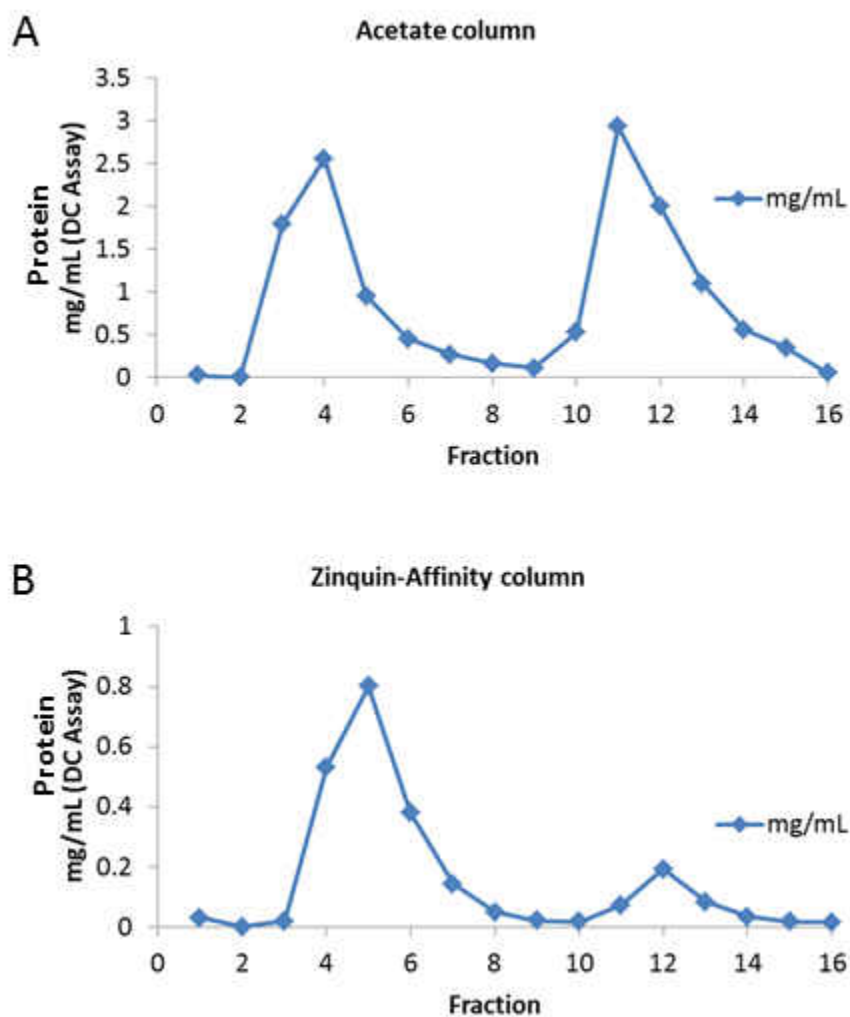
Figure 3.53. Native elution of acetate and ZQ-Aff columns. 25 nmoles (based on Zn^{2+}) of isolated LLC-PK_1 Zn-proteome were chromatographed over acetate (A) and Zinquin-Affinity columns (B). Elution was performed using 20 mM Tris-Cl pH 7.4 containing 1 M NaCl. Protein concentrations were determined using DC protein assay.
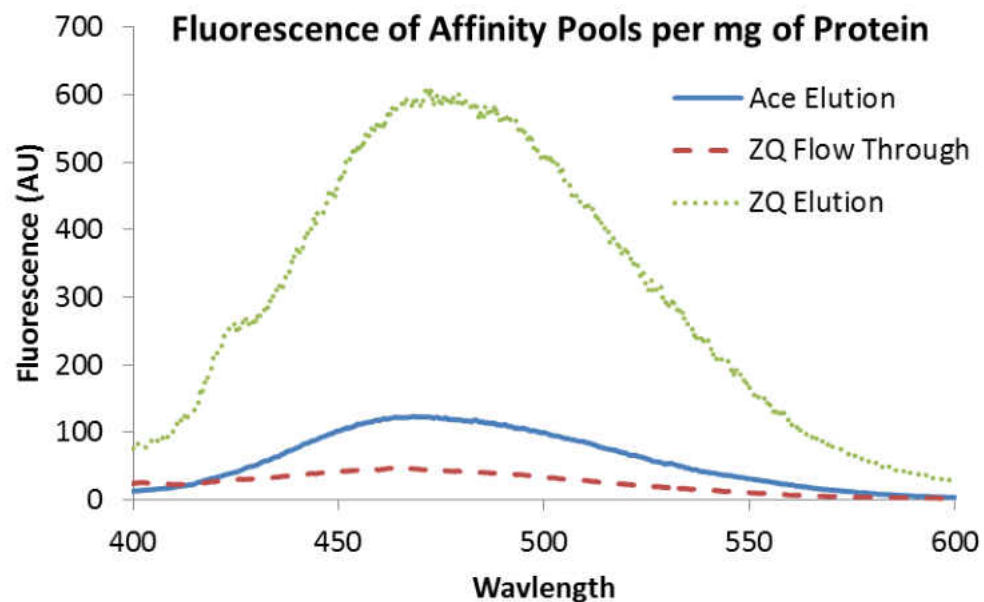
Figure 3.54. Zinquin fluorescence of affinity pools. Protein pools from the chromatography performed in **Figure 3.53** were desalted and reacted with 10 µM ZQ$_{ACID}$ for 30 minutes and the fluorescence was recorded. Fluorescence spectra were adjusted for the amount of protein in each pool.

The fluorescence intensity of the Zinquin elution pool was nearly 6 times higher than the acetate elution pool and 12 times higher than the ZQ flow through pool. Moreover, the emission maximum of this pool was centered at 470 nm, indicative of ZQ-Zn-protein adducts. This result showed that this protocol keeps the proteins in their native state retaining their ability to form adducts with Zinquin. Furthermore, the high fluorescence yield in the ZQ elution pool compared to the other pools showed that this indeed a purification process.

Interestingly, there existed some fluorescence in both the other protein pools as well. The fluorescence in the ZQ flow through pool was most likely due to proteins to which the addition of the linker to the Zinquin molecule prevented binding. The Zn^{2+} cofactor in these proteins are probably more buried and access is restricted when Zinquin is fixed to the agarose bead. The fluorescence associated with the acetate elutant was evidence for a subset of proteins capable of interactions with Zinquin but that also non-specifically binds to the agarose matrix, as suggested in section 3.6.2.   Therefore, this method is not a complete isolation of the Zinquin proteins, but an enhanced purification.

The pool of proteins that was captured by the Zinquin-affinity column was further separated using DEAE ion exchange chromatography. After loading the proteins onto the column, the elution was performed using a 0-500 mM NaCl gradient in 5 mM Tris-Cl pH 8.0 and the fractions were analyzed for absorbance at 280 nm and conductivity (**Figure 3.55**).
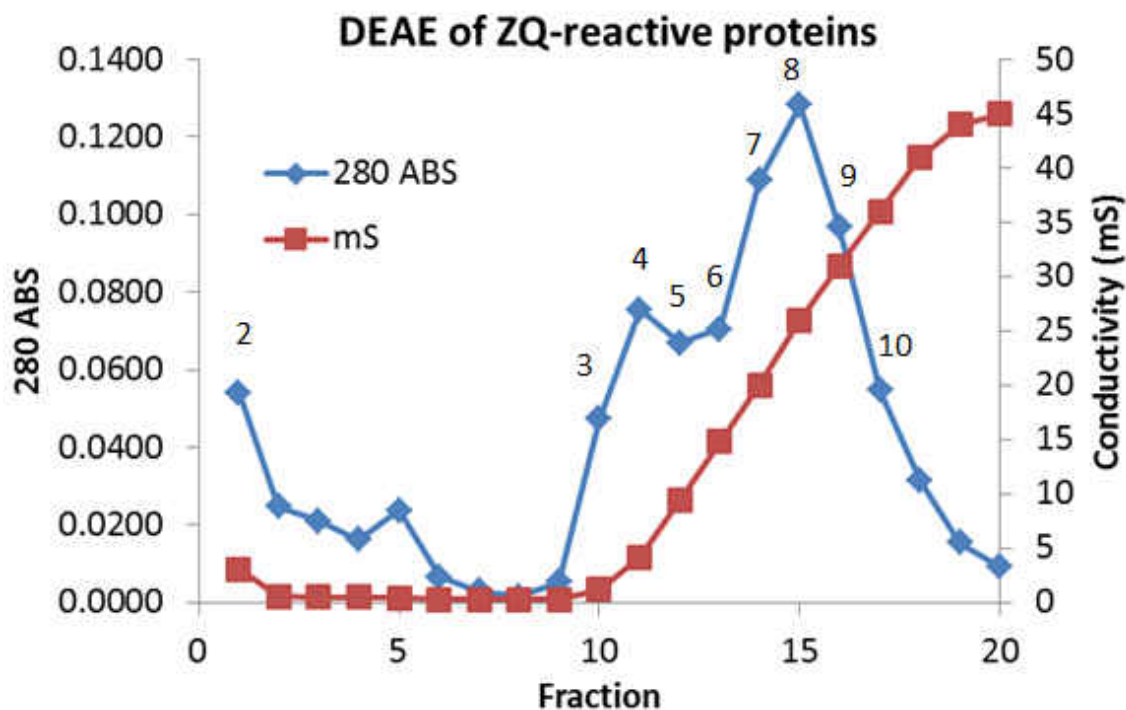
Figure 3.55. DEAE chromatography of Zinquin reactive proteins. Zinquin elution pool from **Figure 3.53** was loaded onto 1 mL DEAE Ceramic HyperD F column in 5 mM Tris-Cl pH 8.0 low conductivity buffer. Column was gradient eluted with 5 mM Tris-Cl pH 8.0 containing 500 mM NaCl. 280 nm absorbance and conductivity were recorded.

Select fractions from the DEAE column (numbered in **Figure 3.55**) were concentrated using a 3 kDa centrifugal filter. As before, this was done three times with low conductivity buffer. The concentrated fractions were then loaded onto a NuPAGE® 12% Bis-Tris Gel and the samples were electrophoresed under denaturing SDS conditions. The gel was first stained using a Coomassie R-250 stain, but no protein bands developed. Using a more sensitive protein detection method, silver staining, the gel showed a vast array of proteins throughout the entire gel (**Figure 3.56**).
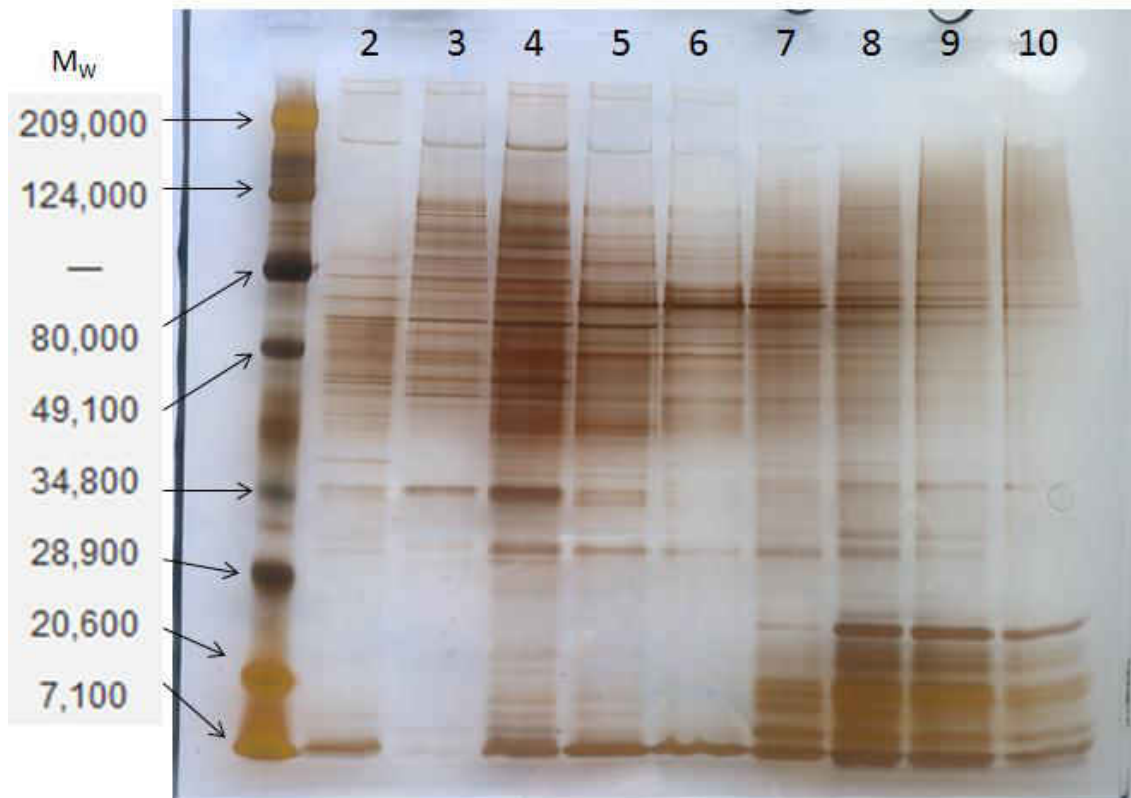
Figure 3.56. SDS-PAGE gel of LLC-PK$_1$ Zinquin proteome. Labeled fractions in **Figure 3.55** were electrophoresed in 12% NuPAGE Bis/Tris gels using SDS-PAGE protocol. Gel was silver stained for detection of protein bands.

Summing the number of stained proteins in each lane led to a total number of over 200 protein bands. Subtracting out bands that appeared near the same position of adjacent lanes led to at least 73 unique proteins isolated. Some of these proteins were in higher concentrations signified by intensely stained bands while others were only faintly visible on the gel. This result provides evidence that the proteins that interact with Zinquin can be isolated using electrophoresis. Furthermore, it shows that the Zinquin interactions occur in a multitude of different proteins.

This initial result called for further optimizations of the protocol. First, this experiment was performed using a modest number of cultured cells (10 plates corresponding to approximately 1×10^8 cells). The PAGE gel of the isolated proteins had bands that were barely visible. Also, since a very sensitive staining technique needed to be used to see the most concentrated proteins, it is possible that some proteins in smaller concentrations were below the limit of detection for this method (LOD of silver stain ≈ 1 ng). In addition, techniques such as LA-ICP-MS (see section 3.8.1) and TSQ staining (see section 3.8.2) require higher concentrations of proteins in order to obtain a signal. Therefore, this method must be scaled up using more cells to get enough protein for analysis. In subsequent experiments, at least 6 times as many cells served as the initial source of the Zn-proteome

The next modification involved the gel electrophoresis method. Up till this point, the methods were done under native conditions to maintain the integrity of the proteins being isolated. However, the SDS-PAGE method is a denaturing process in which proteins subjected to this technique most likely lose any metal cofactors associated with them. This prevents further inorganic analysis of isolated bands. To circumvent this problem, a native SDS-PAGE (NSDS) method was developed to allow for native electrophoretic separations with high resolution. The development of this method is fully described in section 3.7. Furthermore, the applications of this method including Zinquin affinity chromatography are described in section 3.8.

3.7. Development of native sodium dodecyl sulfate gel electrophoresis (NSDS) (In collaboration with William Wobig)

Denaturing sodium dodecyl sulfate polyacrylamide gel electrophoresis (SDS-PAGE) is an extremely common biochemical technique used for small scale separations of protein mixtures with high resolution. It can be used as a way to determine the approximate molecular weight of a protein of interest as well as evaluating the purity of a protein sample. The main drawback of this method is that it is a destructive analytical technique, meaning the electrophoresed protein typically loses all enzymatic activity as well as non-covalently bound subunits. Therefore, subsequent analysis of the cofactors, interactions, and chemistry of the isolated protein is lost. An alternative electrophoretic method is the blue native PAGE method (BN-PAGE). In this technique, the electrophoresed protein maintains its native conformational state, but the resolution of protein bands is significantly diminished, resulting in a protein streak down the lane with poor protein separation. Therefore, there is a pressing need to develop an electrophoretic method that provides acceptable resolution while still maintaining native structure. This is particularly important to the field of metallomics, in which determining the metal ion content of proteins is paramount. In collaboration with William Wobig, the development of such a method is described below.

3.7.1. Formulation of the NSDS Sample Buffer

The first step in development of an effective native electrophoresis method was analyzing the composition of the buffers used in the traditional methodologies, starting

with the buffer that the sample is prepared in. **Table 3.5** describes the composition of

the Invitrogen[TM] LDS Sample Buffer used in SDS-PAGE.

Invitrogen LDS Sample Buffer
106 mM Tris HCl
141 mM Tris Base
2% LDS (Lithium Dodecyl Sulfate)
10% Glycerol
0.51 mM EDTA
0.22 mM SERVA Blue G250
0.175 mM Phenol Red
pH 8.5

Table 3.5. Invitrogen LDS Sample buffer composition

There were two main causes for concern in the makeup of the sample buffer. First, the

high concentration of EDTA in the buffer could lead to chelation of metals from the

proteins in the sample. Strong evidence for this reaction was provided in section 3.3.4.

The second concern was with the LDS concentration. LDS is the detergent molecule that

intercalates into the protein and coats it with a negative charge, thereby allowing it to

migrate in an electric field. However, this intercalation process could result in enough

distortion of the protein structure that leads to the loss of the metal cofactor (reaction

3.25).

$$M^{+a}\text{-Protein} + nLDS \rightleftarrows apoProtein\text{-}LDS_n + M^{+a} \qquad\qquad (3.25)$$

Furthermore, LDS could modify a protein in such a way that it facilitates the chelation of

the metal by the EDTA in the system (reactions 3.26 and 3.27). To circumvent these

problems, EDTA was removed from the sample buffer.

$$M^{+a}\text{-}Protein + nLDS \rightleftarrows M^{+a}\text{-}Protein^*\text{-}LDS_n \qquad (3.26)$$

$$M^{+a}\text{-}Protein^*\text{-}LDS_n + EDTA \rightleftarrows apoProtein\text{-}LDS_n + M^{+n}\text{-}EDTA \qquad (3.27)$$
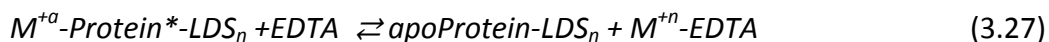
Next, the detergent in the sample buffer was gradually lowered to determine the minimal concentration needed for proper separation. Protein samples were obtained from a DEAE fractionation of the proteome from TE-671 cells. Two different concentrations of protein (≈ 30 μg and 10 μg) were mixed with an array of Tris sample buffers (-EDTA) containing 0, 1, or 2% SDS as well as the commercially available Invitrogen^{TM} LDS sample buffer. Samples were loaded into a 12% NuPAGE Bis-Tris gel and the electrophoresis was performed. Gels were then Coomassie stained to analyze protein migration (**Figure 3.57A**).

The gel in **Figure 3.57A** was run using a modified version of the standard running buffer, removing EDTA as well as the SDS (see section 3.7.2). Samples with SDS in the sample buffer only slightly outperformed the buffer without SDS. However, in all lanes, a majority of the proteins barely entered the gel, and those that did were poorly resolved. This result revealed that SDS is a requirement in the run buffer for proper electrophoresis. The gel in **Figure 3.57B** on the other hand contained 0.1% SDS, the concentration typically used in traditional SDS-PAGE. In this gel, proteins migrated the same in all lanes, regardless of sample buffer. Taken together, to obtain proper resolution, no SDS is required in the sample buffer so long as it is present in the run buffer.
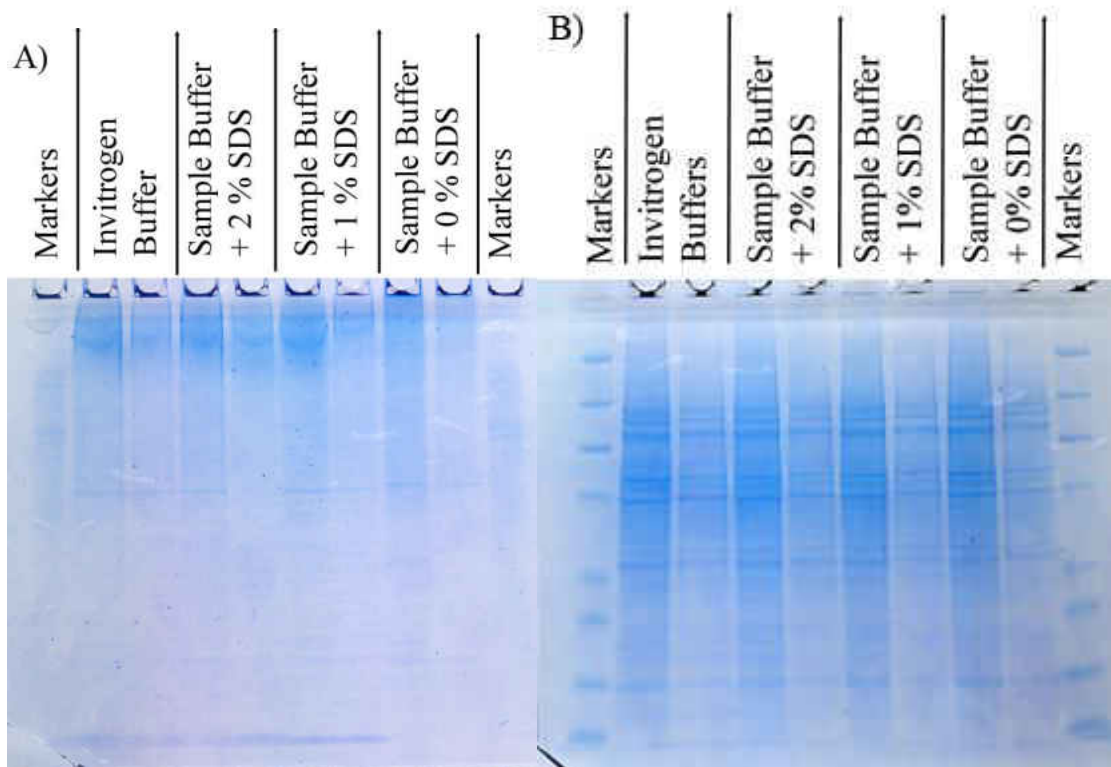
Figure 3.57. Effects of SDS concentration in sample buffer. Protein samples were obtained from a DEAE separation of TE-671 proteome. Approximately 30 and 10 µg samples were prepared in Invitrogen sample buffer and homemade sample buffer containing 2%, 1%, and 0% SDS and electrophoresed through 12% NuPAGE® Bis/Tris gels at 200V in run buffer containing 0% (A) and 0.1% (B) SDS.

Therefore, the sample buffer without SDS was used for all subsequent NSDS experiments.

3.7.2. Formulation of the NSDS Run Buffer

The next variable tested was the chemical composition of the run buffer, starting with what is used in the commercially available run buffer from Invitrogen^{TM} (**Table 3.6**).

Invitrogen MOPS SDS Run Buffer
50 mM Tris
50 mM MOPS
0.1% SDS
1 mM EDTA
pH 7.7

Table 3.6. Invitrogen MOP SDS running buffer composition

The experiment in section 3.7.1 implied that at least some SDS was required in the run buffer. To determine the effects of the SDS concentration in the run buffer on electrophoresis, a series of run buffers were made containing 0.0125%, 0.025%, 0.05%, and 0.1% SDS. Again, for reasons already noted, EDTA was excluded from the new run buffer formulations. Multiple concentrations of Zn_2-ADH were prepared in the revised sample buffer, loaded into four 4-12% NuPAGE® Bis-Tris gels, and the electrophoresis was performed at 200 volts using the four different run buffers. To determine the effects of the SDS on the enzymatic function, and therefore protein structure, an in-gel activity assay was performed prior to protein staining (see section 3.7.4).

The amount of activity retained by the protein was negatively correlated to the amount of SDS in the run buffer, suggesting that indeed SDS has harmful effects on protein stability (**Figure 3.58A**). Conversely, Coomassie staining the gels showed that the resolution was positively correlated to the amount of SDS in the run buffer, reinforcing the need of SDS in the buffer for achieve proper separation (**Figure 3.58B**). Yet, even the 0.1% SDS still showed signs of streaking. This was indicative of overloading the gel, protein degradation, or a combination of the two. Nonetheless, the visual evidence from the activity and staining pattern pointed to an optimal concentration somewhere between 0.05 and 0.025% SDS.

Based on this initial result, the scope of testing the run buffer conditions was expanded. Included in this experiment was a run buffer containing 0.0375% SDS as well as the Invitrogen^{TM} MOPS run buffer. As a comparison, the commercial buffers and protocols for SDS-PAGE and BN-PAGE were used and followed as well.

To probe the effects of SDS concentration in the run buffer in terms of resolution, a mixture of model proteins was used. Alcohol Dehydrogenase, β-galactosidase, Carbonic Anhydrase and Superoxide Dismutase were loaded in equal quantities onto 12% NuPAGE® Bis-Tris gels for the newly synthesized run buffers as well as the Invitrogen MOPS SDS buffer. For the BN-PAGE system, protein samples were loaded on a 4-16% NativePAGE^{TM} gel. Since
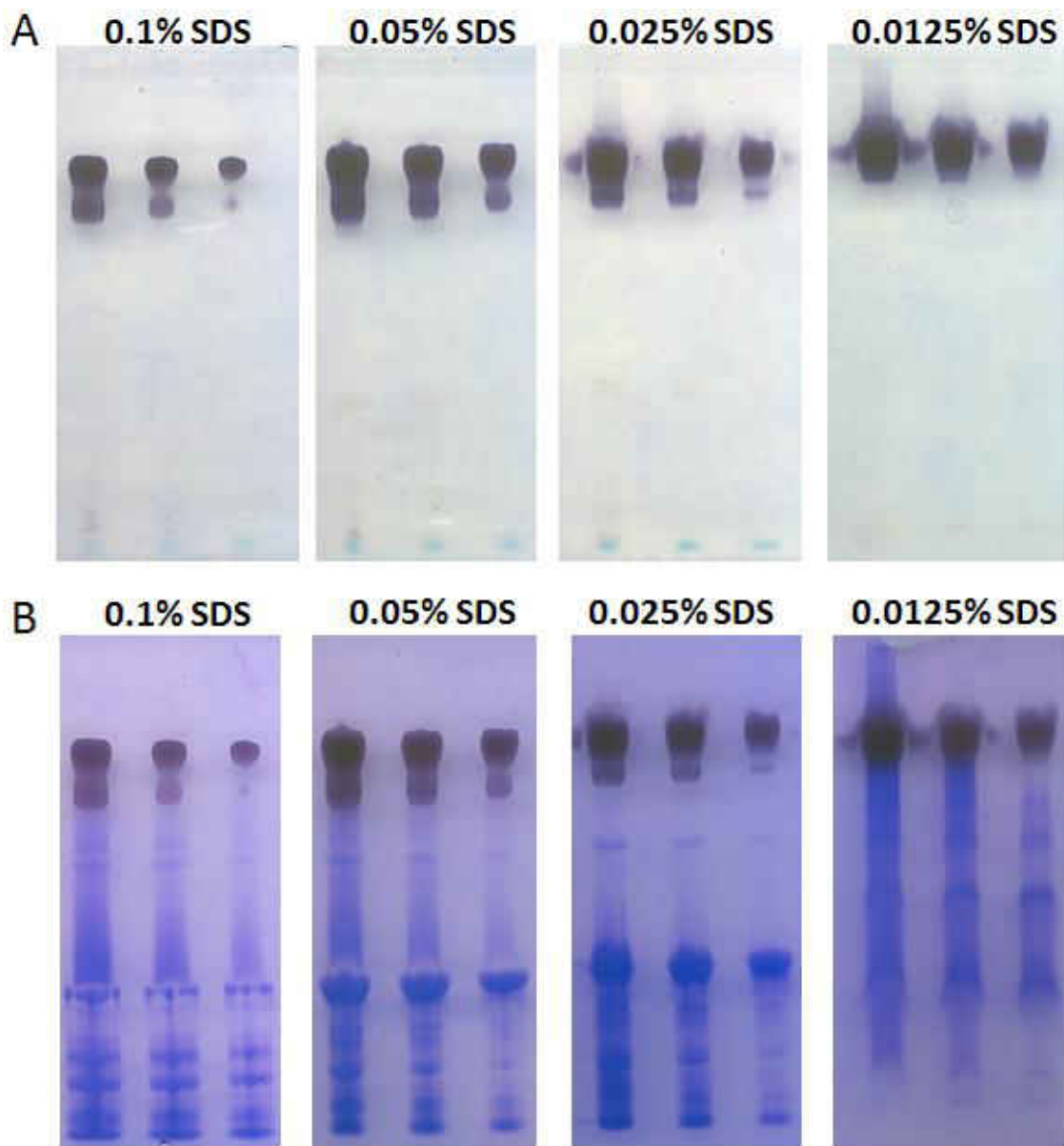
Figure 3.58. Effects of SDS concentration in the run buffer. 150, 75 and 37.5 μg of Zn_2-ADH were prepared in modified sample buffer and electrophoresed at 200 V through 12% NuPAGE Bis/Tris gels in run buffer containing 0.1%, 0.05%, 0.025%, and 0.0125% SDS. Proteins were tested for activity (A) and stained with Coomassie R-250 (B).

Invitrogen indicates that BN-PAGE should be performed at 150V, the developed buffers were also run at this voltage while the denaturing SDS-PAGE gel was run at 200V. Samples were run in duplicate, one to stain for protein and one to test for the enzymatic activity of alcohol dehydrogenase (see section 3.7.4.).

The results of the protein stain for 50 µg, 25 µg, and 12.5 µg samples as well as the activity of the 50 µg sample are shown in **Figure 3.59**. As expected, the resolution of the BN-PAGE gel was quite poor despite having only four proteins in the system (not accounting for any contaminants). Moving to the 0.0125% SDS buffer, the proteins still streaked through most of gel, including the protein markers (lane M for 0.0125% SDS). At 0.025% SDS, bands started to become more resolved but streaking still occurred in the lower half of the gel. Distinct protein bands appeared once a concentration of 0.0375% SDS was used. This became apparent when looking at the densitometry plots of lane 1 for 0.0375% SDS as well as all of the gels tested (**Figure 3.60**).

Increasing the SDS concentration beyond 0.0375% did not significantly improve resolution. However, as the concentration went up, bands at the tops of the gels (green arrows in **Figure 3.59**) began to decrease in intensity. In conjunction, bands further down the lanes started growing in intensity (red arrows). Moreover, in the SDS-PAGE gel, new bands began to appear (yellow arrows). This was strong evidence for the dissociation of the multimeric proteins in this proteins mixture—namely alcohol dehydrogenase and β-galactosidase—at higher SDS concentrations. Also, there was a decrease in ADH activity (lanes A in **Figure 3.59**) as the SDS concentration increased over
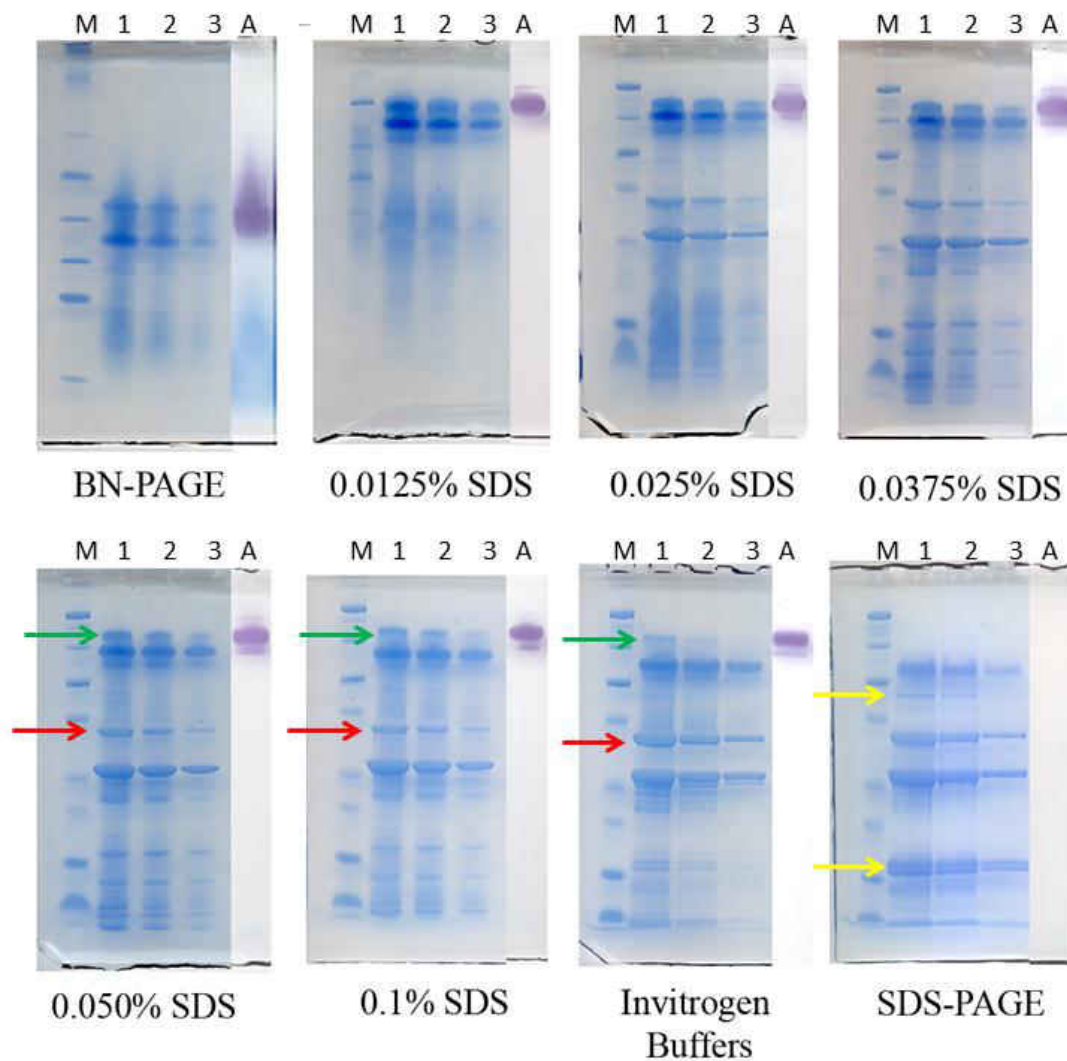
Figure 3.59. Gel electrophoresis using different run buffers and techniques. Gels were loaded with proteins markers (M), 50 µg (1), 25 µg (2), and 12.5 µg (3) of ADH, β-Gal, CA, and SOD and electrophoresed using different run buffers (0.0125%-0.1% SDS, Invitrogen run buffer) and techniques (BN-PAGE and SDS-PAGE). ADH activity of the 50 µg sample was tested in lane A. As the concentration of SDS increased, the ADH tetramer (green arrow) decreased while ADH monomer (red arrow) increased. SDS-PAGE resulted in new protein bands (yellow arrow)
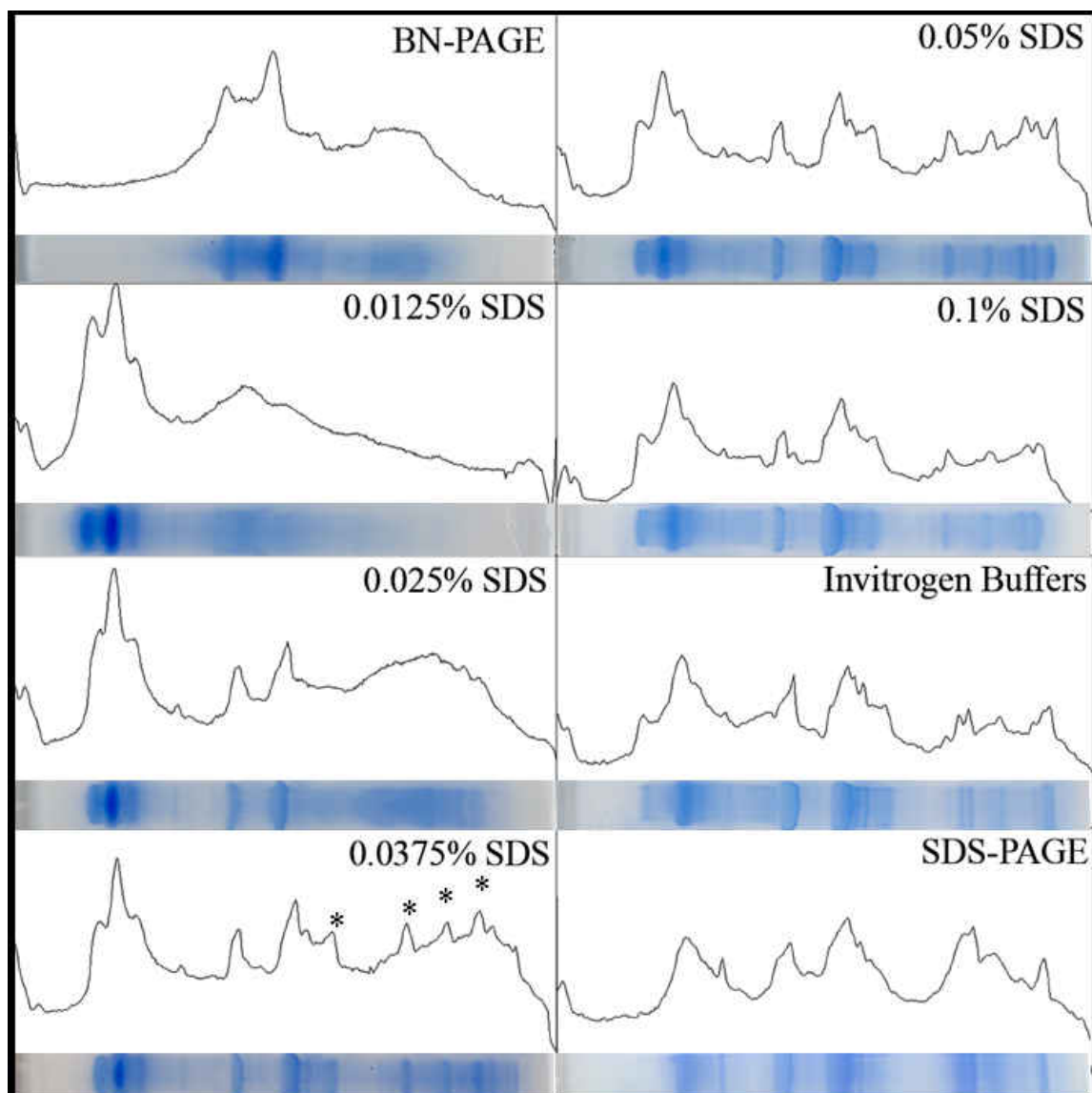
Figure 3.60. Densitometry plot of PAGE gels 50 μg protein lanes in **Figure 3.59** were plotted using ImageJ software. * indicates protein bands that became resolved at 0.0375% SDS.

0.0375% SDS, further supporting the hypothesis of protein denaturation via subunit disassembly at higher SDS concentrations.

As noted, there was a significant difference between the 0.1% SDS buffer and the Invitrogen[TM] MOPS running buffer (0.1% SDS, 1 mM EDTA) in regards to the stained proteins at the green and red arrows. It was determined from the activity assay that the protein at the green arrow corresponded to alcohol dehydrogenase. Moreover, based on the molecular weight standards, the green arrow corresponded to the intact tetramer (160 kDa) whereas the red arrow corresponded to monomer (40 kDa). The increase in the amount of monomeric ADH using the Invitrogen buffer suggests that the presence of EDTA exacerbated the denaturation process of this Zn-protein in the presence of SDS. This was likely mediated by a chelation of the structural Zn^{2+} which destabilized the protein, making it more susceptible to SDS infiltration and denaturation. Nonetheless, the remaining tetrameric ADH still retained some enzymatic function.

Also worth mentioning are the differences between the modified technique using the Invitrogen[TM] MOPS running buffer and the Invitrogen[TM] SDS-PAGE protocol with the same buffer. There are two main deviations in the procedure that led to the two different electrophoretograms. First, traditional SDS-PAGE protocols call for heating the proteins in sample buffer before loading them into the gel. Since this is an obvious cause of protein denaturation, it was removed from the modified technique. Also, as noted before, SDS-PAGE methods suggested performing the electrophoresis at 200V

while the modified technique was performed at 150V, a voltage consistent with native

PAGE conditions.   It was these two modifications that resulted in the two different

electrophoresis patterns, including the full depletion of alcohol dehydrogenase activity.

Taken together, it was determined that a concentration of 0.0375% SDS in the run

buffer was all that was needed to perform electrophoretic separations with acceptable

resolution with higher SDS concentrations leading to protein denaturation.   Therefore,

this was the concentration of SDS used for all subsequent gels run under NSDS

conditions.

3.7.3. Additional protocol optimizations

It has been shown that the presence of unpolymerized acrylamide in a PAGE gel can

negatively affect the resolution of gel electrophoresis.[93] The amount of unpolymerized

acrylamide within a gel is dependent upon the duration of the polymerization reaction

in which the gel is made.[93] Since this duration is unknown for commercially produced

pre-cast gels, there may be a significant amount of unreacted acrylamide still present in

these gels. To test this, fractions from a DEAE separation of the LLC-PK$_1$ proteome were

loaded into a 12% NuPAGE® Bis-Tris gel taken straight from the packaging while a

second sample set was loaded into a gel that had been electrophoresed in ddH$_2$O at

200V for 45 minutes.   Gels were run using the NSDS method and stained using

SimplyBlue[TM] Coomassie stain (**Figure 3.61**).
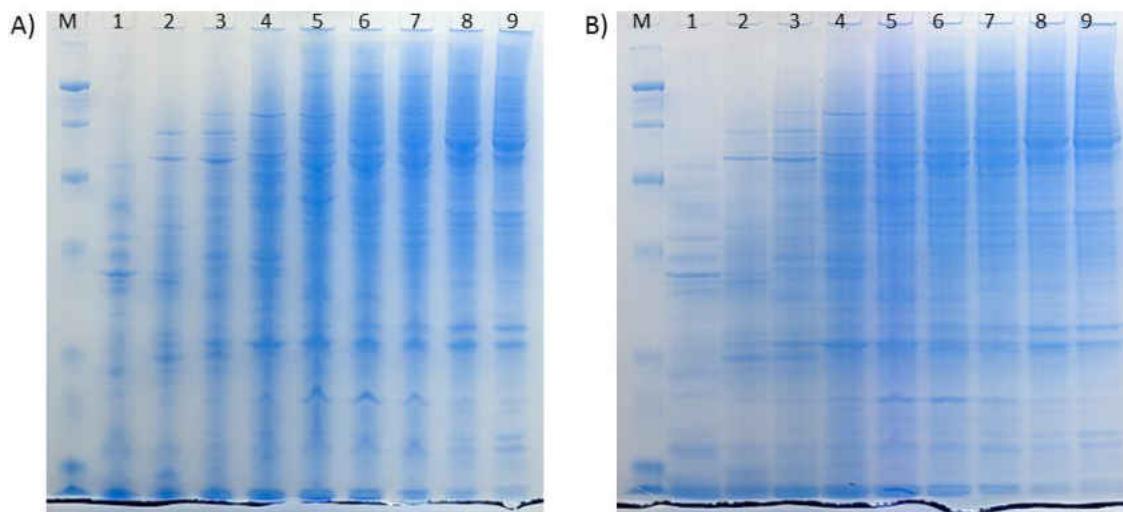
Figure 3.61. Effects of pre-running gels for NSDS-PAGE. Protein fractions from a DEAE separation of LLC-PK$_1$ proteome were loaded in a 12% NuPAGE Bis/Tris pre-cast gel directly out of the package (A) and one electrophoresed in ddH$_2$O at 200V for 30 min (B). Gels were run using NSDS-PAGE method and stained in SimplyBlue^{TM} Safe Stain.

The proteins in the gel without the pre-run tended to streak down the center of the well with modest resolution. However, the gel that was pre-electrophoresed showed much better separation. In addition, unlike the bands in the first gel that showed some "smiling," the bands in the pre-run gel were more evenly distributed throughout the width of the lane. This leads to the conclusion that the commercially available pre-cast gels contain unpolymerized acrylamide or some other chemical that reduces resolution but can be removed by an initial electrophoretic run before the samples are loaded. Hence, this step was included in the new technique.

Pre-running the gel in ddH$_2$O provides an additional advantage. It was determined by William Wobig that the storage solution in which the precast gel is shipped contains approximately 1 µM of Zn^{2+} as measured by ICP-MS.[94] In addition, the digestion of a

pre-run 12% NuPAGE Bis-Tris gel in nitric acid revealed that Zn^{2+} was present in a concentration of 1.00-1.25 µg/g acrylamide (15.2-19 µM). After an electrophoretic run, Zn^{2+} migrated into the run buffer, resulting in a concentration of Zn^{2+} in the gel of 0.17 µg/g acrylamide. Therefore, performing a pre-run removes background Zn^{2+} within the gel. This ion removal is a crucial step for increasing the limit of detection using LA-ICP-MS for subsequent metal analysis of PAGE gels.[94]

A last modification involved chilling the run buffer to 4 °C. This protects against thermal buildup from the electrophoresis process that may damage the protein sample.

3.7.4. Evaluations of SDS-, NSDS-, BN-PAGE for resolution and enzymatic activity

To provide further evidence that this new technique achieves the goal of high resolution non-denaturing separation, a multitude of enzymes were subjected to NSDS-PAGE. Also, to show that this method is an improvement upon the established PAGE techniques, the NSDS-PAGE results were compared with SDS-PAGE and BN-PAGE. The modified buffer recipe and protocol for the NSDS-PAGE method as well as buffers and procedures for the commercially available native and denaturing methods are summarized in **Table 3.7.** All proteins tested were run under these conditions, using 12% NuPAGE® Bis-Tris gels for the SDS and NSDS methods and 4-12% NativePAGE™ Bis-Tris gels for the BN-PAGE method.

Electrophoretic Method		
SDS-PAGE (Invitrogen[TM])	**NSDS-PAGE** (Nowakowski, Wobig, Petering)	**BN-PAGE** (Invitrogen[TM])
Sample Buffer 106 mM Tris HCl 141 mM Tris Base 0.51 mM EDTA 0.22 mM SERVA Blue G-250 0.175 mM Phenol Red 2% LDS 10% Glycerol pH 8.5	100 mM Tris HCl 150 mM Tris Base 0.22 mM Coomassie G-250 0.175 Phenol Red 10% Glycerol pH 8.5	50 mM BisTris 50 mM NaCl 6 N HCl 10% Glycerol 0.001% Ponceau S pH 7.2
Run Buffer 50 mM MOPS 50 mM Tris Base 1 mM EDTA 0.1% SDS pH 7.7	50 mM MOPS 50 mM Tris Base 0.0375% SDS pH 7.7	<u>Cathode</u> pH 6.8 50 mM BisTris 50 mM Tricine 0.02% Coomassie G-250 <u>Anode</u> pH 6.8 50 mM BisTris 50 mM Tricine
Sample Prep 70 °C for 10 min	--	--
Gel Prep --	Run in ddH$_2$O 30 min @200V	--
Temperature Room Temp	4 °C	Room Temp
Voltage 200 V (constant)	150 V (constant)	150 V (constant)
Run Time 45-55 min	70-80 min	85-100 min

Table 3.7. Summary of electrophoretic protocols

Since most of the NSDS development process was centered on alcohol dehydrogenase, the first evaluation of the three methods began using this protein run by itself. The protein staining pattern of 10 µg ADH after electrophoresis is shown in **Figure 3.62**.

As expected, using the SDS-PAGE method resulted in the denaturation of the ADH tetramer into the individual 40 kDa monomers. In contrast, the NSDS-PAGE method kept the protein mostly intact, running as a tight band at a position near 160 kDa according to the protein markers. In the BN-PAGE system, the protein ran as two streaks which neither correlating to 160 kDa as measured by the protein markers. This underscores the fact that BN-PAGE can provide inaccurate molecular weight determinations. Hence, the NSDS-PAGE showed better resolution than BN-PAGE while, unlike the SDS-PAGE, kept the protein in its multimeric state.

To see whether or not the enzyme was still functional, an in-gel activity assay was performed. In this assay, functional ADH oxidizes ethanol to acetaldehyde, in the process reducing NAD to NADH. In the presence of PMS, NADH can reduce MTT to formazan, an insoluble product with a dark purple color that can easily be visualized.[60] Incubating the three gels in the assay solution resulted in the production of formazan in the NSDS- and BN-PAGE gels, but not in the SDS-PAGE gel. Therefore, subjecting ADH to NSDS-PAGE not only preserved the tetrameric structure with high resolution but also maintained the functionality of the protein, a statement that could not be said about either SDS- or BN-PAGE.
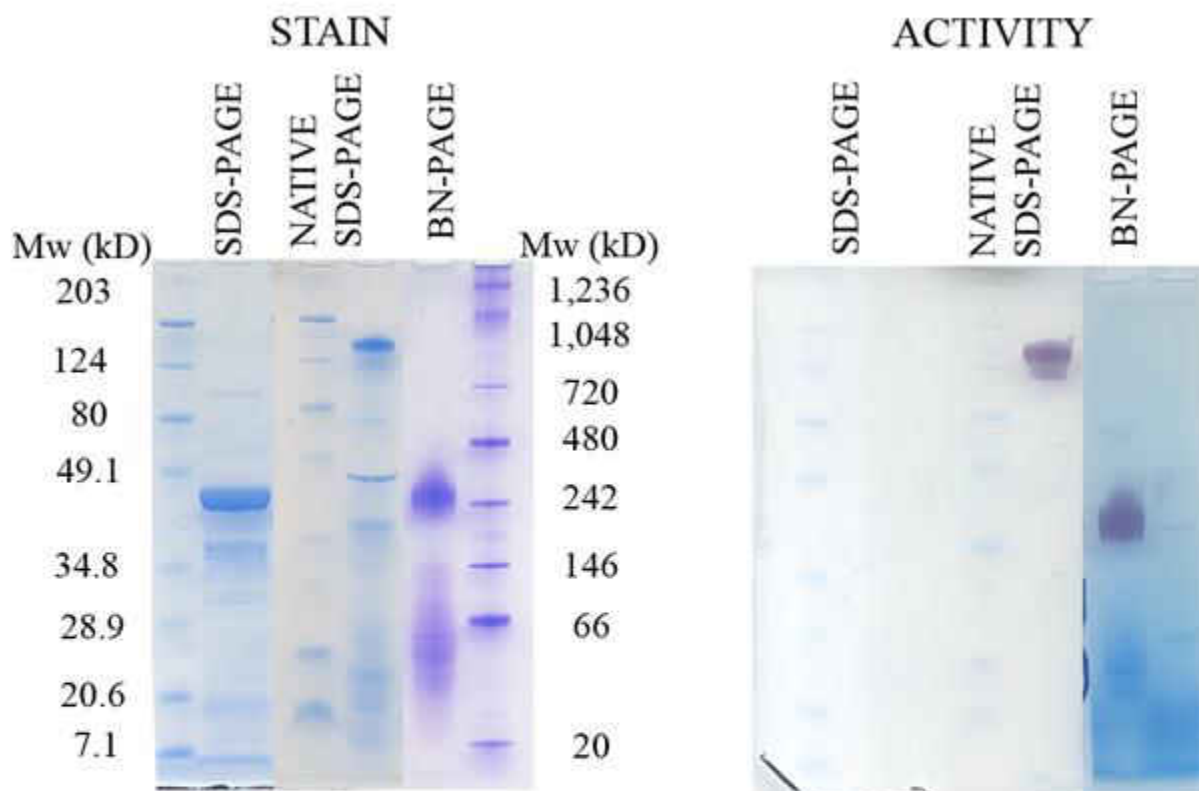
Figure 3.62. SDS-, NSDS-, and BN-PAGE of ADH. 10 µg of ADH were electrophoresed using the SDS-, NSDS-, and BN-PAGE methods, stained, and test for enzymatic activity. Visualization scheme from Manchenko.[60]

The next enzyme tested was β-galactosidase from *Aspergillus oryzae*. Again, 10 µg were run in duplicate for all three electrophoretic techniques, one for protein staining and one for activity (**Figure 3.63**). After staining the gel with Coomassie stain, two bands appeared in the SDS-PAGE gel, while only one band appeared in both the NSDS- and BN-PAGE gels. The molecular weights of the two bands in the SDS-PAGE gel—one slightly higher than 80 kDa and one slightly lower than 80 kDa—summed up the approximate molecular weight in the NSDS-PAGE gel. This strongly suggests that the SDS-PAGE technique dissociated the dimer—seen in NSDS-PAGE—into two non-equivalent monomers. Interestingly, the reported size of β-galactosidase from *Aspergillus oryzae* is 105 kDa, which may correspond to the top band in the SDS-PAGE gel.[95]

To test for function, another activity assay was performed. Here, β-galactosidase cleaves galactose from 5-bromo-4-chloro-3-indolyl-β-D-galactopyranoside (X-Gal) yielding 5-bromo-4-chloro-3-hydroxyindole, which dimerizes during its reduction by nitro blue tetrazolium. This produces insoluble formazan and an insoluble Indigo analog, both having a deep purple color. Again, only the NSDS- and BN-PAGE gels showed active β-galactosidase, supporting the fact that NSDS-PAGE is a native method.

Next, superoxide dismutase from bovine erythrocytes was tested. Superoxide dismutase is a Cu, Zn protein comprised of two covalently-linked monomers with a total molecular weight of 32 kDa.[96] Running 10 µg of protein using the three electrophoretic

156

Figure 3.63. SDS-, NSDS-, and BN-PAGE of β-Gal. 10 µg of β-Gal were electrophoresed using the SDS-, NSDS-, and BN-PAGE methods, stained, and test for enzymatic activity. Visualization scheme from Manchenko.[60]

methods resulted in SOD migrating to three different positions on the gels (**Figure 3.64**). In the SDS-PAGE gel, the protein migrated to a position corresponding to its expected molecular weight of 32 kDa. However, in the gel run using the NSDS-PAGE technique, the protein ran as a tetramer near 124 kDa, while the protein in the BN-PAGE method ran as an apparent hexamer.

The activity assay for this enzyme is a reverse stain. In the presence of phenazine methosulfate and light, MTT will spontaneously convert to formazan, turning the entire gel dark purple. Using molecular oxygen, SOD within the gel will convert formazan back to MTT, creating a clear spot on the gel. Both NSDS- and BN-PAGE gels showed distinct clear regions, indicative of active SOD. Moreover, the BN-PAGE gel had multiple clear bands. These bands most likely correlate to other oligomers, namely a tetramer and a trimer. The NSDS-PAGE gel appeared to also have both tetramer and trimer bands. In the SDS-PAGE gel, no activity was found in the SOD monomer, signifying that it is denatured. However, there existed a faint band in the SDS-PAGE gel located near the trimer region.

Further examination of SOD under SDS-, NSDS- and BN-PAGE was performed by William Wobig. Using LA-ICP-MS, it was determined that both Cu^{2+} and Zn^{2+} were unperturbed in both the NSDS- and BN-PAGE systems while Zn^{2+} was lost from the protein in the SDS method.[94]   In addition, there was no Cu^{2+} associated with the monomer band, but a small amount still existed in the trimer band.[94] Therefore, the faint clear band seen in
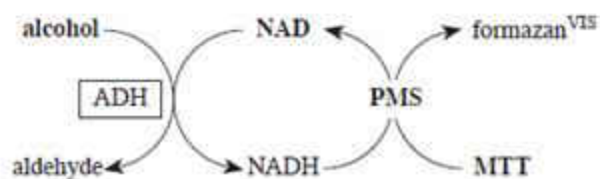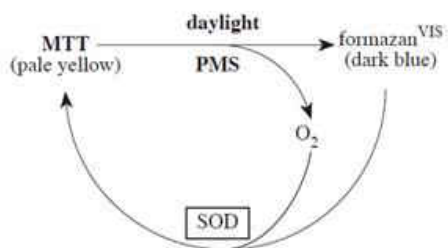
Figure 3.64. SDS-, NSDS-, and BN-PAGE of SOD. 10 µg of SOD were electrophoresed using the SDS-, NSDS-, and BN-PAGE methods, stained, and test for enzymatic activity. Visualization scheme from Manchenko.[60]

the SDS gel could either be due to a functioning enzyme or simply a result of the powerful redox capability of the copper ion.

The PAGE methods were also evaluated using bovine mucosa alkaline phosphatase purchased from Sigma (**Figure 3.65**). Despite being a high resolution method, the stained SDS-PAGE gel revealed protein streaks near the top of the gel in addition to a few resolved bands. This suggested that the purchased enzyme contained multiple contaminants in addition to alkaline phosphatase. Hence, the stained NSDS-PAGE gel showed protein streaking near the top of the gel as well. This poor resolution was exacerbated in the BN-PAGE method in which protein ran throughout the entire length of the gel. Thus, due to the large amount of contaminants, proper evaluation of the protein resolution using these PAGE methods could not be made using this enzyme.

Despite the enzyme impurities, the gels were tested for alkaline phosphatase activity. In this assay, active phosphatases will hydrolyze 5-bromo-4-chloro-3-indoyl phosphate to a phosphate and 5-bromo-4-chloro-3-hydroxyindole. From here, the reaction scheme is the same as for the β-galactosidase assay in which the 5-bromo-4-chloro-3-hydroxyindole dimerizes in the presence of NBT to form dark purple products. As seen with the other enzymes, proteins in both NSDS- and BN-PAGE gels retained their enzymatic activities while proteins in the SDS-PAGE gel did not. This provides further evidence that NSDS-PAGE is a native method.
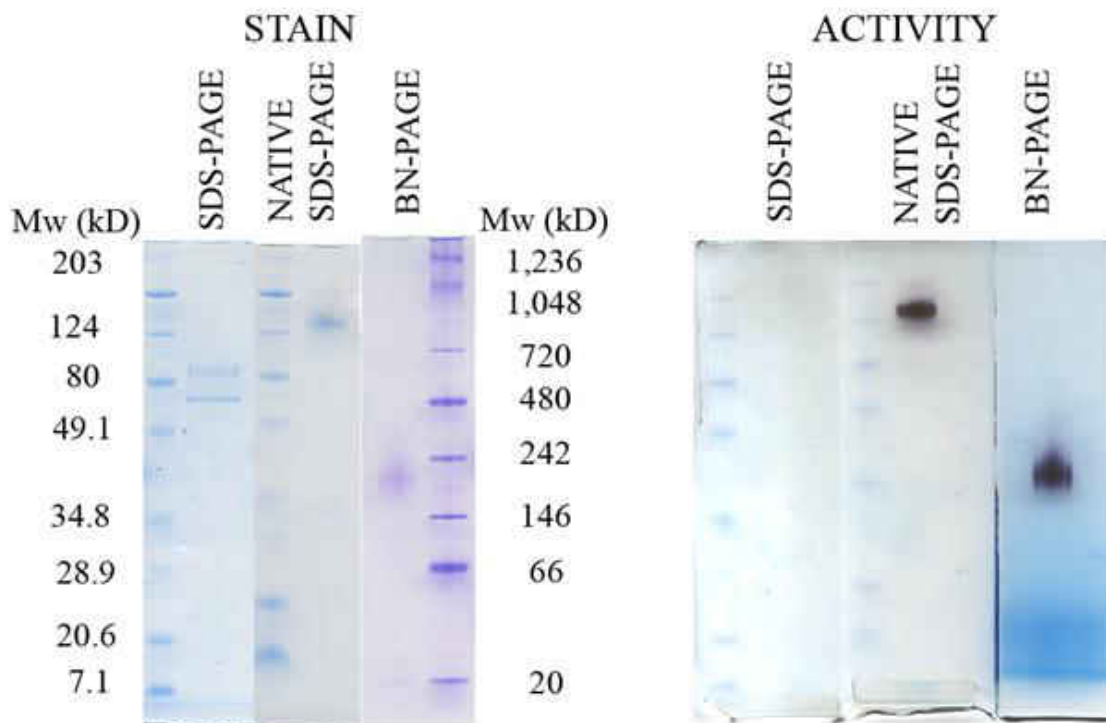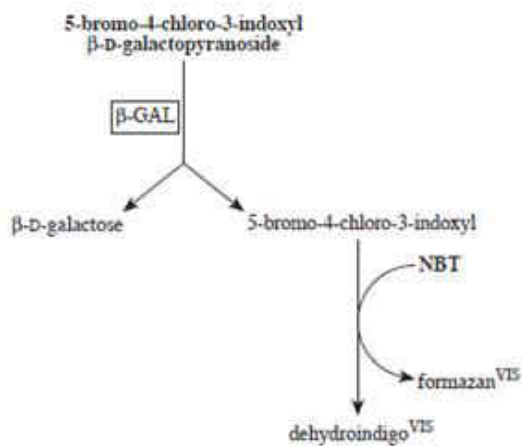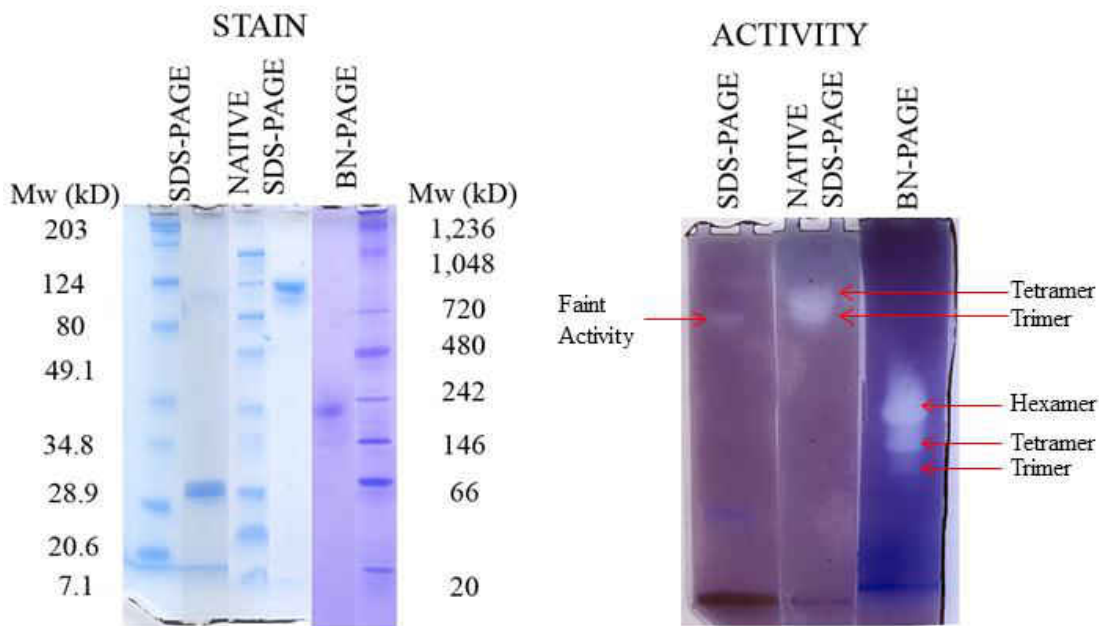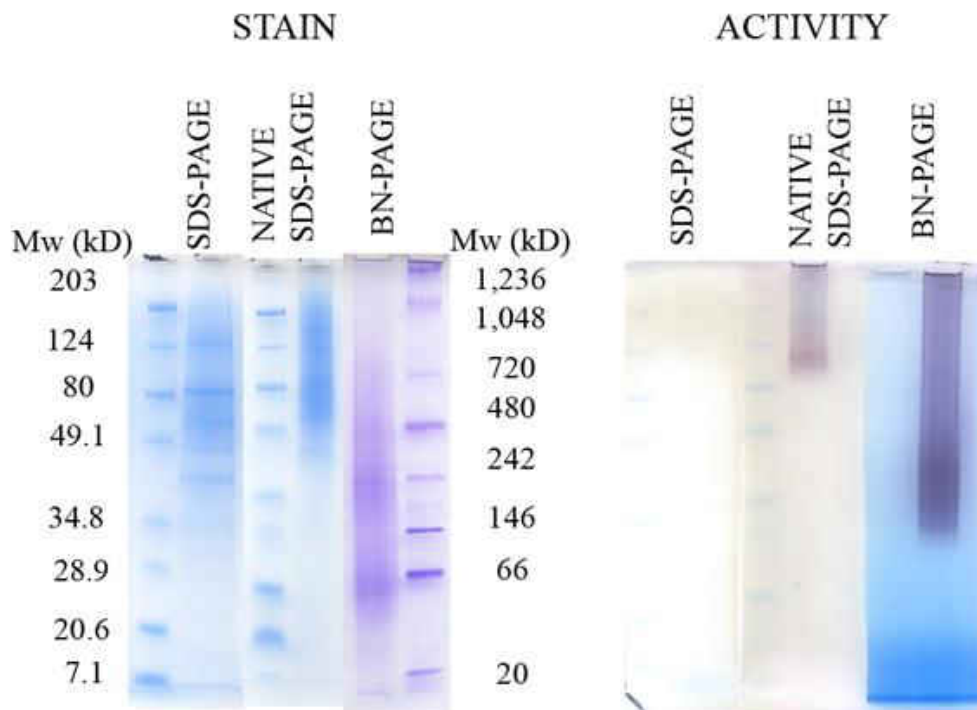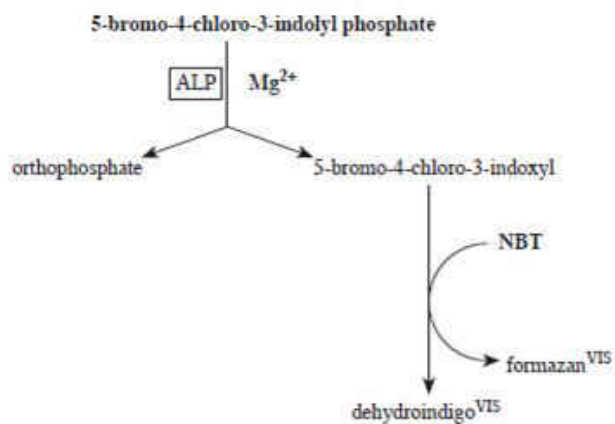
Figure 3.65. SDS-, NSDS-, and BN-PAGE of AP. 10 μg of AP were electrophoresed using the SDS-, NSDS-, and BN-PAGE methods, stained, and test for enzymatic activity. Visualization scheme from Manchenko.[60]

In all, 9 enzymes were tested for activity after electrophoretic seperation. As shown in **Table 8**, with the exceptions of trace activity from urease and superoxide dismutase, proteins run under the SDS-PAGE method lost all of their enzymatic function.

Protein	Enzyme Activity After Electrophoresis		
	SDS-PAGE	NSDS-PAGE	BN-PAGE
Alcohol Dehydrogenase	-	++	++
β-galactosidase	-	++	++
Superoxide Dismutase	Trace	++	++
Alkaline Phosphatase	-	++	++
Urease	Trace	++	++
Peroxidase	-	++	++
Carbonic Anhydrase	-	++	++
L-amino acid oxidase	-	-	++
Glucose-6-Phosphate Dehydrogenase	-	-	++

Table 3.8. Enzymatic activity after SDS-, NSDS-, and BN-PAGE

Conversely, all proteins were active after BN-PAGE. Seven out of the nine proteins retained their activities after electrophoresis using NSDS-PAGE. The results from this survey of enzymes suggest that NSDS-PAGE is a viable native method for most, but not all, enzymes.

The detection of active proteins after electrophoresis was expanded from isolated proteins to an entire proteome. The proteome from LLC-PK$_1$ cells was isolated, loaded onto a DEAE column and a stepwise elution was performed (**Figure 3.66**). After elution,

select peaks were pooled and desalted using centrifugal filters. Proteome fractions were loaded into 6 gels—one for staining and one for activity for each method—then electrophoresed using SDS-, NSDS-, and BN-PAGE (**Figure 3.67**). The SDS- and NSDS-PAGE gels showed relatively similar protein staining patterns, with the SDS-PAGE gel having marginally better resolution. These gels were in stark contrast with the BN-PAGE gel in which the proteins streaked down the gel with very poor resolution.

The gels were then tested for phosphatase activity as described above. In both the NSDS- and BN-PAGE gels, phosphatase activity was found in multiple lanes with the most occurring in fraction 5 (see arrows). In contrast, the SDS-PAGE gel displayed no activity in any lane. Taken together, NSDS-PAGE provides markedly improved electrophoretic separation of a complex proteome sample versus traditional native electrophoresis. Also, unlike SDS-PAGE, the increase in resolution is not at the expense of enzymatic function, in this case the phosphatase activity within a proteome.
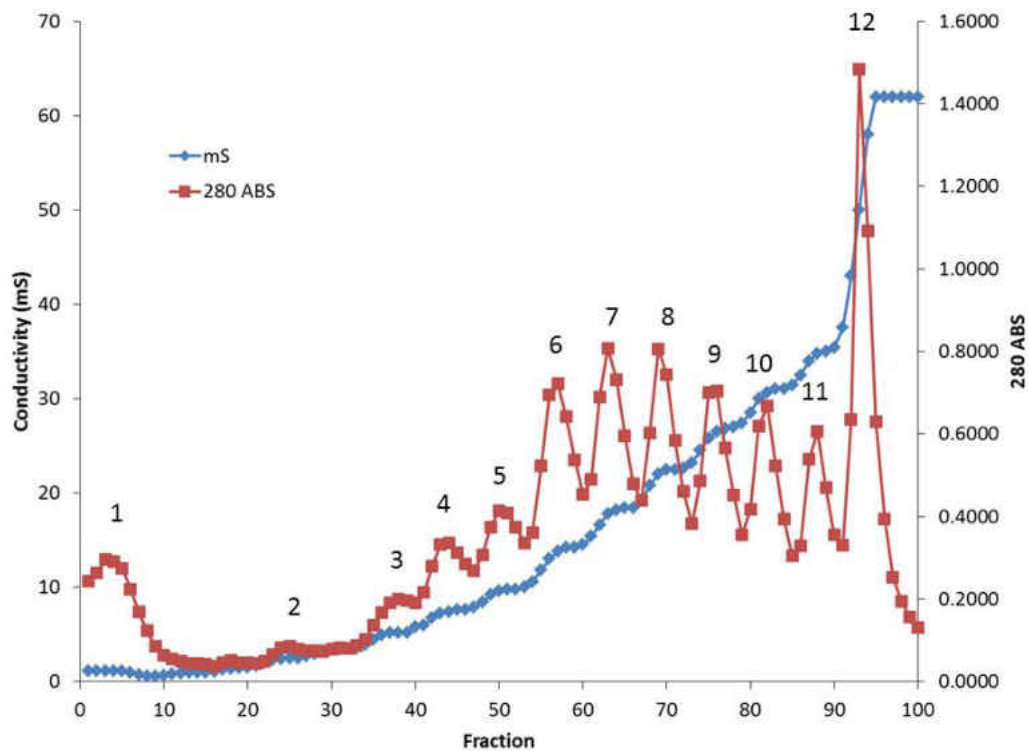
Figure 3.66. Stepwise DEAE elution of LLC-PK$_1$ proteome. Isolated LLC-PK$_1$ proteome in 5 mM Tris-Cl pH 8.0 was loaded onto a 5 mL Macro-Prep DEAE column. Column was eluted stepwise in 50 mM NaCl increments to a final concentration of 500 mM NaCl in 5 mM Tris-Cl pH 8.0. Conductivity and absorbance at 280 nm were recorded.
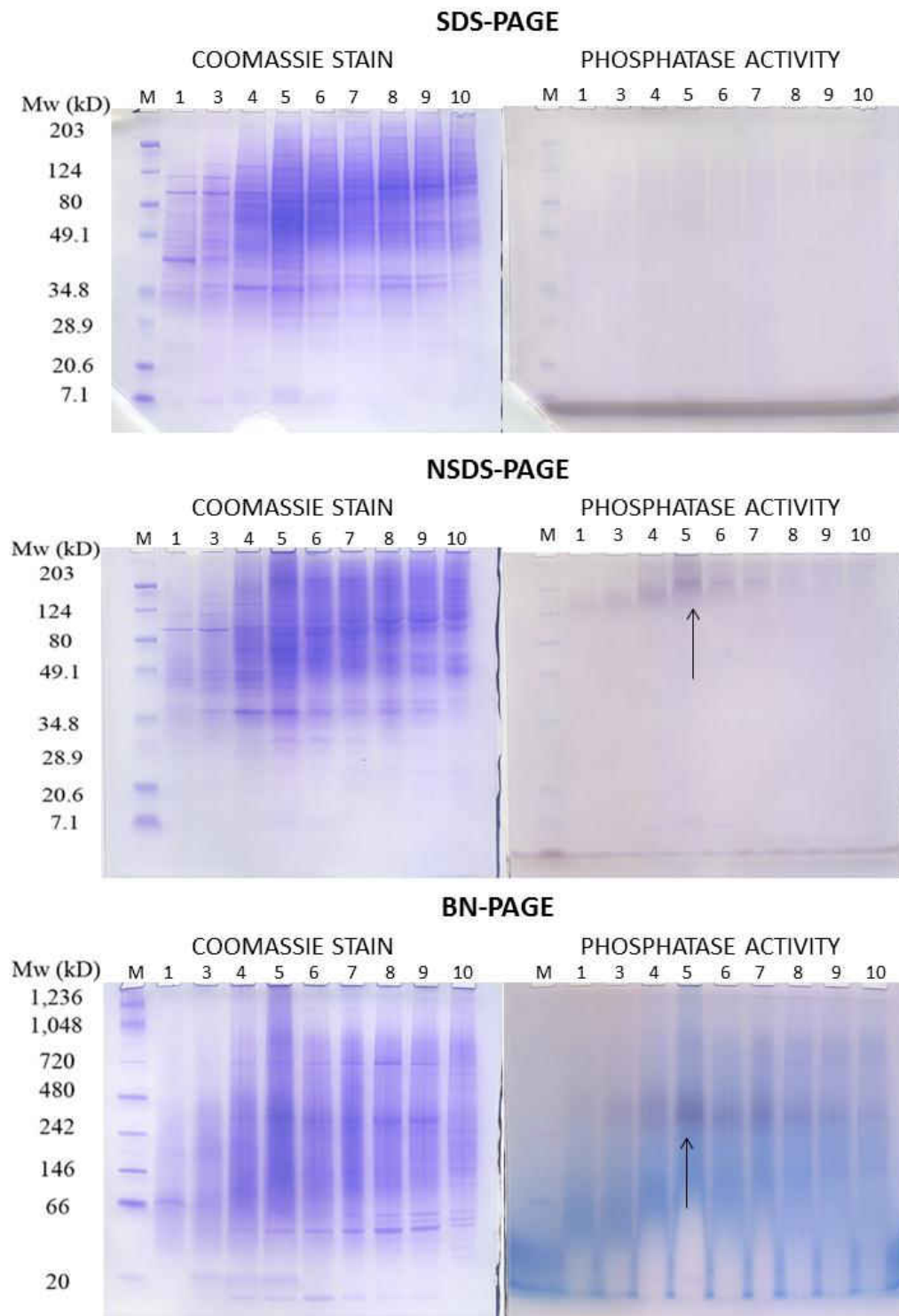
Figure 3.67. SDS-, NSDS-, and BN-PAGE of LLC-PK$_1$ proteome. Numbered peaks in **Figure 3.66** were electrophoresed using SDS-, NSDS, and BN-PAGE techniques. Gels were stained and tested for phosphatase activity.

3.7.5. Alternative alkyl-sulfate solutions as run buffers

SDS has been the classical detergent used in polyacrylamide gel electrophoresis for decades. However, the main drawback of using SDS is that it normally leads to denaturation of the protein of interest. Although the above experiments showed that lowering the concentration of SDS in the run buffer can help preserve the native state, there may be other detergents that do a better job of effectively coating proteins with negative charge without disrupting structure. Therefore, other alkyl-sulfate compounds were tested as possible substitutes for SDS (**Figure 3.68**).
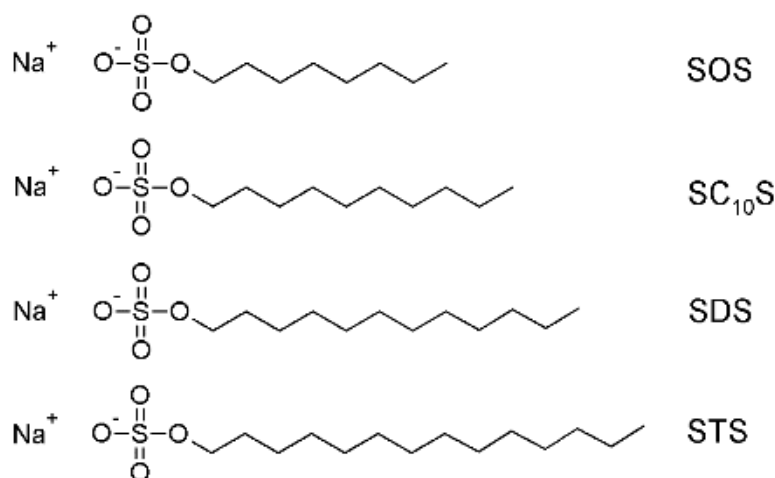
Figure 3.68. Alkyl-Sulfate detergents

To start, the proteome from LLC-PK$_1$ cells was isolated using Sephadex G-25 gel filtration. The elution was performed using the NSDS-PAGE run buffer without detergent (50 mM MOPS, 50 mM Tris-Cl, pH 7.7) to emulate the conditions under electrophoresis. Starting as a base point, the proteome was reacted with different concentrations of SDS

and the extent of denaturation was loosely evaluated based on its reactivity with ZQ_{ACID}. The fluorescence spectra for 5 µM proteome reacted in 0-0.1% SDS assayed with 5 µM ZQ_{ACID} are shown in **Figure 3.69A**.

As the concentration of SDS in the buffer increased, the ratio of fluorescence at 492 nm to 467 nm increased as well. This meant that treatment with SDS made the proteome more susceptible to Zn^{2+} chelation by Zinquin (reactions 3.28 and 3.29).

$$Zn\text{-}proteome + nSDS \rightleftarrows Zn\text{-}proteome^*\text{-}SDS_n \qquad (3.28)$$
$$Zn\text{-}proteome^*\text{-}SDS_n + 2\ ZQ_{ACID} \rightleftarrows Zn(ZQ_{ACID})_2 + apo\text{-}proteome^*\text{-}SDS_n \qquad (3.29)$$
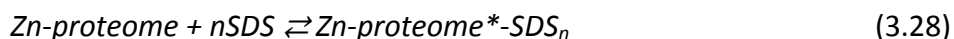
In order for this process to occur, the SDS had to perturb the protein structure enough to either allow Zinquin to access a buried Zn^{2+} ion or simply cause Zn^{2+} to be released. Either way, treatment with SDS resulted in some form of protein distortion and/or denaturation. Further evidence of this was inferred by the decrease in background fluorescence of the proteome with increased concentrations of SDS (**Figure 3.69C**). Although the exact source of this background fluorescence is not known, the change in emission behavior suggests SDS is interacting with the proteome. Taking this background depletion in effect, corrected fluorescence spectra are displayed in **Figure 3.69D**. These corrected spectra further illustrate the point of denaturation by the increase in intensity and the red-shifted emission.

The experiment was repeated using sodium octyl sulfate (SOS) as the detergent. Here, the addition of SOS to the proteome had no effect on the Zinquin-based fluorescence at any concentration tested (**Figure 3.70**).
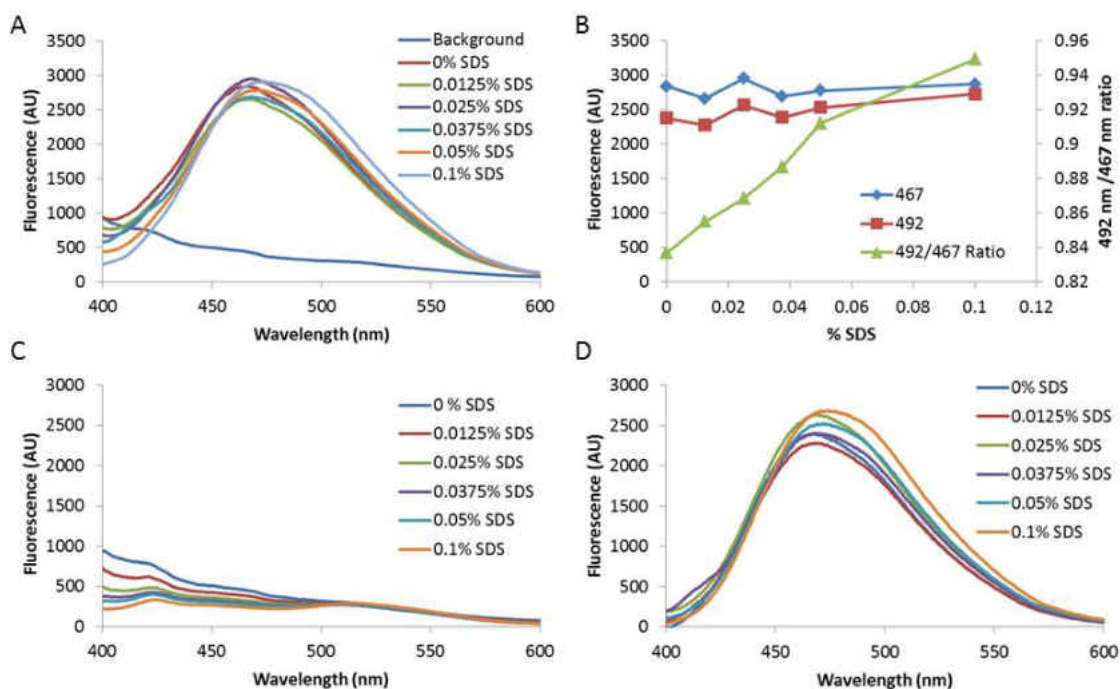
Figure 3.69. Effects of SDS on LLC-PK$_1$ proteome measured by ZQ$_{ACID}$5 µM (based on Zn^{2+}) LLC-PK$_1$ Zn-proteome was reacted with 0-0.1% SDS in 50 mM MOPS 50 mM Tris pH 7.7 for 20 minutes before reaction with 5 µM ZQ$_{ACID}$. After 30 minutes, the fluorescence (A) and spectral changes (B) were recorded. (C) Fluorescence of Zn-proteome in different SDS concentrations. (D) Fluorescence of ZQ-Zn-proteome corrected for SDS concentration.
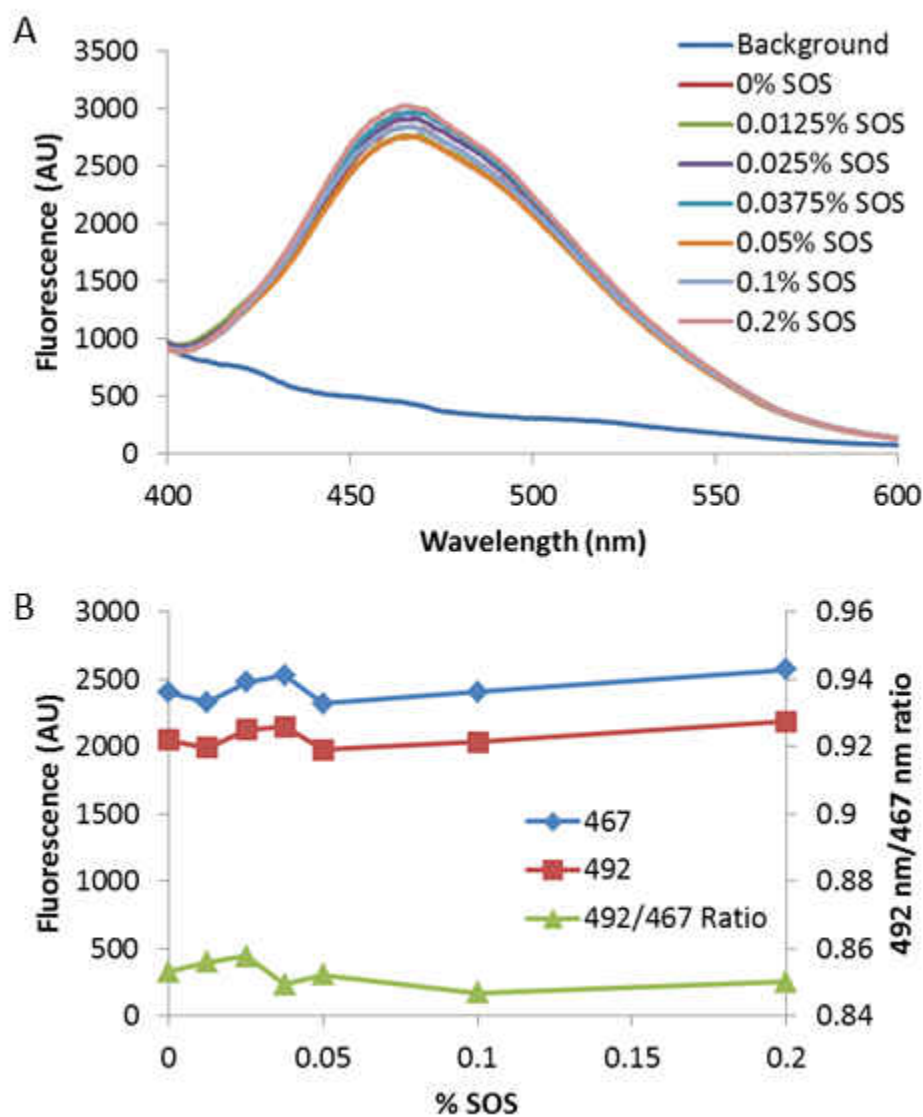
Figure 3.70. Effects of SOS on LLC-PK$_1$ proteome measured by ZQ$_{ACID}$ 5 μM (based on Zn^{2+}) LLC-PK$_1$ Zn-proteome was reacted with 0-0.2% SOS in 50 mM MOPS 50 mM Tris pH 7.7 for 20 minutes before reaction with 5 μM ZQ$_{ACID}$. After 30 minutes, the fluorescence (A) and spectral changes (B) were recorded.

This can be interpreted two ways: either the SOS coated proteins without significantly affecting their structures or SOS did not associate with the proteins. To test this, electrophoresis was performed on a proteomic sample from a Zinquin affinity prep using the NSDS run buffer containing 0.2% SOS as the detergent. This gel was compared to an electrophoresis of the same samples using the standard NSDS run buffer containing 0.0375% SDS (**Figure 3.71**).

In the SOS gel, most of the proteins barely entered into the gel, and those that did streaked down the lane. Moreover, the protein markers did not separate into distinct bands. This is in contrast to the NSDS-PAGE gel in which there was acceptable resolution for both the markers and the complex protein mixtures. Since the resolution of the SOS gel was quite poor, it is unlikely that SOS had any interactions with the proteins in the sample. Therefore, SOS is not a suitable detergent for use in electrophoresis.

Next, the effects sodium decyl sulfate ($SC_{10}S$) and sodium tetradecyl sulfate (STS) on the proteome were investigated. 5 µM LLC-PK$_1$ proteome was reacted with 5 µM ZQ_{ACID} in the presence of either $SC_{10}S$ (**Figure 3.72A,B**) or STS (**Figure 3.72C,D**). Unlike SOS, there was a slight shift and increase in the emission spectra of the ZQ-exposed proteome as the concentration of $SC_{10}S$ increased from 0 to 0.1%. However, this shift was not as dramatic as that seen in the SDS treated proteome as measured by the ratio of fluorescence at 492nm to 467 nm ($\Delta_{492/467nm\ ratio}$ = 0.11 for SDS, $\Delta_{492/467nm\ ratio}$ = 0.073 for $SC_{10}S$).
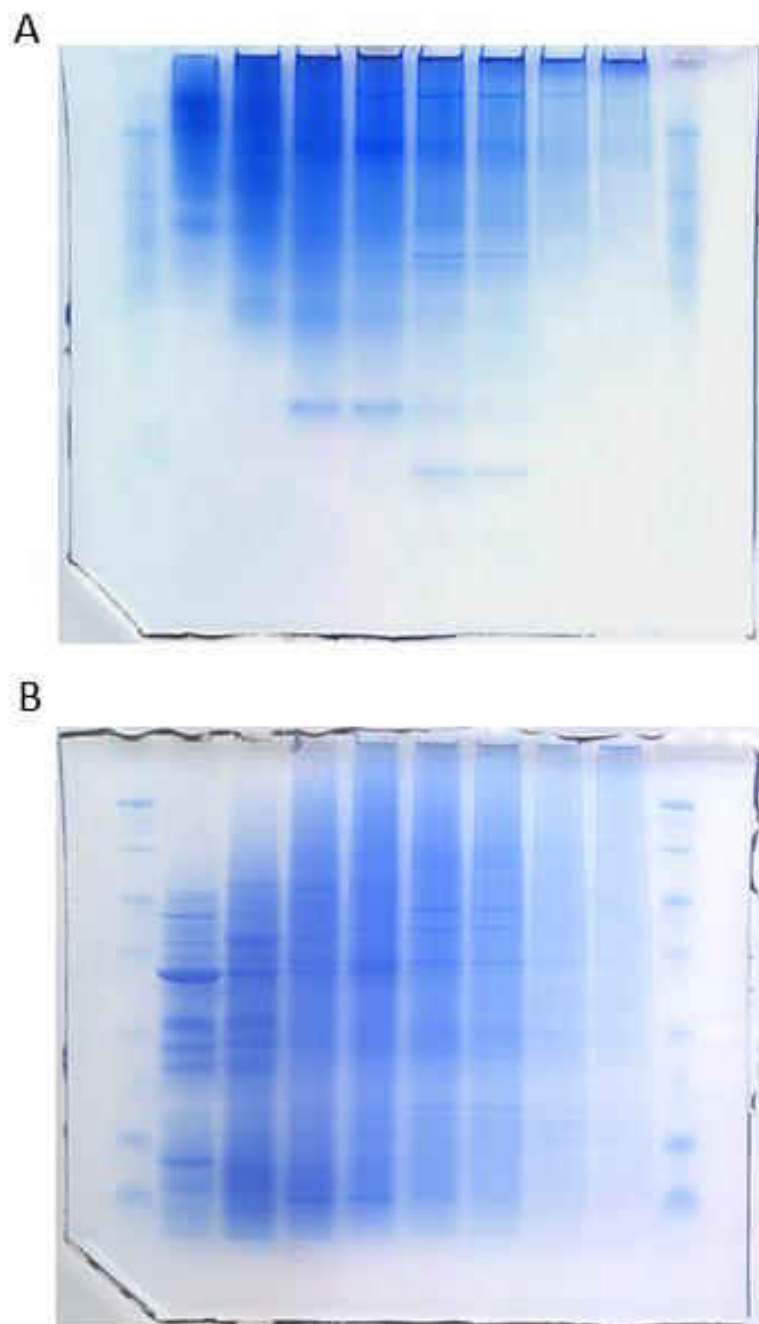
Figure 3.71. SOS- and NSDS-PAGE of LLC-PK$_1$ Zinquin proteome. Protein samples from LLC-PK$_1$ were obtained using Zinquin-Affinity chromatography and prepared in NSDS-PAGE sample buffer. Samples were loaded in 12% NuPAGE Bis/Tris gels and electrophoresed at 150V for 75 min using the NSDS-PAGE run buffer containing 0.2% SOS (A) and 0.0375% SDS (B).
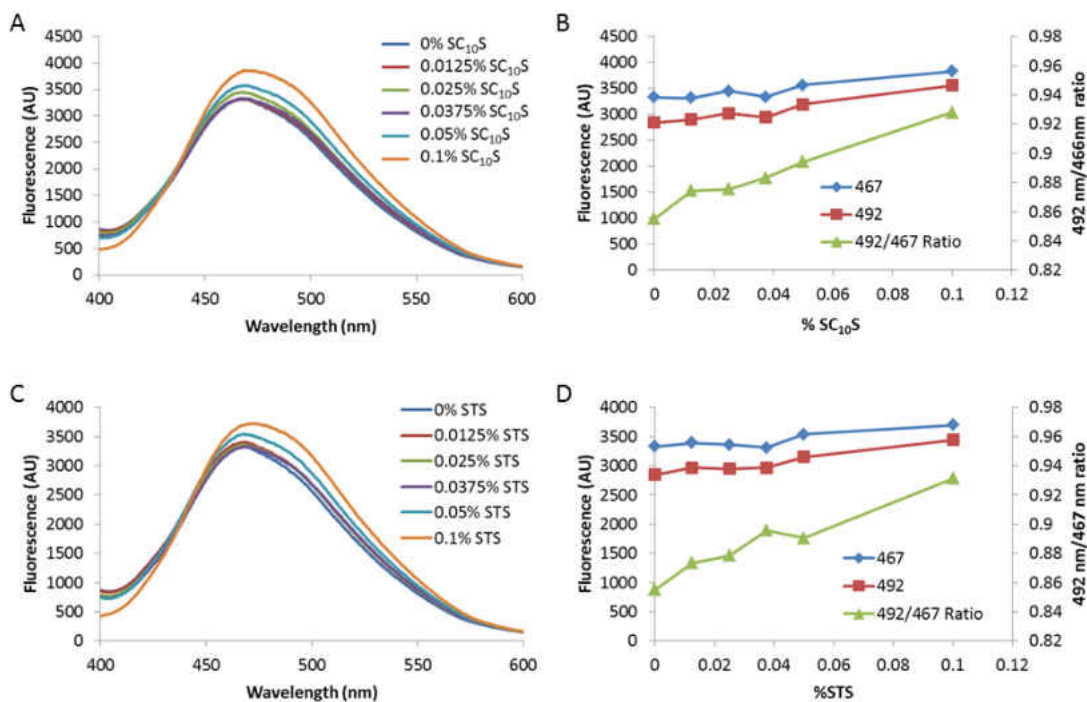
Figure 3.72. Effects of SC$_{10}$S and STS on LLC-PK$_1$ proteome measured by ZQ$_{ACID}$. 5 µM (based on Zn^{2+}) LLC-PK$_1$ Zn-proteome was reacted with 0-0.1% SC$_{10}$S (A, B) and 0-0.1% STS (C, D) in 50 mM MOPS 50 mM Tris pH 7.7 for 20 minutes before reaction with 5 µM ZQ$_{ACID}$. After 30 minutes, the fluorescence and spectral changes were recorded.

This was also the case for the STS treated proteome in which the emission spectra began to red-shift upon increasing the detergent concentration. The change in the ratio of fluorescence at 492 to 467 nm from 0 to 0.1% STS was 0.076, again less that that seen in the SDS-treated proteome at the same concentrations. Since the presence of these detergents had less of an effect on the proteome as measured by Zinquin, $SC_{10}S$ and STS were potential candidates for replacing SDS in native electrophoresis.

The proteome from $LLC-PK_1$ cells was separated by DEAE chromatography. Select fractions were then loaded into 12% NuPAGE® gels and electrophoresed using the NSDS run buffer (50 mM MOPS, 50 mM Tris-Cl, pH 7.7) with a variety of detergents. After electrophoresis, the gels were soaked in the alkaline phosphatase assay solution for 45 minutes (**Figure 3.73**). The only gel that displayed detectable phosphatase activity was the gel run using the NSDS-PAGE buffer containing 0.0375% SDS (arrow). Next, the gels were Coomassie stained to visualize the separations (**Figure 3.74**). Starting with 0.05% $SC_{10}S$ in the run buffer, most of the proteins did not enter the gel; those that did were not resolved. However, performing the electrophoresis with higher $SC_{10}S$ concentrations (0.1% and 0.2%) resulted in more proteins entering the gel with slightly better resolution. This was also the case using 0.1% STS in the run buffer. Yet, the NSDS-PAGE buffer with 0.0375% SDS still yielded better resolution than the $SC_{10}S$ and STS buffers. The resolution of the NSDS-PAGE was still less than traditional SDS-PAGE, but enzymatic activity was retained in the NSDS-PAGE gel and not in the SDS-PAGE gel.
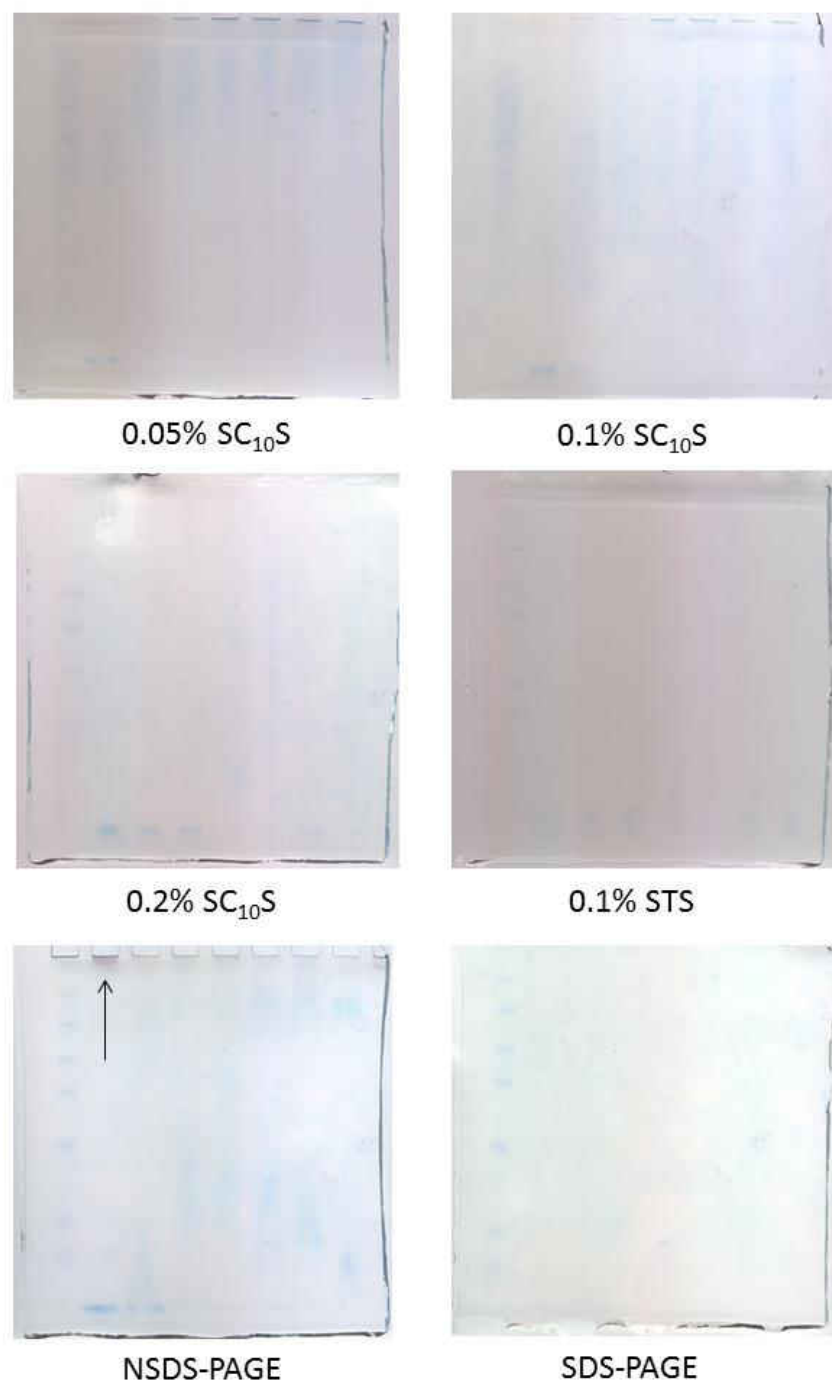
Figure 3.73. Phosphatase activity in SC$_{10}$S-, STS-, NSDS- and SDS-PAGE. Protein samples from a DEAE separation of the LLC-PK$_1$ proteome were loaded in 12% NuPAGE Bis/Tris gels and electrophoresed in run buffers containing various detergent concentrations. Gels were tested for phosphatase activity (arrow).
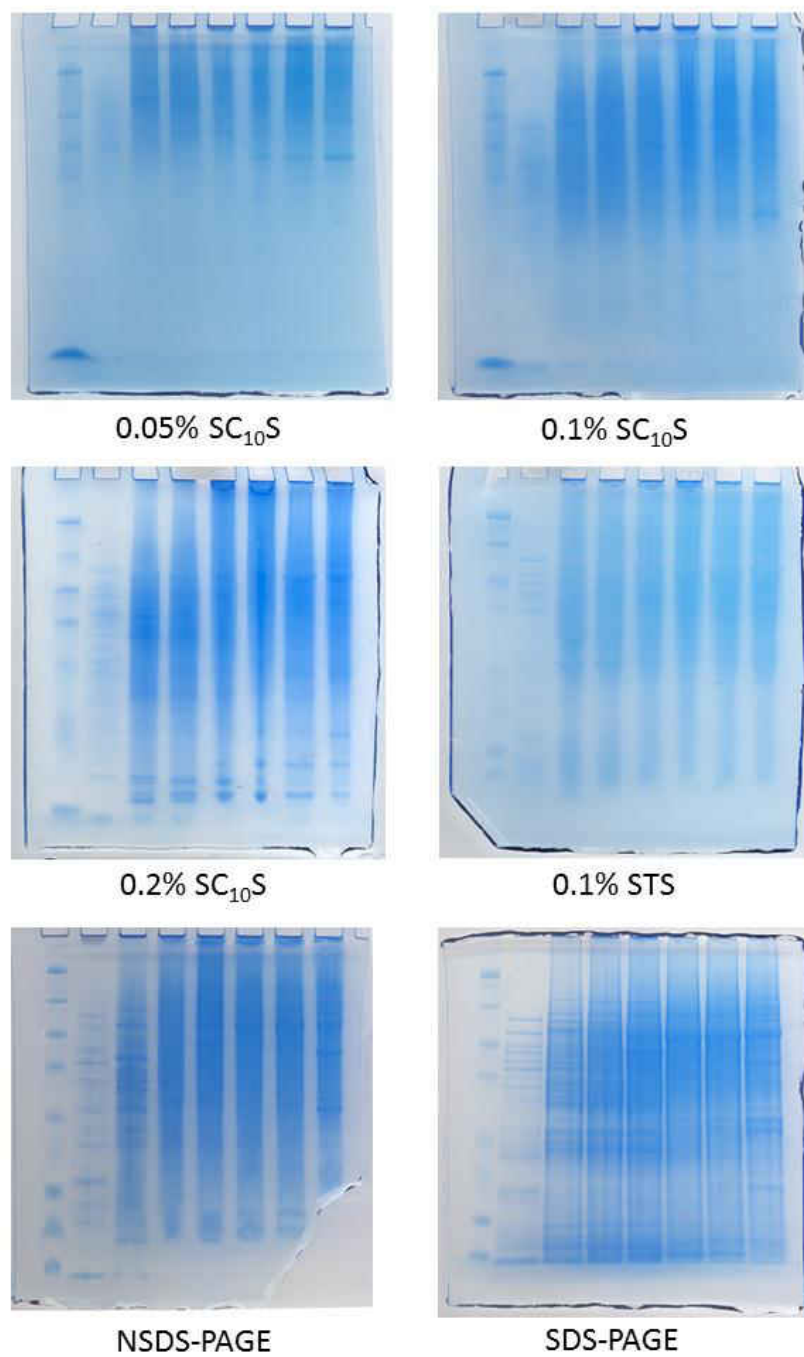
Figure 3.74. SC$_{10}$S-, STS-, NSDS- and SDS-PAGE of LLC-PK$_1$ proteome Gels from **Figure 3.73** were stained with SimplyBlue^{TM} Safe Stain to visualize protein migration.

2.5 µg of ADH was run in the last lane of all the gels. This lane was cut from the rest of

the gel and incubated in the alcohol dehydrogenase assay solution. Only the 0.05%

$SC_{10}S$, 0.01% $SC_{10}S$, and NSDS-PAGE buffer showed any evidence of activity (**Figure 3.75**).

Since the STS buffer did not show adequate resolution at the concentration used and,

more importantly, did not retain enzymatic activity of either ADH or proteomic

phosphatases, it was no longer considered an adequate substitute for SDS.
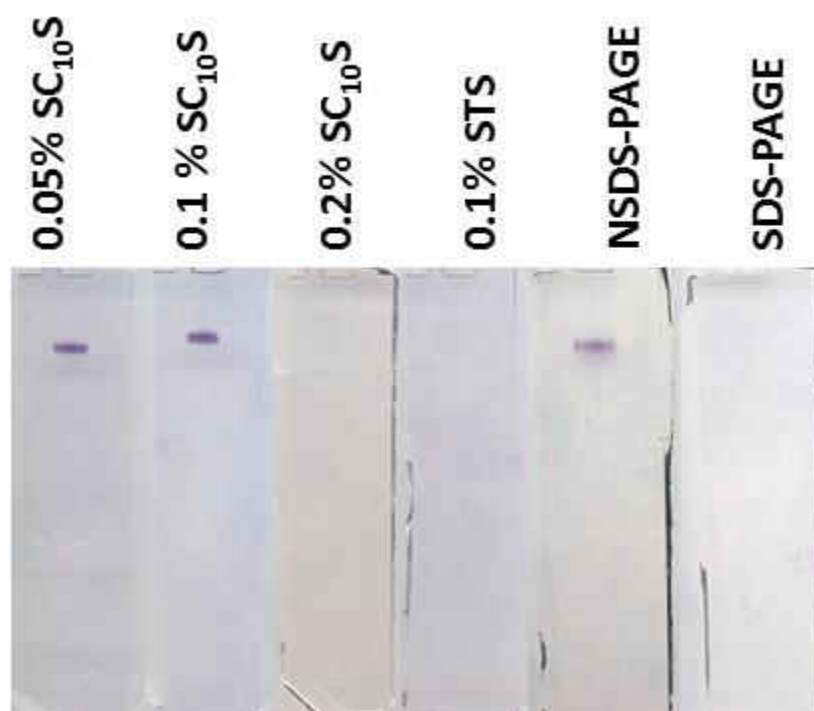
Figure 3.75. ADH activity using $SC_{10}S$-, STS-, NSDS- and SDS-PAGE. Residual activity of
2.5 µg of ADH electrophoresed in the gels from **Figure 3.73.**

The $SC_{10}S$ buffer, on the other hand, retained ADH activity at lower concentrations. Yet, only at higher concentrations of $SC_{10}S$ in the run buffer were the gels starting to see satisfactory resolution. Therefore, it was further explored to use a combination of SDS and $SC_{10}S$ in the run buffer to yield gels with properly resolved bands.

A matrix combination of $SC_{10}S$ and SDS in the run buffer was made varying the $SC_{10}S$ concentration from 0.025% - 0.5% and SDS concentration from 0 to 0.025% SDS. The gels run using these buffers were compared to gels run using the NSDS-, and SDS-PAGE methods. Again, electrophoretic samples were obtained from a DEAE separation of the LLC-PK$_1$ proteome. **Figure 3.76** displays the gels run with 0% and 0.0125% SDS in the run buffer containing 0.025%, 0.0375% and 0.05% $SC_{10}S$. The addition of $SC_{10}S$ to the 0% SDS run buffer appeared to have little effect on the overall separation of the proteins within the samples. In the 0.0125% SDS run buffers, the gel resolutions were enhanced compared to the 0% SDS run buffers, but again the additions of $SC_{10}S$ to the run buffer had little effect on the electrophoresis. Lastly, 0.025%, 0.0375%, and 0.05% $SC_{10}S$ were added to run buffers containing 0.025% SDS (**Figure 3.77**). The electrophoresis of the proteome samples in these buffers showed satisfactory resolution in all three gels. Yet, as seen in the other two SDS sample sets, the resolution did not change with the addition of more $SC_{10}S$ to the run buffer. Since the concentration of $SC_{10}S$ did not have a significant effect on resolution, it is unlikely that it interacted with the proteins within this sample.
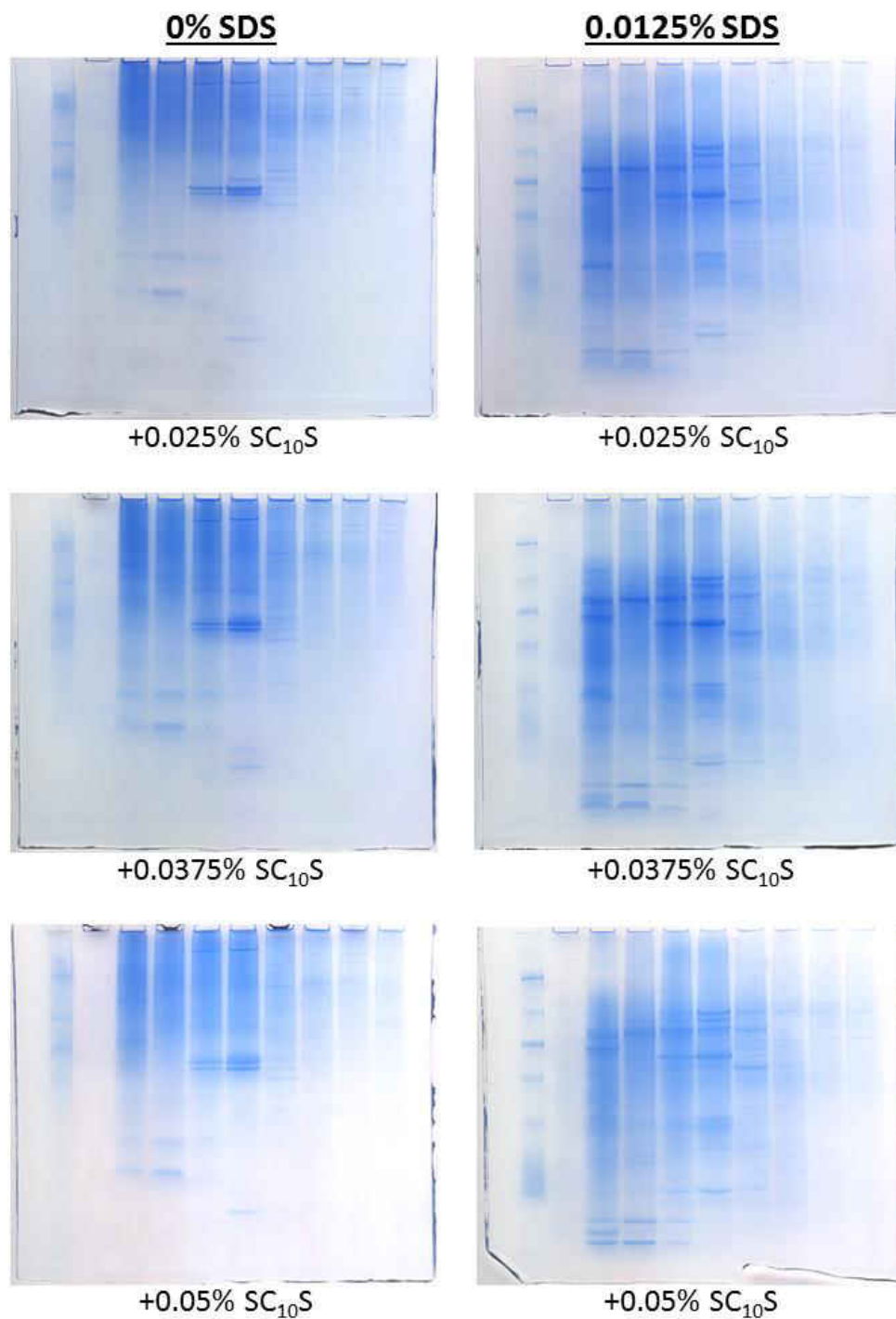
Figure 3.76. SC$_{10}$S-/SDS-PAGE of LLC-PK$_1$ proteome. Protein samples from a DEAE separation of the LLC-PK$_1$ proteome were loaded in 12% NuPAGE Bis/Tris gels and electrophoresed in run buffers containing 0.025-0.05% SC$_{10}$S and 0-0.0125% SDS. Gels were stained using SimplyBlue^{TM} Safe Stain.
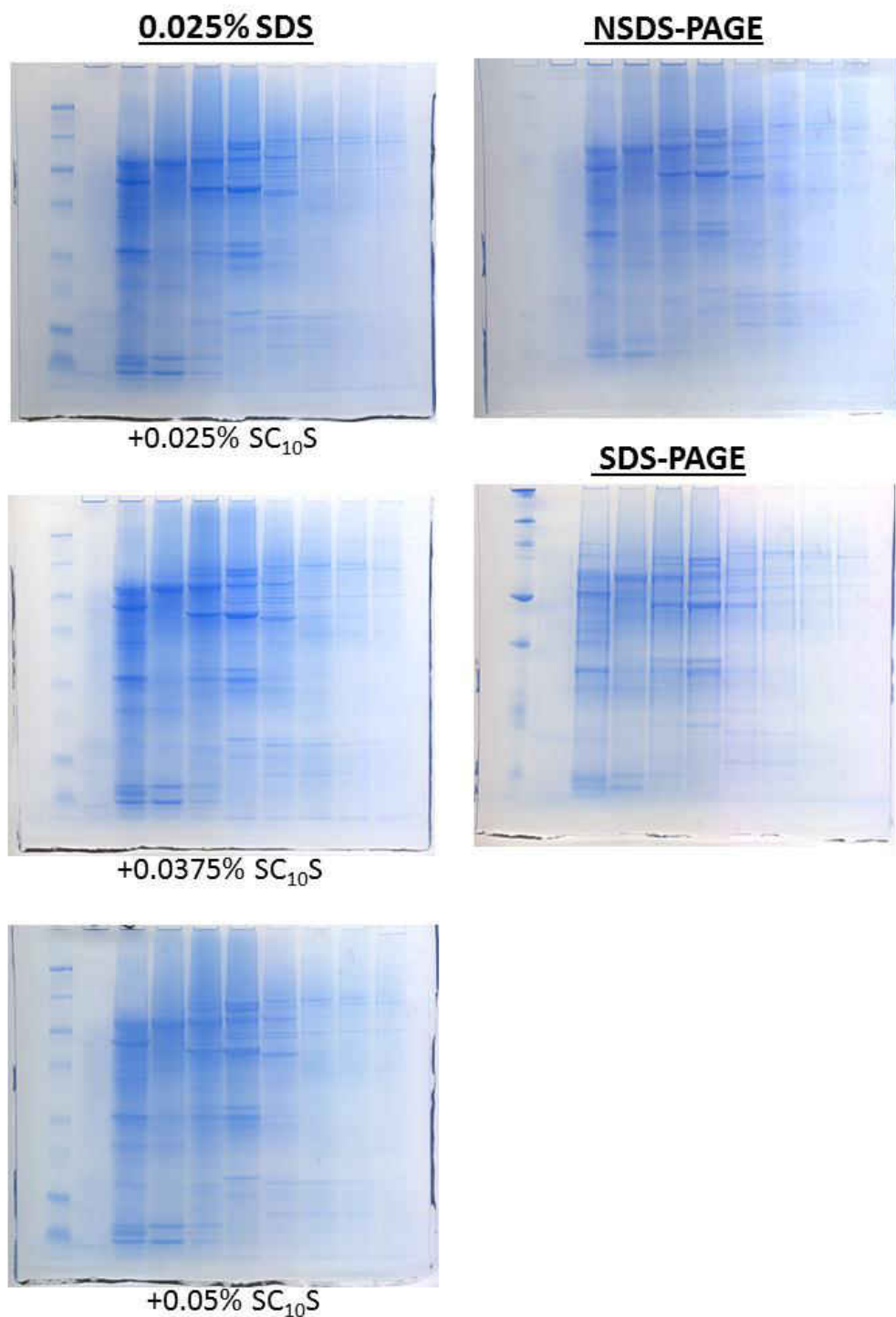
Figure 3.77. SC$_{10}$S-/SDS-PAGE of LLC-PK$_1$ proteome (cont.) Protein samples from a DEAE separation of the LLC-PK$_1$ proteome were loaded in 12% NuPAGE Bis/Tris gels and electrophoresed in run buffers containing 0.025-0.05% SC$_{10}$S and 0.25% SDS. As a comparison samples were run using the NSDS- and SDS-PAGE methods. Gels were stained using SimplyBlue^{TM} Safe Stain.

Interestingly, the resolutions of the 0.025% SDS gels were on par with the NSDS-PAGE method. Therefore, it is possible that using a smaller concentration of 0.025% SDS in conjunction with $SC_{10}S$ may provide adequate separations. Since resolution is not affected by the $SC_{10}S$ concentration, the enhanced resolution may be due to the buffer being more conductive than the 0.0375% NSDS run buffer which may aid in electrophoresis. Further investigations, including the evaluations of enzymatic activities used in section 3.7.4., would need to be revisited with the $SC_{10}S$/ 0.025% SDS run buffer to warrant the replacement of the NSDS-PAGE run buffer.

3.8. Applications of NSDS-PAGE

3.8.1. LA-ICP-MS metal analysis of NSDS-PAGE gels (a collaboration with William Wobig)

As mentioned before, Laser Ablation-Inductively Coupled Plasma-Mass Spectrometry, or LA-ICP-MS is a method used for determining the elemental content of a solid sample. In this technique, a pulsed high-energy laser is focused on the solid analyte, ablating the sample into an aerosol.[97] The aerosol is then transported using an inert gas—in this case Helium—to an inductively coupled plasma where it is completely atomized and ionized and the composition is carried to a mass analyzer.[97,98] This technique was initially designed for analyzing geological materials, but over the past decade, the uses LA-ICP-MS have expanded to studying biological samples, including PAGE gels.[99-102] The main drawback in using this technique in conjunction with gel electrophoresis has been metal loss due to the denaturing conditions of SDS-PAGE or poor resolution from BN-PAGE.[101,103] The development of the NSDS-PAGE method addresses both of these problems. A thorough investigation performed by William Wobig showed a significant increase in protein metal retention using the NSDS-PAGE method compared to SDS-PAGE.[94] Likewise, the results described in section 3.7 showed that there is a marked improvement in resolution using NSDS-PAGE versus BN-PAGE. Therefore, LA-ICP-MS is a viable method for subsequent metal analysis of electrophoresed proteins using NSDS-PAGE.

In continuation with section 3.6.4, the process of isolating the Zinquin proteome from LLC-PK$_1$ was scaled up using 60 plates of LLC-PK$_1$ cells ($\approx$7 x10^8 cells). In addition, aliquots were taken throughout the procedure to determine the degree of purification (**Table 3.9**).

	Lysate	HMW	Ace FT	Ace EL	ZQ FT	ZQ EL
Volume (mL)	4.65	6.6	7.4	7	6.4	4
Aliquot (µL)	100	100	100	100	100	100
F Aliquot (µL)	80	80	80	80	80	80
Total Volume	800	800	800	800	800	800
Dilution	10	10	10	10	10	10
F @ 470 nm	2554.552	1707.432	1681.917	661.982	1658.808	492.452
F x Dil	25545.52	17074.32	16819.17	6619.82	16588.08	4924.52
DC Aliquot (µL)	5	5	5	5	5	5
Dilution	5	5	5	5	5	5
mg/mL	3.2076634	2.11828	1.042888	0.80334	0.896751	0.120959
mg/mL x Dil	16.038317	10.5914	5.214441	4.016702	4.483757	0.604795
Total mg	74.578175	69.90325	38.58686	28.11691	28.69604	2.419178
ZQ Activity (F/mg)	342.53346	244.2565	435.8781	235.4391	578.0616	2035.617
ZQ Activity F/(mg/mL)	7963.9029	8060.463	16127.49	8240.367	18497.97	40712.33

Table 3.9. Purification of the Zinquin-proteome from LLC-PK$_1$ cells

The amount of Zinquin fluorescence per milligram of protein was again highest in the elution fraction from the Zinquin-affinity column, providing credence for the purification process. The Zinquin elution pool was further separated using DEAE chromatography (**Figure 3.78A**) and select fractions were concentrated and electrophoresed using the NSDS-PAGE method (**Figure 3.78B**).
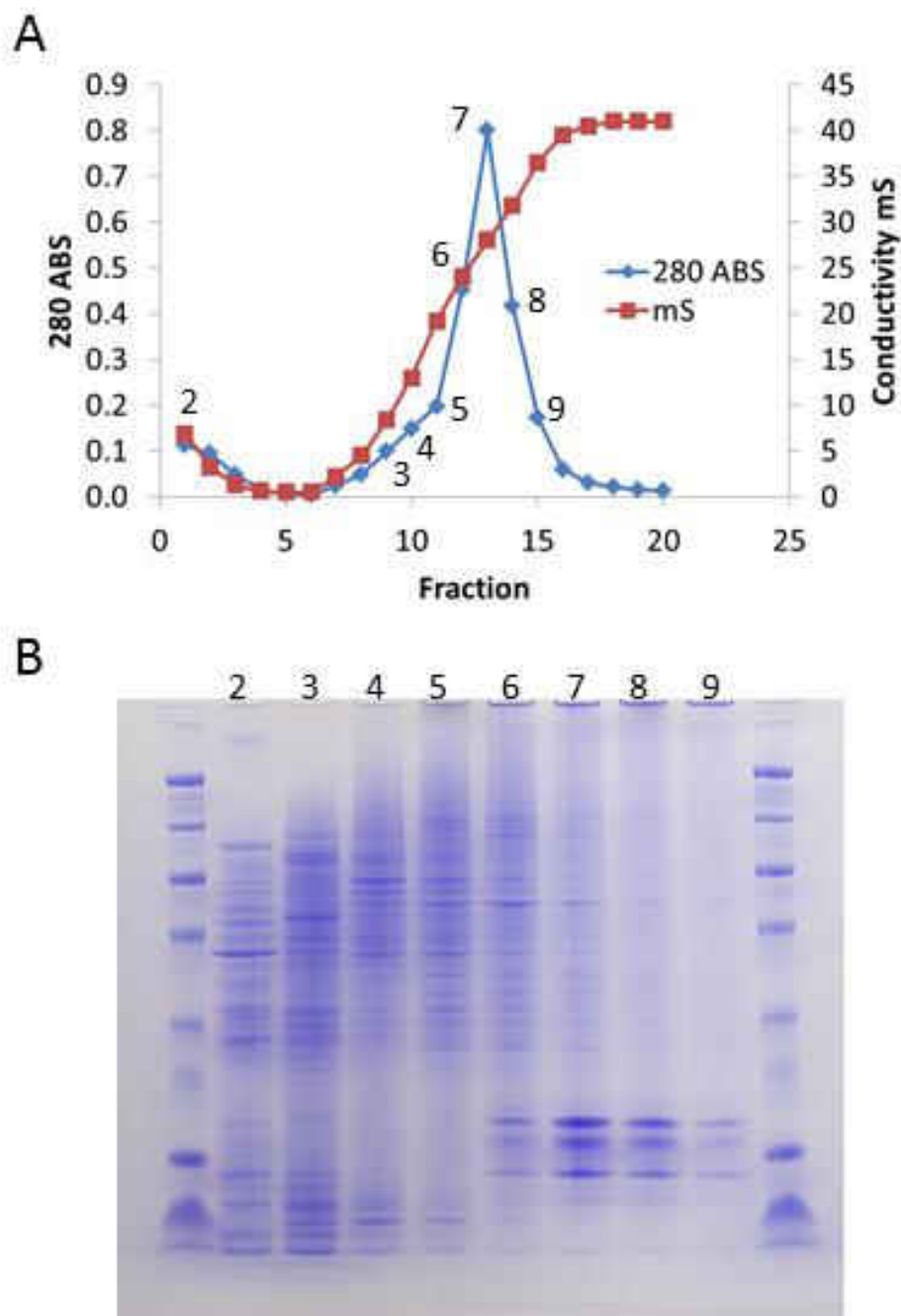
Figure 3.78. DEAE and NSDS-PAGE of the LLC-PK$_1$ Zinquin-proteome. Zinquin-proteome was loaded onto 1 mL DEAE Ceramic HyperD F column in 5 mM Tris-Cl pH 8.0. Column was gradient eluted with 5 mM Tris-Cl pH 8.0 containing 500 mM NaCl. 280 nm absorbance and conductivity were recorded (A). Numbered fractions were electrophoresed using NSDS-PAGE and stained using Coomassie R-250 (B).

In agreement with the previous experiment, Coomassie staining of the NSDS-PAGE gel revealed a variety of isolated proteins. This supports the hypothesis that Zinquin is interacting with multiple intracellular targets.

To determine the metal content of the electrophoresed proteins, a second gel was run and analyzed for ^{66}Zn, ^{63}Cu, and ^{56}Fe via LA-ICP-MS. The examination of Lane 2 showed numerous ^{66}Zn response peaks throughout the length of the gel (**Figure 3.79A**). These peaks that correspond to protein bands are the likely Zn-proteins with which Zinquin is interacting.

In addition, analysis of Lane 7 showed three ^{63}Cu response peaks that appear to line up with three proteins on the stained gel (**Figure 3.79B**). Hence, the Zinquin affinity column was able to capture some copper proteins as well. Zinquin binds Cu^{2+} one order of magnitude stronger than Zn^{2+}, but does not fluoresce.[29,31] This happens despite the fact that Cu^{2+} prefers square planar geometry to the tetrahedral coordination favored by Zinquin complexes caused by the steric hindrance of the 2' methyl group.[31,104] Therefore, it is conceivable that Zinquin may interact with members of the Cu-proteome to form non-fluorescent Zinquin-Cu-protein adducts.

The protein marked in **Figure 3.79A** was sent to the Innovation Center Mass Spectrometry Facility at the Medical College of Wisconsin for identification. The top ranked protein match was Annexin A1, a Ca^{2+} dependent phospholipid-binding protein. Despite having a ^{66}Zn response associated with this band, this protein is not thought of as a Zn^{2+}-binding protein. However, there are solvent accessible cysteine and histidine
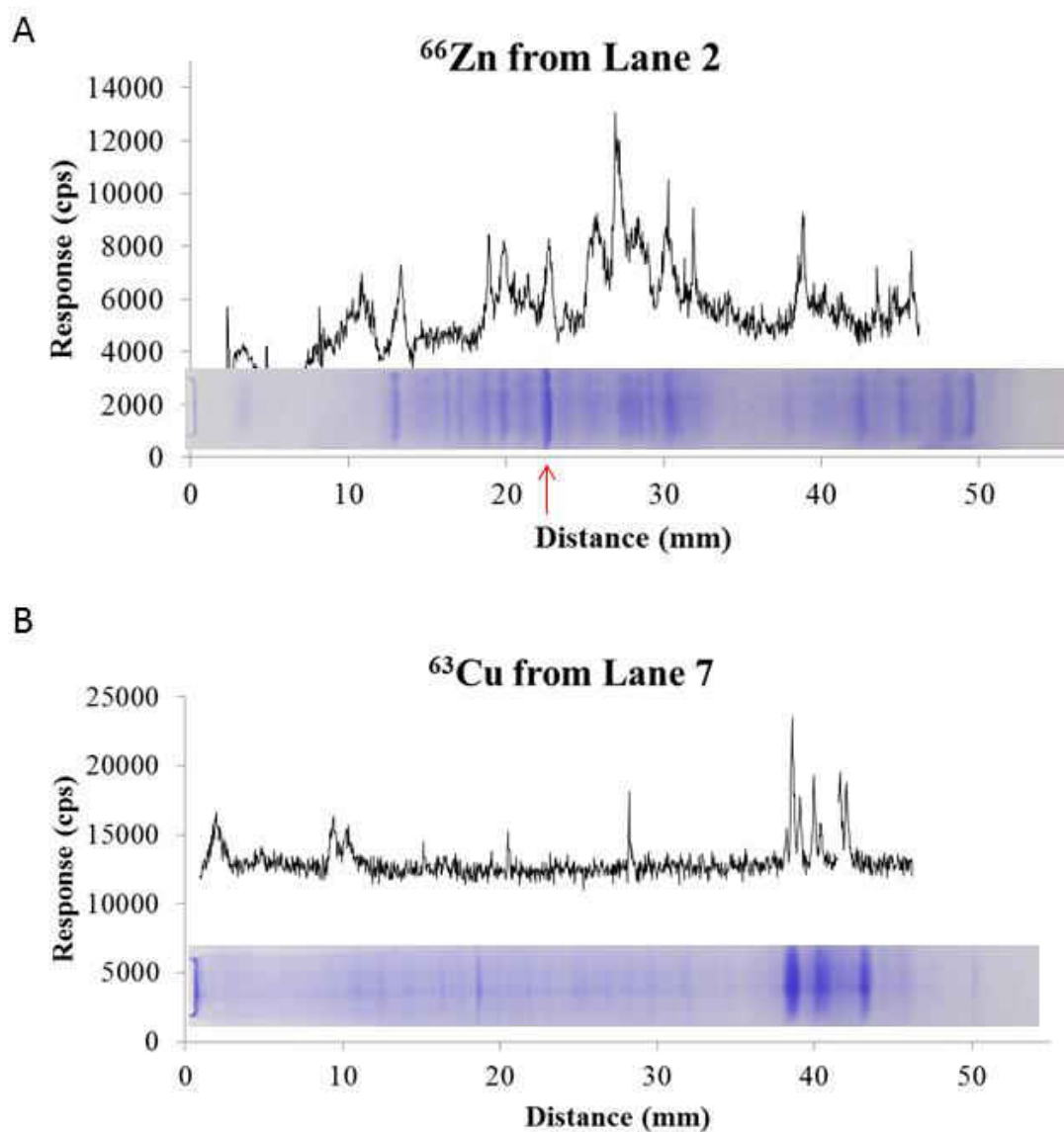
Figure 3.79. LA-ICP-MS of ZQ-proteome ran using NSDS-PAGE Duplicate unstained gel from **Figure 3.78** was dried and analyzed using LA-ICP-MS. Laser parameters: 100% energy, 200 μm spot size, 40 μm/min scan rate, 1000 mL/min He. [66]Zn response trace from Lane 2 is in (A) and [63]Cu response trace from Lane 7 is in (B).

residues which may serve as a coordination site for Zn^{2+}.[105] Whether this is functionally significant or an anomalous result is still to be determined. Else, the second ranked result—malate dehydrogenase—was a protein known to be activated by Zn^{2+}.[106] Yet, purifications of this enzyme via ammonium sulfate and cation exchange chromatography resulted in a metal free protein.[107] However, this can be attributed to the inclusion of mM amounts of EDTA added in the purification buffers.[107] Therefore, it is possible that this is the Zn-protein being captured by the Zinquin column.

The ^{56}Fe analysis of the gel revealed no iron peaks associated with protein bands. This result most likely means that Zinquin has little to no affinity for Fe-proteins. However, the background ^{56}Fe response was extremely high in all the lanes (>30,000 cps), making the detection of Fe-proteins in this system difficult. This was most likely due to iron contamination during the production of the precast gels. Therefore, if the NSDS-PAGE-LA-ICP-MS method is to be used to test for iron proteins, samples should be made using a rare isotope of iron to dampen the background response. In addition, gels should be pre-run in ddH_2O to aid in the removal of the contaminant metals within the precast gel (see section 3.7.3.).

To improve upon this method, LLC-PK$_1$ cells were grown in the presence of ^{70}Zn. Growing the cells in this rare isotope (natural abundance = 0.6%) accomplishes two complementary goals. First, the response from any contaminant Zn^{2+} will be less when analyzing a rare isotope as opposed to an isotope of higher abundance. Second, growing cells in only ^{70}Zn results in every Zn-protein having the same isotope and not

the natural distribution of isotopes. This means that the ICP-MS response obtained from a Zn-protein grown in ^{70}Zn represents close to 100% of that protein whereas the ICP-MS response from a Zn-protein grown normally only correlates to the natural abundance of the analyzed isotope. Hence, the ^{70}Zn enriched LLC-PK$_1$ proteome was separated using an HPLC DEAE column and select fractions were concentrated and electrophoresed using NSDS-PAGE.

Before the samples were analyzed by LA-ICP-MS, the laser ablation parameters were optimized. There are four different parameters that affect the efficiency of ablation: (1) the spot size of the laser, (2) the energy of the laser, (3) the rate at which the laser moves across the sample, and (4) the flow of the carrier gas over the ablated material. To test the effects of these variables on zinc response obtained from ICP-MS, 12.5 μg of alcohol dehydrogenase was electrophoresed using the NSDS-PAGE method and subsequently located in the gel by incubation in the ADH activity assay solution. The activity bands were then cut from the gel, dried, and analyzed by LA-ICP-MS. Varying these four parameters of the ablation process led to quite different ^{64}Zn response patterns (**Figure 3.80**). Most notably, lowering the scan rate of the ablation led to a more resolved ^{64}Zn response. This was due to the fact that a lower scan rate ablated more sample and also allowed for the acquisition of more data points from the ICP-MS. Yet, lowering the scan rate to a certain degree resulted in a lower Zn response. This was most likely due to the thermal dispersion of the laser energy rather than ablation. This could be ameliorated by lowering the laser energy during the scan (green traces versus
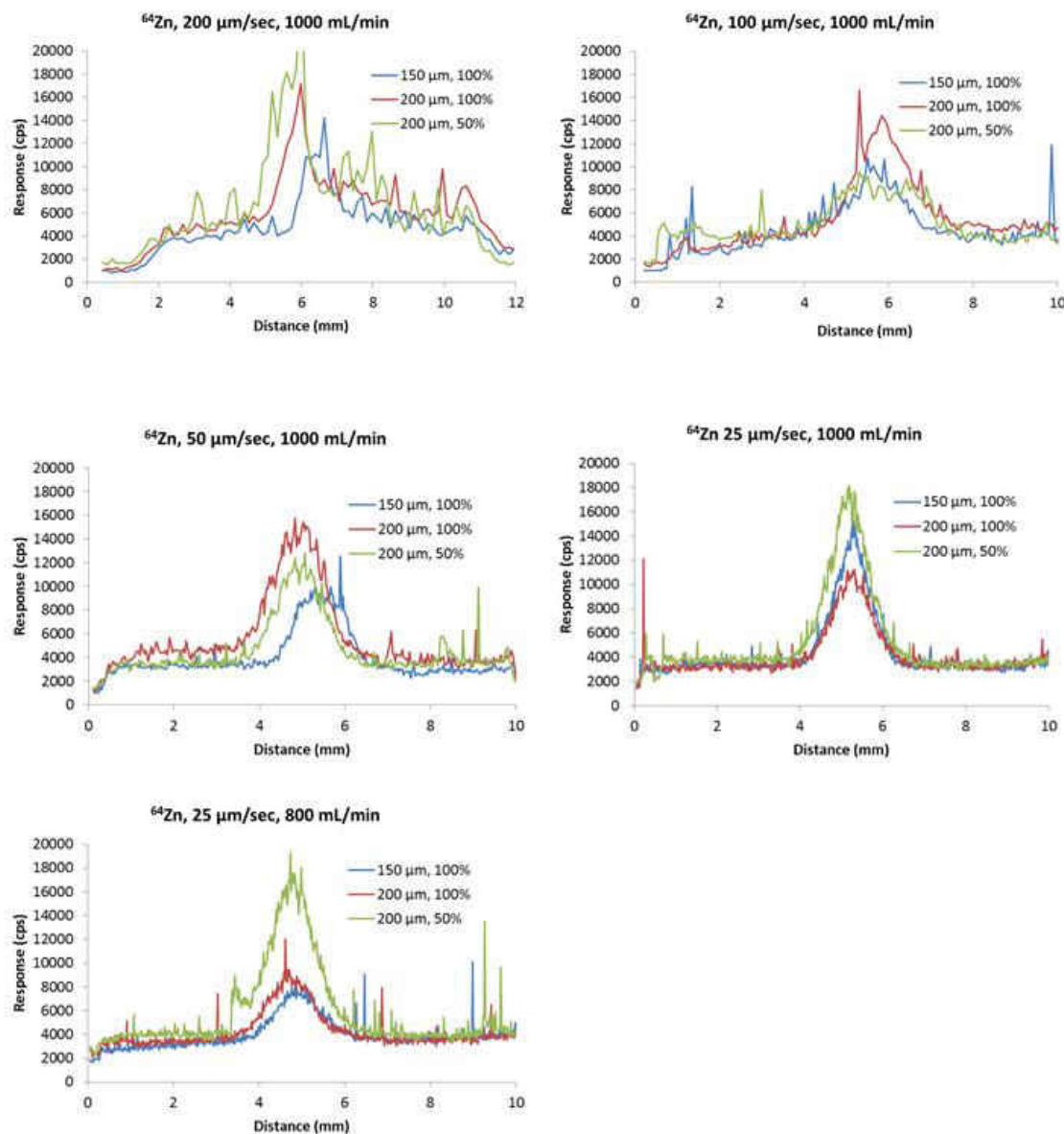
Figure 3.80. Optimization of LA-ICP-MS parameters 12.5 µg of ADH was electrophoresed using NSDS-PAGE method and analyzed for ^{64}Zn via LA-ICP-MS. Laser parameters were varied to determine optimal instrument settings.

the red/blue traces in the 25 µm/sec scans). Also, a higher carrier gas flow (1000 mL/min versus 800 mL/min) resulted in narrower response peak presumably due to more streamlined transfer of the ablated material to the ICP-MS. Therefore, scans were now performed at 50% laser energy with a 200 µm spot size scanned at 25 µm/sec and a carrier gas flow rate of 1000 mL/min.

To provide semi-quantitative results, 0.5 µL of ^{70}Zn standards were spotted onto the gel, dried for one hour, and ablated (**Figure 3.81A**). By using this rare zinc isotope, the background was nearly eliminated and ^{70}Zn could be faithfully detected down to 29 ppb (limit of detection was defined by a response three times greater than the background).[98] This result is a significant improvement compared to other LA-ICP-MS studies in which the limits of detection for zinc were nearly 100 times higher (2-6 ppm).[101,108,109] In addition, both the 9.8 and 20 ppb spots could be visualized, but the response values (ca 150 and 180 cps, respectively) were only slightly above the background (ca 80 cps). Next, the average response obtained from each standard spot was plotted versus the concentration of ^{70}Zn in the standard (**Figure 3.81B**). The resulting linear regression analysis showed excellent correlation (R^2 = 0.9975) throughout the tested standards and was used to determine the approximate concentration of ^{70}Zn in the protein bands in the gel.
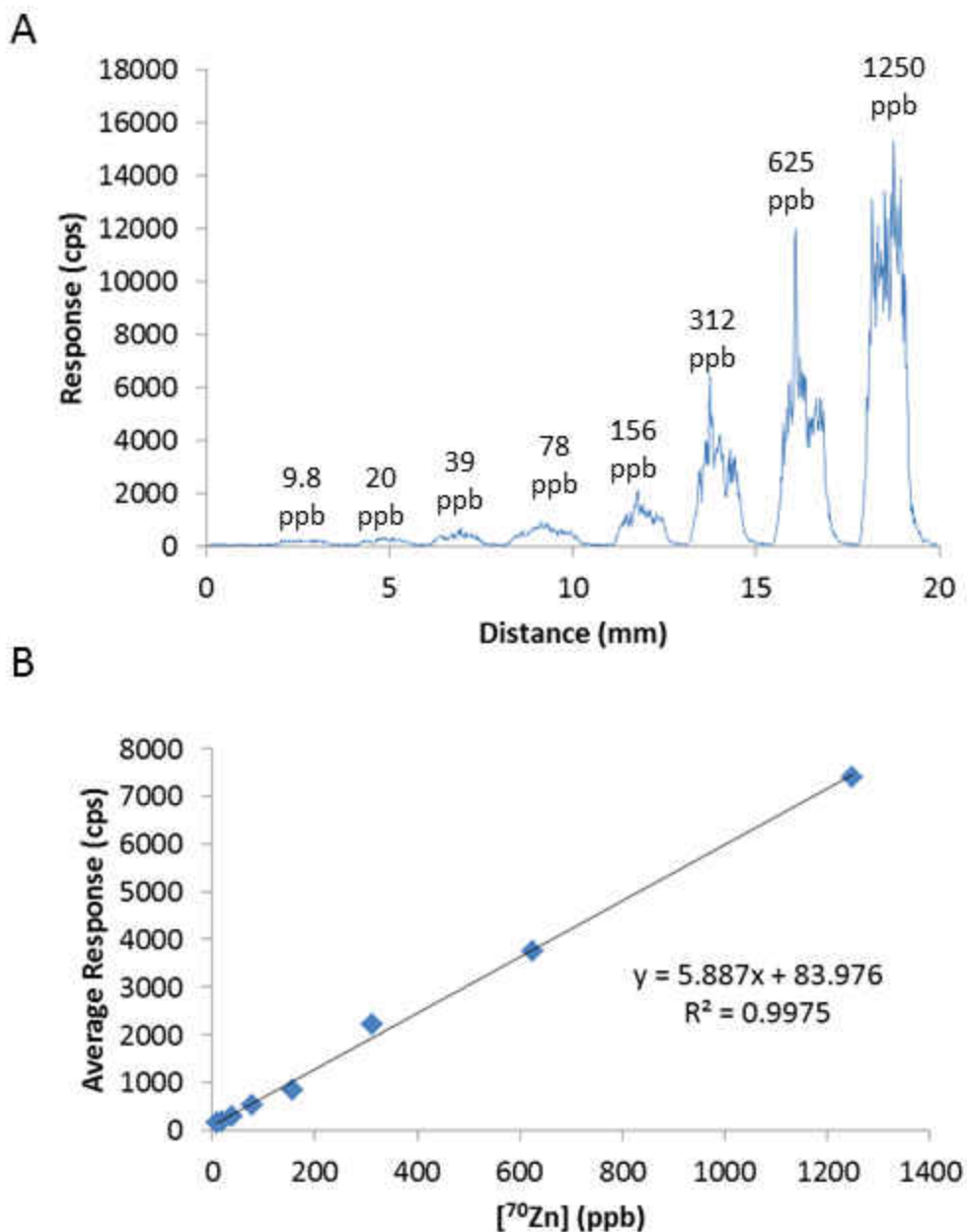
Figure 3.81. LA-ICP-MS analysis of [70]Zn standards. 0.5 µL of 9.8-1250 ppb [70]Zn standards were spotted on the edge of a PAGE gel and dried for one hour before LA-ICP-MS analysis. Laser parameters: 50% laser energy, 200 µm spot size, 25 µm/min scan rate, 1000 mL/min He. (A) [70]Zn response from ablating through the standards. (B) Linear regression of the average response from ablated standards vs. [[70]Zn].
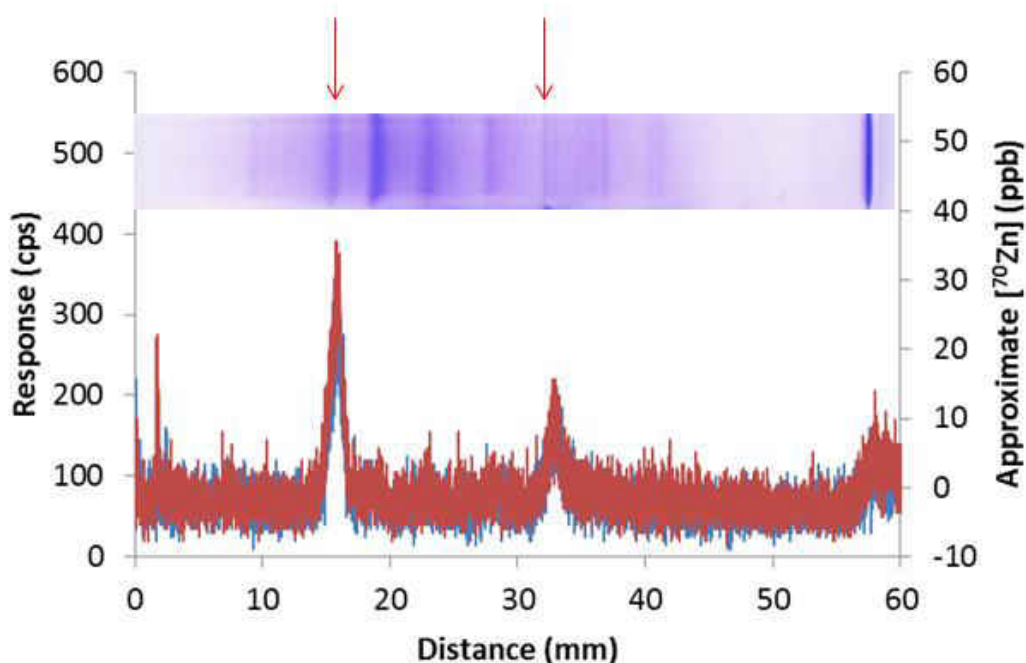
Figure 3.82. LA-ICP-MS of LLC-PK$_1$ ^{70}Zn-proteome. LLC-PK$_1$ ^{70}Zn-proteome was separated using HPLC DEAE and electrophoresed using NSDS-PAGE. LA-ICP-MS analysis revealed 2 isolated proteins containing ^{70}Zn (arrows). Laser parameters: 50% laser energy, 200 μm spot size, 25 μm/min scan rate, 1000 mL/min He.

The LA-ICP-MS trace from one of the gel lanes is shown in **Figure 3.82**. There were two ^{70}Zn response peaks that correlated to two protein bands on the Coomassie stained gel (red arrows). Importantly, due to the low concentration, these zinc peaks would not have been detected by traditional LA-ICP-MS techniques (without using ^{70}Zn). Thus, using an isotope-enriched sample, NSDS-PAGE-LA-ICP-MS is an innovative method that can be used for detecting metal cofactors associated with members of a cellular proteome.

3.8.2. TSQ Staining of NSDS-PAGE gels

Based on metal analysis using LA-ICP-MS and activity assays, the metal cofactors of many proteins were retained in the NSDS-PAGE process.[94]   Therefore, since TSQ and Zinquin are known to bind to Zn-proteins, incubating NSDS-PAGE gels in a TSQ/ZQ solution should result in fluorescent signals from bands corresponding to members of the Zn-proteome.[56,71]

Hence, the Zinquin-proteome was isolated from LLC-PK$_1$ cells and electrophoresed using the NSDS-PAGE method. To check for background fluorescence, the gel was placed on a UV transilluminator and excited using the long wavelength setting (≈365 nm) and an image of the gel was taken using a 470 nm emission filter (**Figure 3.83A**). The gel was then soaked in a 25 µM TSQ staining solution for 30 minutes, washed twice in ddH$_2$O, and the fluorescence image was captured (**Figure 3.83B**). Upon TSQ staining, numerous protein bands became fluorescent, suggesting that TSQ bound to the Zn-proteins in the gel which can be visualized by this method.

To show that this is a Zn-dependent phenomenon, the gel was soaked for 45 minutes in a solution containing 100 µM TPEN, a strong chelator of Zn^{2+}. The resulting fluorescence image showed that most, but not all, of the fluorescence in the gel was quenched. This was consistent with what was seen in TSQ-treated cells reacted with TPEN in which a majority of the cellular fluorescence was depleted, by not completely quenched.[56] The loss of fluorescence was due to either extraction of Zn^{2+} from a TSQ-Zn-protein adduct (reaction 3.30), or a ligand substitution reaction between TPEN and TSQ (reaction 3.31).
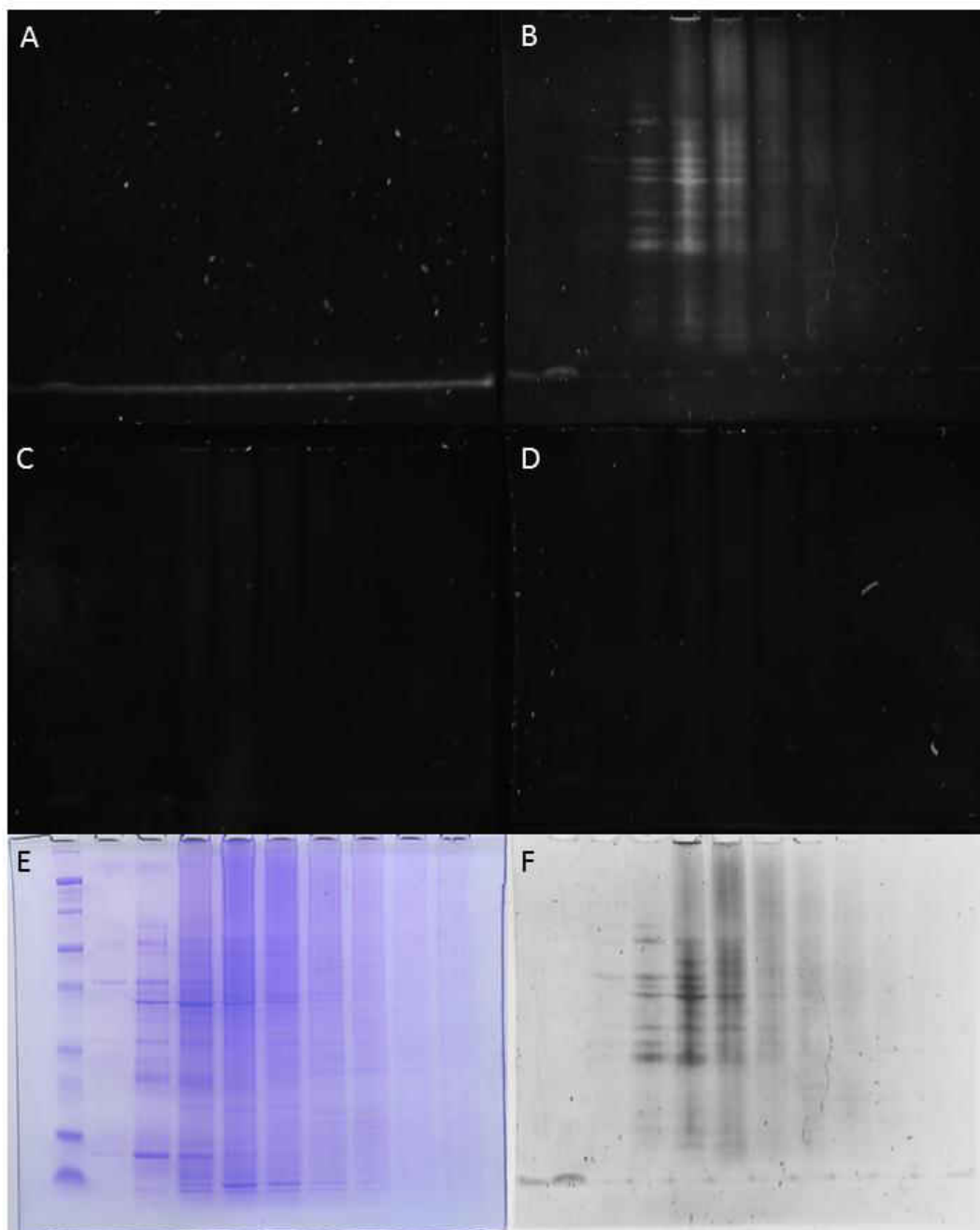
Figure 3.83. TSQ Stain of Zinquin proteome on NSDS-PAGE gel. Zinquin proteome was run using NSDS-PAGE. Electrophoresed gel was excited at 365 nm and images were captured using 470 nm filter and 3 second exposure for background (A), followed by 25 µM TSQ 30 min (B), followed by 100 µM TPEN 45 min (C), followed by 25 µM TSQ 45 min (D). Gel was stained using Coomassie R-250 stain (E) and compared to the inverted TSQ stain (F).

$$TPEN + TSQ\text{-}Zn\text{-}Protein \rightleftarrows ZnTPEN + TSQ + apo\text{-}Protein \qquad (3.30)$$
$$TPEN + TSQ\text{-}Zn\text{-}Protein \rightleftarrows TPEN\text{-}Zn\text{-}Protein + TSQ \qquad (3.31)$$
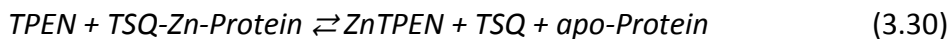
In an attempt to elucidate which reaction is occurring, the gel was re-soaked in 25 µM

TSQ for 45 minutes. If TPEN is chelating Zn^{2+} from the proteins (reaction 3.28), Zn-TPEN

should enter in solution and be unperturbed by TSQ due to its high affinity for Zn^{2+}. If

TPEN is replacing TSQ in Zn-proteins (reaction 3.29), then the addition of excess TSQ in

the absence of "free" TPEN may force the equilibrium back to the left and fluorescent

protein bands may be recovered. However, this assumes that TPEN-Zn-protein adducts

are kinetically labile and that the formation constant of a TPEN-Zn-protein adduct is

near the formation constant of a TSQ-Zn-protein adduct and thus the equilibrium can be

perturbed. Nonetheless, the re-stained TSQ gel did not exhibit any enhancement of

fluorescence (**Figure 3.83D**). Therefore, either the assumptions of the reactivity of TPEN

adducts were incorrect or TPEN chelated out a majority of the Zn^{2+} from Zn-proteins.

The above result provided initial evidence that TSQ can be used to image Zn-proteins

within polyacrylamide gels. Importantly, the amount of fluorescence observed in these

TSQ-stained gels should be correlative to the amount of Zn^{2+} in the protein band, not

the quantity of protein. To test this, a Zn-deficient alcohol dehydrogenase was prepared

by reacting Zn_2-ADH with TPEN and isolating Zn-ADH via gel filtration (see section

3.3.5.). 25 µg of both forms of the enzyme were electrophoresed using the SDS-, NSDS-

, and BN-PAGE methods and subsequently stained in 25 µM TSQ (**Figure 3.84**).
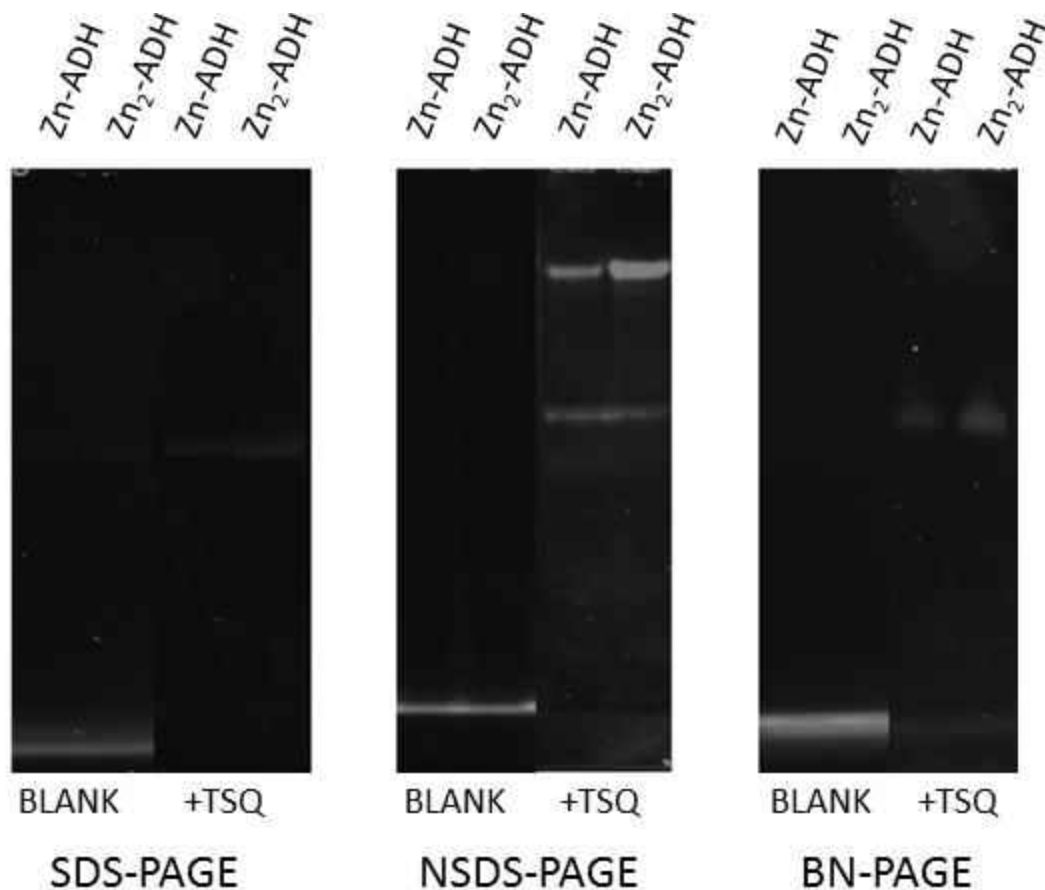
Figure 3.84. TSQ stain of ADH using SDS-, NSDS-, and BN-PAGE. 25 μg of Zn-ADH (prepared as described in section 3.3.5) and Zn_2-ADH were electrophoresed using SDS-, NSDS-, and BN-PAGE methods. Electrophoresed gels were excited at 365 nm and images were captured using 470 nm filter and 3 second exposure. Background fluorescence was recorded (BLANK) and after exposure to 25 μM TSQ for 30 min (TSQ) for the 3 gels.

As expected, TSQ staining of the SDS-PAGE gel resulted in minimal fluorescence enhancement from the background, presumably due to the loss of Zn^{2+} from ADH during the SDS-PAGE protocol. The small amount of fluorescence that was observed after staining was similar in both gel lanes and did not correlate to the amount of Zn^{2+} loaded in each lane. This suggests that a small amount of exogenous Zn^{2+} in solution—most likely from the destruction of Zn_2-ADH—bound to those denatured proteins to which

TSQ formed a fluorescent adduct. Else, some Zn^{2+} was still associated with these bands despite the loss of activity (see section 3.7.4.).

Examining Zn-ADH and Zn_2-ADH run using the NSDS-PAGE method showed significant fluorescence enhancement after treating the gel with TSQ. Importantly, there was less fluorescence in the Zn-ADH sample compared to the Zn_2-ADH sample despite each lane containing the same amount of protein. This supports the notion that the fluorescence is dependent on the Zn^{2+} content of the bands, not on the protein itself.

Interestingly, exposing the BN-PAGE gel to TSQ showed only moderate fluorescence enhancement when compared to the NSDS-PAGE gel. This is in spite of the fact that the BN-PAGE method keeps Zn_2-ADH in its native form during the separation (see section 3.7.4.). A possible explanation for the lower fluorescence is that the protein streaked down the BN-PAGE gel, whereas in the NSDS-PAGE gel, the protein moved in a concentrated band and therefore yielded higher fluorescence. Nevertheless, the Zn_2-ADH lane stained brighter than Zn-ADH lane, further validating this method as a way to image Zn-proteins in polyacrylamide gels.

Lastly, this staining technique was used to test whether TSQ and Zinquin react with the same Zn-proteins. The LLC-PK$_1$ proteome was separated using DEAE chromatography and a select fraction (0.1 nmoles of total Zn^{2+}) was reacted with 0.4 nmoles of TSQ, ZQ_{ACID}, or ZQ_{EE} for 1 hour before loading into a PAGE gel. Also included in the gel was the proteomic fraction reacted with 0.2 nmoles of $^{70}Zn(TSQ)_2$, $^{70}Zn(ZQ_{ACID})_2$, and $^{70}Zn(ZQ_{EE})_2$. The gel was run using the NSDS-PAGE technique and the fluorescence

image of the gel was recorded (**Figure 3.85**). Since the fluorescent probes were run with the protein sample, the gels were not incubated in the TSQ staining solution.

The TSQ-treated sample showed fluorescence throughout the entire length of the gel, suggesting that TSQ formed ternary adducts with many of the Zn-proteins in the sample. There were also multiple fluorescent bands in the proteome fraction reacted with ZQ_{EE}; yet, the staining pattern was quite different compared to the TSQ sample (red arrow vs. green arrow in **Figure 3.85A**).   A histogram of the both the TSQ and ZQ_{EE} lanes revealed that both fluorophores reacted with many of the same proteins as evidenced by the overlap of intensity peaks (**Figure 3.85B**).   However, the majority of the Zinquin fluorescence was located in Zn-proteins near the top of the gel, while TSQ fluorescence was mainly associated with Zn-proteins further down the gel. In addition, there were a few fluorescence peaks that were associated with only one of the two fluorophores (color coded dots in **Figure 3.85B**).   Taken together, these data imply that these two closely related Zn sensors prefer different Zn-proteins and thus image different subsets of the Zn-proteome.

Importantly, the fluorescence patterns of the TSQ-treated fraction and the $Zn(TSQ)_2$ treated fraction were quite similar to one another.   This was also the case in the ZQ_{EE} and $Zn(ZQ_{EE})_2$ fractions as well. This result strengthens the case that both $Zn(TSQ)_2$ and $Zn(ZQ_{EE})_2$ are capable of rearranging to form sensor-Zn-protein adducts as proposed in section 3.4.
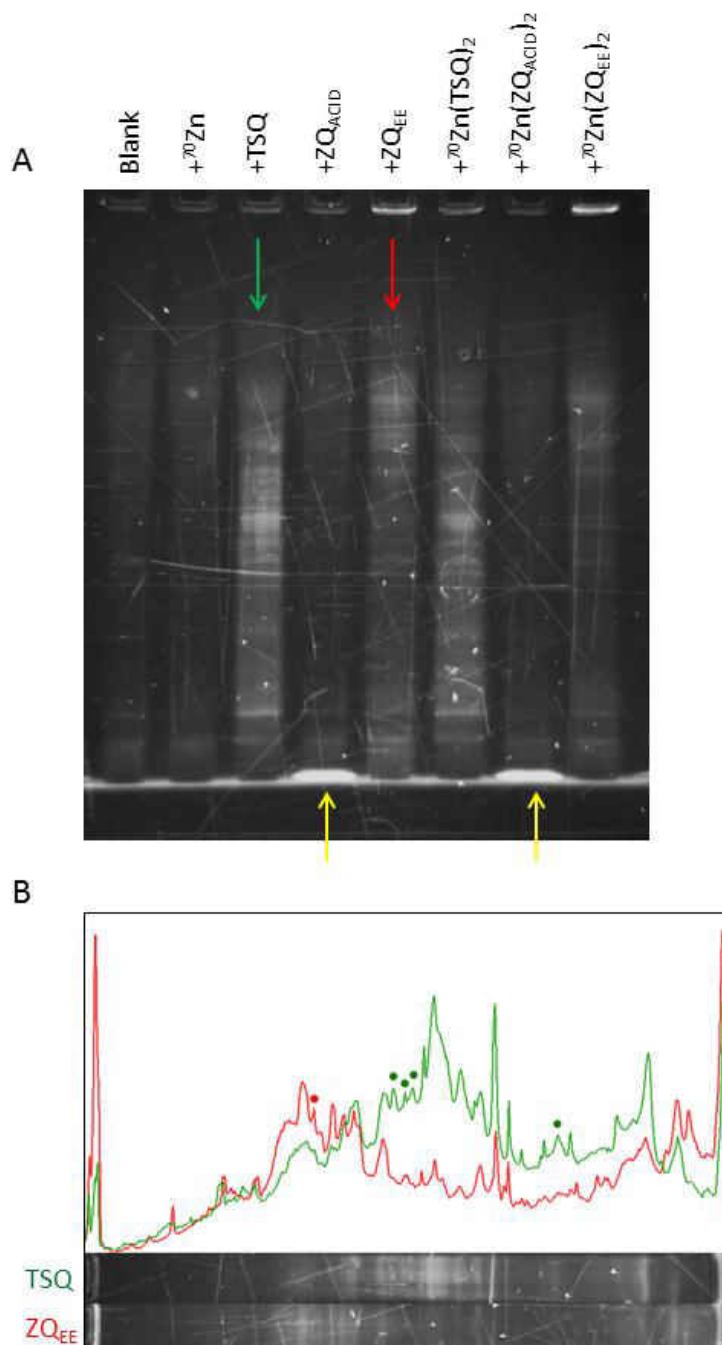
Figure 3.85. NSDS-PAGE of Zn-proteome reacted with sensors and Zn(sensors)$_2$. LLC-PK$_1$ Zn-proteome was fractionated using DEAE chromatography. 0.2 nmoles of Zn-proteome were reacted with 0.4 nmoles of TSQ, ZQ$_{ACID}$, ZQ$_{EE}$, and 0.2 nmoles of ^{70}Zn(TSQ)$_2$, ^{70}Zn(ZQ$_{ACID}$)$_2$, ^{70}Zn(ZQ$_{EE}$)$_2$ for one hour and electrophoresed using NSDS-PAGE. (A) Gels were excited at 365 nm and images were captured using 470 nm filter and 5 second exposure. (B) Densitometry plot of the TSQ (green) and ZQ$_{EE}$ (red) lanes constructed using ImageJ. Color-coded dots signify unique protein bands for each sensor

The lanes treated with ZQ_{ACID}—both as free ZQ_{ACID} and as $Zn(ZQ_{ACID})_2$—resulted in the majority of fluorescence located at the dye front (yellow arrows in **Figure 3.85A**). Unlike neutrally charged TSQ and ZQ_{EE}, ZQ_{ACID} is negatively charged at the pH in which the electrophoresis is performed. Therefore, the application of an electric field resulted in ZQ_{ACID} running with the other negatively charged dyes in the sample buffer to the dye front at the bottom of the gel. Hence, this method cannot be used to faithfully detect Zn-proteins if the samples are treated with Zinquin acid prior to electrophoresis.

4. <u>Discussion</u>

Over the past few decades, there has been a paradigm shift in the understanding of the functions of Zn^{2+} in biological systems. Originally thought of as just another enzymatic cofactor, Zn^{2+} has emerged as a major player in a variety of physiological processes including regulation of apoptosis, cognition, and wound healing.[3,110-114] Moreover, Zn^{2+} dyshomeostasis has been linked to numerous human ailments ranging from stunted growth, to neurodegenerative disorders, to compromised immunity.[111,115,116] Therefore, there is a growing imperative to understand the underlying chemical mechanisms of Zn^{2+} metabolism.

(2-methyl-8-p-toluenesulfonamido-6-quinolyloxy)acetate (Zinquin) and its analogues have been staple tools used as a means to monitor the intracellular Zn^{2+} status. Much of our understanding of Zn^{2+} biology is rooted in the use of these fluorescent sensors.[24-26] Yet, beyond proof of principle experiments, there are limited examinations of the chemical nature of these sensors, specifically with respect to how they may react in a cellular environment. If the chemistry of the sensor used has not been thoroughly characterized, how can the chemistry of the studied process be properly understood?

The bidentate binding nature of Zinquin and its analogues is cause for concern that it may interact with Zn^{2+} coordinated to another intracellular ligand, not transient Zn^{2+} (reaction 3.1). Indeed, Hendrickson et. al. verified that Zinquin acid could form fluorescent adduct species with small organic ligands, but the extrapolation to larger

ligands—such as Zn-proteins—was not investigated.[53] Although adduct formation with Zn-proteins had been postulated by some[22,29,53,54], no thorough investigation into the intracellular reactions of Zinquin had been undertaken. Therefore, one of the main goals of this study was to elucidate the types of reactions Zinquin may undergo in a cellular context, including adduct formation.

The use of fluorescence spectrophotometry over microscopy was crucial in the understanding of the reactions of Zinquin. The most important advantage was the ability to obtain spectral data from a fluorescent Zinquin species. The fluorescence spectrum of $Zn(ZQ_{ACID})_2$ has a wavelength maximum at 492 nm, whereas Zinquin ternary adducts have blue-shifted emissions centered near 470 nm as determined by reactions of Zinquin with the Zn-proteome (section 3.2.1.), model proteins (sections 3.2.2., 3.2.3., and 3.4.1.), and small organic ligands (section 3.3.4.). The same spectral properties hold true for TSQ as well.[56] This provided a physical handle to distinguish between adduct formation and free Zn-sensor complexes. Importantly, these data could not have been obtained by simply measuring emission intensity in fluorescence microscopy or by single wavelength fluorimetry. This validates the need for more probing analytical techniques.

Another advantage includes the number of cells in each experiment. Obtaining spectrofluormetric data from cells in a cuvette suspension involves the fluorescence contribution from millions of cells in the system. In contrast, fluorescence microscopy analyzes only the few cells within the field of view. Therefore, using fluorescence spectrophotometry removes researcher bias from choosing select cells in a field of

potentially millions of cells on a microscope plate as representatives of the entire system.

Along the same lines, the concentration of the cells being tested can easily be adjusted when cells are in suspension. This is important because treating cells with fluorophores such as Zinquin is, in essence, a chemical reaction. Therefore, a variation in cell concentration is, in effect, a variation of the reactant concentration which can ultimately affect the products formed, in this case fluorescent Zinquin species. It stands to reason that performing experiments on sparsely populated microscope plates may result in different reactions than ones that occur on densely populated plates. By adjusting the concentration of cells in the cuvette to a set value—in this case 5×10^6 cells/mL—for all *in vivo* exposures, this variable effect is eliminated from experiment to experiment.

In all of the seven cell types tested, the fluorescence spectra after exposure to Zinquin were centered near 470 nm, not 492 nm as expected for $Zn(ZQ_{ACID})_2$ (see section 3.1.2). This provided initial evidence that Zinquin is reacting with members of the Zn-proteome to form adducts (reaction 3.1). Also, the fluorescence intensities in each cell type after exposure were near the intensity of 1 μM $Zn(ZQ_{ACID})_2$. Since free $[Zn^{2+}]$ is thought to be in the low nM range and total $[Zn^{2+}]$ in the μM range, the Zn-proteome must be considered a target for Zinquin to account for the amount of fluorescence observed.[4,23,55]

In a parallel study performed by the Petering group, it was determined that TSQ—a Zinquin predecessor—reacted solely with protein-bound Zn^{2+} when exposed to cells.[56] Gel filtration experiments involving the lysates from Zinquin exposed cells showed that, like TSQ, the majority of Zinquin-based fluorescence was due to interactions with Zn-proteins (section 3.1.3.). However, unlike TSQ, Zinquin was also able to chelate out Zn^{2+} from some Zn-proteins that eluted as LMW $Zn(ZQ_{ACID})_2$. Moreover, the extent to which Zinquin chelation occurred was dependent on the cell line tested, varying from negligible amounts ($LLC\text{-}PK_1$) to up to 20% of the total Zn^{2+} (TE-671 cell). Therefore, not only are the intracellular reactions of Zinquin different from a related Zn-sensor, but they are also different depending upon what cell type is being used.

The amount of Zn-proteins that react with Zinquin was initially estimated by correlating the fluorescence observed in the proteomic fractions to a standard curve of $Zn(ZQ_{ACID})_2$ (see section 3.1.2). The assumption made was that the free complex and the ternary adduct have similar fluorescence yields. This was later supported by the titration of $Zn(ZQ_{ACID})_2$ with BSA to form ZQ-Zn-BSA which exhibited 90% of the fluorescent intensity of $Zn(ZQ_{ACID})_2$ (see section 3.4.1.). Depending upon the cell type, 15-30% of the Zn-proteins reacted with Zinquin to form adducts and thus represented the main source of Zinquin fluorescence. Moreover, the variation in reactivity between cell types adds to the complexity of the exact ZQ-Zn-proteins being observed.

The end products of exposing cells to Zinquin are the formation of Zinquin-Zn-protein adducts and in some cases the chelation of Zn^{2+} from Zn-proteins as free $Zn(ZQ_{ACID})_2$.

However, this result is further complicated by the fact that $Zn(ZQ_{ACID})_2$ is not immune to undergoing reactions with proteins having modest Zn^{2+} binding sites (see section 3.4, K_D BSA ≈ 50 nM, most eukaryotic Zn-binding proteins K_D ≈ 1-100 pM).[91] Conceivably, Zinquin may initially chelate out Zn^{2+} from a Zn-protein, but then immediately react with an adventitious Zn^{2+} binding site, forming a new Zinquin-Zn-protein adduct (reactions 3.16 and 3.17). Therefore, it is possible that Zinquin aids in the redistribution of Zn^{2+} within the proteome.

The extent of which $Zn(ZQ_{ACID})_2$ reacts with the proteome is most likely dependent on the type of cell being investigated. The fact that $Zn(ZQ_{ACID})_2$ is present in variable amounts after cellular exposure to Zinquin in a variety of cell types indicates that this reaction is cell dependent (see section 3.1.2). With respect to changes in "free" Zn^{2+}, the extent of this reaction is also cell-dependent. In C6 cells, the treatment with NEM resulted in a net increase in $Zn(ZQ_{ACID})_2$ that did not react with the proteome (see section 3.5.2). Yet, the exogenous introduction of $Zn(ZQ_{ACID})_2$ to the LLC-PK$_1$ proteome resulted in a significant reaction in terms of new Zinquin adduct formations (see section 3.4.3). Therefore, the possible reaction of $Zn(ZQ)_2$ with the host proteome must also be kept in mind.

In addition, most Zn^{2+} sensor experiments also involve subsequent exposure to TPEN after incubation with the fluorescent probe to show that fluorescence is Zn^{2+} dependent.[20,29,36,37,40,117-123] Yet, TPEN not only quenches the Zn-sensor fluorescence, but also reacts with Zn-proteins, resulting in the chelation of Zn^{2+} or the formation of

TPEN-Zn-protein adducts (see section 3.3.4, 3.8.2). Therefore, there is a significant danger of altering not just the transient Zn^{2+} concentration within the cell but also Zn^{2+} discretely bound to proteins when TPEN is added to the system.

Figure 4.1 provides a summary of the reactions Zinquin and TPEN may undergo in a cellular environment as evidenced in this report. Traditionally, Zinquin ethyl ester was thought to enter the cell, be hydrolyzed to Zinquin acid, and react with Zn^{2+} ions to form fluorescent $Zn(ZQ_{ACID})_2$ which can be quenched with TPEN. However, there is mounting evidence for a number of other reactions that ultimately give rise to Zinquin fluorescence as described above.

The complexity of this scheme is intensified when considering the number of Zn-proteins affected in the system, each with its own thermodynamic and kinetic variables with respect to reactions with Zinquin and TPEN. Furthermore, the reactivity of $Zn(ZQ_{EE})_2$ was not included in this scheme, which may give rise to additional fates of Zinquin. Therefore, all of these reactions need to be considered when exposing cells to Zinquin and/or TPEN.

To gain further information about the Zn-proteins that are targets for Zinquin, Zinquin-affinity chromatography was developed. This technique revealed that the $\approx$20% of Zn-proteins that react with Zinquin corresponds to approximately 5% of the total proteome as measured by mass (see section 3.6.1.). Further analysis using SDS-PAGE showed that, at a minimum, there are nearly 100 different Zinquin-reactive proteins ranging in size
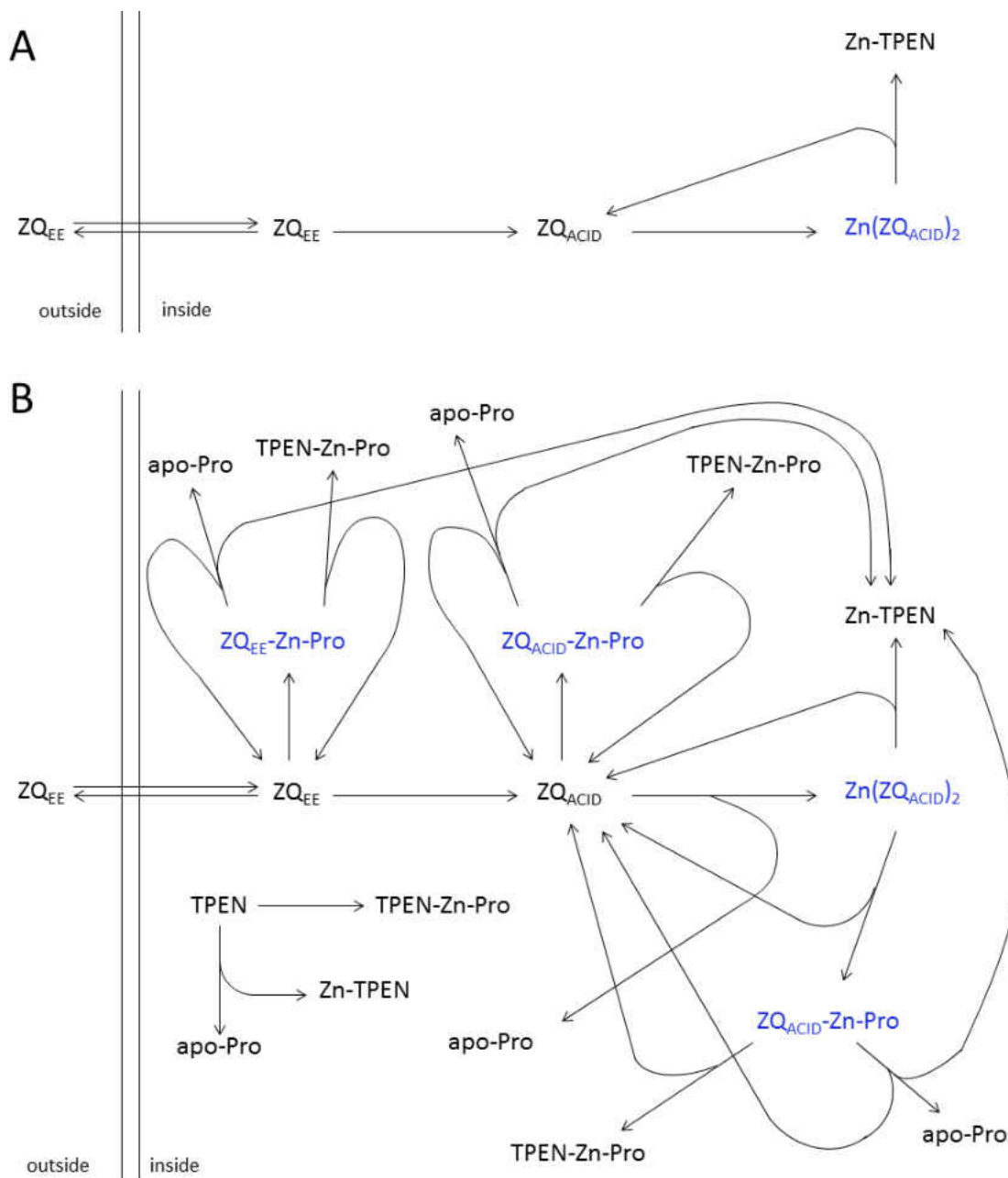
Figure 4.1. Possible intracellular reactions of Zinquin and TPEN. (A) Traditional reaction scheme of cellular exposure to Zinquin followed by TPEN. (B) Types of reactions Zinquin and TPEN undergo in an intracellular environment as presented in this report. Blue species signify fluorescent compounds

and expressed quantity (see section 3.6.4.). This says that Zinquin reacts with a significant percentage of the total number of cellular proteins. This percentage is made larger when considering that not all of the proteins that bind Zinquin were able to be captured by the Zinquin affinity column. These isolated Zinquin proteins can be identified using traditional proteomic techniques, thus beginning to answer the question of the intracellular targets of Zinquin (see section 3.8.1.).

The development of Zinquin-affinity chromatography has greater implications than simply identifying which proteins bind Zinquin. It is a way to begin to isolate some Zn-proteins—and more generally metalloproteins—from a complex cellular lysate. This technique is essentially the reverse of traditional metal affinity chromatography. Instead of a metal binding region on a protein (typically an engineered Histidine-tag on the desired protein) associating with an immobilized metal-column (typically Ni or Co), here, a metallo-specifc ligand is in the immobilized phase, to which the eluted metalloproteins in a complex solution bind. Indeed, LA-ICP-MS analysis of a subset of the proteome captured by this technique revealed numerous Zn^{2+} peaks corresponding to Zn-proteins (see section 3.8.1.). In theory, the Zinquin molecule ligated to the affinity column could be additionally modified to capture differing subsets of the Zn-proteome. This concept was supported by the in gel TSQ/ZQ staining in which ZQ_{EE} and TSQ preferentially reacted with different Zn-proteins in the same sample (see section 3.8.2). Moreover, since some copper proteins were also captured by the Zinquin-affinity column, this system may be applicable to other metallomes as well (see section 3.8.1.).

With these new spectral and experimental design insights in mind, a study claiming intracellular Zn^{2+} redistribution after exposure to *N*-ethylmaleimide was revisited.[34,35] Indeed, exposure to NEM resulted in red-shifted fluorescence spectra, indicative of Zn^{2+} release as monitored by Zinquin (see section 3.5.2.). Also, gel filtration experiments showed a depletion of HMW Zn^{2+} recovered in the LMW fractions after NEM-exposure, and thus would support the hypothesis that *N*-ethylmaleimide is a liberator of Zn^{2+} ions. However, when this process was monitored by TSQ, the release of Zn^{2+} was *not* observed as measured spectrophotometrically or using AAS (see section 3.5.3.). This means that Zn^{2+} redistribution was a function of the Zn-sensor being used and was not necessarily representative of the reaction being investigated, in this case *N*-ethylmaleimide with Zn-proteins in C6 cells. Furthermore, since both experiments involving Zinquin and TSQ resulted in similar fluorescence enhancements after exposure to NEM, they may be indistinguishable using traditional fixed-window fluorescence microscopy, despite having different cellular Zn^{2+} distributions.

Zinquin and its analogue TSQ are common Zn^{2+} sensors used in the biological and biochemical community. They have been used in a variety of cell types to detect not only basal Zn^{2+} levels, but also changes in intracellular free Zn^{2+}.[15,20,29,30,32-42,44-50] However, a broad survey of seven different cell systems showed that the main source of fluorescence was from reactions with the Zn-proteome, not Zn^{2+}. In addition, the types of intracellular reactions, including adduct formation and chelation of proteomic Zn^{2+} by Zinquin, were dependent on the cell system used. Furthermore, even closely-related sensors reacted quite differently with intracellular Zn^{2+} sources, either when measuring

basal fluorescence (TSQ/ZQ staining in section 3.8.2) or when attempting to stimulate Zn^{2+} release (NEM reactions in section 3.5.4.) Taken together, this underscores the fact that these sensors are not passive observers of Zn^{2+}, but active participants in the Zn^{2+} biochemistry within the tested cell. Given the nature of these interactions, Zinquin and TSQ do not measure transient Zn^{2+} within a cell. Moreover, these new insights into the cellular reactions of these sensors make conclusions drawn from their use suspect. These investigations need to be revisited and accompanied with additional extensive analyses—such as fluorescence spectroscopy and chromatography—to truly describe the chemistry performed by the Zn^{2+} sensor in use.

Although most of this report focused on sensors used for studying transient Zn^{2+}, there is a growing demand for the basic understanding of which proteins bind Zn^{2+}.[124-126] Early bioinformatic studies estimate the size of the Zn^{2+} metallome to be around 2,800 proteins, yet most of these proteins have not been isolated and identified.[5,124] Of the variety of metallomic approaches, LA-ICP-MS has emerged as a promising technique for accessing the metal content of proteins run on polyacrylamide gels.[109,127,128] The main problem with this method is the potential for metal loss during the electrophoretic separation.[101] Hence, there was an impetus to develop a PAGE technique that maintains protein integrity while still effectively separating a complex protein mixture. Moreover, using this method may help elucidate which proteins sensors such as Zinquin are interacting with.

By making simple modifications to the traditional PAGE methods, samples of isolated proteins and complex cellular protein mixtures were able to be separated with high resolution while still maintaining enzymatic function (see section 3.7.4.). The most glaring modification that needed to be made was the removal of EDTA from all buffers. Supposedly added to inhibit metalloproteases, the astute metallobiochemist would recognize the dangers of introducing such a powerful metal chelator to the system.[129] These fears were realized when investigating the reactions of the Zn-proteome with a variety of metal chelators, including EDTA, in which 30% of the total Zn^{2+} was removed from the proteome (see section 3.3.4.). Furthermore, the presence of EDTA in the run buffer assisted in the destruction of the ADH tetramer during the electrophoresis, presumably by removing the structural Zn^{2+} (see section 3.7.2).

Another key modification was the amount of detergent present in the buffers. Scaling back the SDS concentration to 0.0375% (1.3 mM) in the run buffer resulted in adequate protein resolution while still maintaining activity of many proteins (see section 3.7.2.). During the original development of SDS-PAGE back in the early 1970's, a key paper investigated the binding of SDS to a variety of protein peptides.[130] The SDS binding isotherms for the seven different proteins tested were all biphasic in nature. The authors agreed with an earlier report that, in the early phase of the reaction, SDS associates with the proteins a single molecule at a time (reactions 4.1).[131]

$$SDS + SDS_n\text{-Protein} \rightleftarrows SDS_{n+1}\text{-Protein} \quad \text{where } n \geq 0 \qquad (4.1)$$
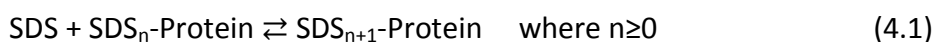
As the concentration of SDS is increased, more SDS binds to a point where the protein begins to unfold, exposing more binding sites for SDS. Thus, cooperative binding is then observed, signified by a sharp increase in the SDS binding curve (reaction 4.2).

$$nSDS + SDS_m\text{-Protein} \rightleftarrows SDS_{m+n}\text{-protein} \tag{4.2}$$
$$\text{where } n \geq 2, m = \# \text{ of bound SDS}$$
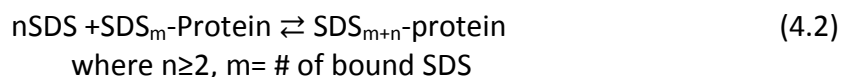
The point at which the phase change occurred was at an equilibrium concentration of SDS between 1.2-1.5 mM for all proteins tested. Therefore, running proteins in a buffer containing 1.3 mM SDS coats the proteins with the maximal amount of electric charge before significantly altering the protein structure.

It should be noted that the point at which SDS binding cooperativity occurs, and thus denaturation occurs, varies from protein to protein.[130] Therefore, an SDS concentration of 1.3 mM still may be enough to disrupt the structure of some more sensitive proteins. This was evident by the loss of enzymatic activity of L-amino oxidase and Glucose-6-Phosphate dehydrogenase after NSDS-PAGE analysis (see section 3.7.4.). Yet, for a majority of the enzymes tested, activity remained intact. Thus NSDS-PAGE is a viable, but not perfect, native separation method.

The applications of NSDS-PAGE are profound. By providing higher resolution separation than BN-PAGE, enzymes from cellular lysates can be resolved and located using direct in-gel activity assays (see section 3.7.5.) Also, Zn-proteins can be located on the NSDS gel by incubation in a TSQ solution, resulting in formation of fluorescent TSQ-Zn-proteins that can be visualized (see section 3.8.2.). In theory, this concept of TSQ

staining could be expanded to include other small molecules such as drugs or other toxic agents to determine novel binding interactions with electrophoresed proteins. Moreover, this method could aid in the identification of native protein-protein interactions as well.

One of the most promising applications of NSDS-PAGE is to the field of metallomics. LA-ICP-MS analysis performed by William Wobig demonstrated a vast improvement in metal retention for both model proteins and proteomic fractions from cell lysates in gels run using the NSDS-PAGE method compared to traditional SDS-PAGE.[94] This occurred without major sacrifices in resolution that were observed in other native-PAGE methods (see section 3.7.4.). Therefore, the addition of this method to the arsenal of techniques used in metallomics allows for vast improvements in the ability to identify novel metal-binding proteins.

References:

1. Vallee, B. L., and Auld, D. S. Zinc coordination, function, and structure of zinc enzymes and other proteins. *Biochemistry* (1990) **29**, 5647-5659

2. Andreini, C., Banci, L., Bertini, I., and Rosato, A. Zinc through the Three Domains of Life. *Journal of Proteome Research* (2006) **5**, 3173-3178

3. Vallee, B. L. Zinc biochemistry: A perspective. *Trends Biochem. Sci* (1976) **1**, 88-91

4. Outten, C. E., O'Halloran, and V., T. Femtomolar Sensitivity of Metalloregulatory Proteins Controlling Zinc Homeostasis. *Science* (2001) **292**, 2488-2492

5. Andreini, C., Banci, L., Bertini, I., and Rosato, A. Counting the zinc-proteins encoded in the human genome. *Journal of proteome research* (2006) **5**, 196-201

6. Zhang, B., Georgiev, O., Hagmann, M., Günes, Ç., Cramer, M., Faller, P., Vasák, M., and Schaffner, W. Activity of Metal-Responsive Transcription Factor 1 by Toxic Heavy Metals and H2O2 In Vitro Is Modulated by Metallothionein. *Mol. Cell. Biol.* (2003) **23**, 8471-8485

7. Andrews, G. Cellular zinc sensors: MTF-1 regulation of gene expression. *BioMetals* (2001) **14**, 223-237

8. Petering, D. H., Zhu, J., Krezoski, S., Meeusen, J., Kiekenbush, C., Krull, S., Specher, T., and Dughish, M. Apo-Metallothionein Emerging as a Major Player in the Cellular Activities of Metallothionein. *Exp. Biol. Med.* (2006) **231**, 1528-1534

9. Petering, D. H., Loftsgaarden, J., Schneider, J., and Fowler, B. Metabolism of cadmium, zinc and copper in the rat kidney: the role of metallothionein and other binding sites. *Environ. Health Perspect.* (1984) **54**, 73-81

10. Budde, T., Minta, A., White, J. A., and Kay, A. R. Imaging free zinc in synaptic terminals in live hippocampal slices. *Neuroscience* (1997) **79**, 347-358

11. Paoletti, P., Vergnano, A. M., Barbour, B., and Casado, M. Zinc at glutamatergic synapses. *Neuroscience* (2009) **158**, 126-136

12. Kay, A. R., and Toth, K. Is Zinc a Neuromodulator? *Sci. Signal.* (2008) **1**, re3-

13. Takeda, A. Zinc Signaling in the Hippocampus and Its Relation to Pathogenesis of Depression. *Mol. Neurobiol.* (2011) **44**, 166-174

14. Tsuchiya, D., Hong, S., Suh, S. W., Kayama, T., Panter, S. S., and Weinstein, P. R. Mild Hypothermia Reduces Zinc Translocation, Neuronal Cell Death, and Mortality After Transient Global Ischemia in Mice. *J Cereb Blood Flow Metab* (2002) **22**, 1231-1238

15. Jayasooriya, A. P., Ackland, M. L., Mathai, M. L., Sinclair, A. J., Weisinger, H. S., Weisinger, R. S., Halver, J. E., Kitajka, K., and Puskás, L. G. Perinatal ω-3 polyunsaturated fatty acid supply modifies brain zinc homeostasis during adulthood. *Proceedings of the National Academy of Sciences of the United States of America* (2005) **102**, 7133-7138

16. Kawahara, M., Arispe, N., Kuroda, Y., and Rojas, E. Alzheimer's disease amyloid beta-protein forms Zn(2+)-sensitive, cation-selective channels across excised membrane patches from hypothalamic neurons. *Biophys. J.* (1997) **73**, 67-75

17. Gaither, L. A., and Eide, D. Eukaryotic zinc transporters and their regulation. *BioMetals* (2001) **14**, 251-270

18. Murakami, M., and Hirano, T. Intracellular zinc homeostasis and zinc signaling. *Cancer Sci.* (2008) **99**, 1515-1522

19. Krebs, N. F., Hambidge, K. M., Westcott, J. E., Miller, L. V., Sian, L., Bell, M., and Grunwald, G. Exchangeable Zinc Pool Size in Infants Is Related to Key Variables of Zinc Homeostasis. *The Journal of Nutrition* (2003) **133**, 1498S-1501S

20. Truong-Tran, A. Q., Ruffin, R. E., and Zalewski, P. D. Visualization of labile zinc and its role in apoptosis of primary airway epithelial cells and cell lines. *American Journal of Physiology - Lung Cellular and Molecular Physiology* (2000) **279**, L1172-L1183

21. Canzoniero, L. M. T., Turetsky, D. M., and Choi, D. W. Measurement of Intracellular Free Zinc Concentrations Accompanying Zinc-Induced Neuronal Death. *The Journal of Neuroscience* (1999) **19**, RC31

22. Petering, D. H. *Chemtracts-Inorganic Chemistry* (2004) **17**, 569-580

23. Vinkenborg, J. L., Nicolson, T. J., Bellomo, E. A., Koay, M. S., Rutter, G. A., and Merkx, M. Genetically encoded FRET sensors to monitor intracellular Zn2+ homeostasis. *Nat Meth* (2009) **6**, 737-740

24. Thompson, R. B. Studying zinc biology with fluorescence: ain't we got fun? *Curr. Opin. Chem. Biol.* (2005) **9**, 526-532

25. Domaille, D. W., Que, E. L., and Chang, C. J. Synthetic fluorescent sensors for studying the cell biology of metals. *Nat Chem Biol* (2008) **4**, 168-175

26. Jiang, P., and Guo, Z. Fluorescent detection of zinc in biological systems: recent development on the design of chemosensors and biosensors. *Coord. Chem. Rev.* (2004) **248**, 205-229

27. Frederickson, C. J., Kasarskis, E. J., Ringo, D., and Frederickson, R. E. A quinoline fluorescence method for visualizing and assaying the histochemically reactive zinc (bouton zinc) in the brain. *J. Neurosci. Methods* (1987) **20**, 91-103

28. Reyes, J. G., Santander, M., Martinez, P. L., Arce, R., and Benos, D. J. A fluorescence method to determine picomole amounts of Zn(II) in biological systems. *Biological Research* (1994) **27**, 49-56

29. Zalewski, P. D., Forbes, I. J., and Betts, W. H. Correlation of apoptosis with change in intracellular labile Zn(II) using zinquin [(2-methyl-8-p-toluenesulphonamido-6-quinolyloxy)acetic acid], a new specific fluorescent probe for Zn(II). *The Biochemical journal* (1993) **296 (Pt 2)**, 403-408

30. Nasir, M. S., Fahrni, C. J., Suhy, D. A., Kolodsick, K. J., Singer, C. P., and O'Halloran, T. V. The chemical cell biology of zinc: structure and intracellular fluorescence of a zinc-quinolinesulfonamide complex. *J. Biol. Inorg. Chem.* (1999) **4**, 775-783

31. Fahrni, C. J., and O'Halloran, T. V. Aqueous Coordination Chemistry of Quinoline-Based Fluorescence Probes for the Biological Chemistry of Zinc. *J. Am. Chem. Soc.* (1999) **121**, 11448-11458

32. Colvin, R. A., Laskowski, M., and Fontaine, C. P. Zinquin identifies subcellular compartmentalization of zinc in cortical neurons. Relation to the trafficking of zinc and the mitochondrial compartment. *Brain Res.* (2006) **1085**, 1-10

33. Coyle, P., Zalewski, P. D., Philcox, J. C., Forbes, I. J., Ward, A. D., Lincoln, S. F., Mahadevan, I., and Rofe, A. M. Measurement of zinc in hepatocytes by using a fluorescent probe, zinquin: relationship to metallothionein and intracellular zinc. *Biochem. J.* (1994) **303**, 781-780

34. Haase, H., and Beyersmann, D. Uptake and intracellular distribution of labile and total Zn(II) in C6 rat glioma cells investigated with fluorescent probes and atomic absorption. *BioMetals* (1999) **12**, 247-254

35. Haase, H., and Beyersmann, D. Intracellular zinc distribution and transport in C6 rat glioma cells. *Biochem. Biophys. Res. Commun.* (2002) **296**, 923-928

36. Haase, H., Ober-Blöbaum, J. L., Engelhardt, G., Hebel, S., Heit, A., Heine, H., and Rink, L. Zinc Signals Are Essential for Lipopolysaccharide-Induced Signal Transduction in Monocytes. *The Journal of Immunology* (2008) **181**, 6491-6502

37. Kaltenberg, J., Plum, L. M., Ober-Blöbaum, J. L., Hönscheid, A., Rink, L., and Haase, H. Zinc signals promote IL-2-dependent proliferation of T cells. *Eur. J. Immunol.* (2010) **40**, 1496-1503

38. Klaus-D, K. Cellular stress and intracellular zinc dyshomeostasis. *Arch. Biochem. Biophys.* (2007) **463**, 183-187

39. Palmiter, R. D., and Findley, S. D. Cloning and functional characterization of a mammalian zinc transporter that confers resistance to zinc. *EMBO J.* (1995) **14**, 639-649

40.   Pearce, L. L., Wasserloos, K., St. Croix, C. M., Gandley, R., Levitan, E. S., and Pitt, B. R. Metallothionein, Nitric Oxide and Zinc Homeostasis in Vascular Endothelial Cells. *The Journal of Nutrition* (2000) **130**, 1467S-1470S

41.   Smith, P. J., Wiltshire, M., Davies, S., Chin, S.-F., Campbell, A. K., and Errington, R. J. DNA damage-induced [Zn2+]i transients: correlation with cell cycle arrest and apoptosis in lymphoma cells. *American Journal of Physiology - Cell Physiology* (2002) **283**, C609-C622

42.   Smith, P. J., Wiltshire, M., Furon, E., Beattie, J. H., and Errington, R. J. Impact of overexpression of metallothionein-1 on cell cycle progression and zinc toxicity. *American Journal of Physiology - Cell Physiology* (2008) **295**, C1399-C1408

43.   Snitsarev, V., Budde, T., Stricker, T. P., Cox, J. M., Krupa, D. J., Geng, L., and Kay, A. R. Fluorescent Detection of Zn2+-Rich Vesicles with Zinquin: Mechanism of Action in Lipid Environments. *Biophys. J.* (2001) **80**, 1538-1546

44.   Spahl, D. U., Berendji-Grün, D., Suschek, C. V., Kolb-Bachofen, V., and Kröncke, K.-D. Regulation of zinc homeostasis by inducible NO synthase-derived NO: Nuclear metallothionein translocation and intranuclear Zn2+ release. *Proceedings of the National Academy of Sciences* (2003) **100**, 13952-13957

45.   St. Croix, C. M., Wasserloos, K. J., Dineley, K. E., Reynolds, I. J., Levitan, E. S., and Pitt, B. R. Nitric oxide-induced changes in intracellular zinc homeostasis are mediated by metallothionein/thionein. *American Journal of Physiology - Lung Cellular and Molecular Physiology* (2002) **282**, L185-L192

46.   Tang, Z.-L., Wasserloos, K., Liu, X., Stitt, M., Reyolds, I., Pitt, B., and St. Croix, C. (2002) Nitric oxide decreases the sensitivity of pulmonary endothelial cells to LPS-induced apoptosis in a zinc-dependent fashion. in *Oxygen/Nitrogen Radicals: Cell Injury and Disease* (Vallyathan, V., Shi, X., and Castranova, V. eds.), Springer US. pp 211-217

47.   Zalewski, P. D., Millard, S. H., Forbes, I. J., Kapaniris, O., Slavotinek, A., Betts, W. H., Ward, A. D., Lincoln, S. F., and Mahadevan, I. Video image analysis of labile zinc in viable pancreatic islet cells using a specific fluorescent probe for zinc. *Journal of Histochemistry & Cytochemistry* (1994) **42**, 877-884

48.   Cortese, M. M., Suschek, C. V., Wetzel, W., Kröncke, K.-D., and Kolb-Bachofen, V. Zinc protects endothelial cells from hydrogen peroxide via Nrf2-dependent stimulation of glutathione biosynthesis. *Free Radical Biol. Med.* (2008) **44**, 2002-2012

49.   Zalewski, P. D., Forbes, I. J., Seamark, R. F., Borlinghaus, R., Betts, W. H., Lincoln, S. F., and Ward, A. D. Flux of intracellular labile zinc during apoptosis (gene-directed cell death) revealed by a specific chemical probe, Zinquin. *Chem. Biol.* (1994) **1**, 153-161

50.   Palmiter, R. D., Cole, T. B., and Findley, S. D. ZnT-2, a mammalian protein that confers resistance to zinc by facilitating vesicular sequestration. *EMBO J* (1996) **15**, 1784-1791

51.   Brand, I. A., and Kleineke, J. Intracellular Zinc Movement and Its Effect on the Carbohydrate Metabolism of Isolated Rat Hepatocytes. *J. Biol. Chem.* (1996) **271**, 1941-1949

52.   Zhu, J., Meeusen, J., Krezoski, S., and Petering, D. H. Reactivity of Zn-, Cd-, and Apo-Metallothionein with Nitric Oxide Compounds: In Vitro and Cellular Comparison. *Chem. Res. Toxicol.* (2010) **23**, 422-431

53.   Hendrickson, K. M., Geue, J. P., Wyness, O., Lincoln, S. F., and Ward, A. D. Coordination and Fluorescence of the Intracellular Zn2+ Probe [2-methyl-8-(4-Toluenesulfonamido)-6-quinolyloxy]acetic Acid (Zinquin A) in Ternary Zn2+ Complexes. *J. Am. Chem. Soc.* (2003) **125**, 3889-3895

54.   Kimura, E., and Koike, T. Recent development of zinc-fluorophores. *Chem. Soc. Rev.* (1998) **27**, 179-184

55.   Krężel, A., and Maret, W. Zinc-buffering capacity of a eukaryotic cell at physiological pZn. *J. Biol. Inorg. Chem.* (2006) **11**, 1049-1062

56.   Meeusen, J. W., Tomasiewicz, H., Nowakowski, A., and Petering, D. H. TSQ, a Common Fluorescent Sensor for Cellular Zinc, Images Zinc Proteins. *Inorg. Chem.* (2011)

57. Hendrickson, K. M., Rodopoulos, T., Pittet, P.-A., Mahadevan, I., Lincoln, S. F., David Ward, A., Kurucsev, T., Duckworth, P. A., Forbes, I. J., Zalewski, P. D., and Henry Betts, W. Complexation of zinc(II) and other divalent metal ions by the fluorophore 2-methyl-8-(toluene-p-sulfonamido)-6-quinolyloxyacetic acid in 50% aqueous ethanol. *J. Chem. Soc., Dalton Trans.* (1997) **0**, 3879-3882

58. Mosmann, T. Rapid colorimetric assay for cellular growth and survival: Application to proliferation and cytotoxicity assays. *J. Immunol. Methods* (1983) **65**, 55-63

59. Ellman, G., and Lysko, H. A precise method for the determination of whole blood and plasma sulfhydryl groups. *Anal. Biochem.* (1979) **93**, 98-102

60. Manchenko, G. P. *Handbook of detection of enzymes on electrophoretic gels*, (2003) 2nd ed ed., Boca Raton, CRC Press

61. Brewer, G. J. *An introduction to isozyme techniques*, (1970), Academic Press

62. Shows, T., Scrafford-Wolff, L., Brown, J., and Meisler, M. GM1-gangliosidosis: Chromosome 3 assignment of theβ-galactosidase-A gene (β GAL A). *Somat Cell Mol Genet* (1979) **5**, 147-158

63. Brewer, G. J. Achromatic regions of tetrazolium stained starch gels: inherited electrophoretic variation. *Am. J. Hum. Genet.* (1967) **19**, 674-680

64. Dingjan, P. G., Postma, T., and Stroes, J. A. P. Quantitative differentiation of human serum alkaline phosphatase isoenzymes with polyacrylamide disc gel electrophoresis. *Z Klin Chem Klin Biochem* (1973) **11**, 167-171

65. Fishbein, W. N. THE STRUCTURAL BASIS FOR THE CATALYTIC COMPLEXITY OF UREASE: INTERACTING AND INTERCONVERTIBLE MOLECULAR SPECIES (WITH A NOTE ON ISOZYME CLASSES)*. *Ann. N.Y. Acad. Sci.* (1969) **147**, 857-881

66. Taketa, K. A tetrazolium method for peroxidase staining: Application to the antibody-affinity blotting of α-fetoprotein separated by lectin affinity electrophoresis. *Electrophoresis* (1987) **8**, 409-414

67.   Tashian, R. E. (1969) The esterases and carbonic anhydrases in human erythrocytes. in *Biochemical methods in red cell genetics*, Academic Press. pp 307

68.   Feinstein, R. N., and Lindahl, R. Detection of oxidases on polyacrylamide gels. *Anal. Biochem.* (1973) **56**, 353-360

69.   Shaw, C., and Prasad, R. Starch gel electrophoresis of enzymes—A compilation of recipes. *Biochem. Genet.* (1970) **4**, 297-320

70.   Lakowicz, J. R. *Principles of Fluorescence Spectroscopy*, (2006) 3rd ed., Springer

71.   Nowakowski, A. B., and Petering, D. H. Reactions of the Fluorescent Sensor, Zinquin, with the Zinc-Proteome: Adduct Formation and Ligand Substitution. *Inorg. Chem.* (2011) **50**, 10124-10133

72.   Rana, U., Kothinti, R., Meeusen, J., Tabatabai, N. M., Krezoski, S., and Petering, D. H. Zinc binding ligands and cellular zinc trafficking: Apo-metallothionein, glutathione, TPEN, proteomic zinc, and Zn-Sp1. *J. Inorg. Biochem.* (2008) **102**, 489-499

73.   Meeusen, J. W., Nowakowski, A., and Petering, D. H. Reaction of Metal-Binding Ligands with the Zinc Proteome: Zinc Sensors and N,N,N',N'-Tetrakis(2-pyridylmethyl)ethylenediamine. *Inorg. Chem.* (2012) **51**, 3625-3632

74.   Pulido, P., Kägi, J. H. R., and Vallee, B. L. Isolation and Some Properties of Human Metallothionein*. *Biochemistry* (1966) **5**, 1768-1777

75.   Namdarghanbari, M. A., Meeusen, J., Bachowski, G., Giebel, N., Johnson, J., and Petering, D. H. Reaction of the zinc sensor FluoZin-3 with Zn7-metallothionein: Inquiry into the existence of a proposed weak binding site. *J. Inorg. Biochem.* (2010) **104**, 224-231

76.   Chatterjee, A., Moulik, S. P., Sanyal, S. K., Mishra, B. K., and Puri, P. M. Thermodynamics of Micelle Formation of Ionic Surfactants: A Critical Assessment for Sodium Dodecyl Sulfate, Cetyl Pyridinium Chloride and Dioctyl Sulfosuccinate (Na Salt) by Microcalorimetric, Conductometric, and Tensiometric Measurements. *The Journal of Physical Chemistry B* (2001) **105**, 12823-12831

77. Ballestín, R., Molowny, A., Marín, M. P., Esteban-Pretel, G., Romero, A. M., Lopez-Garcia, C., Renau-Piqueras, J., and Ponsoda, X. Ethanol Reduces Zincosome Formation in Cultured Astrocytes. *Alcohol Alcohol.* (2011) **46**, 17-25

78. Magonet, E., Hayen, P., Delforge, D., Delaive, E., and Remacle, J. Importance of the structural zinc atom for the stability of yeast alcohol dehydrogenase. *Biochem J* (1992) **287 (Pt 2)**, 361-365

79. Bortolato, M., Besson, F., and Roux, B. Role of metal ions on the secondary and quaternary structure of alkaline phosphatase from bovine intestinal mucosa. *Proteins: Structure, Function, and Bioinformatics* (1999) **37**, 310-318

80. Lu, H., Pang, W., Hu, Y.-D., Yang, H. P., Huang, C.-Y., and Jiang, Y.-G. Effects of intracellular zinc depletion on the expression of VDAC in cultured hippocampal neurons. *Nutr. Neurosci.* (2011) **14**, 80-87

81. Shin, J.-H., Jung, H. J., An, Y. J., Cho, Y.-B., Cha, S.-S., and Roe, J.-H. Graded expression of zinc-responsive genes through two regulatory zinc-binding sites in Zur. *Proceedings of the National Academy of Sciences* (2011) **108**, 5045-5050

82. Bernhardt, M. L., Kim, A. M., O'Halloran, T. V., and Woodruff, T. K. Zinc Requirement During Meiosis I–Meiosis II Transition in Mouse Oocytes Is Independent of the MOS-MAPK Pathway. *Biol. Reprod.* (2011) **84**, 526-536

83. Trotman, C. N., and Greenwood, C. Effects of zinc and other metal ions on the stability and activity of Escherichia coli alkaline phosphatase. *Biochem J* (1971) **124**, 25-30

84. Masuoka, J., and Saltman, P. Zinc(II) and copper(II) binding to serum albumin. A comparative study of dog, bovine, and human albumin. *J. Biol. Chem.* (1994) **269**, 25557-25561

85. Gibon, J., Tu, P., Frazzini, V., Sensi, S. L., and Bouron, A. The thiol-modifying agent N-ethylmaleimide elevates the cytosolic concentration of free Zn2+ but not of Ca2+ in murine cortical neurons. *Cell Calcium* (2010) **48**, 37-43

86. Gregory, J. D. The Stability of N-Ethylmaleimide and its Reaction with Sulfhydryl Groups. *J. Am. Chem. Soc.* (1955) **77**, 3922-3923

87. Yap, L.-P., Sancheti, H., Ybanez, M. D., Garcia, J., Cadenas, E., and Han, D. (2010) Chapter 6 - Determination of GSH, GSSG, and GSNO Using HPLC with Electrochemical Detection. in *Methods Enzymol.* (Enrique, C., and Lester, P. eds.), Academic Press. pp 137-147

88. Shaw Iii, C. F., He, L., Muñoz, A., Savas, M. M., Chi, S., Fink, C. L., Gan, T., and Petering, D. H. Kinetics of reversible N-ethylmaleimide alkylation of metallothionein and the subsequent metal release. *JBIC* (1997) **2**, 65-73

89. Muylle, F. R., Adriaensen, D., Coen, W., Timmermans, J.-P., and Blust, R. Tracing of labile zinc in live fish hepatocytes using FluoZin-3. *BioMetals* (2006) **19**, 437-450

90. Nowakowski, A., and Petering, D. Sensor specific imaging of proteomic Zn2+ with zinquin and TSQ after cellular exposure to N-ethylmaleimide. *Metallomics* (2012) **4**, 448-456

91. Maret, W., and Li, Y. Coordination dynamics of zinc in proteins. *Chem Rev* (2009) **109**, 4682-4707

92. Meister, A. Glutathione metabolism and its selective modification. *J. Biol. Chem.* (1988) **263**, 17205-17208

93. Talian, I., Kováčová, V., Petrovič, M., and Sabo, J. Impact of un-polymerized acrylamide monomer residues onto protein identification by MALDI TOF MS. *cent.eur.j.chem.* (2012) **10**, 1073-1078

94. Wobig, W. Methods in Metallomics, Proteomics, and Toxicology: Development and Applications of Laser Ablation Inductively Coupled Plasma Mass Spectrometry and Native SDS-PAGE. UW-Milwaukee, Milwaukee, 2013.

95. TANAKA, Y., KAGAMIISHI, A., KIUCHI, A., and HORIUCHI, T. Purification and Properties of β-Galactosidase from Aspergillus oryzae. *J. Biochem.* (1975) **77**, 241-247

96. Keele, B. B., McCord, J. M., and Fridovich, I. Further Characterization of Bovine Superoxide Dismutase and Its Isolation from Bovine Heart. *J. Biol. Chem.* (1971) **246**, 2875-2880

97. Koch, J., and Günther, D. Review of the State-of-the-Art of Laser Ablation Inductively Coupled Plasma Mass Spectrometry. *Appl. Spectrosc.* (2011) **65**, 155A-162A

98. Skoog, D. A., Holler, F. J., and Crouch, S. R. *Instrumental analysis*, (2007), Brooks/Cole, Cengage Learning

99. Günther, D., Jackson, S. E., and Longerich, H. P. Laser ablation and arc/spark solid sample introduction into inductively coupled plasma mass spectrometers. *Spectrochimica Acta Part B: Atomic Spectroscopy* (1999) **54**, 381-409

100. Becker, S. J., Lobinski, R., and Becker, S. J. Metal imaging in non-denaturing 2D electrophoresis gels by laser ablation inductively coupled plasma mass spectrometry (LA-ICP-MS) for the detection of metalloproteins. *Metallomics* (2009) **1**, 312-316

101. Jiménez, M. S., Rodriguez, L., Gomez, M. T., and Castillo, J. R. Metal–protein binding losses in proteomic studies by PAGE–LA-ICP-MS. *Talanta* (2010) **81**, 241-247

102. Raab, A., Pioselli, B., Munro, C., Thomas-Oates, J., and Feldmann, J. Evaluation of gel electrophoresis conditions for the separation of metal-tagged proteins with subsequent laser ablation ICP-MS detection. *Electrophoresis* (2009) **30**, 303-314

103. Sussulini, A., and Becker, J. S. Combination of PAGE and LA-ICP-MS as an analytical workflow in metallomics: state of the art, new quantification strategies, advantages and limitations. *Metallomics* (2011) **3**, 1271-1279

104. Lippard, S. J., and Berg, J. M. *Principles of Bioinorganic Chemistry*, (1994), University Science Books

105. Rosengarth, A., Gerke, V., and Luecke, H. X-ray structure of full-length annexin 1 and implications for membrane aggregation. *J. Mol. Biol.* (2001) **306**, 489-498

106. Blonde, D. J., Kresack, E. J., and Kosicki, G. W. THE EFFECTS OF IONS AND FREEZE–THAWING ON SUPERNATANT AND MITOCHONDRIAL MALATE DEHYDROGENASE. *Can. J. Biochem.* (1967) **45**, 641-650

107. Mathewson, P. R., Yost Jr, F. J., and Harrison, J. H. The absence of zinc in the mitochondrial and supernatant forms of malate dehydrogenase. *Biochimica et Biophysica Acta (BBA) - Enzymology* (1973) **321**, 413-422

108. Becker, J. S., Zoriy, M., Matusch, A., Wu, B., Salber, D., Palm, C., and Becker, J. S. Bioimaging of metals by laser ablation inductively coupled plasma mass spectrometry (LA-ICP-MS). *Mass Spectrom. Rev.* (2010) **29**, 156-175

109. Becker, J. S., Zoriy, M., Becker, J. S., Pickhardt, C., Damoc, E., Juhacz, G., Palkovits, M., and Przybylski, M. Determination of Phosphorus-, Copper-, and Zinc-Containing Human Brain Proteins by LA-ICPMS and MALDI-FTICR-MS. *Anal. Chem.* (2005) **77**, 5851-5860

110. Truong-Tran, A. Q., Carter, J., Ruffin, R., and Zalewski, P. D. New insights into the role of zinc in the respiratory epithelium. *Immunol Cell Biol* (2001) **79**, 170-177

111. Sensi, S. L., Paoletti, P., Bush, A. I., and Sekler, I. Zinc in the physiology and pathology of the CNS. *Nat Rev Neurosci* (2009) **10**, 780-791

112. Fukamachi, Y., Karasaki, Y., Sugiura, T., Itoh, H., Abe, T., Yamamura, K., and Higashi, K. Zinc Suppresses Apoptosis of U937 Cells Induced by Hydrogen Peroxide through an Increase of the Bcl-2/Bax Ratio. *Biochem. Biophys. Res. Commun.* (1998) **246**, 364-369

113. Flinn, J. M., Hunter, D., Linkous, D. H., Lanzirotti, A., Smith, L. N., Brightwell, J., and Jones, B. F. Enhanced zinc consumption causes memory deficits and increased brain levels of zinc. *Physiol. Behav.* (2005) **83**, 793-803

114. Fujiwara, Y., Watanabe, S., Sakamoto, M., and Kaji, T. Repair of wounded monolayers of cultured vascular endothelial cells after simultaneous exposure to lead and zinc. *Toxicol. Lett.* (1998) **94**, 181-188

115. Brown, K. H., Peerson, J. M., Rivera, J., and Allen, L. H. Effect of supplemental zinc on the growth and serum zinc concentrations of prepubertal children: a meta-analysis of randomized controlled trials. *The American Journal of Clinical Nutrition* (2002) **75**, 1062-1071

116. Maggini, S., Wenzlaff, S., and Hornig, D. Essential Role of Vitamin C and Zinc in Child Immunity and Health. *Journal of International Medical Research* (2010) **38**, 386-414

117. Sauer, G. R., Smith, D. M., Cahalane, M., Wu, L. N. Y., and Wuthier, R. E. Intracellular zinc fluxes associated with apoptosis in growth plate chondrocytes. *J. Cell. Biochem.* (2003) **88**, 954-969

118. Back, C. J., Sistonen, L., Enkvist, M. O. K., Heikkilä, J. E., and Åkerman, K. E. O. Ca2+ and Zn2+ Dependence of DNA Synthesis in Untransformed and in Ha-rasval-12-Expressing NIH 3T3 Cells. *Exp. Cell Res.* (1993) **208**, 303-310

119. Tatsumi, T., and Fliss, H. Hypochlorous Acid Mobilizes Intracellular Zinc in Isolated Rat Heart Myocytes. *Journal of Molecular and Cellular Cardiology* (1994) **26**, 471-479

120. Cuajungco, M. P., and Lees, G. J. Nitric oxide generators produce accumulation of chelatable zinc in hippocampal neuronal perikarya. *Brain Res.* (1998) **799**, 118-129

121. Ho, L. H., Ratnaike, R. N., and Zalewski, P. D. Involvement of Intracellular Labile Zinc in Suppression of DEVD-Caspase Activity in Human Neuroblastoma Cells. *Biochem. Biophys. Res. Commun.* (2000) **268**, 148-154

122. Rudolf, E., Červinka, M., and Cerman, J. Zinc has ambiguous effects on chromium (VI)-induced oxidative stress and apoptosis. *J. Trace Elem. Med Biol.* (2005) **18**, 251-260

123. Haase, H., Hebel, S., Engelhardt, G., and Rink, L. Zinc ions cause the thimerosal-induced signal of fluorescent calcium probes in lymphocytes. *Cell Calcium* (2009) **45**, 185-191

124. Cvetkovic, A., Menon, A. L., Thorgersen, M. P., Scott, J. W., Poole Ii, F. L., Jenney Jr, F. E., Lancaster, W. A., Praissman, J. L., Shanmukh, S., Vaccaro, B. J., Trauger, S. A., Kalisiak, E., Apon, J. V., Siuzdak, G., Yannone, S. M., Tainer, J. A., and Adams, M. W. W. Microbial metalloproteomes are largely uncharacterized. *Nature* (2010) **466**, 779-782

125. Kemsley, J. MERGING METALS INTO PROTEOMICS. *Chemical & Engineering News Archive* (2011) **89**, 28-30

126. Waldron, K. J., and Robinson, N. J. How do bacterial cells ensure that metalloproteins get the correct metal? *Nat Rev Micro* (2009) **7**, 25-35

127. Binet, M. R. B., Ma, R., McLeod, C. W., and Poole, R. K. Detection and characterization of zinc- and cadmium-binding proteins in Escherichia coli by gel electrophoresis and laser ablation-inductively coupled plasma-mass spectrometry. *Anal. Biochem.* (2003) **318**, 30-38

128. Becker, J. S., Mounicou, S., Zoriy, M. V., Becker, J. S., and Lobinski, R. Analysis of metal-binding proteins separated by non-denaturating gel electrophoresis using matrix-assisted laser desorption/ionization mass spectrometry (MALDI-MS) and laser ablation inductively coupled plasma mass spectrometry (LA-ICP-MS). *Talanta* (2008) **76**, 1183-1188

129. Auld, D. S. (1995) Removal and replacement of metal ions in metallopeptidases. in *Methods Enzymol.* (Alan, J. B. ed.), Academic Press. pp 228-242

130. TAKAGI, T., TSUJII, K., and SHIRAHAMA, K. Binding Isotherms of Sodium Dodecyl Sulfate to Protein Polypeptides with Special Reference to SDS-polyacylamide Gel Electrophoresis. *J. Biochem.* (1975) **77**, 939-947

131. Steinhardt, J., and Reynolds, J. A. *Multiple equilibria in proteins*, (1969), Academic Press

CURRICULUM VITAE

Andrew B. Nowakowski

Education

University of Milwaukee-Wisconsin
Ph.D. in Chemistry   August 2013
Advisor: Distinguished Professor Dr. David H. Petering
Dissertation: Zinc Chemical Biology: The Pursuit of the Intracellular Targets of Zinquin

University of Milwaukee-Wisconsin
B.S. in Biochemistry, Pre-Medicinal Certificate   December 2006
Magna cum laude
GPA 3.72/4.00
Undergraduate Research Advisor: Associate Professor Dr. Michael K. Reddy

Experience

Research Assistant at University of Wisconsin-Milwaukee
January 2009- August 2012, July-August 2013 (3 years, 10 months)
Performed chemical research in the fields of biochemistry, metallomics, proteomics, and bio-analytical chemistry. Responsible for initial experimental design, data analysis, and subsequent protocol optimizations. Received McFarland Award for graduate research (2010). Developed multiple novel methods including:
- New affinity-based chromatography for partial purifications of proteins containing Zn
- High resolution native gel electrophoresis (provisional patent filed)
- Optimization of laser ablation inductively couple mass spectrometry for analysis of trace metals.

Teaching Assistant at University of Wisconsin Milwaukee
August 2006- December 2008, September 2012 –May 2013 (4 years, 1 month)
Created lesson plans for teaching one-hour discussions each week involving reinforcement of topics taught during separate lectures. Directed hands-on chemistry performed by students in laboratory setting with emphasis on proper technique and scientific method. Responsible for proctoring, grading, and discussing all exams and quizzes. Courses taught:
- CHEM 100: Chemical Science
- CHEM 101: Chemical Science (Chemistry for Nursing and Related Fields)
- CHEM 102: General Chemistry (taught while in undergraduate program)

- CHEM 103: Survey of Biochemistry
- CHEM 603: Introduction to Biochemistry Laboratory

Selected Presentations

1. **Nowakowski, A.B.**, Petering, D.H. The chemical biology of zinquin: what is being imaged? *2nd Canadian Conference of Biological Inorganic Chemistry,* May 2009.
2. **Nowakowski, A.B.**, Petering, D.H. Fluorescent Zn2+ sensor chemical biology – reexamination of possible intracellular targets *3rd Canadian Conference of Biological Inorganic Chemistry,* May 2011.

Publications

1. Meeusen, J.W., Tomasiewicz, H., **Nowakowski, A.B.**, Petering, D.H. TSQ (6-Methoxy-8-p-Toluenesulfonamido-Quinoline), a Common Fluorescent Sensor for Cellular Zinc, Images Zinc Proteins. *Inorg. Chem.* **2011**, 50(16) 7563-73.
2. **Nowakowski, A.B.**, Petering, D.H. Reactions of the Fluorescent Sensor, Zinquin, with the Zinc-Proteome: Adduct Formation and Ligand Substitution. *Inorg. Chem*. **2011**, 50(20) 10124-33.
3. Rush, T., Liu, X.Q., **Nowakowski, A.B.**, Petering, D.H., Lobner, D. Glutathione-mediated neuroprotection against methylmercury neurotoxicity in cortical culture is dependent on MRP1. *Neurotoxicology.* **2011**, 33(3) 476-81.
4. Meeusen, J.W., **Nowakowski, A.B.**, Petering, D.H. Reaction of Metal Binding Ligands with the Zinc Proteome: Zinc Sensors and TPEN. *Inorg. Chem.* **2011**, 51(6), 3625–3632.
5. **Nowakowski, A.B.**, Petering, D.H., Sensor Specific Imaging of Proteomic Zn2+ with Zinquin and TSQ after Cellular Exposure to N-ethylmaleimide. *Metallomics*. **2012,** 4, 448-456

Manuscripts in Progress

1. **Nowakowski, A.B.**, Meeusen, J.W., Menden, H. Petering, D.H. Chemical-Biological Properties Zinc Sensors TSQ and Zinquin: Formation of Sensor-Zn-Protein Adducts vs. Zn(Sensor)2 Complexes. Manuscript in Progress.
2. **Nowakowski, A.B.**, Wobig, W.J, Petering, D.H. Native SDS-PAGE: High Resolution Electrophoretic Separation of Proteins with Retention of Native Properties. Manuscript in Progress